THE ROLE OF SIALIC ACID BINDING IN REOVIRUS NEUROPATHOGENESIS

By

Johnna McKeeta Frierson

Dissertation

Submitted to the Faculty of the

Graduate School of Vanderbilt University

in partial fulfillment of the requirements

for the degree of

DOCTOR OF PHILOSOPHY

in

Microbiology and Immunology

December 2012

Nashville, Tennessee

Approved:

Dr. Bruce Carter

Dr. Terence Dermody

Dr. Wonder Drake

Dr. Eric Skaar

Dr. John Williams

To all my family and loved ones, whose love, prayers, and encouragement have fueled me each and every step of the way

ACKNOWLEDGEMENTS

My graduate experience has been like no other endeavor I've ever pursued. It has been a time of great growth, life changes, and learning. I'm so honored and appreciative to have had this opportunity. There are so many people that have helped me along the way, and I know that I could have not made it without them. In addition to the family I was born into, I have been fortunate to build a family here at Vanderbilt. It has been a wonderful place to be. I would be remiss if I didn't take the opportunity to say a word of thanks to those who have invested into me during my time in graduate school.

• My mother, father, and stepmother, Felicia, for their endless encouragement, support, and prayers. Mom and Dad, I thank you for instilling in me a strong moral character and love of God. My faith has gotten me though many challenges over the years and has shaped the person I am today. My success is a reflection of you and the fact that you always gave me the confidence and freedom to dream big.

• The entire Allen, Flemming, and Frierson families. We have a lot of love in our family and that loving spirit has always stayed with me no matter how far from home I may roam.

• My best friends Dawn Salters and Camelia Ashley. I thank you for being true friends and sisters to me. You ladies are wonderful, and I could never thank you enough for your friendship and support.

• My “Furman” family- Parthenia, Manie, Chris, and Alex. We’ve been friends for quite some time now. I thank you for your love, friendship, and cheers over the years. We’ve seen each other through so many different phases in life already, and I can’t wait to see what is in store for us next.

• The many wonderful friends and classmates that I have met over the years at Vanderbilt. Thank you for the joy, laughter, and friendship you’ve brought into my life. I am especially thankful for the friendship of Klarissa Hardy, Nekeithia Wade, and Isi Tolliver. We began IGP together and have supported each other through our separate journeys all the way until the end. My time at Vanderbilt would not have been the same without you, and we have made memories that will surely last a lifetime.

• I would like to thank Michelle Grundy, Linda Sealy and Roger Chalkley. When I graduated from Furman University, I was not sure what my next step would be. Michelle, I thank you for your advice and encouragement to apply to the IMSD postbaccalaureate program. Your gentle assurance that I really had a chance to be successful in graduate school opened my eyes to a world of possibilities. You have played an integral role in my education and career, and I’ll never forget that. I thank Linda and Roger of the IMSD program for your tireless efforts to help under-represented students realize their true scientific potential. Thank you for being our advocate.

• I thank Terry Dermody for being such an outstanding mentor. I was blessed to have trained with you and the lab environment you work so hard to create. You have taught me

many scientific and life lessons that I will always carry with me. Thank you for believing in me and being invested in my success. I look forward to keeping in touch with you for many years to come.

• My dissertation committee, Eric Skaar, Wonder Drake, John Williams, and Bruce Carter for insightful advice not only for helping me to become a better scientist, but for helping me to grow as an individual.

• Past and present members of the Dermody Lab. Words can't express how much I value the relationships I've built in our lab. I truly think of you like members of my family. I'll always remember the special times I've shared with everyone.

• Karl Boehme for being "my postdoc". You taught me practically everything I know in the lab and took me under your wing when I joined. I wish you much success in the future and look forward to seeing your career take off and your family prosper.

• Thank you to the Division of Pediatric Infectious Disease, the Department of Pathology, Microbiology, and Immunology, and the Lamb Center for Pediatric Research for educational and financial support.

• Most importantly, I would like to thank my husband, Sterling. Thank you for being such a loving, strong, and faithful partner to me throughout our time together. Your quiet strength is a continuous comfort. It is a strength that I appreciate more every day we are

together. I could have not made it through those times of uncertainty without you. I look forward to the next chapter of our lives together. God truly blessed me when He brought you into my life.

TABLE OF CONTENTS

Page

DEDICATION ii

ACKNOWLEDGEMENTS iii

LIST OF TABLES ix

LIST OF FIGURES x

LIST OF ABBREVIATIONS xii

Chapter

I. BACKGROUND 1

Introduction 1
Virus-receptor interactions 2
Carbohydrates as virus receptors 6
Structure and function of reovirus attachment protein σ1 5
Interactions of σ1 with SA 9
Adhesion strengthening mechanism of reovirus attachment to cells 12
Reovirus tropism and neuropathogenesis 13
Significance of research 16

II. CRYSTAL STRUCTURE OF REOVIRUS ATTACHMENT PROTEIN σ1 IN COMPLEX WITH SIALYLATED OLIGOSACCHARIDES 18

Introduction 18
Results 19
Construct Design and Structure Determination 19
Overall Structure of σ1 20
Structure of σ1 in Complex with α-2,3-Sialyllactose 24
Structures of σ1 in Complex with α-2,6-Sialyllactose and α-2,8-Disialyllactose 26
Discussion 28

III. SIALIC ACID BINDING DETERMINANTS IN THE σ1 ATTACHMENT PROTEIN OF SEROTYPE 3 REOVIRUS 33

Introduction 33
Results 34
Residues in Reovirus σ1 Required for Sialic Acid Binding 34
Discussion 37

IV. UTILIZATION OF SIALYLATED GLYCANS AS CORECEPTORS ENHANCES THE NEUROVIRULENCE OF SEROTYPE 3 REOVIRUS....39
Introduction....39
Results....40
SA binding enhances reovirus neurovirulence and spinal cord injury....40
SA binding influences reovirus replication at sites of secondary infection....43
SA binding enhances reovirus neurovirulence and replication in the brain....46
SA binding does not alter reovirus tropism in the brain....48
SA binding enhances infection of and replication in murine primary cortical neurons....48
Discussion....52

V. SUMMARY AND FUTURE DIRECTIONS....56

VI. MATERIALS AND METHODS
Cells....66
Viruses....66
Protein Expression and Purification....68
X-ray Structure Determination....68
HA assay....69
Reovirus Infection of L929 and MEL Cells....70
Infection of Mice....70
Preparation of cortical neuron cultures from embryonic mice....71
Assessment of reovirus infectivity by indirect immunofluorescence....72
Assessment of reovirus replication by plaque assay....73
Quantification of viral RNA using RT-qPCR....73
Histology and immunohistochemical staining for reovirus antigen....74

Appendices

A. CRYSTAL STRUCTURE OF REOVIRUS ATTACHMENT PROTEIN σ1 IN COMPLEX WITH SIALYLATED OLIGOSACCHARIDES....75

B. THE REOVIRUS SIGMA1S PROTEIN IS A DETERMINANT OF HEMATOGENOUS BUT NOT NEURAL VIRUS DISSEMINATION IN MICE....87

C. INTESTINAL MICROBIOTA PROMOTE ENTERIC VIRUS REPLICATION AND SYSTEMIC PATHOGENESIS....99

D. UTILIZATION OF SIALYLATED GLYCANS AS CORECEPTORS ENHANCES THE NEUROVIRULENCE OF SEROTYPE 3 REOVIRUS.....105

REFERENCES 143

LIST OF TABLES

Table Page

II-1. Data collection and refinement statistics for σ1-oligosaccharide structures.....61

V-1. Predicted glycan specificity of T1/T3 σ1 β-spiral exchange chimeras.....61

V-2. Predicted neural tropism and glycan specificity of T1/T3 σ1 domain exchange chimeras 64

LIST OF FIGURES

Figure Page

I-1. Organization and structure of a reovirus virion 6

I-2. Computer-processed negative-stain electron micrographs of σ1 7

I-3. Full-length model of reovirus σ1 9

I-4. Crystal structures of the hJAM-A and mJAM-A extracellular domains.....10

I-5. Reovirus T1L binds and infects M cells that overlie Peyer's patches 15

II-1. Structure of T3D σ1 22

II-2. Structural features of the T3D σ1 body domain and sequence alignments with T1L and T2J σ1 23

II-3. Interactions between σ1 and SA 25

II-4 The σ1 protein in complex with SA in different linkages 27

II-5. Structural adaption of the binding site 31

III-1. HA assay of T3D σ1 point mutants 35

III-2. Identification of σ1 residues required for binding to cell-surface SA 36

IV-1. SA-binding capacity enhances reovirus virulence and paralysis following IM inoculation.....41

IV-2. SA binding is associated with higher peak titers of reovirus in neural tissues 44

IV-3 Binding to SA is not required for dissemination by hematogenous routes 45

IV-4 SA-binding capacity enhances reovirus neurovirulence and replicative capacity following IC inoculation 47

IV-5 Binding to SA does not alter reovirus tropism in the brain.....49

IV-6 SA-binding capacity increases the efficiency of reovirus infection of primary cortical neurons.....51

IV-7 Comparison of T3D and T3D-σ1R202W σ1 interactions with the terminal SA of α(2,3) sialyllactose 55

V-1. Construct design of T1/T3 σ1 β-spiral exchange chimeras. 62

V-2. Construct design of T1/T3 σ1 domain exchange chimeras 65

LIST OF ABBREVIATIONS

3S6X	α-2,3-sialyllactose
3S6Y	α-2,6-sialyllactose
3S6Z	α-2,8-sialyllactose
AAV	adeno-associated virus
AFP	acute flaccid paralysis
CNS	central nervous system
ds	double-stranded
FBS	fetal bovine serum
HA	hemagglutination
hJAM-A	human JAM-A
IC	intracranial
IM	intramuscular
JAM-A	junction adhesion molecule-A
JAM-B	junction adhesion molecule-B
JAM-C	junction adhesion molecule-C
L cell	murine L929 cell
M cell	microfold cell
MEL	murine erythroleukemia
mJAM-A	murine JAM-A
MOI	multiplicity of infection
PBS	phosphate buffered saline

PFU	plaque forming units
reovirus	mammalian orthoreovirus
qRT-PCR	quantitative real-time PCR
RT-PCR	reverse transcription PCR
SA	sialic acid
T1L	type 1 Lang
T2J	type 2 Jones
T3	type 3
T3D	type 3 Dearing
TX-100	Triton X-100

CHAPTER I

BACKGROUND

Introduction

The process by which viruses cause disease consists of a complex series of steps involving many host and viral factors. Virus must employ mechanisms necessary to successfully invade a host, replicate in target cells, and subsequently be transmitted to the next host. The capacity of a virus to infect some types of cells in the host can lead to the production of disease. As such, the first step in the viral replication cycle, attachment of the virus to cell-surface receptors, is important for establishing infection and serves a critical function in viral pathogenesis. Therefore, studies aimed at gaining an understanding of the precise nature of pathogen-receptor interactions can provide valuable insights into mechanisms of tissue injury and disease in an infected host. In the work presented in this thesis, I use mammalian orthoreoviruses (called reoviruses here), a highly tractable experimental model for the study of viral pathogenesis, to gain a better understanding of virus-receptor interactions and the influence of these interactions in central nervous system (CNS) disease.

When this work was initiated, it was well established that sialic acid (SA) serves as a co-receptor for type 3 (T3) reovirus and allows reovirus to more efficiently attach to and infect cultured cells. It was also known that residues 198, 202, and 204 of T3 σ1 influence the capacity of σ1 to interact with SA. However, whether and how these σ1 residues engage SA was not known. Moreover, the crystal structure of the SA-binding

domain of the σ1 of T3 reovirus had not been determined, and the possible contributions of other σ1 residues to SA binding were unclear. Finally, while it was known that SA binding enhances reovirus dissemination from the intestine to the CNS and confers tropism for bile duct epithelium, the role of SA binding in reovirus infection of the CNS was not well understood.

In Chapter II, I report the crystal structure of the T3 reovirus attachment σ1 protein in complex with sialylated oligosaccharides. In Chapter III, I present work that defines functional SA-binding determinants in the T3 reovirus σ1 attachment protein. In Chapter IV, I report that utilization of sialylated glycans by T3 reovirus enhances neurovirulence. These findings reveal the structural and molecular basis of T3 σ1-SA interactions and suggest that SA-binding enhances reovirus infection of the murine CNS.

Virus-receptor interactions

Viral attachment to specific host molecules is the initial step in viral infection. This process is substantially more complex than a simple binary interaction between virus and receptor and often involves multiple viral and cellular determinants. These interactions also may be accompanied by dramatic conformational rearrangements of viral structural proteins (24, 53, 103, 114, 131) and, in some cases, viral receptors (85). Many viruses employ an adhesion-strengthening attachment strategy in which primary virus-cell interactions require low-affinity adhesion of the virus to common cell-surface molecules that are often carbohydrate in nature (123, 127). This initial phase of attachment is then followed by higher-affinity binding to a secondary receptor that triggers virus entry through either direct membrane fusion or receptor-mediated

endocytosis (31, 114, 124, 131). In addition, several viruses use independent receptors for attachment and internalization. For example, adenovirus uses the coxsackievirus and adenovirus receptor to attach to host cells (12, 113) and αvβ3 and αvβ5 integrins to induce endocytosis (71, 125).

Receptor engagement can influence many aspects of viral pathogenesis, most prominently dissemination and tropism. For example, tropism of human immunodeficiency virus (68), poliovirus (92), and SARS-coronavirus (30) is strongly influenced by the capacity of these viruses to bind specific receptors. Strains of adeno-associated virus (AAV) show a pattern of tropism in the CNS dependent on carbohydrate binding specificity. AAV4 utilizes α-2,3-linked SA as a receptor and infects ependymal cells. In contrast, AAV5 uses α-2,3- and α-2,6-linked SA to infect neurons (55). Thus, both proteinaceous and carbohydrate receptors can influence the types of diseases caused by viruses.

Carbohydrates as virus receptors

A large number of viruses, including many that cause human disease, use sialylated oligosaccharides present on proteins or lipids to attach to cells. Given their ubiquitous expression on the cell surface and wide distribution on various cell types throughout the host, it is not surprising that glycans terminating in SA are an important class of virus receptors. For example, coxsackievirus A24 variant and enterovirus 70, which cause acute hemorrhagic conjunctivitis and have pandemic potential, attach to sialylated oligosaccharides (2, 83). The human JC and BK polyomaviruses cause a fatal demyelinating disease and kidney graft loss, respectively, in immunocompromised

individuals. Both viruses use glycans terminating in SA as receptors (67, 78). Lastly, rotavirus, which is a member of the *Reoviridae* family, causes severe gastroenteritis in children. These viruses vary in SA-binding capacity as judged by sensitivity or resistance to neuraminidase treatment (13, 51). Neuraminidase-insensitive strains were thought to use non-sialylated receptors. However, the "neuraminidase-insensitive" rotavirus strain Wa attaches to the ganglioside GM1 (48). Because of its branched structure, this carbohydrate is difficult to cleave with neuraminidase (72, 109). Therefore, SA should be considered as a possible receptor component even for viruses whose infectivity is not affected by pre-treatment of cells with neuraminidase.

One of the most well characterized roles of SA in viral pathogenesis is in influenza virus infection and disease. Influenza viruses engage SA to infect cells of the airway epithelium (108). The specificity of the interactions between the influenza hemagglutinin and SA play a key role in tropism and host restriction. Avian influenza strains preferentially recognize the α-2,3-linked SA found in intestinal and upper airway epithelium of birds. In contrast, and human influenza strains preferentially bind to α-2,6-linked SA, which is enriched in the lower airway epithelium of humans (43, 107, 108). Mutations in the influenza hemagglutinin that change the SA specificity of an avian strain (α-2,3-linked SA) to that of a human strain (α-2,6-linked SA) allow an expansion of the viral host range to include humans with potentially devastating consequences. This insight strengthens the rationale to conduct studies to gain a better understanding of mechanisms that viruses use to engage carbohydrate receptors and understand the precise function of these receptors in viral pathogenesis.

Structure and function of reovirus attachment protein σ1

Reoviruses, members of the *Reoviridae* family, form icosahedral, nonenveloped particles that are approximately 850 Å in diameter (26) (Figure I-1). The ten segments of dsRNA that compose the reovirus genome are encapsidated within two concentric protein shells, the outer capsid and inner core (Figure I-1A). Together, the outer capsid and core are composed of eight structural proteins. The bulk of the outer capsid consists of the tightly-associated μ1 and σ3 proteins (65). There are turrets formed by the pentameric λ2 protein at each of the twelve icosahedral vertices of the virion from which the viral attachment protein, σ1, extends (6, 23, 33, 39, 42) (Figure I-1B). Three reovirus serotypes have been described, which are represented by prototype strains type 1 Lang (T1L), type 2 Jones (T2J), and type 3 Dearing (T3D) (89, 99).

The σ1 protein belongs to a class of fiber proteins constructed from triple β-spirals, a motif that was first identified in the adenovirus fiber (87). Before crystallographic structures of σ1 were determined, information about the structure came from composite transmission electron micrographs of σ1 molecules purified from virions (39) (Figure I-2). These images confirmed earlier predictions of a fiber-like structure of σ1 (10) and clearly revealed two distinct morphological domains: a long N-terminal fibrous tail that inserts into the virion capsid and a C-terminal globular head that projects away from the virion surface. As high-resolution atomic structures of σ1 became available (23, 91), the initial model of the morphological domains was revised to include a third domain encompassing a region of sequence in the middle portion of the molecule: the body domain.

Thus, the σ1 protein is a filamentous trimer about 480 Å in length with three discrete domains: the tail, body, and head (23, 39, 91) (Figure I-3).

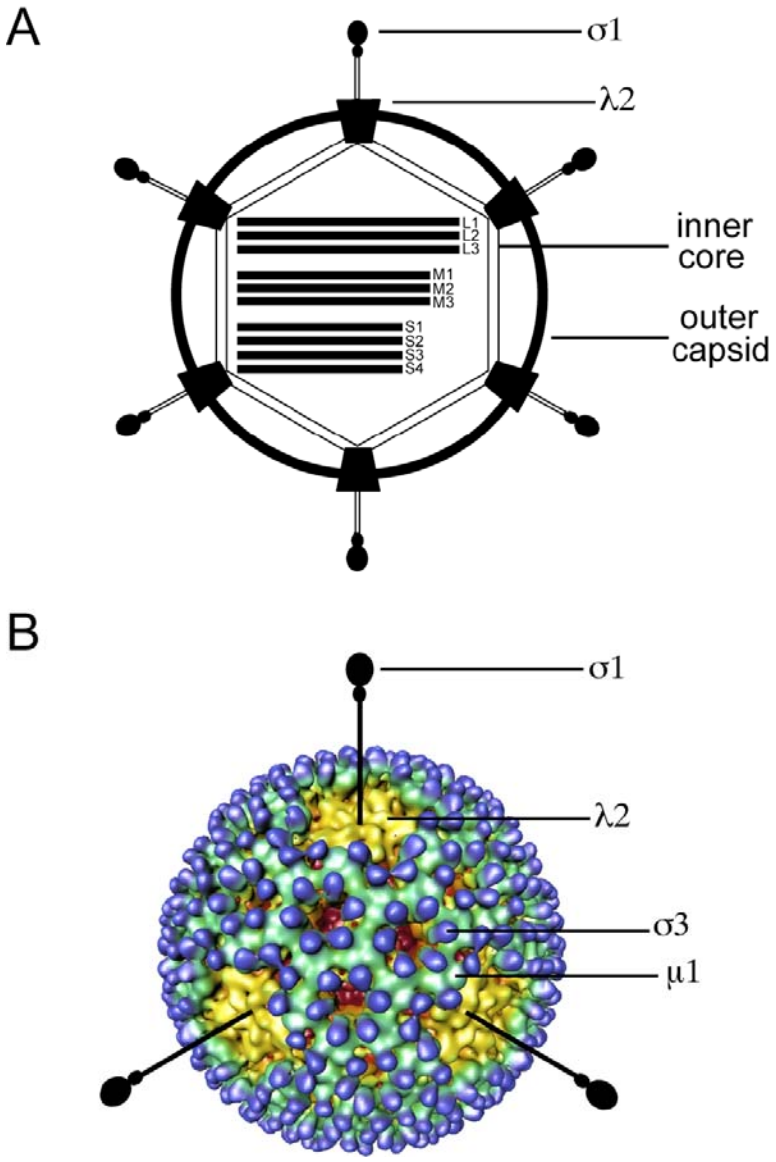

FIGURE I-1. Organization and structure of a reovirus virion. (A) Schematic representation of a reovirus virion. Outer capsid, inner core, viral attachment protein σ1, the λ2 base into which σ1 inserts, and ten viral dsRNA genome segments are indicated. (B) Cryo-electron microscopic image reconstruction of a reovirus virion. Major outer capsid proteins are pseudocolored and indicated. σ1 molecules are represented schematically. Image adapted from Nason et al. (76).

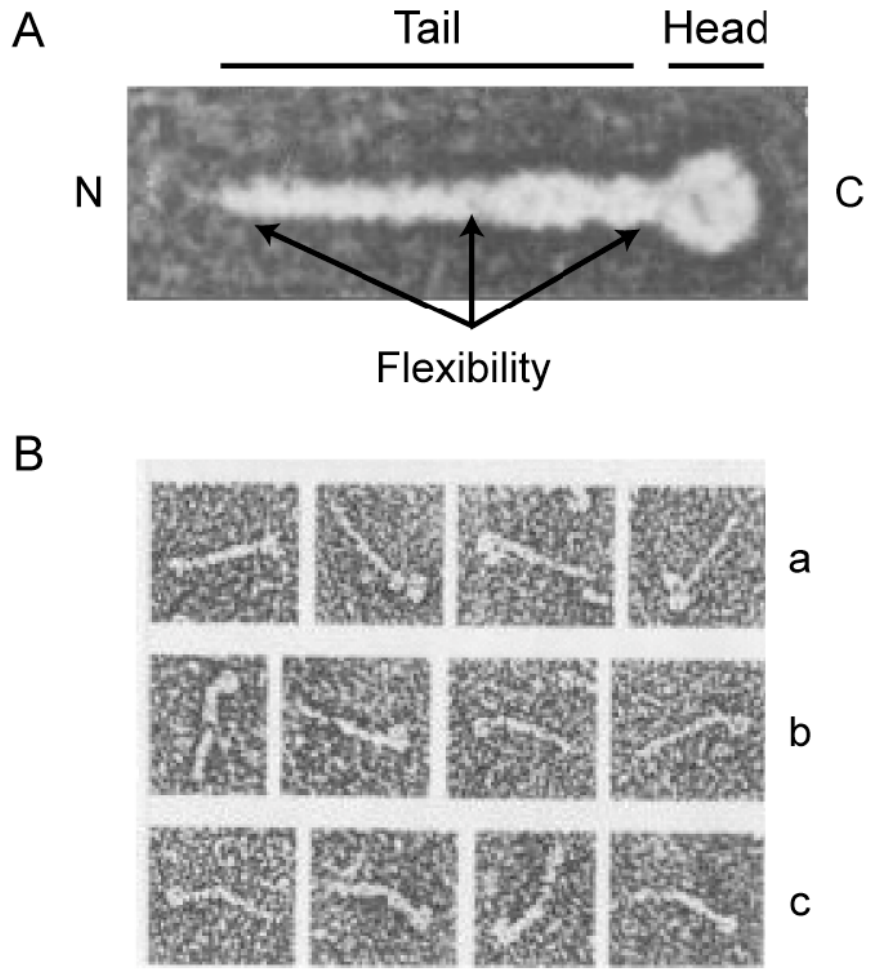

FIGURE I-2. Computer-processed negative-stain electron micrographs of σ1. (A) Composite electron micrograph of σ1. N and C termini, head and tail domains, and regions of observed flexibility of the molecule are indicated. (B) Individual electron micrographs of σl molecules, highlighting distinct morphologies: (a) the head appears multi-lobed; (b) the tail is kinked immediately adjacent to the head; (c) the tail is kinked near its midpoint. Images adapted from Fraser et al. (38).

Residues 1 to 160 encompass the σ1 tail domain, which inserts into the virion capsid (23, 42) (Figure I-3). This region of the molecule is predicted to form an α-helical coiled coil (35, 81). The σ1 body domain encompasses residues 170 to 309 and is comprised of a β-spiral repeat motif interrupted by a short α-helical coiled coil (91) (Figure I-3). The globular head domain of σ1 incorporates residues 310 to 455 and folds

into an 8-stranded β-barrel (23, 57, 91, 101) (Figure I-3). Sequences in the σ1 body domain mediate SA binding by type 3 strains (21, 91), whereas sequences in the σ1 head domain engage junctional adhesion molecule A (JAM-A) (57) (Figure I-3).

JAM-A (F11R/JAM/JAM1) serves as a receptor for all three reovirus serotypes (8, 18). JAM-A is a member of the immunoglobulin (Ig) superfamily postulated to regulate formation of intercellular tight junctions (66, 70, 126). The molecule contains two extracellular Ig-like domains, a short transmembrane region, and a cytoplasmic tail possessing a PDZ-domain-binding motif (70, 126) (Figure I-4). There are three recognized JAM family members (JAM-A, JAM-B, and JAM-C) (4, 5, 25, 64, 75). Both the murine (m) and human (h) homologs of JAM-A function as reovirus receptors (8, 18); JAM-B and JAM-C do not confer reovirus receptor activity.

The σ1 protein exhibits a substantial degree of flexibility, which can be attributed to regions that partition the main σ1 domains (34, 39, 80) (Figure I-2 and I-3). T3D σ1 contains a four-residue insertion between the two most C-terminal β-spiral repeats that lie just below the σ1 head that confers flexibility in this region (19, 23, 39). Sequence alignments of T1L and T2J σ1 predict six-residue insertions at this same position (23). The second region of flexibility is observed towards the middle of the σ1 protein and is thought to correspond to the junction between the α-helical coiled-coil tail and the β-spiral body of the protein (Figure I-3). A third region of flexibility is found in the N-terminal portion of the protein, which may form the virion-insertion domain (23, 39, 46, 81) (Figure I-2 and I-3).

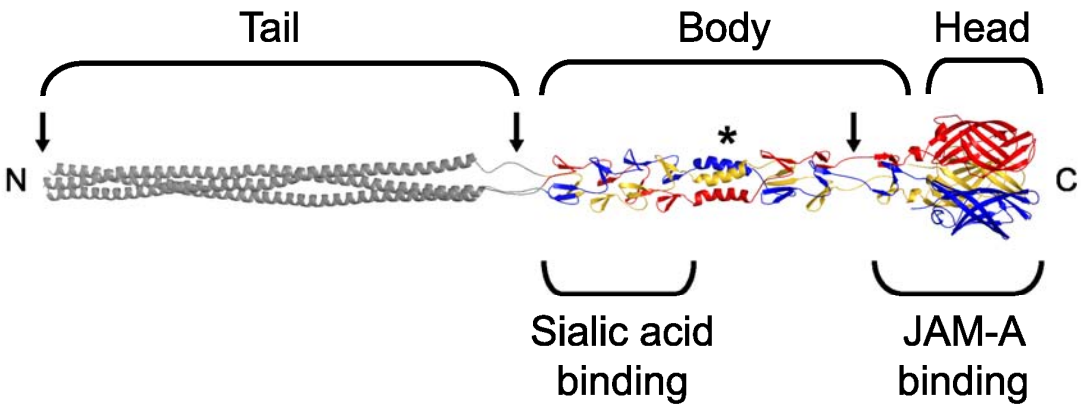

FIGURE I-3. Full-length model of reovirus σ1. A full-length depiction of σ1 was generated by modeling a predicted trimeric a-helical coiled coil and linking it to the N-terminus of the largest crystallized fragment of σ1 (residues 246-455 of strain T3D σ1) (91). The three monomers of the crystallized fragment are shown in blue, red, and yellow; the model is shown in grey. Tail, body, and head regions are indicated. Regions of flexibility are marked by arrows. A sequence polymorphism that confers susceptibility to cleavage by intestinal proteases is indicated with an asterisk. The approximate locations of binding sites for sialic acid and junctional adhesion molecule-A (JAM-A) are shown. Amino (N)- and carboxy (C)-termini are indicated.

Interactions of σ1 with SA

The earliest evidence that reoviruses engage cell-surface SA was gathered from hemagglutination (HA) assays, a sensitive assay for SA-binding capacity, in the early 1960's (63). Reoviruses exhibit the capacity to agglutinate erythrocytes of several mammalian species (63). Subsequent studies revealed that terminal α-linked SA residues on the protein glycophorin A mediate T3 reovirus agglutination of erythrocytes (44, 84). Accordingly, neuraminidase treatment of erythrocytes, which removes cell-surface SA,

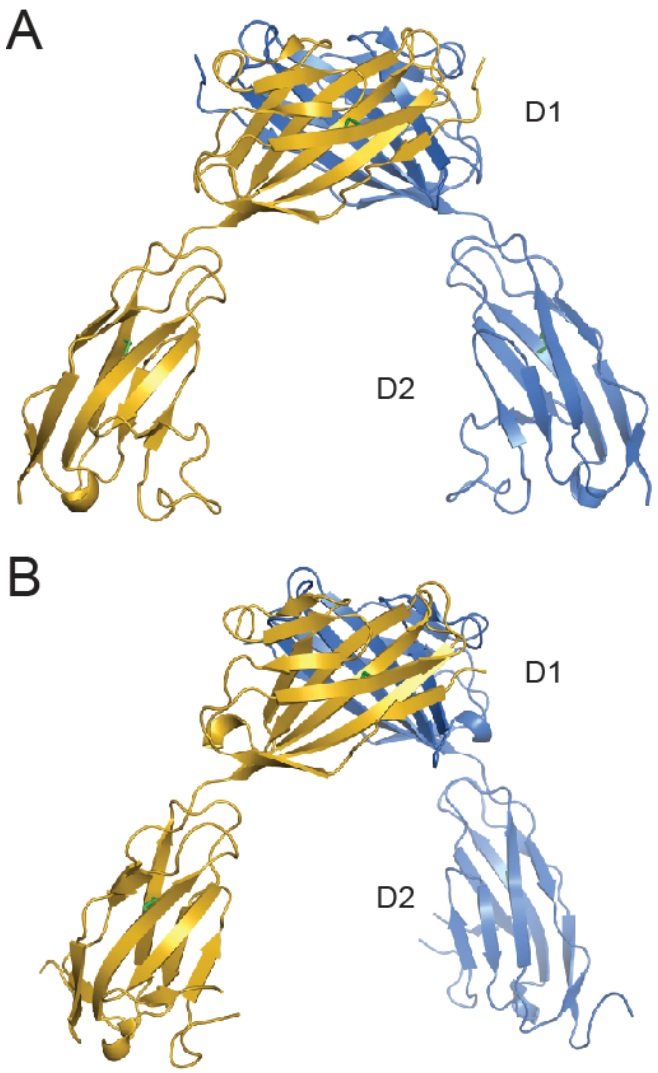

FIGURE I-4. Crystal structures of the hJAM-A and mJAM-A extracellular domains. (A-B) Ribbon drawings of the hJAM-A dimer (A) and the mJAM-A dimer (B), with one monomer shown in orange and the other in blue. Disulfide bonds are shown in green. Dimerization is mediated by the membrane-distal D1 immunoglobulin domain. Both human and murine JAM-A serve as reovirus receptors. Images adapted from Prota et al (86) (A) and Kostrewa et al (60) (B) by Eva Kirchner.

decreases the HA capacity of strain T3D (44). In addition, SA serves as an important coreceptor for reovirus binding to and infection of certain types of cells in culture, such as murine erythroleukemia (MEL) cells (22, 98).

Although naturally circulating strains of reovirus incapable of binding SA exist, the majority of field isolates do exhibit the capacity to interact with SA and agglutinate erythrocytes (27). Sequence analysis and assays of SA-binding capacity revealed that sequence polymorphisms within the σ1 body domain at residues 198, 202, and 204 determine the capacity of field-isolate strains to bind SA (27, 97). This genetic linkage was further strengthened by the finding that non-SA binding reovirus strains could be adapted to infect and replicate in MEL cells, which require binding to SA to support infection. When the S1 genes of these non-SA binding strains were analyzed, sequence changes were observed in a discrete region of σ1 corresponding to a putative SA-binding domain (22). Structural studies of T3 reovirus σ1 performed as a part of this thesis demonstrated more specifically that interactions between σ1 and SA involve residues at the N-terminal portion of the body domain, between β-spiral repeats 2 and 3, where the SA moiety docks into a shallow pocket that is formed mainly by residues in the third β-spiral repeat (91) (Figure I-3). Interestingly, the T3 σ1 SA-binding domain is highly permissive for glycan-binding and can engage α-2,3-, α-2,6-, and α-2,8-linked SA moieties (91).

The carbohydrate receptors for other serotypes of reovirus have not been as well characterized. While it is known that T1 reoviruses also bind to SA in some contexts, it is apparent that that the nature of the carbohydrate engaged by T1 and T3 reovirus strains differ. For example, T1L, but not T3D, binds to the apical surface of microfold (M) cells, but not to enterocytes, in tissue sections of rabbit Peyer's patches (49). Pre-treatment of the tissue sections with neuraminidase or with lectins that specifically recognize α-2-3-linked sialic acid inhibits infection by T1L, a property that segregates with the S1 gene.

More recently, glycan microarrays along with crystallographic studies of T1 reovirus σ1 have revealed that, in contrast to T3 reovirus, sequences in the head domain of the T1 σ1 protein are responsible for binding to the sialylated ganglioside, GM2 (90).

Adhesion-strengthening mechanism of reovirus attachment to cells

The first evidence that σ1 contains two distinct receptor-binding domains came from the realization that the SA-binding domain of T3 σ1 genetically mapped to the body domain of the σ1 protein (22, 27). To gain a better understanding of the function of SA in reovirus attachment and tropism, *in vitro* studies using monoreassortant viruses containing the S1 gene of either non-SA-binding strain T3C44 (28) (strain T3SA-) or SA-binding strain T3C44-MA (22) (strain T3SA+) and all other gene segments from T1L (7). T3SA- and T3SA+ demonstrate cell-specific interactions attributed to the S1 gene segments of their respective T3 parental strains, with T3SA+, but not T3SA-, capable of hemagglutination and growth in MEL cells. In concordance with these results, studies using surface plasmon resonance demonstrated that T3SA+ binds SA with a K_D of ~ 5 x 10^{-9} M, while T3SA- displays no specific interaction with SA (7).

These reovirus strains also exhibit differences in binding and growth in other cells in culture. Although both T3SA+ and T3SA- replicate with equivalent efficiency in L cells, T3SA+ replicates 100-fold more efficiently in HeLa cells than does T3SA- (7). Moreover, the avidity of these strains for L cells is nearly equivalent (K_D 3 x 10^{-11} M) as shown by radioligand binding assays, but the avidity of T3SA+ for HeLa cells is five-fold higher than that of T3SA- (7). Kinetic binding studies indicate that the capacity to engage SA functionally serves to increase the k_{on} of virus attachment to HeLa cells. Binding of

T3SA+ to HeLa cells proceeds through a time-dependent adhesion-strengthening process, which is initially characterized by a rapid k_{on} and k_{off}, and then transitions to a higher-avidity binding state with a slower k_{off} (7). Preincubation of virus with sialyllactose dramatically reduces the efficiency of T3SA+ infection, yet has no effect on T3SA- infectivity (7). Therefore, the enhanced infectivity of T3SA+ is mediated by the interaction of σ1 with cell-surface SA. However, this SA-mediated enhancement of T3SA+ infection is only effective during the initial phases of virus-cell interaction, since sialyllactose does not inhibit productive binding of T3SA+ after the first 30 min of virus adsorption (7). In contrast, Fab fragments of an antibody directed to the σ1 head efficiently neutralize infection of either T3SA+ or T3SA-, even when added at late times during adsorption (7).

Results of binding studies using T3SA+ and T3SA- indicate that the interaction of reovirus with the cell surface is complex, with multiple cellular molecules engaging σ1 in an elegantly coordinated process that determines the outcome of the attachment event. These insights have led to the current model of reovirus attachment in which receptors are engaged by a multistep adhesion-strengthening process in which σ1 first binds to an abundant cell-surface carbohydrate with low affinity (7), which is followed by high-affinity interactions with JAM-A or other proteinaceous receptors that remain to be indentified(6, 8) .

Reovirus tropism and neuropathogenesis

Reoviruses exhibit a broad host range in nature, infecting many mammalian species, including humans (26). However, while reoviruses have the capacity to infect

humans, disease is restricted to the very young (69, 111). Reoviruses infect most children (110) and can cause mild respiratory or gastrointestinal illnesses (26). In addition, reoviruses serve as important models for studies of viral replication and pathogenesis and in particular for analysis of viral determinants of CNS injury.

Reoviruses enter animal hosts by both respiratory and enteric routes (119). Following peroral inoculation of newborn mice, reoviruses adhere selectively to surface projections on the luminal surface of M cells (119, 128-130) (Figure I-5). These epithelial cells overlie the Peyer's patches in the intestine. Ultrastructural studies of the fate of virus in the intestinal tract suggest that virions are endocytosed by M cells and subsequently transported across these cells within cytoplasmic vesicles (128). Upon reaching the submusocal zone beneath the M cells, viruses can either spread to intestinal tissue in close proximity by infecting the basal surface of intestinal epithelial cells (95, 96, 120) or disseminate to secondary sites in the host by neural, lymphoid, or hematogenous pathways.

T1 reovirus spreads to the CNS by hematogenous routes to infect ependymal cells, leading to non-lethal hydrocephalus (115, 121, 122). In contrast, T3 reovirus spreads primarily via axonal transmission to the CNS (73, 115), infects neurons, and causes lethal encephalitis (73, 115, 121, 122). Following intramuscular (IM) inoculation into the hind limb, T3D spreads to the spinal cord through the sciatic nerve (115). The σ1-encoding S1 gene dictates these serotype-specific disease patterns (115, 121, 122), most likely via selective recognition of cell-surface receptors by σ1.

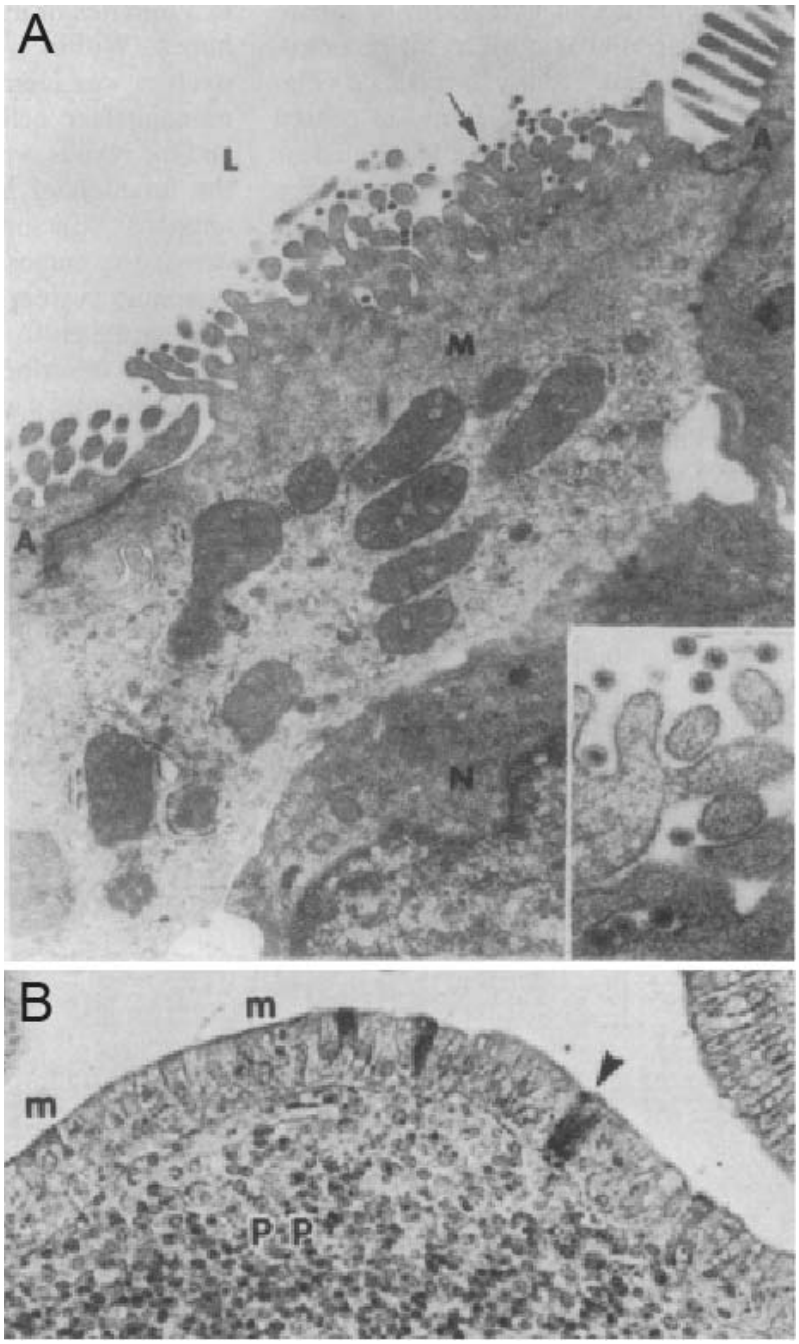

FIGURE I-5. Reovirus T1L binds and infects M cells that overlie Peyer's patches. (A) An electron micrograph demonstrating T1L virions (arrow) adhering to the luminal (L) surface of an M cell (M) in a closed ileal loop 30 minutes after virus inoculation. The M cell surrounds a mononuclear cell (N) and borders two absorptive (A) cells that lack adherent virus (x13,400). Inset: higher magnification of M cell surface with adherent virions (x38,800). (B) A photomicrograph of adult mouse intestine 48 h after inoculation with 5 x 109 PFU T1L demonstrates reovirus antigen-positive (arrowhead) M cells (m) overlying Peyer's patches (PP). Images adapted from Wolf et al (130) (A) and Rubin et al (95) (B).

Although the functions in disease pathogenesis of the two known reovirus receptors (JAM-A and SA) are not completely understood, careful *in vivo* studies have been performed that have enhanced an understanding of the roles played by these receptors in reovirus infection in the host. Studies using JAM-A-knockout mice indicate that JAM-A is dispensible for reovirus growth in the intestine following peroral inoculation but is required for efficient hematogenous spread from primary to secondary sites of replication (3). In addition, JAM-A is required for reovirus infection of vascular endothelial cells, which may provide a portal into the bloodstream. Studies comparing pathogenesis in newborn mice of reovirus strains that differ in glycan utilization (strains T3SA+ and T3SA-) revealed that SA-binding enhances spread from the intestine to peripheral sites of replication such as the liver, spleen, and brain (9). Furthermore, the capacity to bind SA confers reovirus tropism for bile duct epithelium (9). However, it is not known whether SA-binding influences reovirus dissemination, tropism, and replication within the CNS.

Significance of the research

Receptor utilization is an important determinant of many aspects of reovirus disease, including dissemination and tropism. Mechanisms underlying reovirus spread to and within the CNS are not well understood. Examination of carbohydrate coreceptor utilization by reovirus in the pathogenesis of neural injury will improve an understanding of how carbohydrates function as viral receptors and define mechanisms by which neurotropic viruses infect the host. Many clinically important neurotropic viruses produce neural injury similar to that caused by reovirus. Knowledge of pathologic mechanisms

gained from this research may establish general principles of viral neuropathogenesis, thereby improving our ability to develop antiviral therapeutics. Morever, an enhanced understanding of the molecular interactions that occur between σ1 and its cellular receptors will aid in the continued development of reovirus as an oncolytic agent and vaccine vector.

My work focused on elucidating the molecular basis of SA binding by T3 reovirus and defining the contribution of SA engagement to reovirus neuropathogenesis. Using structure-guided mutagenesis, I defined a discrete network of residues in T3 σ1, centered on Arg202, that are required for SA binding. Furthermore, data gathered from *in vivo* experiments comparing strains that differ in the capacity to bind SA suggest that SA-binding enhances reovirus neurovirulence by allowing more efficient infection of CNS tissues. These studies have enhanced an understanding of mechanisms of viral attachment to cell-surface glycans and CNS disease caused by neurotropic viruses.

CHAPTER II

CRYSTAL STRUCTURE OF REOVIRUS ATTACHMENT PROTEIN σ1 IN COMPLEX WITH SIALYLATED OLIGOSACCHARIDES

Introduction

Previous studies revealed that sequences in the T3D σ1 body domain bind to carbohydrates (21). Sequence analysis of reovirus variants identified three residues, Asn198, Arg202, and Pro204, which genetically segregate with the capacity of T3 σ1to interact with SA. These residues lie near the midpoint of the protein, at the lower end of the body domain, about 100 Å away from residues in the head that interact with JAM-A. Previous structural analyses of T3D σ1 (23, 57, 101) were based on constructs that did not include this putative carbohydrate-binding site. It is therefore unclear how σ1 achieves its specificity for SA, or whether σ1 undergoes rearrangements after engaging its carbohydrate receptor.

To enhance an understanding of mechanisms by which viral attachment proteins engage cell-surface glycans, we determined the crystal structure of T3D σ1 in complex with α-2,3-sialyllactose, α-2,6-sialyllactose, and α-2,8-disiallylactose. All three carbohydrates terminate in SA but feature different linkages that are present in various physiologic glycans. These studies shed light on the structural basis of σ1-SA interactions and define a new carbohydrate-binding structural motif in a viral attachment protein.

The research described in this chapter was performed in collaboration with the laboratory of Dr. Thilo Stehle (Universitat Tübingen). Dirk Reiter (Universitat Tübingen) purified, crystallized, and solved the structure of the C-terminal half of T3D σ1 alone and

in complex with α-2,3-sialyllactose, α-2,6-sialyllactose, and α-2,8-disiallylactose. Dirk also prepared the structural figures shown in this chapter. I assisted in construct design, helped to choose glycans to soak with σ1, and contributed to data interpretation. Based on information gathered from the crystal structures, I performed functional studies to determine what residues in T3 σ1 are important for mediating binding to SA. Results from these experiments are presented in Chapter III.

Results

Construct Design and Structure Determination - The σ1 protein belongs to a class of fiber proteins constructed from triple β-spirals, a motif that was first identified in the adenovirus fiber (117). In a previous study, we crystallized a smaller region of σ1, spanning residues 246 to 455 and containing three β-spiral repeats as well as the globular head domain (23). While this structure provided no insights into the carbohydrate-binding region of σ1, it served as a basis to predict that β-spiral repeats form the entire body domain of the protein (residues 167-309) (23). Near residue 170, the body domain transitions into a long α-helical coiled-coil region that forms the N-terminal tail domain (residues 1-156).

To determine the structure of a longer fragment of σ1 including the predicted sialic-acid binding residues 198, 202, and 204, we designed a construct for the expression of residues 170-455. This construct excluded the long α-helical coiled-coil region to simplify protein expression, purification, and crystallization. Prototype strain T3D σ1 is sensitive to trypsin-mediated cleavage after Arg245 (20). However, a sequence

polymorphism occurring in the majority of T3 field-isolate strains, Thr249Ile, renders the protein resistant to trypsin (20). A construct containing Ile249 was therefore used in our study. Trimerization was promoted by using a hexahistidine-tagged trimerization domain, a modified GCN4 sequence (47), at the N-terminus of the expressed protein. This domain was proteolytically removed before final purification and crystallization.

Overall Structure of σ1 - The structure of σ1 residues 170 to 455 reveals a highly elongated, symmetric trimer that measures about 200 Å in length (Table II-1 and Figure II-1A and II-1B). Tail residues N-terminal to amino acid 170, which were not included in the crystallized protein, are predicted to form an α-helical coiled-coil structure that adds another 200 Å in length to the protein (Figure II-1C). As expected, the structure of the globular head domain (residues 310 to 455) is essentially identical to that described previously (23). However, the body domain displays a number of unusual features. Although sequence-based predictions suggested that this region would be composed of eight consecutive triple β-spiral repeats (23), we find that the body domain contains a mixture of α-helical coiled-coil and β-spiral repeats (Figure II-1). Four β-spiral repeats at the N-terminus (β1-β4, residues 170 to 235) are followed by a short α-helical coiled-coil (cc, residues 236 to 251) and three additional β-spiral repeats (β5-β7, residues 252 to 309) (Figure II-2). Inspection of the sequence indicates a likely reason for the deviation from the β-spiral fold at the center of the body (Figure II-2B). Three hydrophilic residues (Thr236, Ser244, and Ser252) are located at positions that are typically occupied by hydrophobic side chains in β-spirals. Moreover, Ser241 replaces a characteristic proline or glycine at the turn in a β-spiral repeat. While some deviations from the β-spiral

consensus sequence can be tolerated, even residues replacing the glycine or proline (e.g., residues Gln224 or Thr278), the cumulative effect of the four non-consensus residues results in a β-spiral no longer being the optimal fold. The α-helical coiled-coil structure contains two heptad-repeat sequences, starting with Phe239 and ending with Gln251 (Figure II-2A and II-2C).

Table II-1. Data collection and refinement statistics for σ1-oligosaccharide structures.

σ1 in complex with	α-2,3-sl	α-2,6-sl	α-2,8-di-sl
Space group	$P2_12_12$	$P2_12_12$	$P2_12_12$
Unit cell dimensions (Å)	a = 87.15 b = 333.18 c = 58.49	a = 87.61 b = 333.06 c = 58.29	a = 87.19 b = 331.84 c = 58.13
Unit cell angles (°)	α = β = γ = 90	α = β = γ = 90	α = β = γ = 90
Resolution range (Å)	38.6-2.25	48.05-2.79	48.06-2.28
Completeness (%)	95.37	98.65	96.03
Total reflections	369038	547842	277926
Unique reflections	78324	43203	75913
R_{merge} (%)[#]	10.8	6.2	9.6
I/ σI	13.5	18.6	18.6
R_{work} (%)*	15.77	15.69	17.31
R_{free} (%)*	19.89	20.48	22.03
r.m.s.d. bond lengths (Å)	0.006	0.007	0.006
r.m.s.d. bond angles (°)	0.960	1.12	1.01

r.m.s.d., root-mean-square deviation. sl, sialyllactose.
* $R_{work} = R_{free} = \Sigma| |F_{obs}(hkl)| - |F_{calc}(hkl)| | / \Sigma |F_{obs}(hkl)|$. R_{free} was calculated with 5% of the data.
[#] $R_{merge} = \Sigma | I - \langle I \rangle | / \Sigma I$

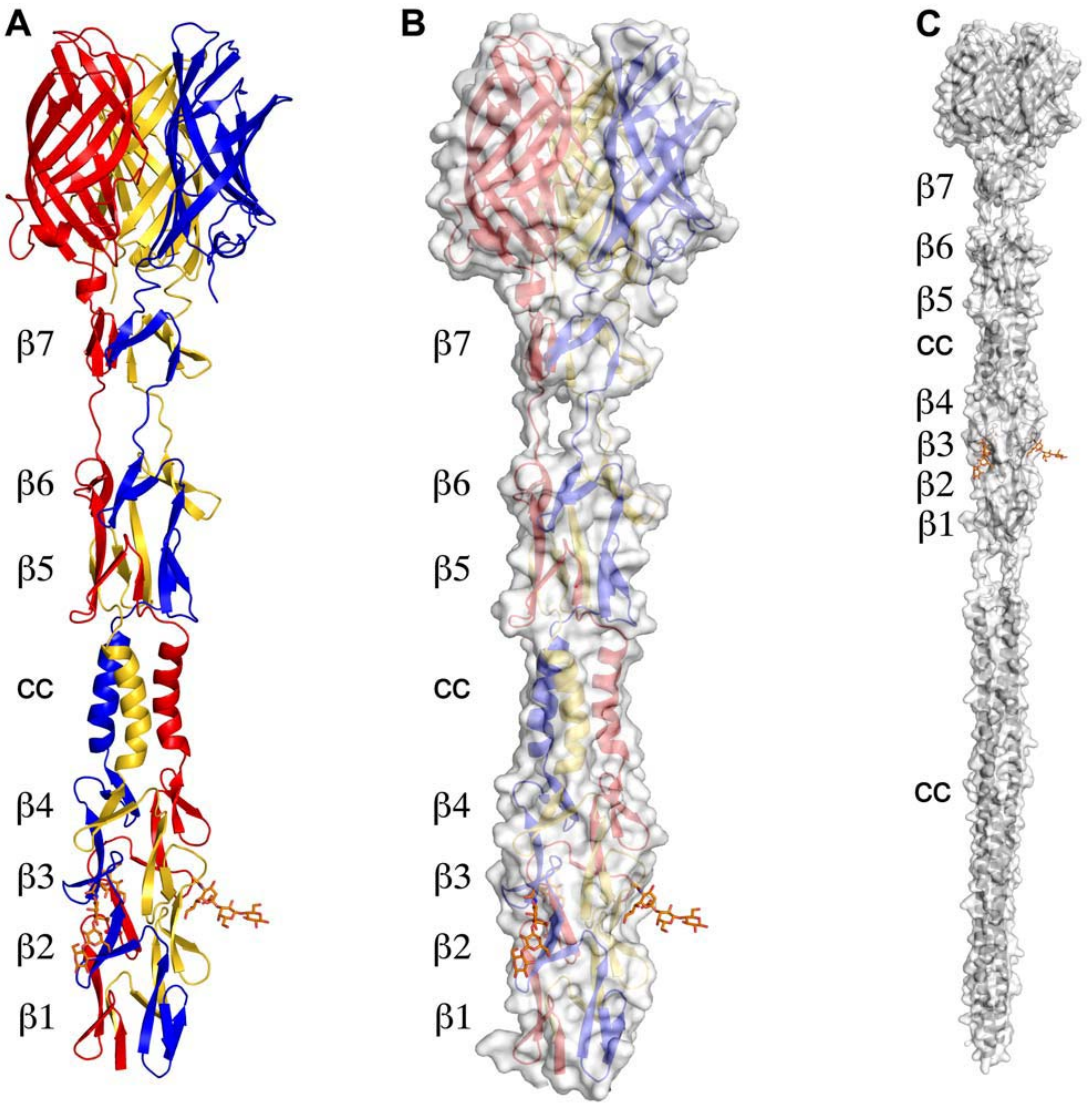

FIGURE II-1. Structure of T3D σ1. (A) Ribbon drawing of the T3D σ1 body and head domains in complex with α-2,3-sialyllactose. The σ1 monomers are shown in red, blue, and yellow. The body domain consists of seven triple β-spiral repeats (β1- β7) and an α-helical coiled-coil domain (cc) that is inserted between β-spiral repeats β4 and β5. The bound α-2,3-sialyllactose is shown in stick representation and colored in orange. (B) Molecular surface of the σ1 structure, shown in semitransparent white coloring. (C) Model of full-length σ1, including a computer-generated trimeric α-helical coiled coil structure spanning σ1 residues 1-160 at the N-terminus (91).

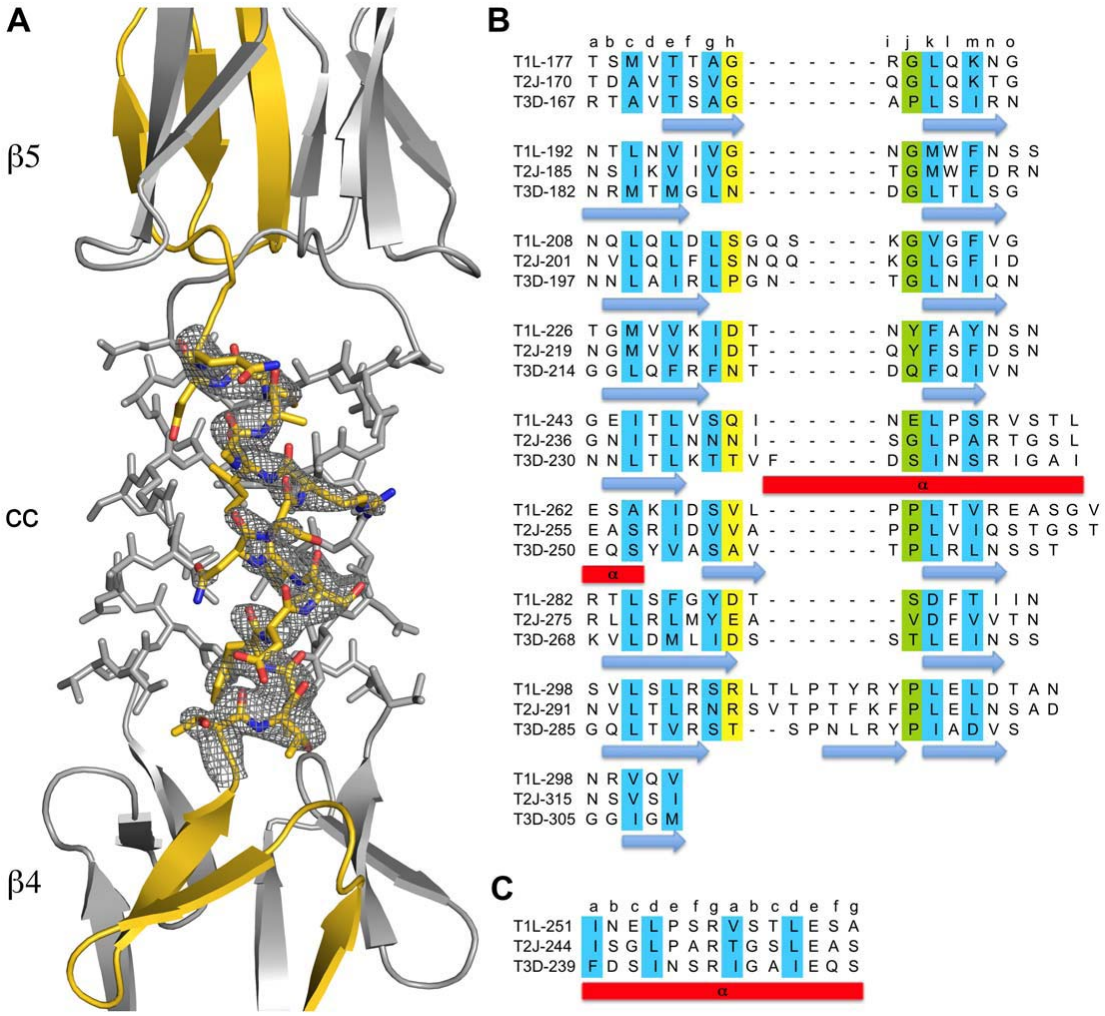

FIGURE II-2. Structural features of the T3D σ1 body domain and sequence alignments with T1L and T2J σ1. (A) Close-up view of the α-helical coiled-coil that separates β-spirals 4 and 5 in the T3D σ1 body domain. The coiled-coil region is shown as a stick model, while the adjacent β-spiral repeats are depicted as a ribbon drawing. A simulated annealing omit difference map for one chain is shown with a radius of 2.2 Å and a contour level of 3σ. (B) The residues are aligned according to the triple β-spiral consensus sequence (a-o), with typically hydrophobic residues (c, e, g, k, and m) indicated in cyan and the position in the β-turn usually occupied by proline or glycine (j) in green. (C) Sequence analysis of the coiled-coil region in the body domain. Residues 239-252 are organized in heptads (a-g), and the coiled-coil consensus is indicated with typically hydrophobic residues (a and d) highlighted in cyan (91).

Structure of σ1 in Complex with α-2,3-Sialyllactose - To elucidate the structural basis of the interaction of the reovirus attachment protein σ1 with its carbohydrate coreceptor, we prepared a complex by soaking crystals of σ1 with 10 mM α-2,3-sialyllactose, a compound that terminates in α-linked SA. The subsequent structure, determined at 2.25 Å resolution (Table II-1), unambiguously demonstrated the location of the carbohydrate in an unbiased difference electron-density map (Figure II-3A). The oligosaccharide binds in a shallow groove next to the loop connecting the second and third β-spiral repeats. The σ1 protein contains three identical binding sites, one on each chain, and all three are occupied by α-2,3-sialyllactose molecules, with the SA making identical and extensive contacts in each chain (Figure II-3B and II-3C). The lactose moieties face different directions, probably as a result of internal flexibility and participation in crystal contacts (Figure II-3C).

SA contains four characteristic functional groups: a carboxylate at C1, a hydroxyl group at C4, an N-acetyl group at C5, and a glycerol chain at C6. All four groups are recognized by σ1 (Figure II-3B). Arg202 forms a bidentate salt bridge with the carboxyl group. A single hydrogen bond links the hydroxyl group at C4 to the carbonyl of Gly205. The amide of the N-acetyl group is engaged in a hydrogen bond with the backbone carbonyl of Leu203, and the N-acetyl methyl group is facing into a partially hydrophobic cavity. The glycerol chain lies parallel to the peptide backbone, forming direct hydrogen bonds with the backbone carbonyl of Ile201 and the amide nitrogen of Leu203. In some of the binding sites, the glycerol chain forms water-mediated hydrogen bonds with the Asn210 side chain and the amide nitrogen of Ile211. We note that Arg202, which was previously shown to influence SA binding (22), provides a key contact to the ligand.

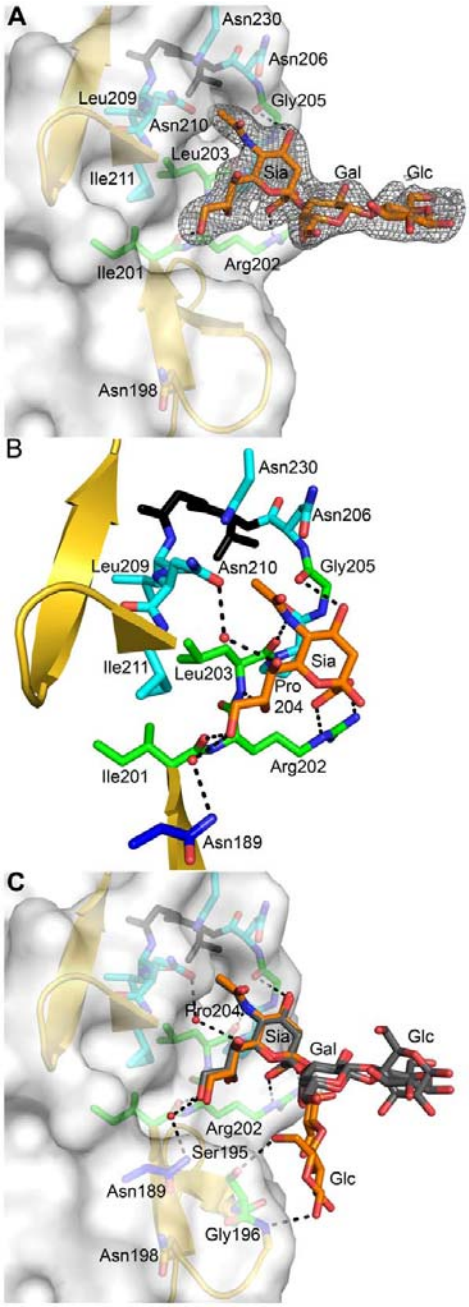

FIGURE II-3. Interactions between σ1 and SA. (A) Simulated annealing omit difference density map contoured at 3σ and displayed with a radius of 2.2 Å around the bound α-2,3-sialyllactose. The sugar moieties are labeled Sia (sialic acid), Gal (galactose), and Glc (glucose) here and in subsequent figures. (B) Detailed interactions between σ1 and the terminal sialic acid of α-2,3-sialyllactose. Residues in the binding region are drawn in ball and stick representation, while the rest of the protein is shown as a ribbon drawing. The σ1 residues forming hydrogen bonds or salt bridges with the ligand are shown in green, and residues forming van der Waals contacts are shown in cyan. The side chain of Asn189 (colored dark blue) is contributed by a neighboring σ1 monomer (see also Figure 1A). Sialic acid is shown in ball-and-stick representation, with carbons colored orange, oxygens colored red, and nitrogens colored blue. Bridging waters are shown as orange spheres. Hydrogen bonds and salt bridges are represented with broken lines. (C) Superposition of all three bound ligands into a single binding site. The superposition was performed using σ1 residues only. While the orientation of the terminal sialic acid is nearly identical, the lactose moieties are facing in different orientations as a result of their participation in different crystal contacts (91).

Moreover, Pro204, which also had been implicated in SA binding (22), is part of a structure that shapes the ligand-binding site.

Structures of σ1 in Complex with α-2,6-Sialyllactose and α-2,8-Disialyllactose - As contacts in the complex of σ1 with α-2,3-sialyllactose exclusively involve the SA moiety, we hypothesized that σ1 should be capable of binding SA in different naturally occurring linkages, including α-2,6- and α-2,8-linked SA. We therefore determined crystal structures of σ1 in complex with α-2,6-sialyllactose (Figure II-4A) and α-2,8-disialyllactose (Figure II-4B). Refinement statistics for both structures are provided in Table II-1. In each case, only two of the binding sites are occupied, as the third is partially blocked by crystal contacts. For the α-2,6-sialyllactose complex, the electron density allowed us to unambiguously identify all three sugar residues (Figure II-4A). The electron density for the α-2,8-disialyllactose complex did not allow us to model the terminal glucose. Comparison of these structures with each other and with the α-2,3-sialyllactose complex shows that the terminal SA is bound in the same conformation and with identical contacts in all three cases. However, the remaining moieties of the glycans differ in conformation and contacts with σ1. The α-2,3-sialyllactose and α-2,8-disialyllactose ligands assume an elongated shape in which the lactose groups face away from the protein (Figure II-3C and Figure II-4B). Inspection of the α-2,8-disialyllactose complex shows that the N-acetyl group of the second SA forms a hydrogen bond to the side chain of Ser195. In contrast, σ1 binds α-2,6-sialyllactose in a folded-back conformation (Figure II-4A). This conformation is stabilized by an intramolecular hydrogen bond and the galactose O2 and O3 hydroxyl groups, which form hydrogen

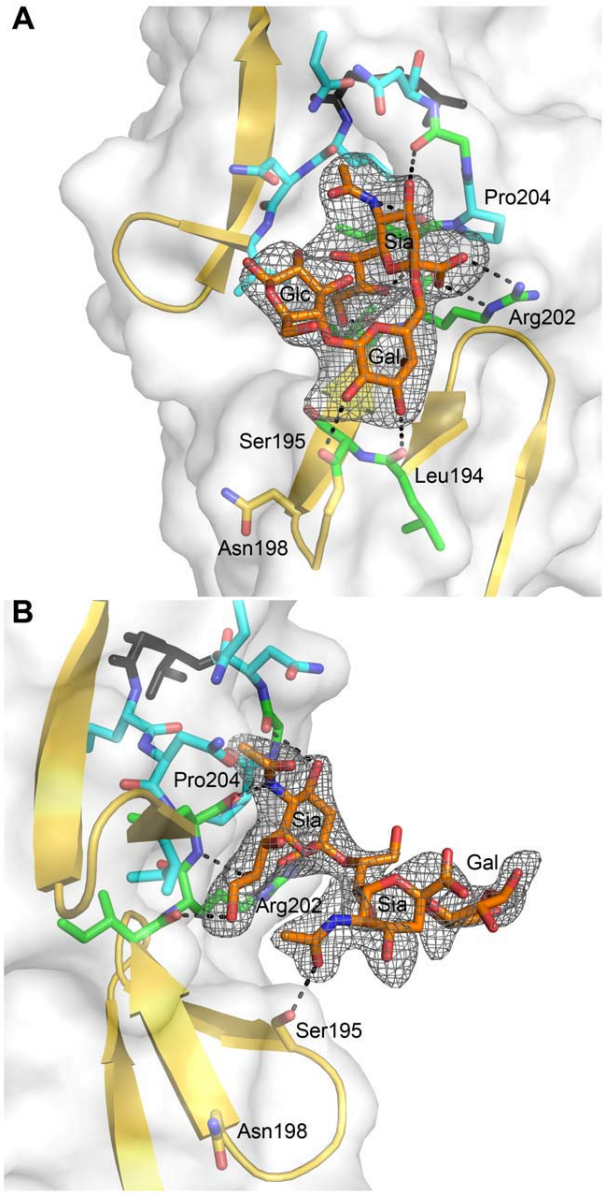

FIGURE II-4. The σ1 protein in complex with SA in different linkages. (A) View into the carbohydrate-binding site of the complex of σ1 with α-2,6-sialyllactose. (B) View into the carbohydrate-binding site of the complex of σ1 with α-2,8-disialyllactose. The orientation in panel (A) differs by 60 degrees along a vertical axis from the orientations shown in panel (B) and Figure 3 to provide a clearer view into of the binding site. In both panels, σ1 residues directly contacting the ligand are shown in green, and surrounding residues making van der Waals contacts are shown in cyan. The ligands are shown in ball-and-stick representation, with carbons colored orange, oxygens colored red, and nitrogens colored blue. Hydrogen bonds are represented with broken black lines. The maps are simulated annealing omit difference density maps contoured at 3σ and displayed with a radius of 2.2 Å around the ligands (91).

bonds to the backbone carbonyl atoms of Ser195 and Leu194, respectively. Collectively, these results confirm that the sialic-acid-binding site of T3D σ1 is in the body domain of the attachment protein as suggested by genetic and functional evidence from previous studies (22, 27). Furthermore, while T3D σ1 exhibits a broad SA binding capacity, the contacts made between σ1 and the SA moieties of the oligosaccharides are highly conserved.

Discussion

The σ1 protein uses a complex network of contacts to engage terminal SA, which is a common feature of all three glycans used in this study. The interactions involve σ1 residues at the lower end of the body domain, between β-spirals 2 and 3. At this location, the SA moiety docks into a shallow pocket that is formed mainly by residues in the third β-spiral. All four functional groups of SA make contacts with σ1 through an elaborate network of hydrogen bonds and van der Waals interactions. Although all three ligands used for complex formation with σ1 contain additional carbohydrates, these moieties make very few interactions. The complex with α-2,8-disialyllactose identified a hydrogen bond between the N-acetyl group of the second SA and the side chain of Ser195 (Figure II-4B). However, the results from mutagenesis experiments, presented in Chapter III, demonstrate that a Ser195Ala mutation has no effect on either HA capacity or viral growth. Therefore, the observed contact is unlikely to have physiologic relevance. The interactions between σ1 and α-2,6-sialyllactose identified two hydrogen bonds that link the galactose to the protein and may help to stabilize the folded-back conformation of the ligand (Figure II-4A). As both contacts involve main chain atoms of σ1, their functional

significance cannot be easily probed by site-directed mutagenesis. Nevertheless, it is likely that the observed contacts lead to a modest increase in the affinity of σ1 for compounds terminating in α-2,6-linked SA. It is unclear if such an increase in affinity is biologically significant.

A large collection of structures of viruses or viral attachment proteins in complex with sialylated oligosaccharide receptors is available (14, 17, 32, 36, 41, 78, 79, 104-106, 123, 132, 133), and these have produced significant insights into mechanisms of SA binding, receptor specificity, and viral pathogenesis. However, the interactions observed between T3D σ1 and SA differ in important ways from those found in all other virus-receptor complexes, offering new insights into the parameters that guide viral attachment and specificity. In all cases in which structures are available, the receptors are bound by a globular domain in a region that projects farthest from the viral capsid and is easily accessible for interactions with the cell surface. In contrast, the highly elongated T3D σ1 protein engages its carbohydrate ligand at its midpoint, about 150 Å away from the region that projects farthest from the virion. Although the σ1 protein possesses some flexibility at defined regions (23, 39), the location of the SA-binding site would not appear optimal for engagement of membrane-bound receptors that feature sialylated ligands close to the membrane. The region of JAM-A that is engaged by the σ1 head domain is fairly close to the membrane (57). Even when allowing for considerable flexibility between the σ1 head and body, it is difficult to envision a conformation in which the tail of σ1 is still inserted into the virus and the SA binding site can closely approach the membrane. However, σ1 could more easily engage SA that projects far

above the membrane, perhaps by being located on a large protein or projecting from prominent loops.

Prior to this study, structural information had been available only for the C-terminal portion of the σ1 protein (23). Based on analysis of that structure, as well as sequence comparisons with the related adenovirus fiber protein, full-length σ1 was predicted to fold into three distinct regions: an N-terminal α-helical coiled coil (termed the tail), a region containing eight consecutive β-spiral repeats (the body), and a globular β-barrel (the head). Our structural analysis of a fragment comprising the body and head domains show that this model must be revised, as we find an insertion of a short α-helical coiled coil that interrupts the β-spiral sequence in the body, replacing one β-spiral repeat with a helical structure. Thus, it is clear that the structure of σ1 features several transitions between α-helical and β-spiral regions. This topological relationship differs from that of the adenovirus fiber, in which the shaft domain is thought to consist entirely of β-spiral repeats (88). Examination of the T3D body domain sequence shows that it contains a nearly perfect heptad repeat pattern, which is typical for α-helical coiled coils, in a short stretch of 14 residues (Figure II-2). A similar pattern is observed in the T1L and T2J σ1 sequences, but a proline residue within the consensus makes it unlikely that these proteins also feature a continous α-helical coiled coil at the equivalent location.

To our knowledge, the structures presented here are the first examples of any fibrous viral protein engaging a ligand via its repetitive fiber region. Other viral attachment proteins contain fibrous- or stalk-like structures, but they usually engage receptors with globular head domains placed on top of these structural elements, as observed in complexes of adenovirus fiber proteins with their receptors (85). Globular

head domains offer higher variability in engaging ligands and can more easily create recessed binding pockets suitable for high-affinity binding. Instead, fiber-like structures generally feature short connections between their repeating units and a relatively flat surface, limiting binding options. However, inspection of the β-spirals in σ1 reveals subtle modifications in a single repeat that allow it to create a shallow binding site for SA. One of the hallmarks of β-spirals is a highly conserved β-turn between two strands, involving residues at positions g, h, i, and j (Figure II-2). The residue at position j is usually a proline or glycine. This turn is enlarged by two amino acids in the σ1 repeat that engages SA, transforming the turn into a small loop (Figure II-5).

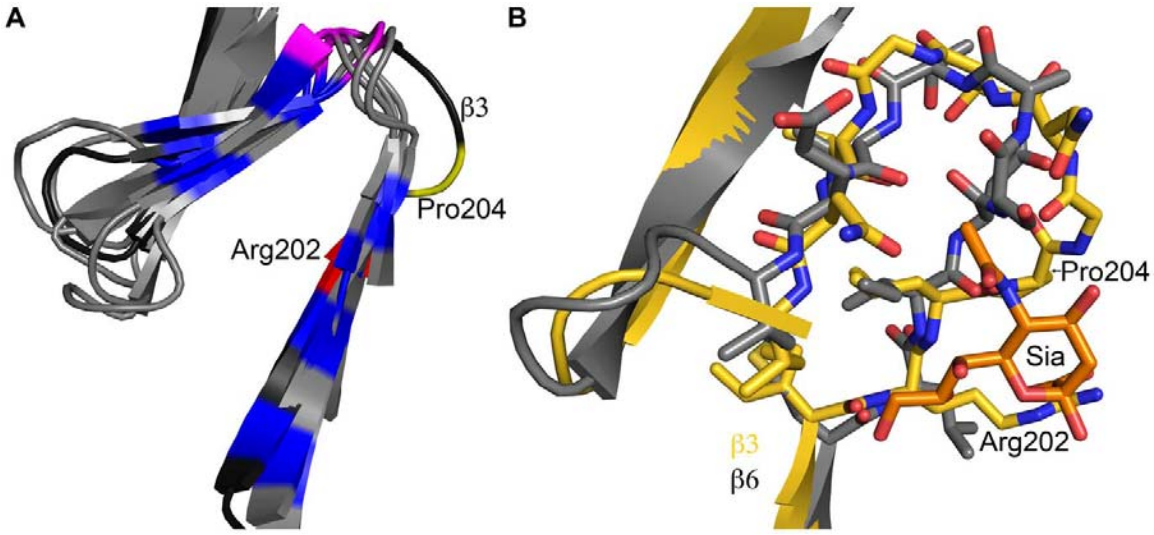

FIGURE II-5. Structural adaption of the binding site. (A) Superposition of all seven β-spiral repeats. Repeat β3, which is shown in darker shading, interacts with sialic acid and deviates markedly in its structure from the other repeats. Conserved hydrophobic residues are colored in blue, the position in the β-turn that is usually occupied by proline or glycine is shown in magenta. Arg202 and Pro204, which are part of repeat β3, are highlighted in red and yellow, respectively. (B) Superposition of a prototypical β-spiral repeat (β6) onto the sialic acid binding repeat β3. Amino acids are shown in ball and stick representation, and residues Arg202 and Pro204 in β3 are labeled. Panel B is enlarged to provide a clearer view (91).

Interestingly, Pro204 introduces a kink after a β-strand, causing the chain to deviate from the β-spiral motif at this position to provide a pocket for the ligand. Thus, alteration of the typical repeating motif identifies a ligand-binding site in the case of σ1. It is conceivable that similar aberrations in other fibrous protein sequences also might indicate binding sites. The location of a SA binding site in an elongated fiber-like structure also raises the possibility of creating a small SA binding cassette that could be transferred into a variety of trimeric fiber-like proteins constructed from α-helical coiled coils or β-spirals. Our work thus enhances an understanding of reovirus-glycan interactions and may also guide the construction of new SA binding platforms to facilitate structure-function analyses and SA-mediated cell targeting.

CHAPTER III

SIALIC ACID BINDING DETERMINANTS IN THE σ1 ATTACHMENT PROTEIN OF SEROTYPE 3 REOVIRUS

Introduction

Residues Asn198, Arg202, and Pro204 of T3D σ1 have been implicated in SA binding by sequence comparisons of reovirus strains that differ in SA coreceptor utilization (27, 98) and genetic analysis of reovirus mutants adapted to growth in MEL cells (22). To determine whether these sequences influence SA binding by T3 reovirus in an otherwise isogenic background, I used structure-guided mutagenesis to identify residues in σ1 that functionally engage SA.

In this study, I generated a panel of T3D mutant viruses containing point mutations in the σ1 protein. I tested the capacity of these viruses to bind to SA by assessing the hemagglutination capacity of each virus. In complementary experiments, I tested the capacity of these viruses to replicate in MEL cells, which require SA-binding for productive infection. The results reveal that residues 198, 202, 203, 204, and 205 are required for functional binding to SA by reovirus.

My findings, along with the structural studies presented in Chapter II, identify a discrete SA-binding domain in σ1 and a network of residues that are required for mediating σ1-SA interactions. I acknowledge the contributions of Takeshi Kobayashi (Osaka University) and Elizabeth Halvorson (Wake Forest University) for generating virus strains rsT3D-σ1N198D, rsT3D-σ1R202W, and rsT3D-σ1P204L.

Results

Residues in Reovirus σ1 Required for Sialic Acid Binding - To identify sequences that influence SA binding, I used plasmid-based reverse genetics (58, 59) to introduce point mutations into the σ1 protein of reovirus strain T3D. Mutant viruses were isolated following co-transfection of murine L929 cells with RNA-encoding plasmids corresponding to the T3D *L1-L3*, *M1-M3*, and *S2-S4* genes and a plasmid corresponding to the σ1-encoding *S1* gene incorporating site-specific mutations. Thus, each recombinant virus is isogenic, with the exception of the *S1* gene and its protein product, σ1. Guided by the structure of the σ1-SA complexes shown in Chapter II, I engineered individual alanine substitutions of amino acids ranging from Asn189 to Asn210. By their location in the structure, we hypothesized that these residues would be required for functional SA binding. In addition, substitutions N198D, R202W, and P204L, which have been implicated in SA binding by sequence comparisons of reovirus strains that differ in SA utilization (27, 98) and genetic analysis of reovirus mutants adapted to growth in MEL cells (22), were engineered to define the effect of these polymorphisms in an otherwise isogenic background.

After confirming the σ1-encoding S1 gene nucleotide sequences, the mutant viruses were tested for HA capacity (Figure III-1) and growth in L929 cells and MEL cells (Figure III-2). In comparison to rsT3D, rsT3D-σ1N198D, rsT3D-σ1R202A, rsT3D-σ1R202W, rsT3D-σ1L203A, rsT3D-σ1P204A, rsT3D-σ1P204L, and rsT3D-σ1G205A produced little or no agglutination of calf erythrocytes, a sensitive assay for SA binding (27). However, rsT3D-σ1N189A, rsT3D-σ1S195A, and rsT3D-σ1N210A produced HA titers that were comparable to those of wild-type rsT3D. Each of the point-mutant viruses

produced approximately 1000-fold yields of viral progeny after growth in L929 cells (Figure III-2A), a cell line that does not require sialic-acid-binding for reovirus to replicate (98). In contrast, those containing mutations N198D, R202A, R202W, L203A, P204A, P204L, and G205A displayed attenuated growth in MEL cells (Figure III-2B), a cell line permissive only to SA binding reovirus strains (98). These findings indicate that viruses with mutations of residues 198, 202, 203, 204, and 205 are altered in SA binding efficiency, suggesting that these residues serve a functional role in T3D σ1-SA interactions.

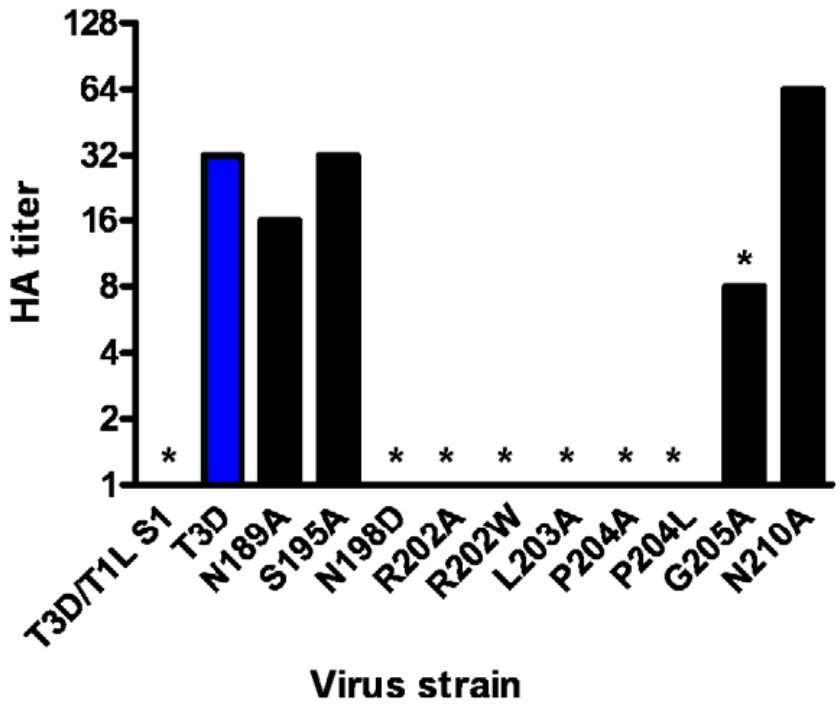

FIGURE III-1. HA assay of T3D σ1 point mutants. Purified reovirus virions (10^{11} particles) were serially diluted in 0.05 ml of PBS in 96-well U-bottom microtiter plates. Bovine erythrocytes were washed twice with PBS and resuspended at a concentration of 1% (vol/vol) in PBS. Erythrocytes (0.05 ml) were added to wells containing virus and incubated at 4°C for at least 2 h. HA titer is expressed as 10^{11} particles divided by the number of particles/HA unit. One HA unit equals the number of particles sufficient to produce HA. *, $P < 0.05$ in comparison to T3D by Student's *t* test (91).

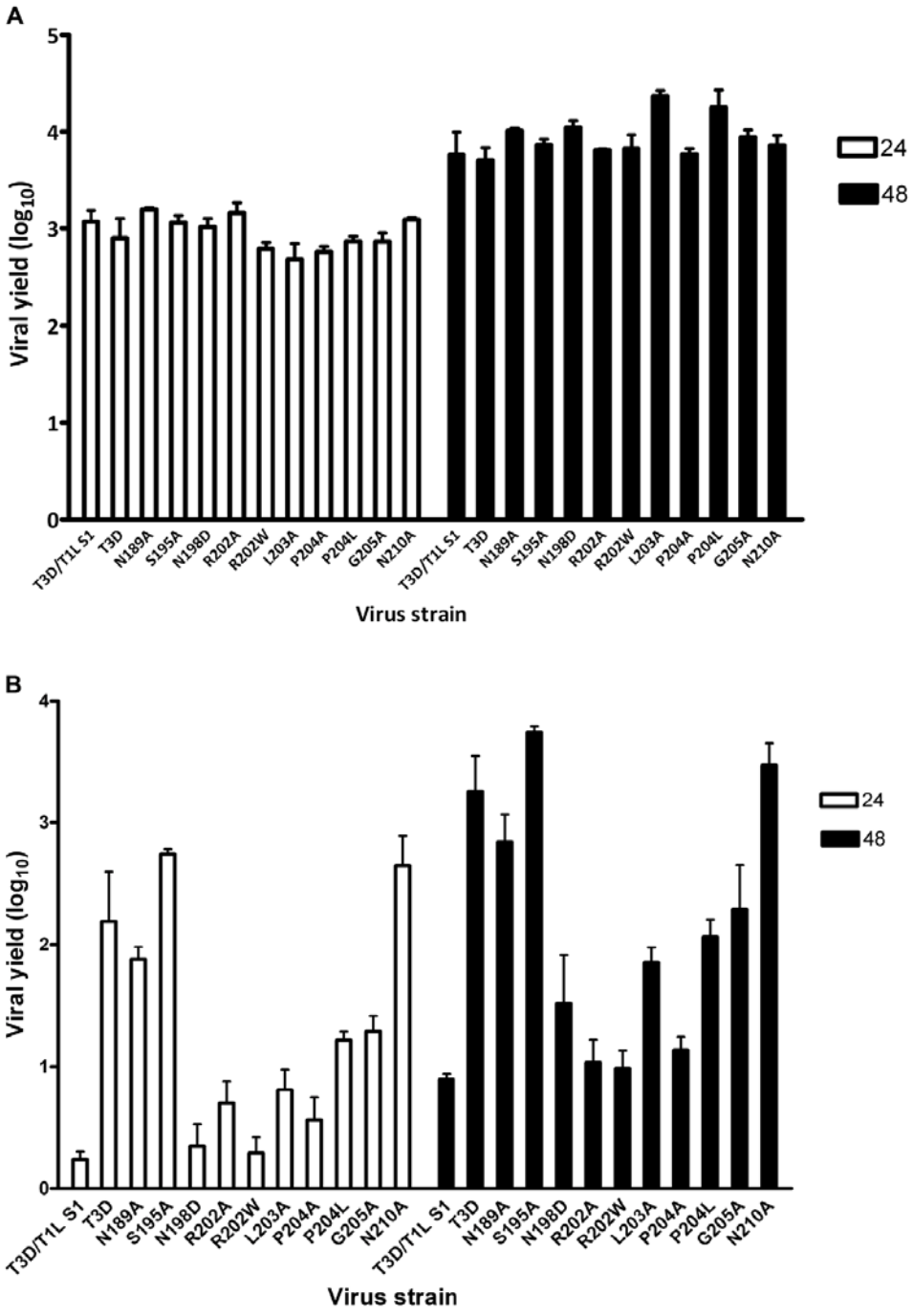

FIGURE III-2. Identification of σ1 residues required for binding to cell-surface SA. (A) Infection of murine fibroblast (L929) cells or (B) murine erythroleukemia (MEL) cells by wild-type or point-mutant viruses. Cells were adsorbed with virus at an MOI of 1 PFU/cell. Following incubation at room temperature for 1 h, the inoculum was removed, and cells were incubated at 37°C for 24 and 48 h. Viral titers were determined by plaque assay. The results are expressed as viral yields (log_{10} titer at t = 24 or 48 h minus log_{10} titer at t = 0 h) for triplicate samples. Error bars indicate S.D. *, $P < 0.05$ in comparison to T3D by Student's t test (91).

Discussion

Naturally occurring sequence variability at three amino acid positions (residues 198, 202, and 204) has been linked to the SA-binding capacity of T3 σ1 (22, 28). Our structures, presented in Chapter II, readily identify two of these residues, Arg202 and Pro204, as key determinants of SA binding. The side chain of Arg202 forms a salt bridge with the SA carboxylate group, while the Pro204 side chain stacks against the Arg202 guanidinium group. Moreover, the carbonyl oxygen in the peptide bond linking Leu203 and Pro204 forms a hydrogen bond with SA. Substitutions of either Arg202 or Pro204, as seen in the R202W and P204L variants, would be predicted to decrease the affinity for SA, which is confirmed by the mutagenesis data. In contrast, the critical role of residue 198 in ligand recognition is not apparent from the crystal structures. Mutagenesis data (Figure III- and Figure III-), in conjunction with previous results (22), clearly demonstrate that Asn198 is required for successful SA-dependent infection, with viruses carrying an N198D mutation having substantially reduced infectivity in MEL cells. However, the crystal structures show that Asn198 is not involved in direct or water-mediated contacts with any of the three oligosaccharides. Furthermore, the Asn198 side chain is solvent-exposed, forming a single hydrogen bond with the Asn189 side chain. However, mutation of Asn189 to alanine does not affect SA binding (Figure III- and Figure III-), suggesting that the observed Asn198-Asn189 hydrogen bond is not relevant for ligand recognition. It is possible that the introduction of a negatively charged side chain at position 198, as is the case with the N198D mutation, leads to long-range electrostatic effects or structural rearrangements that indirectly affect receptor binding. However, given the distance of Asn198 from the binding site and its surface-exposed

location, this possibility appears remote. It is more likely that Asn198 serves as a contact point with a part of the functionally relevant glycan, which has not been included in the structural analysis. Although my results define the interactions of σ1 with terminal SA, the actual receptor may be a more complex sialylated glycan, perhaps carrying several branches. Such complex receptor structures, which can be attached to proteins or lipids, are true ligands for several adenoviruses and polyomaviruses (78, 79, 82). Therefore, Asn198 may well define a second receptor contact point for reovirus σ1.

Taken together, results from this study identify reovirus SA binding determinants in T3 σ1. This work enhances an understanding of the molecular basis of T3 σ1-SA interactions and establishes a foundation for future studies aimed at identifying the physiologically relevant sialylated glycans bound by reovirus *in vivo*.

CHAPTER IV

UTILIZATION OF SIALYLATED GLYCANS AS CORECEPTORS ENHANCES THE NEUROVIRULENCE OF SEROTYPE 3 REOVIRUS

Introduction

While all reovirus serotypes engage JAM-A (18, 86), they differ in carbohydrate coreceptor utilization, suggesting that carbohydrate binding by σ1 influences reovirus pathology in the CNS. Studies comparing the pathogenesis in newborn mice of reovirus strains that differ in glycan utilization revealed that SA-binding enhances spread from the intestine to peripheral sites of replication such as the liver, spleen, and brain (9). In addition, the capacity to bind SA confers reovirus tropism for bile duct epithelium (9). However, it is not known whether SA-binding influences reovirus dissemination, tropism, and replication within the CNS.

In this study, we sought to define the function of carbohydrate binding in reovirus neuropathogenesis. I monitored survival of newborn mice inoculated with wild-type T3D and T3D-σ1R202W, a T3D point-mutant virus that does not bind SA (91), and quantified viral loads in various organs of infected animals. I found that the wild-type virus was more virulent and produced higher titers in neural tissues than the mutant virus following intramuscular (IM) or intracranial (IC) inoculation. Furthermore, I found that the wild-type virus displayed an increased capacity to infect and replicate in primary cultures of cortical neurons in an SA-dependant manner. Collectively, these results suggest that binding to SA enhances the kinetics of reovirus replication in neural tissues and point to a functional role for sialylated glycan engagement in reovirus neurovirulence.

The research described in this chapter was performed in collaboration with other investigators. I performed the animal experiments and infectivity studies, and collected organs for histopathological analysis. Dr. Ty Abel (Department of Pathology, Microbiology, and Immunology at the Vanderbilt University School of Medicine) guided the histologic analyses of brain sections and captured representative images. Drs. Jennifer Konopka and Andrea Pruissjers (Department of Pediatrics at the Vanderbilt University School of Medicine) assisted in the extraction and culture of mouse cortical neurons. Dirk Reiter in the Thilo Stehle laboratory (Universitat Tübingen) prepared the structural figures shown in this chapter.

Results

SA binding enhances reovirus neurovirulence and spinal cord injury- To determine whether SA binding influences reovirus neuropathogenesis, we monitored survival and clinical signs of disease in two-day-old mice following IM inoculation with 5×10^6 PFU of either T3D or T3D-σ1R202W (Figure IV-1A). Reovirus strain T3D-σ1R202W contains a point mutation in σ1 that ablates SA-binding capacity (91). Mice were observed for 21 days after inoculation and euthanized when moribund. Significantly fewer mice infected with T3D survived in comparison to those infected with T3D-σ1R202W. The survival frequency of mice infected with T3D was 25.9% compared with 63.6% for mice infected with T3D-σ1R202W ($P < 0.005$). These results suggest that SA binding enhances reovirus virulence.

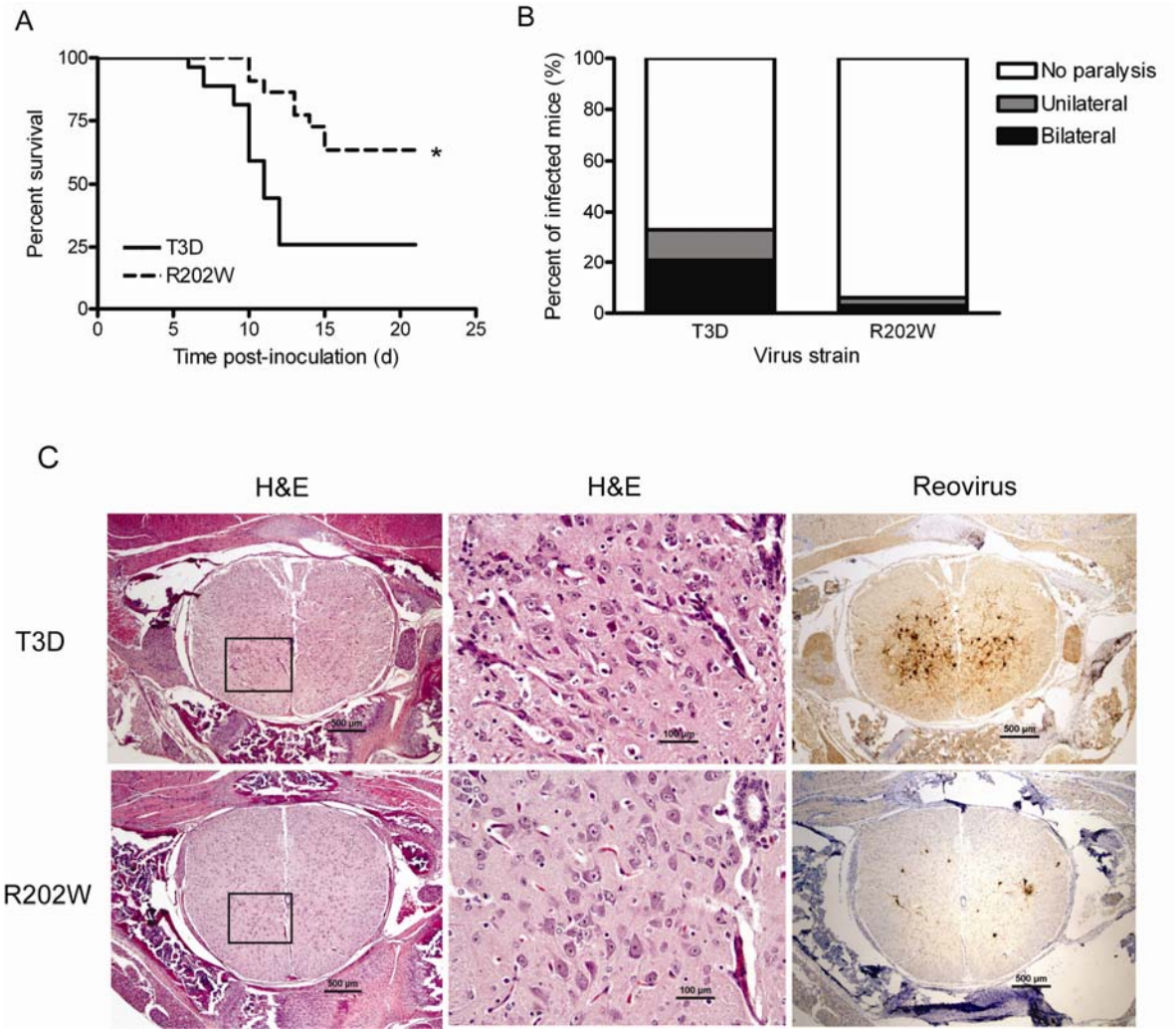

FIGURE IV-1. SA-binding capacity enhances reovirus virulence and paralysis following IM inoculation. Newborn C57/BL6 mice were inoculated in the right hindlimb with 5×10^6 PFU of either T3D or T3D-σ1R202W (R202W). (A) Mice (n = 22-27 for each virus strain) were monitored for survival for 21 days. *, $P < 0.005$ as determined by log-rank test in comparison to T3D. (B) Mice were monitored for development of reovirus-induced AFP on day 8 post-inoculation (n = 32-44 for each virus strain). Complete paralysis was first observed at this time point; survival frequencies of wild-type and mutant-infected mice at this time point were comparable. (C) On day 8 post-inoculation, spinal cords of infected mice were resected. Consecutive lumbosacral sections of the inferior spinal cord were stained with hematoxylin and eosin (H&E) or polyclonal reovirus antiserum (Reovirus). Representative sections of spinal cord matched for lumbar depth are shown. Scale bars, 5.0 mm. Boxes indicate areas of enlargement in the middle panel. Scale bars, 1.0 mm.

Following IM inoculation of newborn mice, T3 reovirus causes acute flaccid paralysis (AFP) between 8 and 10 days post-inoculation (45). Infected mice exhibit ipsilateral, followed by contralateral, hindlimb paralysis as a consequence of injury within the anterior horn of the spinal cord associated with motor neuron loss and spread of viral antigen (45). We observed differences in development of AFP in mice infected with wild-type and mutant virus. On day 8 post-inoculation, mice infected with wild-type virus displayed hindlimb paralysis at a five-fold greater frequency than those infected with the mutant virus (33% vs. 6%, respectively) (Figure IV-1B). Furthermore, the percentage of mice infected with wild-type virus exhibiting bilateral hindlimb paralysis was almost four times greater than that in mice infected with the mutant virus (11% vs. 3%, respectively) (Figure IV-1B). These data are concordant with results gathered from the survival experiments and provide further evidence that SA binding enhances reovirus virulence.

To investigate whether enhanced virulence and AFP development in mice infected with wild-type virus compared with mutant virus corresponds with more extensive reovirus infection and tissue damage in the spinal cord, we compared histologic sections of spinal cords resected from mice inoculated intramuscularly with 5×10^6 PFU of either T3D or T3D-σ1R202W (Figure IV-1C). Transverse sections of the inferior spinal cord were sectioned and processed for H&E staining or staining for reovirus antigen. Following H&E staining, spinal cords of mice infected with wild-type virus displayed more widespread injury, as indicated by increased apoptotic bodies, reactive endothelium, inflammatory infiltrates, and neurons with eosinophilic cytoplasmic inclusions. Immunohistochemistry for reovirus antigen showed correspondingly more

abundant and intense staining in mice infected with wild-type virus compared with spinal cords from mice infected with the mutant virus. These findings suggest that binding to SA leads to increased reovirus infection and injury to motor neurons in the spinal cord.

SA binding influences reovirus replication at sites of secondary infection- To better understand how SA-binding capacity influences reovirus virulence, we inoculated two-day-old mice intramuscularly with 5×10^6 PFU of either T3D or T3D-σ1R202W and quantified viral titers in the hindlimb, spinal cord, brain, and liver on days 2, 4, 8, and 10 post-inoculation (Figure IV-2A). In the hindlimb muscle, titers of both viruses were comparable, except on day 4 when the mutant virus produced higher titers than the wild-type virus ($P < 0.005$). In the spinal cord and brain, the mutant virus produced significantly higher titers than the wild-type virus at day 4 ($P < 0.05$). However, on days 8 and 10, titers of the wild-type virus were significantly higher than those of the mutant ($P < 0.05$). Interestingly, titers in the liver of mice infected with the wild-type virus were significantly less than those in mice infected with the mutant virus throughout the experimental time course of infection ($P < 0.05$ on day 2 and $P < 0.005$ on days 4 and 8).

To determine whether SA-binding capacity influences the kinetics of hematogenous spread, we again inoculated two-day-old mice intramuscularly with 5×10^6 PFU of either T3D or T3D-σ1R202W. In this experiment, we quantified viral titers in the heart and spleen (Figure IV-3A) and monitored viral genome copies in the serum (Figure IV-3B). On day 4 post-inoculation, the wild-type virus produced higher titer in the heart, but lower titer in the spleen in comparison to the mutant virus. On day 10 post-inoculation, the wild-type virus produced higher titer than the mutant virus in the spleen.

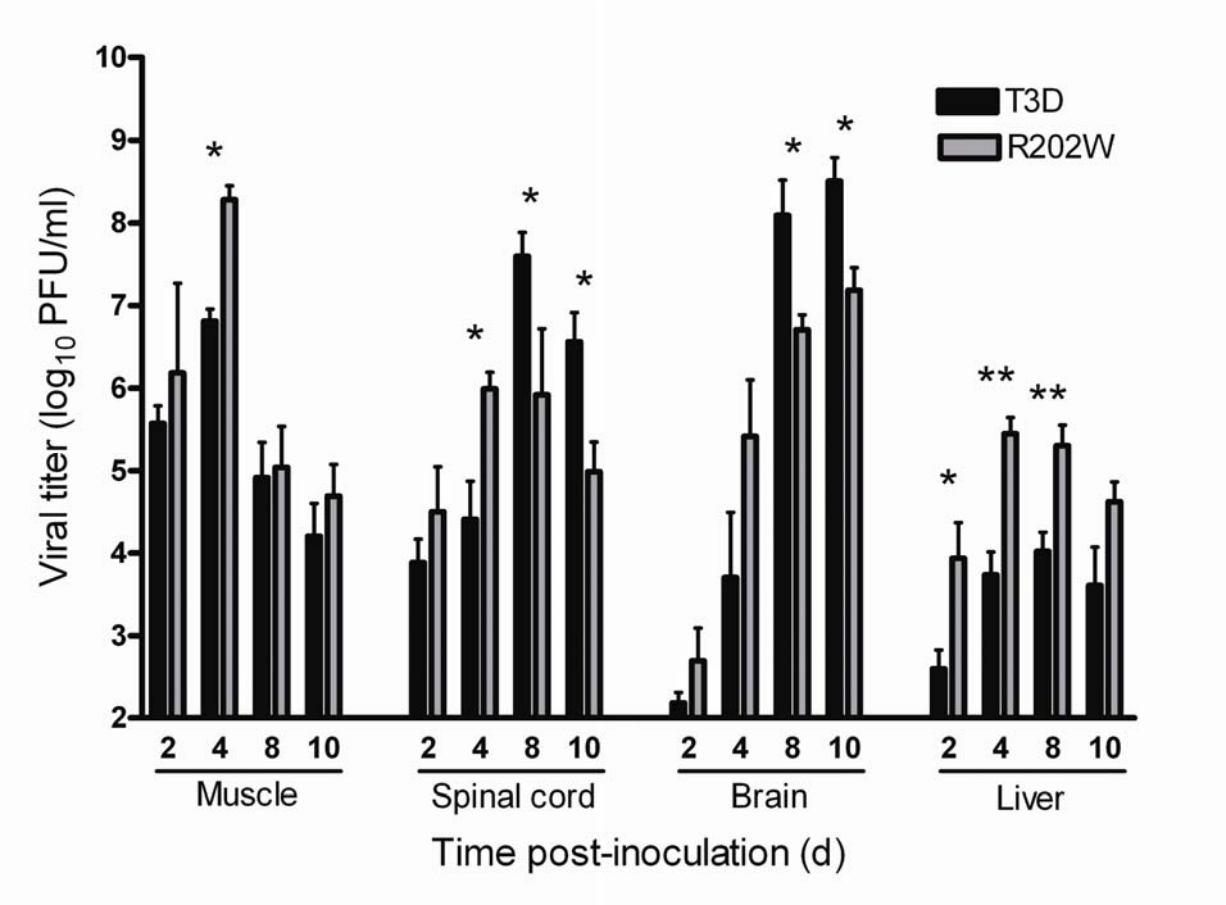

FIGURE IV-2. SA binding is associated with higher peak titers of reovirus in neural tissues. Newborn C57/BL6 mice were inoculated in the right hindlimb with 5×10^6 PFU of either T3D or T3D-σ1R202W. At days 2, 4, 8, and 10 post-inoculation, mice were euthanized, hindlimb muscle, spinal cord, brain, and liver were resected, and viral titers in organ homogenates were determined by plaque assay. Results are expressed as mean viral titers for 6-9 animals for each time point. Error bars indicate SEM. *, $P < 0.05$ and **, $P < 0.005$, as determined by Mann-Whitney test in comparison to T3D.

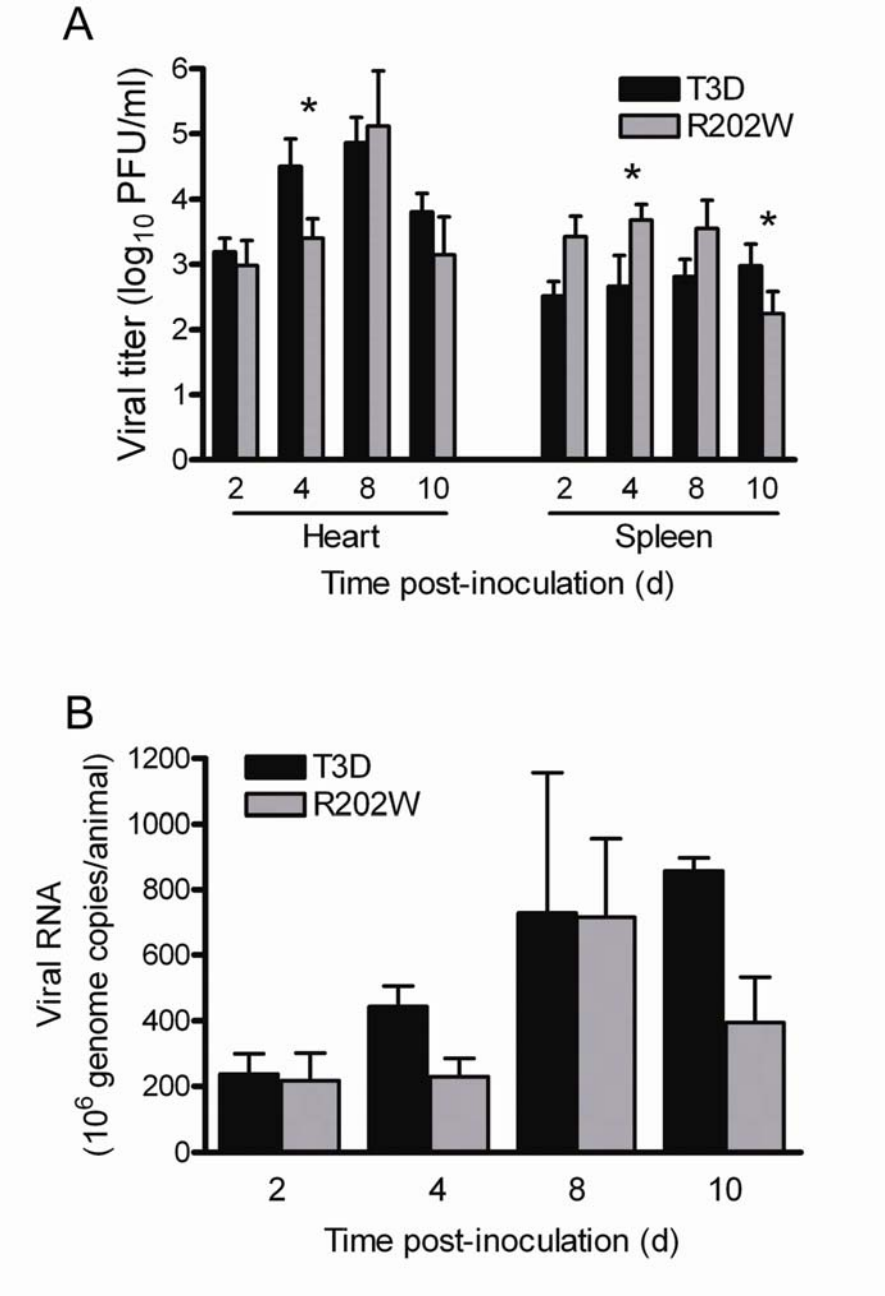

FIGURE IV-3. Binding to SA is not required for dissemination by hematogenous routes. Newborn C57/BL6 mice were inoculated in the right hindlimb with 5×10^6 PFU of either T3D or T3D-σ1R202W. (A) At days 2, 4, 8, and 10 post-inoculation, mice were euthanized, and heart and spleen were resected. Viral titers in organ homogenates were determined by plaque assay. Results are expressed as mean viral titers for 7 to 10 animals for each time point. Error bars indicate SEM. *, $P < 0.05$ as determined by Mann-Whitney test in comparison to T3D. (B) At days 2, 4, 8, and 10 post-inoculation, mice were euthanized, blood was collected, and viral genome copies in serum were determined by RT-qPCR. Results are expressed as mean viral genome copies per animal for 3 to 5 animals at each time point. Error bars indicate SEM.

Although these differences are statistically significant, because of the modest magnitude of the differences, they may not be physiologically important. Furthermore, the number of viral genome copies detected in the serum of mice infected with either virus also was comparable. Thus, SA-binding capacity enhances overall peak titers in the murine CNS. However, utilization of SA is not required for infection of the liver and does not appear to influence hematogenous dissemination in mice.

SA binding enhances reovirus neurovirulence and replication in the brain- Differences in titers produced by T3D and T3D-σ1R202W in the spinal cord and brain could result from more efficient spread of wild-type virus from the muscle to the CNS, enhanced replication of wild-type virus in the CNS, or both effects. To distinguish between these possibilities, we inoculated three-day-old mice intracranially with 2 PFU of either wild-type or mutant virus. We monitored infected mice for survival and clinical signs of disease for 21 days and quantified viral loads in the brain at days 4, 8, and 12 following inoculation (Figure IV-4). We again observed that mice infected with the wild-type virus displayed a lower frequency of survival (33%) compared with those infected with the mutant virus (85%) ($P < 0.001$) (Figure IV-4A). In addition, wild-type virus produced higher titers in the brain than did the mutant following IC inoculation (Figure IV-4B), reaching statistical significance on day 8 post-inoculation ($P < 0.05$). Taken together, these findings suggest that SA binding enhances reovirus virulence by accelerating viral replication in the CNS.

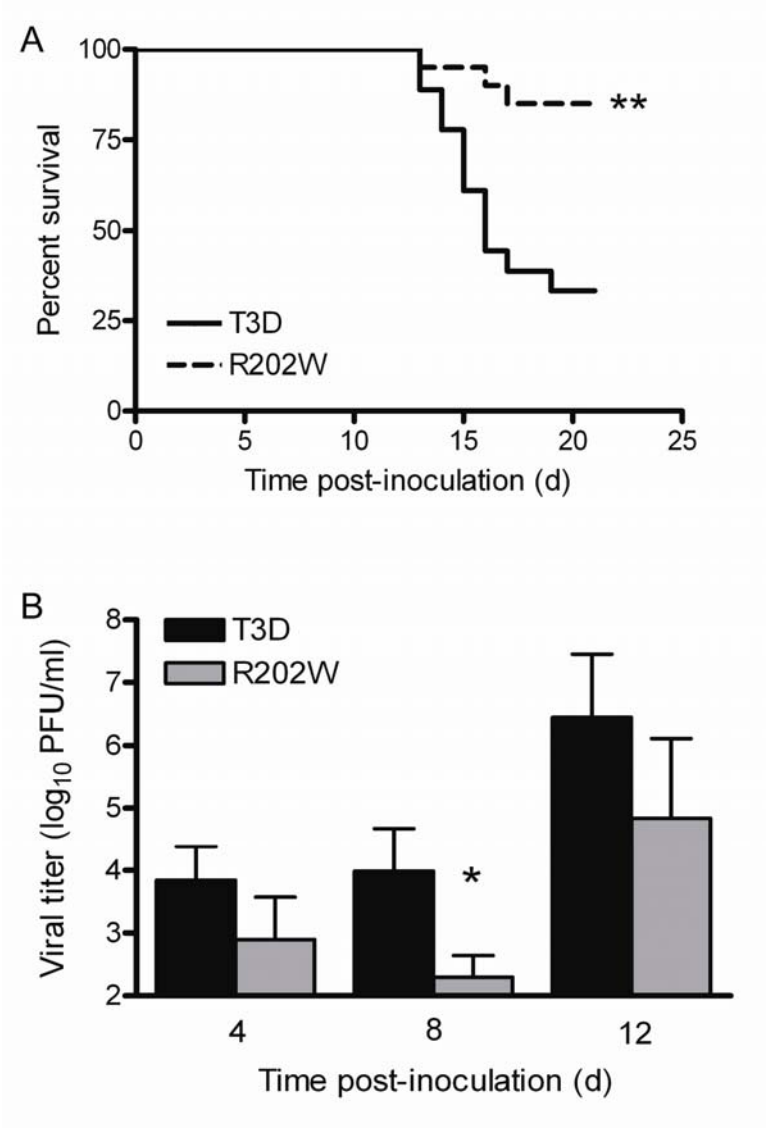

FIGURE IV-4. SA-binding capacity enhances reovirus neurovirulence and replicative capacity following IC inoculation. Newborn C57/BL6 mice were inoculated intracranially with 2 PFU of either T3D or T3D-σ1R202W. (A) Mice (n = 18-21 for each virus strain) were monitored for survival for 21 days. **, $P < 0.001$ as determined by log-rank test in comparison to T3D. (B) At days 4, 8, and 12 post-inoculation, viral titers in brain homogenates were determined by plaque assay. Results are expressed as mean viral titers for 4 to 7 animals for each time point. Error bars indicate SEM. *, $P < 0.05$, as determined by Mann-Whitney test in comparison to T3D.

SA binding does not alter reovirus tropism in the brain- To test whether σ1-SA interactions are required for neural tropism of T3 reovirus, we compared histologic sections of brains resected from mice inoculated intracranially with 100 PFU of either T3D or T3D-σ1R202W (Figure IV-5). Brains chosen for histologic analysis were matched anatomically based on the size and shape of landmarks such as the hippocampus as well as displaying comparable viral titers. The intensity of reovirus antigen staining as well as the cellular distribution of reovirus antigen was similar in brain sections from mice infected with either T3D or T3D-σ1R202W. Characteristic reovirus tropism involving several areas of the brain including the cortex, the C2-C4 region of the hippocampus, and the thalamus was apparent in mice infected with either virus (Figure IV-5A). In addition, involvement of the cerebellum, specifically infection of the Purkinje cells, was observed in brain sections of mice infected with either virus (Figure IV-5B). Therefore, SA-binding capacity of T3 reovirus does not influence targeting of reovirus to specific regions within the brain, but rather appears to influence replication efficiency in brain tissue.

SA binding enhances infection of and replication in murine primary cortical neurons- Results gathered thus far reveal that SA-binding enhances the capacity of reovirus to replicate in the brain following IM or IC inoculation. We hypothesized that this difference is attributable to enhanced infection and replication in neurons by SA-binding reovirus strains. To test this hypothesis, we quantified infection of primary cortical neuron cultures using an immunoflorescence assay (Figure IV-6A and Figure IV-6B) and compared titers of T3D and T3D-σ1R202W following replication in primary

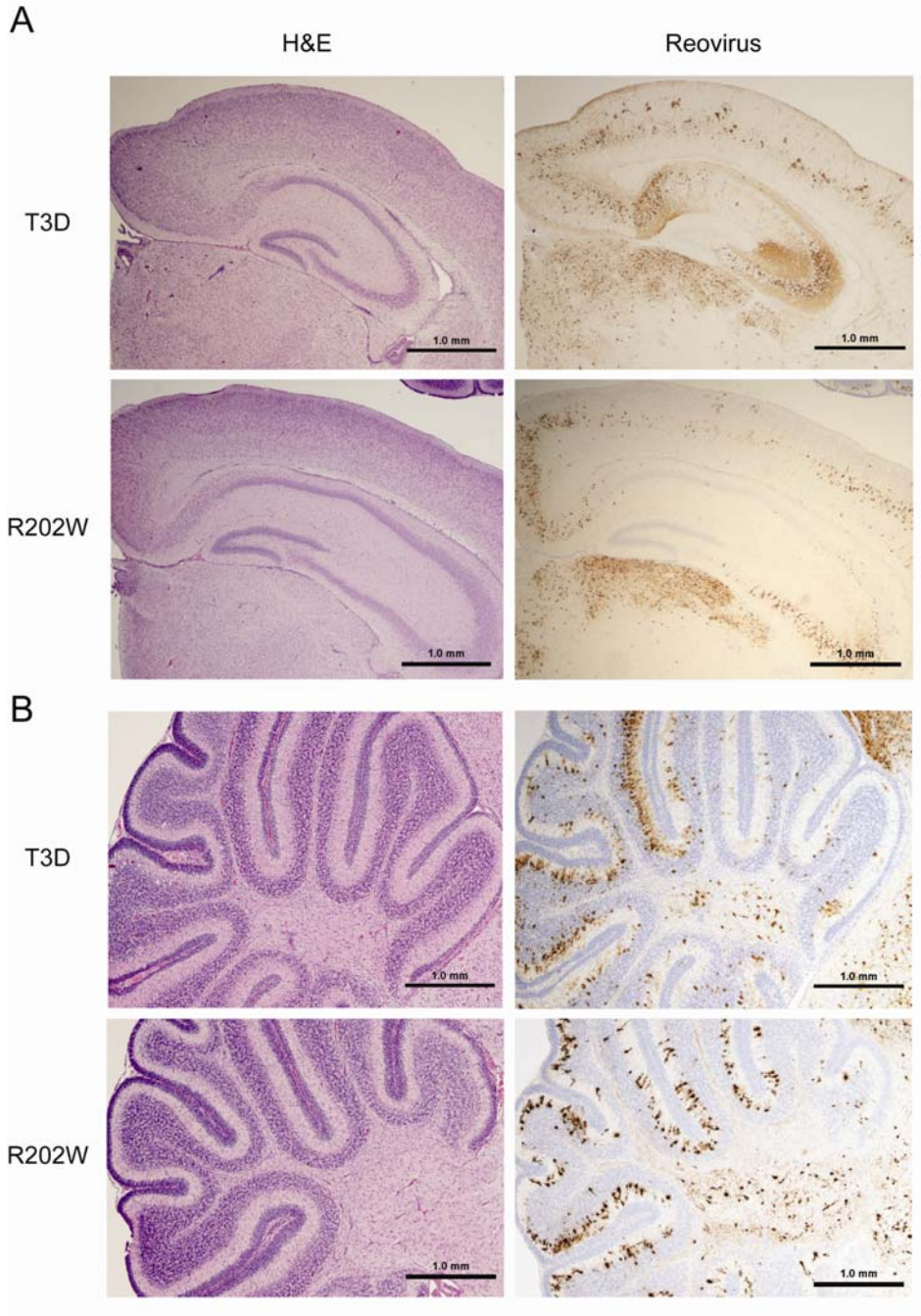

FIGURE IV-5. Binding to SA does not alter reovirus tropism in the brain. Newborn C57/BL6 mice were inoculated intracranially with 100 PFU of either T3D or T3D-σ1R202W (R202W). On day 8 post-inoculation, brains of infected mice were resected. The brains were bisected, and the left hemispheres were processed for histopathology and the right hemispheres were prepared for viral titer determination by plaque assay. Consecutive coronal sections of the brain were stained with hematoxylin and eosin (H&E) or polyclonal reovirus antiserum (Reovirus). Representative sections of brain hemisphere, matched for hippocampal depth, (A) and cerebellum (B) are shown. Scale bars, 1.0mm. T3D-infected brain sections are from the right hemisphere of a brain with a viral titer of 8×10^8 PFU, and R202W-infected brain sections are from the right hemisphere of a brain with a viral titer of 3.5×10^8 PFU.

cortical neuron cultures at 24, 48, and 72 h post-infection (Figure IV-6C). Primary cultures of mouse cortical neurons were established using cerebral cortices of C57/BL6 embryos at developmental day E15 and cultured for 7 days prior to infection (3). Wild-type virus infected a significantly higher percentage of cortical neurons (5%) in comparison to the mutant (1%) ($P < 0.0001$) (Figure IV-6A and Figure IV-6B). Concordantly, at 24 h post-infection, yields of wild-type and mutant virus were comparable (Figure IV-6C). However, by 48 and 72 h post-infection, wild-type virus produced significantly higher yields than those produced by the mutant (Figure IV-6C). These findings suggest that engagement of SA by reovirus enhances infection and replication efficiency in neurons.

To confirm the importance of SA binding for infectivity and replication of primary cultures of neurons, cells were treated with *A. ureafaciens* neuraminidase to remove cell-surface SA. *A. ureafaciens* neuraminidase is a broad-spectrum enzyme that cleaves α-2,3-, α-2,6-, and α-2,8- terminally-linked SA present on glycan chains (116). Neuraminidase treatment diminished the infectivity and replication of wild-type virus to the levels observed for the mutant virus (Figure IV-6A, IV-6B, and IV-6C). These findings demonstrate that both replication and infectivity of primary neuronal cultures by T3 reovirus is enhanced by SA binding. Collectively, these results suggest that the capacity of reovirus to bind cell-surface SA enhances the efficiency with which the virus infects cells in the murine CNS.

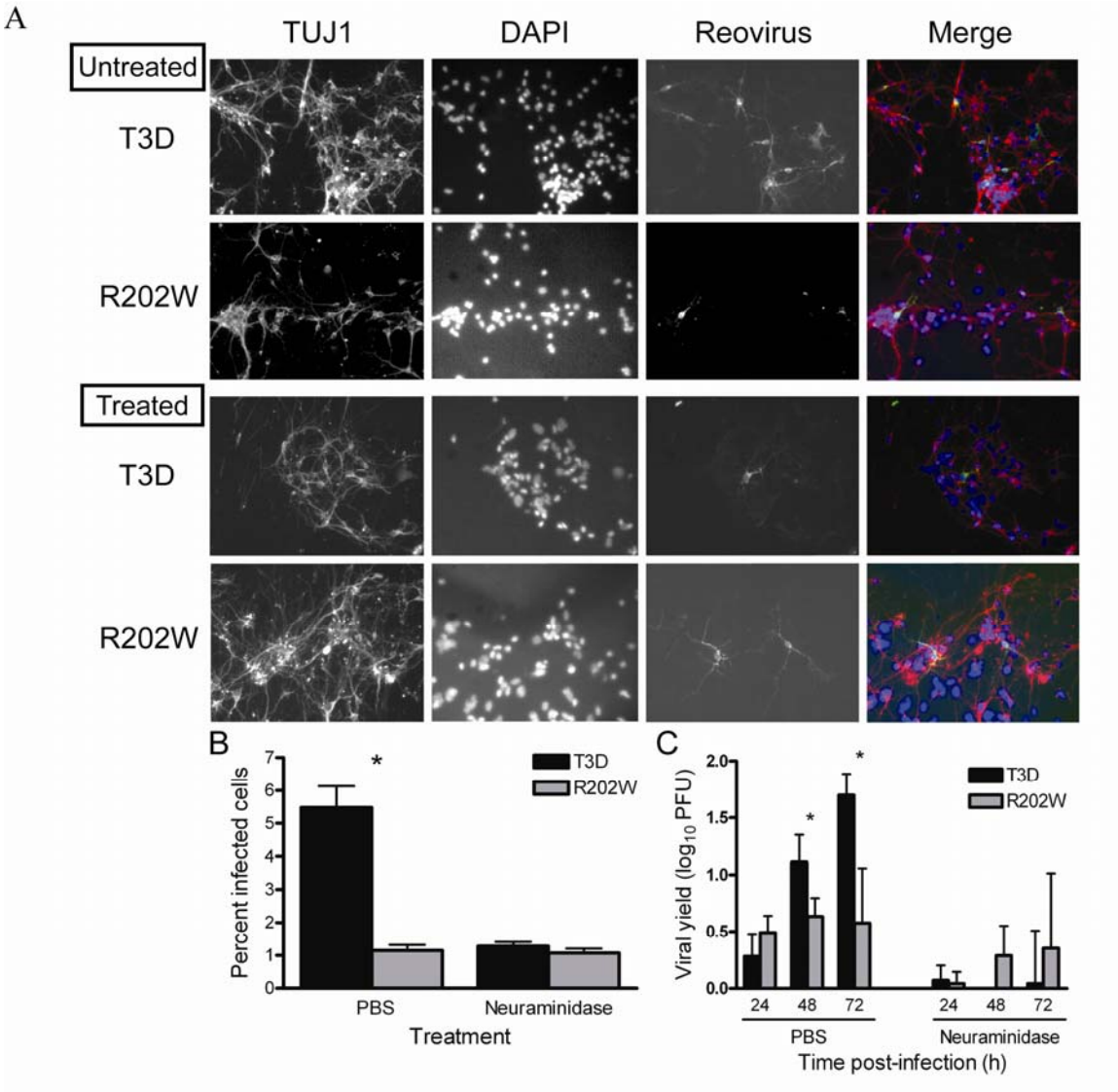

FIGURE IV-6. SA-binding capacity increases the efficiency of reovirus infection of primary cortical neurons. Cortical neurons were harvested from C57/BL6 mouse embryos at developmental day E15.5 and cultured for 5-7 days prior to infection. (A) Neurons were adsorbed with either T3D or T3D σ1-R202W at an MOI of 1000 PFU/cell following pre-treatment with either PBS or 40 mM *A. ureafaciens* neuraminidase and incubated for 21 h. Cells were stained with TUJ1 neural-specific marker to detect neurons (red), DAPI to detect nuclei (blue), and polyclonal reovirus antiserum to detect reovirus antigen (green) and visualized using indirect immunofluorescence microscopy. Representative wells from duplicate experiments are shown. (B) The percentage of infected cells was quantified by dividing the number of neurons exhibiting reovirus staining by the total number of cell nuclei exhibiting DAPI staining in three fields of 400X view in triplicate wells (n=2). Fields of view contained between 200 and 600 nuclei. Error bars indicate SEM. *, $P < 0.0001$, as determined by Student *t* test in comparison to T3D. (C) Neurons were adsorbed with either T3D or T3D σ1-R202W at an MOI of 1 PFU/cell. Titers of virus in cell lysates were determined by plaque assay at the indicated times post-adsorption. Results are expressed as mean viral yield for duplicate samples. Error bars indicate SD. *, $P < 0.05$, as determined by Student *t* test in comparison to T3D.

Discussion

In this study, I found that the capacity to bind cell-surface SA enhances the neurovirulence of T3 reovirus. Following either IM or IC inoculation of newborn mice, wild-type strain T3D was more virulent and produced higher titers in neural tissues compared with non-SA-binding mutant virus T3D-σ1R202W. Furthermore, mice infected with wild-type virus displayed a higher frequency of AFP and enhanced tissue injury compared with mutant-infected mice. The key finding of this study is that SA-binding capacity dictates increased reovirus infectivity and replicative capacity in murine neurons. These data suggest that SA binding enhances the neurovirulence of T3 reovirus by mediating efficient infection of target cells in the CNS, resulting in increased replication and pathology.

I found that wild-type T3D displays increased infectivity and replicative capacity in primary cultures of murine cortical neurons, a phenotype that is dependent on cell-surface SA. Binding of T3 reovirus strains to SA facilitates viral attachment through low-affinity adhesion that places the virus on the cell surface where access to the higher-affinity, but lower-abundance, proteinaceous receptor is thermodynamically favored (7). This adhesion-strengthening mechanism may be the basis for the enhanced replication and neurovirulence of T3D. Although the proteinaceous receptor on neurons for T3 reovirus is not known, my findings suggest that its engagement likely requires initial low-affinity glycan binding to anchor the virus to the cell surface. We favor this scenario because neuraminidase treatment of primary murine cortical neurons decreases but does not abolish infection or replication (Figure IV- 6), consistent with the existence of other host mediators of attachment and cell entry.

I previously identified residues in T3 σ1 that are required for functional binding of reovirus to SA, i.e., binding that results in productive infection (91). Using reverse genetics, I introduced structure-guided mutations in the T3 σ1 molecule and characterized the resultant mutant viruses using assays to quantify SA-binding capacity. This analysis highlighted the importance of Arg202 in the interaction of T3 σ1 with SA. The Arg202 sidechain forms a bidentate salt bridge with the carboxylate moiety of SA, which is an important electrostatic contact between the protein and its carbohydrate ligand. Replacement of Arg202 with a tryptophan in T3D-σ1R202W would remove the electrostatic interaction between the arginine and SA and introduce a structural clash with the glycan (Figure IV-7). It is therefore unlikely that the mutant can bind to SA, even in the improbable case that the overall structure of the binding site is not altered by the mutation. This model provides a structural framework for understanding the decreased virulence displayed by T3D-σ1R202W.

Following IM inoculation, wild-type T3D produced lower titers in the livers of infected mice than did non-SA binding stain T3D-σ1R202W (Figure IV-2). This is an interesting result because previous studies from our laboratory revealed that SA binding confers tropism of reovirus for bile duct epithelium and reovirus-induced injury to the liver (9). The SA-binding strain used in that study, T3SA+, produces higher titers in liver tissue than its non-SA-binding counterpart, T3SA-, at early times after infection. However, SA-binding-capacity is not strictly required for infection and replication in the liver, as T3SA- produces titers in the liver that approximate those of T3SA+ at late times of infection (3, 9). It is possible that the genetic backgrounds of the strains used by Barton et al (9) (T1L) and here (T3D) account for the observed differences. It is also

possible that the routes of inoculation, peroral (9) vs. IM (current study) influence hepatic tropism. We also noted that T3D-σ1R202W produced higher titers than wild-type virus in the spinal cord and brain of infected mice on day 4 post-inoculation. Since reovirus is delivered initially to the CNS by hematogenous routes (3, 15), it is possible that bloodstream dissemination of the mutant virus is subtly enhanced in comparison to wild-type virus, although if so, this difference was not sufficient to permit detection in our assays.

Data presented in this study and others (9) indicate that the capacity of T3 reovirus to bind cell-surface SA can target the virus to specific sites of infection and lead to enhanced replication and disease. These observations suggest that SA-binding capacity confers a fitness advantage for reovirus. For example, it is possible that an SA-mediated replication enhancement leads to increased viral shedding and transmission of virus from host to host. However, there are naturally circulating strains of reovirus that do not bind to SA (28), suggesting that SA-binding capacity is a balanced polymorphism in nature that also imposes a fitness cost. For example, SA-binding capacity diminishes reovirus infection of polarized human airway epithelial cells (38). Strain T3SA+ does not efficiently infect these cells, whereas T3SA- does. Moreover, neuraminidase pre-treatment to remove cell-surface SA enhances infection of airway epithelial cells (38). Determination of the precise contribution of SA binding to viral fitness will require competition studies using strains that vary solely in SA-binding capacity and populations of susceptible mice.

For many viruses, including several important human pathogens, glycan engagement plays an important role in infection and pathogenesis. Here, I demonstrate

that utilization of sialylated glycans as coreceptors enhances the neurovirulence of T3 reovirus. This study broadens an understanding of mechanisms of reovirus attachment to neuronal cells and supports the hypothesis that T3 reovirus-glycan interactions are key determinants of reovirus neurovirulence in the CNS.

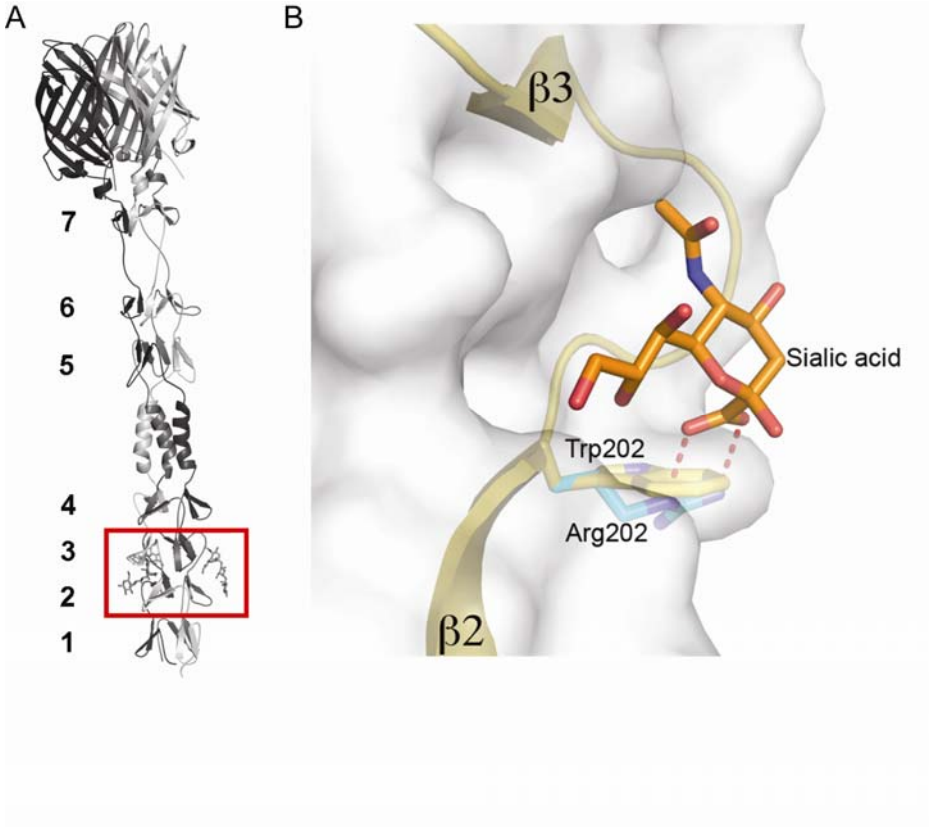

FIGURE IV-7. Comparison of T3D and T3D-σ1R202W σ1 interactions with the terminal SA of α(2,3) sialyllactose. (A) Ribbon drawing of the T3D σ1 body and head domains in complex with α(2,3) sialyllactose. The σ1 monomers are shown in red, blue, and yellow. The body domain consists of seven triple β-spiral repeats (β1–β7) and an α-helical coiled-coil domain (cc) that is inserted between β-spiral repeats β4 and β5. The bound α(2,3) sialyllactose is shown in stick representation and colored in orange (enclosed by the red box). (B) An enlarged view of the T3D σ1 SA-binding domain. The σ1 residue 202 of a single σ1 monomer is drawn in stick representation, while the remainder of the monomer is shown as a ribbon tracing. The other monomers are shown in a surface-shaded representation. The SA moiety of α(2,3) sialyllactose is shown in stick representation, with carbons colored orange, oxygens colored red, and nitrogens colored blue. Residue Arg202 (cyan) of wild-type T3D forms a salt bridge with the carboxylate group of SA (91). This bond is represented by a dashed red line, illustrating that it is likely lost when Arg202 is replaced with a tryptophan (yellow) in T3D-σ1R202W.

CHAPTER V

SUMMARY AND FUTURE DIRECTIONS

Virus attachment to host cells is the first step in viral replication and serves a central role in determining viral tropism and disease. Defining the precise interactions that mediate virus-receptor engagement is crucial for understanding the mechanisms underlying viral pathogenesis. Although it is known that carbohydrate interactions influence reovirus dissemination and tropism *in vivo*, little is understood about the function of these molecules in reovirus tropism and pathogenesis within the CNS. Studies of pathogen-receptor interactions can therefore provide valuable insight into mechanisms of injury and disease in an infected host and improve our ability to develop antiviral therapeutics. The work described in this dissertation was performed to enhance an understanding of the structural basis of interactions between σ1 and SA and determine the role of SA binding in reovirus virulence within the CNS.

The data presented in this thesis support the following conclusions: 1) T3 reovirus attachment to SA is achieved through binding of β-spiral repeats 2 and 3 of σ1 to the glycan (Chapter II); 2) residues Asn198, Arg202, Leu203, Pro204, and Gly205 of σ1 are required for mediating σ1-SA interactions (Chapter III); and 3) SA binding enhances reovirus neurovirulence (Chapter IV). This chapter summarizes the data presented in this dissertation and highlights future directions for this research.

Molecular mechanisms of reovirus attachment to SA

Results from Chapter II and III reveal the structural and molecular basis for T3 reovirus σ1-SA interactions. In Chapter II, I present the first structure of the SA-binding domain of T3 σ1 alone and in complex with carbohydrates that naturally occur on human cells. Structures of the σ1-glycan complexes represent the first examples of any filamentous viral attachment protein engaging a ligand via repetitive sequence motifs in its fiber region. The findings in Chapter III identify a network of residues that are required for mediating σ1-SA interactions.

Future studies should be directed toward identifying the physiologically relevant glycans engaged by T3 reovirus *in vivo*. Glycan arrays done in collaboration with Ten Feizi (Imperial College) and the Stehle laboratory (Universitat Tübingen) have identified potential candidates: GD1a, GD1b, and GM3. Interestingly, these three gangliosides also constitute a large portion of the gangliosides expressed in the CNS and differ in their expression among various neural cell types during development (61, 62). To test the hypothesis that one or more of these gangliosides are natural ligands for T3 reovirus in the CNS, several experiments should be performed. Infection of murine primary cortical neurons is SA-dependent (40). Therefore, these cells can be used to identify soluble glycans that inhibit reovirus infection of neurons. In complementary experiments, antibodies against the ganglioside candidates could be used to test whether blockade of glycan binding impedes reovirus infection of cortical neurons. In either case, the effect of the soluble glycans or glycan-specific antibodies on reovirus infectivity could be measured by FFU or replication assays. Should results from experiments using murine primary cortical neurons pinpoint particular glycans required for reovirus infection of

neurons, the next step could be to validate the results *in vivo* by assessing virulence and virus replication in reovirus-infected animals that do not express the candidate glycans. Animals that do not express GD1a (GD3/GT3 synthase deficient), GD1b (GD3/GT3 synthase deficient), and GM3 (GM3 synthase deficient) have been generated (50) and would be useful models for these experiments.

An additional important unanswered question that remains from my work is the precise function of σ1 residue Asn198 in σ1-SA interactions. The current crystal structures of σ1 in complex with various oligosaccharides do not show an interaction with Asn198 and SA despite its requirement for reovirus binding to SA (91). To determine the function of Asn198 in σ1-SA interactions and gain insight into the native carbohydrate engaged by T3 reovirus, crystallographic studies should be conducted using T3D σ1 protein. The protein should be expressed in *E. coli*, purified, and crystallized. The T3D σ1 crystals should then be soaked with various physiologically relevant carbohydrates (for example GD1a, GD1b, and GM3 depending on the results of the functional assays), and the structures of the resulting complexes should be solved. These studies will help identify the native carbohydrate coreceptor for T3 reovirus and will further an understanding of protein-ligand interactions. This work is currently ongoing in collaboration with the Stehle laboratory (Universitat Tübingen).

The role of carbohydrate-binding in reovirus serotype-specific neuropathogenesis

The dramatic differences exhibited by T1 and T3 reovirus strains in viral tropism and disease in mice segregate with the σ1-encoding S1 gene (29, 112, 121, 122). Although JAM-A serves as a proteinaceous receptor for both T1 and T3 serotypes (8, 18),

utilization of carbohydrate coreceptors is serotype specific (7, 21, 22, 27, 49). This observation highlights the possibility that carbohydrate coreceptor engagement influences reovirus tropism and pathogenesis in infected animals. Results presented in Chapter IV demonstrate that reovirus engagement of sialylated glycans enhances T3 reovirus neurovirulence, but it is not known whether carbohydrate coreceptor engagement contributes to the differences in pathogenesis observed between T1 and T3 reovirus strains.

To define the contribution of carbohydrate coreceptor engagement to the serotype-specific differences in CNS tropism and pathogenesis, reoviruses expressing T1/T3 chimeric σ1 proteins should be generated and compared in studies of virulence and viral replication in mice. To perform these experiments, a panel of T1/T3 chimeric reoviruses with exchanges of carbohydrate-binding domains in σ1 protein should be generated and characterized for receptor-binding specificity *in vitro* (Table V-1 and Figure V-1). Once receptor-binding specificity has been confirmed, *in vivo* studies should be conducted comparing virulence, disease development, tropism, and replication in mice. If serotype-specific carbohydrate engagement influences tropism and dissemination, the T1/T3 chimeric σ1 viruses should display phenotypes that segregate with the carbohydrate-binding domain. Accordingly, chimeric viruses with the T1 carbohydrate-binding specificity should more closely resemble the CNS tropism of T1 reovirus, and chimeric viruses with the T3 carbohydrate-binding specificity should be similar to T3 reovirus. These studies will shed light on the role of carbohydrate binding in serotype-specific tropism and dissemination.

Table V-1. Predicted glycan specificity of T1/T3 σ1 β-spiral exchange chimeras.

Chimera	T1 glycan specificity	T3 glycan specificity
T1L	+	-
T3D	-	+
T1-X1	+	+
T3-X2	-	-
T1-X3	+	+
T1-X4	+	-
T3-X5	-	-
T3-X6	-	+

T1 and T3 refer to the backbone of the S1 gene from which the construct is derived.

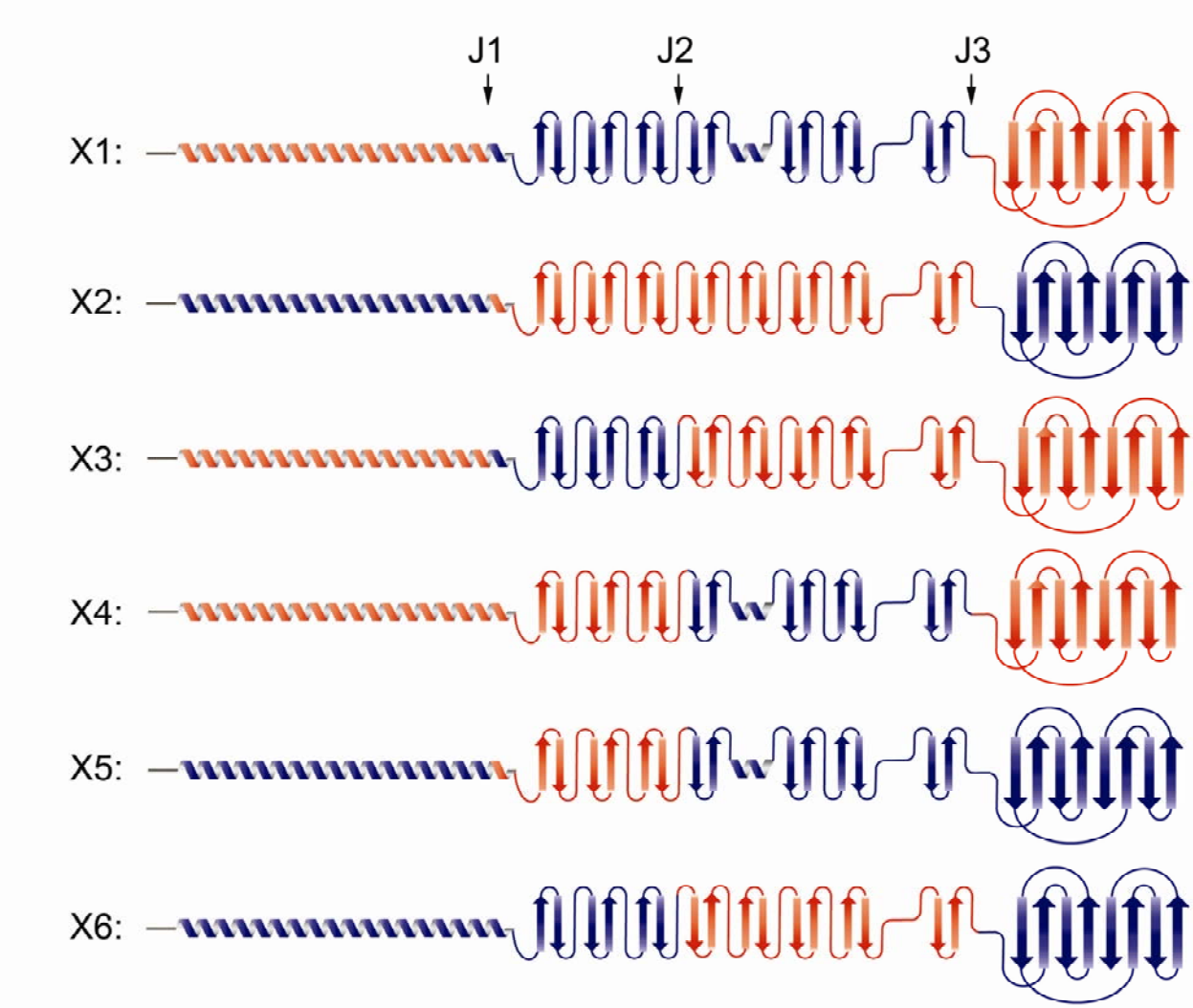

FIGURE V-1. Construct design of T1/T3 σ1 chimeras to exchange SA-binding domains. Proposed reciprocal β-spiral exchanges between T1L (red) and T3D (blue) σ1 proteins are depicted. The exchanges will be made at regions of conserved sequences or structural motifs at three junctions denoted J1, J2, and J3.

Experiments using JAM-A knockout mice and cortical neurons have demonstrated that binding to JAM-A is not required for reovirus infection of the brain or reovirus neurovirulence following IC inoculation (3). Furthermore, while SA-binding

enhances the efficiency of infection of CNS tissues, it is not strictly required for infection (9, 40). These findings suggest that there is a neural-specific receptor engaged by T3 reovirus strains yet to be identified. Although there is some evidence to suggest that sequences in the σ1 head domain of T3 reovirus strains influence reovirus neurovirulence and tropism in the CNS (11, 56), the precise role of the σ1 domains in the dichotomous patterns of tropism and spread exhibited by T1 and T3 reovirus strains is unknown. To define the contribution of each of the domains of σ1 to the serotype specific differences in CNS tropism and pathogenesis, reoviruses expressing T1/T3 chimeric σ1 proteins should be generated and compared in studies of virulence and viral replication in mice. To perform these experiments, a panel of T1/T3 chimeric reoviruses with reciprocal exchanges of the head, body, and tail domains of T1 and T3 σ1 proteins should be generated and characterized for receptor-binding specificity *in vitro* (Table V-2 and Figure V-2). Once receptor-binding specificity has been confirmed, *in vivo* studies should be conducted comparing virulence, disease development, tropism, and replication in mice. Studying this panel of σ1 chimeric viruses will give insight into which domains of σ1 are required for reovirus tropism, dissemination, and disease, and enhance an understanding of the how the discrete domains of σ1 work in concert to dictate reovirus pathogenesis.

Conclusions

With this research, we sought to establish a precise understanding of virus-receptor interactions in reovirus target-cell selection and pathogenesis. Research presented in this dissertation encompasses structural analyses, molecular genetics, and

Table V-2. Predicted neural tropism and glycan specificity of T1/T3 σ1 domain exchange chimeras.

Chimera	T1 neural tropism	T3 neural tropism	T1 glycan specificity	T3 glycan specificity
T1L	+	-	+	-
T3D	-	+	-	+
131	+	-	+	+
313	-	+	-	-
113	-	+	-	-
331	+	-	+	+
133	-	+	-	+
311	+	-	+	-

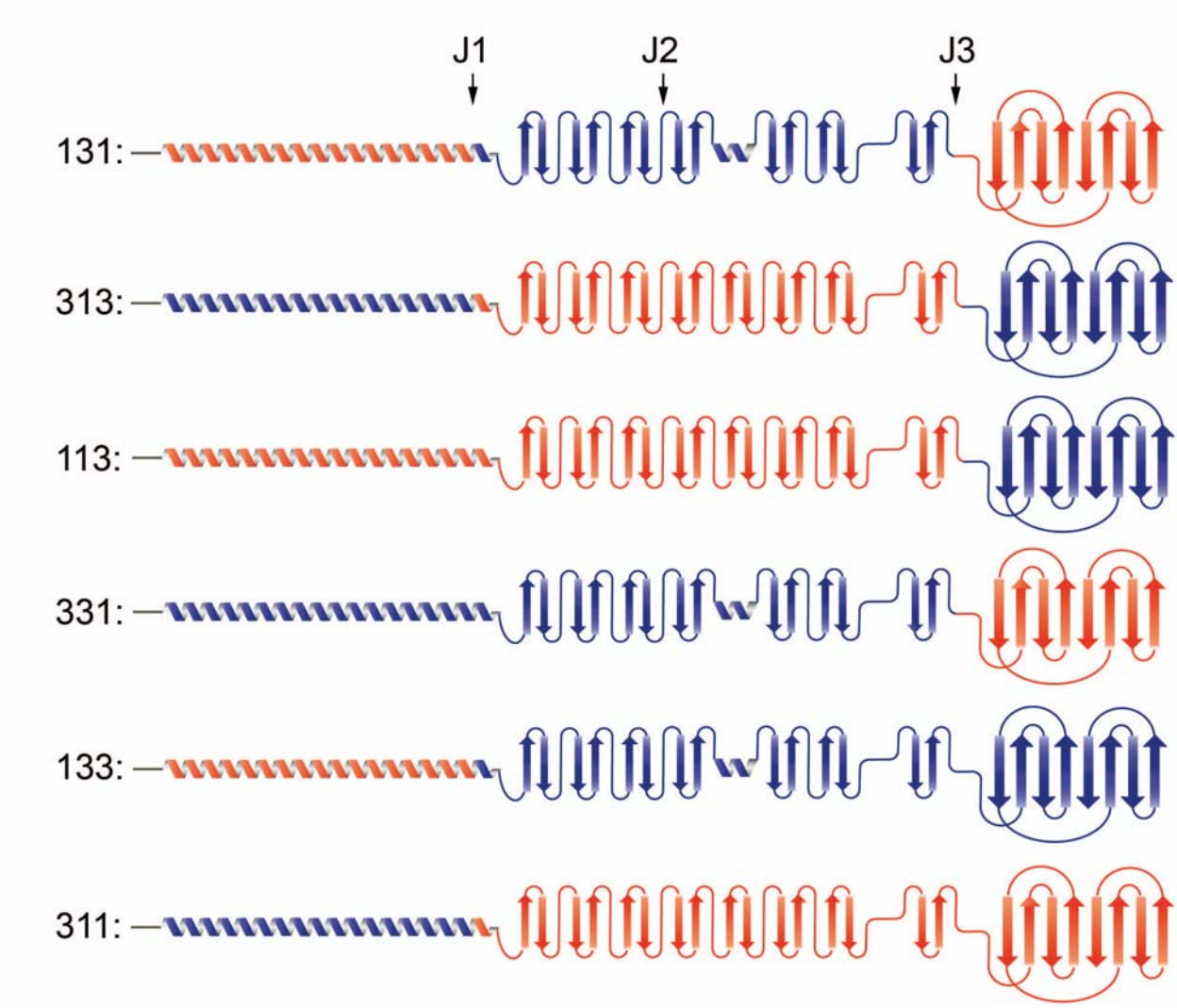

FIGURE V-2. Construct design of T1/T3 σ1 domain exchange chimeras. Proposed reciprocal β-spiral exchanges between T1L (red) and T3D (blue) σ1 proteins are depicted. The exchanges will be made at regions of conserved sequences or structural motifs at junctions denoted J1 and J3.

in vivo studies to provide a thorough assessment of the structure and function of reovirus attachment protein σ1 and its sialylated glycan coreceptors on the cell-surface.

Results from this research have enhanced an understanding of mechanisms of reovirus attachment to neuronal cells and the molecular interactions and structural features that mediate receptor engagement by viral attachment proteins. The long-term goal of this work is to identify and understand key pathogen-host molecular interactions that dictate how reovirus targets cells and disseminates to cause disease in the host. Therefore, the findings presented here can be used as a platform for future studies aimed at elucidating the basis of reovirus serotype-specific differences in spread and infection of the CNS. In addition, knowledge generated by this research adds to the reovirus field by elucidating the role of carbohydrate binding in reovirus neuropathogenesis. The broader implications of this work will be to contribute to an understanding of how neurotropic viruses interact with cellular receptors to cause disease in the CNS, and perhaps aid in the development of novel anti-viral therapies directed at blocking the attachment step. My research also will aid in the continued development of reovirus as an oncolytic agent and vaccine vector. An in-depth understanding of mechanisms used by reovirus to engage cell-surface receptors and how these interactions influence cell-targeting may lead to improved reovirus vectors with enhanced selectivity.

CHAPTER VI

MATERIALS AND METHODS

Cells

L929 cells (100) were maintained in Joklik's minimum essential medium (Sigma-Aldrich) supplemented to contain 5% fetal bovine serum (FBS), 2 mM L-glutamine, 100 U/ml of penicillin, 100 μg/ml of streptomycin, and 25 ng/ml of amphotericin B. MEL cells, previously designated T3cl.2 cells (94), were maintained in Ham's F-12 medium (CellGro) supplemented to contain 10% fetal bovine serum, 2 mM L-glutamine, 100 U/ml penicillin, 100 μg/ml streptomycin, and 25 ng/ml amphotericin B. BHK-T7 cells (16) were grown in DMEM (Invitrogen) supplemented to contain 5% FBS, 2 mm L-glutamine, 2% minimal essential medium amino acid solution (Invitrogen), and 1 mg/ml geneticin (Invitrogen).

Viruses

Recombinant reoviruses were generated by plasmid-based reverse genetics (58, 59). Reovirus strains rsT3D (wild type), rsT3D-σ1N198D, rsT3D-σ1R202W, and rsT3D-σ1P204L were recovered using monolayers of L929 cells at approximately 90% confluence (3×10^6 cells) in 60-mm dishes (Costar) infected with recombinant vaccinia virus rDIs-T7pol (52) at a multiplicity of infection (MOI) of ~ 0.5 $TCID_{50}$. At 1 h post-infection, cells were co-transfected with ten plasmid constructs representing the cloned T3D genome using 3 μl of TransIT-LT1 transfection reagent (Mirus) per μg of plasmid

DNA (58). Reovirus strains rsT3D-σ1N189A, rsT3D-σ1S195A, rsT3D-σ1R202A, rsT3D-σ1L203A, rsT3D-σ1P204A, rsT3D-σ1G205A, and rsT3D-σ1N210A were recovered using BHK-T7 cells at 90% confluence (approximately 3×10^6 cells) seeded in 60-mm dishes. Cells were co-transfected with five plasmids representing the cloned T3D genome using 3 μl of TransIT-LT1 transfection reagent (Mirus) per μg of plasmid DNA (59). The amount of each plasmid used for transfection was identical to that described for L929 cell transfections. Following 3 to 5 days of incubation, recombinant viruses were isolated from transfected cells by plaque purification using monolayers of L929 cells (118).

The σ1 mutant viruses were generated by altering pT7-S1T3D (58) using QuikChange (Stratagene) site-directed mutagenesis. Sequences of the mutant viruses were determined using viral RNA from purified virions and subjected to Onestep reverse transcription-PCR (RT-PCR) (Qiagen) using *L1*- or *S1*-specific primers. The purified PCR products were subjected to sequence analysis for the presence of the introduced mutation in the *S1* gene segment and the noncoding signature mutation in the *L1* gene segment (58).

Purified reovirus virions were prepared using second-passage L929-cell lysate stocks of twice plaque-purified reovirus as described (42). Viral particles were Freon-extracted from infected cell lysates, layered onto CsCl gradients, and centrifuged at 62,000 × *g* for 18 h. Bands corresponding to virions (1.36 g/cm^3) (102) were collected and dialyzed in virion-storage buffer (150 mM NaCl, 15 mM $MgCl_2$, 10 mM Tris-HCl pH 7.4). The concentration of reovirus virions in purified preparations was determined

from an equivalence of one OD unit at 260 nm equals 2.1×10^{12} virions (102). Viral titers were determined by plaque assay using L929 cells (118).

Protein Expression and Purification

The expression of soluble and properly folded T3D σ1 trimers was facilitated by appending a trypsin-cleavable trimerization domain based on the GCN4 leucine zipper (47) N-terminally to a cDNA encoding the entire σ1 body and head domains (amino acids 170-455). The construct was cloned into the pQE-80L expression vector, which encodes a non-cleavable N-terminal hexahistidine-tag. The protein was expressed in *E. coli Rosetta 2 DE3* (Novagen) at 20°C for 16 h post-induction or by autoinduction at 20°C for 48-72 h. Bacteria were lysed by two passages through an EmulsiFlex (Avestin) homogenizer and purified by Ni-IMAC using His-Trap-FF columns (GE-Healthcare). The immobilized protein was eluted by on-column digestion with 0.1 mg/ml trypsin at a flowrate of 0.1ml/min for 12 h. Size-exclusion chromatography (Superdex-200, GE-Healthcare) was used as the final purification step.

X-ray Structure Determination

Crystals of T3D σ1 were grown using 15% PEG200, 0.1M MES (pH 6.5) as a precipitant. The crystals belong to space group $P2_12_12$ and contain one trimer in the asymmetric unit. Complexes with carbohydrate ligands were prepared by soaking crystals with the respective carbohydrate prior to data collection. The crystals were transferred into mother liquor supplemented with 10 mM carbohydrate, incubated for 5 min, and

cryoprotected by incubation for 15 s in 35% PEG200, 0.1M MES, 10 mM carbohydrate (pH 6.5).

Diffraction data were collected at the beamlines PXI (SLS) and ID14-4 (ESRF). Diffraction data were integrated and scaled using XDS (54), and the structure was solved by molecular replacement with AMoRe (77) using the structure of the T3D σ1 head (PDB ID 1KKE) as a search model. Refinement was performed with Refmac5 (74) and Phenix (1), and model building was done in Coot (37). Ligands were placed into weighted F_o-F_c difference density maps at a contour level of 3σ and refined using the CCP4 library and user-defined restraints. Coordinates and structure factors for all three complexes have been deposited in the PDB data bank (www.rcsb.org) with accession codes 3S6X (complex with α-2,3-sialyllactose), 3S6Y (complex with α-2,6-sialyllactose) and 3S6Z (complex with α-2,8-di-sialyllactose).

HA Assay

Purified reovirus virions (10^{11} particles) were distributed into 96-well U-bottom microtiter plates (Costar) and serially diluted twofold in 0.05 ml of phosphate-buffered saline (PBS). Calf erythrocytes (Colorado Serum Co.) were washed twice with PBS and resuspended at a concentration of 1% (vol/vol). Erythrocytes (0.05 ml) were added to wells containing virus particles and incubated at 4°C for at least 2 h. A partial or complete shield of erythrocytes on the well bottom was interpreted as a positive HA result; a smooth, round button of erythrocytes was interpreted as a negative result. HA titer is expressed as 10^{11} particles divided by the number of particles/HA unit. One HA unit equals the number of particles sufficient to produce HA. HA titers from three

independent experiments were compared using an unpaired Student's *t* test as applied in Microsoft Excel. *P* values of less than 0.05 were considered statistically significant.

Reovirus Infection of L929 and MEL Cells

L929 cells or MEL cells (2×10^5 cells/well) were plated in 24-well plates (Costar) and incubated at 37°C for at least 2 h. Cells were adsorbed with reovirus strains at an MOI of 1 plaque forming units (PFU)/cell. Following incubation at room temperature for 1 h, cells were washed three times with PBS and incubated at 37°C for 24 or 48 h. Samples were frozen and thawed twice, and viral titers were determined by plaque assay (118). For each experiment, samples were infected in triplicate. Mean values from three independent experiments were compared using an unpaired Student's *t* test as applied in Microsoft Excel. *P* values of less than 0.05 were considered statistically significant.

Infection of mice

C57BL/6J mice were obtained from Jackson Laboratory to establish breeding colonies. Newborn mice 2-3 days old were inoculated intramuscularly or intracranially with purified reovirus diluted in PBS. IM inoculations (5 μl) were delivered into the right hindlimb, and IC inoculations (5 μl) were delivered into the left cerebral hemisphere, in both cases using a Hamilton syringe and 30-gauge needle. For analysis of viral virulence, mice were monitored for symptoms of disease for 21 days post-inoculation. For virulence experiments, mice were euthanized when found to be moribund (defined by rapid or shallow breathing, lethargy, or paralysis). Death was not used as an endpoint. For analysis of virus replication, mice were euthanized at various intervals following

inoculation, and organs were collected into 1 ml of PBS and homogenized by freezing, thawing, and sonication. For analysis of viremia, mice were euthanized and decapitated at various intervals following inoculation, and whole blood was collected from the neck into a 1 ml syringe containing 100 µl Alsever's solution (Sigma). Viral titers in organ homogenates were determined by plaque assay using L929 cells (118).

For experiments in which viral titers were determined in an organ or blood, the Mann-Whitney test was used to calculate two-tailed *P* values. This test is appropriate for experimental data that display a non-Gaussian distribution (93). *P* values of less than 0.05 were considered to be statistically significant. When all values are less than the limit of detection, a Mann-Whitney test *P* value cannot be calculated. Statistical analyses were performed using Prism software (GraphPad Software, Inc.).

All animal husbandry and experimental procedures were performed in accordance with Public Health Service policy and approved by the Vanderbilt University School of Medicine Institutional Animal Care and Use Committee.

Preparation of cortical neuron cultures from embryonic mice

Primary cultures of mouse cortical neurons were established using cerebral cortices of C57/BL6 embryos at developmental day E15 (3). Fetuses were decapitated, brains were removed, and cortical lobes were dissected and submerged in Hanks' balanced salt solution (Gibco) on ice. Cortices were incubated in 0.6 mg/ml trypsin solution at room temperature for 30 min, washed twice, and manually dissociated twice using a Pasteur pipette. Viable cells were plated at a density of 2.5×10^5 cells/ml in 24-well plates. Wells were treated prior to plating with a 10 µg/ml poly-D-lysine solution (BD Biosciences)

and a 1.64 μg/ml laminin solution (BD Biosciences). Cultures were incubated for the first 24 h in neurobasal medium (Gibco) supplemented to contain 10% FBS (Gibco), 0.6 mM L-glutamine, 50 units/ml penicillin, and 50 μg/ml streptomycin. Cultures were thereafter maintained in neurobasal medium supplemented to contain B27 (Gibco), 50 units/ml penicillin, and 50 μg/ml streptomycin. One-half of the medium was replaced with fresh medium every 3 to 4 days. Neurons were cultivated for 7 days prior to use.

Assessment of reovirus infectivity by indirect immunofluorescence

Monolayers of murine cortical neurons (2.5×10^5 cells/well) seeded in 24-well plates were adsorbed with reovirus at an MOI of 1000 PFU/cell at room temperature for 1 h. Cells were incubated with either PBS or 40 mU *Arthrobacter ureafaciens* neuraminidase at 37°C for 1 h and washed three times with PBS prior to virus adsorption. Following removal of the virus inoculum, cells were washed with PBS and incubated in complete medium at 37°C for 21 h to permit completion of a single cycle of viral replication. Monolayers were fixed with 1 ml of methanol at -20°C for at least 30 min, washed twice with PBS, and blocked with 0.1% Tween-20 (Sigma) and 20% normal goat serum (Vector Laboratories) in PBS. Cells were washed once with PBS and stained with polyclonal rabbit anti-reovirus serum at a 1:1000 dilution in PBS-0.5% Triton X-100 at room temperature for 1 h. Neurons were visualized after washing three times with PBS and staining with a monoclonal mouse anti-β-tubulin antibody (TUJ1; Covance) at a 1:1000 dilution in PBS-0.5% Triton X-100 at room temperature for 1 h. Monolayers were washed twice with PBS-0.5% Triton X-100 and incubated with a 1:1000 dilution of Alexa488-labeled anti-rabbit and Alexa546-labeled anti-mouse IgG (Invitrogen). Nuclei

were stained with 4′,6-diamidino-2-phenylindole (DAPI; Invitrogen) at a 1:10,000 dilution. Monolayers were washed with PBS, and infected cells were visualized by indirect immunofluorescence using an Axiovert 200 fluorescence microscope (Carl Zeiss).

Assessment of reovirus replication by plaque assay

Murine primary cortical neurons (10^5 cells/well) were adsorbed with reovirus strains at an MOI of 1 PFU/cell. Cells were incubated with either PBS or 40 mU *A. ureafaciens* neuraminidase at 37°C for 1 h and washed three times with PBS prior to virus adsorption. Following incubation with virus at room temperature for 1 h, cells were washed three times with PBS and incubated at 37°C for 24, 48, or 72 h. Samples were frozen and thawed twice, and viral titers were determined by plaque assay using L929 cells (118). For each experiment, samples were infected in triplicate. Viral yields were calculated according to the following formula: $\log_{10}\text{yield}_{tx} = \log_{10}(\text{PFU/ml})_{tx} - \log_{10}(\text{PFU/ml})_{t0}$, where t_x is the time postinfection. Mean values from two independent experiments were compared using an unpaired Student's *t* test as applied in Microsoft Excel. *P* values of less than 0.05 were considered to be statistically significant.

Quantification of viral RNA using RT-qPCR

Total RNA was extracted from 200 μl of whole blood/Alsever's mixture using the High Pure Viral RNA kit (Roche). RNA was eluted into a final volume of 40 μl. RT-qPCR was performed using an ABI 7000 sequence detection system (Applied Biosystems) and EZ RT-PCR (Roche) according to the manufacturer's instructions with minor modifications. Reovirus RNA was quantified using 10 μl of RNA extract. Forward

(S4 83F, 5′-CGCTTTTGAAGGTCGTGTATCA-3′) and reverse (S4 153R, 5′-CTGGCTGTGCTGAGATTGTTTT-3′) primers corresponding to the viral S4 gene were used for RT and qPCR amplification. The S4-specific fluorogenic probe used was 5′-dFAM-AGCGCGCAAGAGGGATGGGA-BHQ-1-3′ (Biosearch Technologies). RT was performed at 50°C for 2 min, followed by incubation at 60°C for 30 min. The reaction was terminated by incubation at 95°C for 5 min. Subsequently, 40 cycles of qPCR were performed at 95°C for 15 s followed by incubation at 60°C for 30 s. Standard curves relating threshold cycle values to copies of plasmid DNA template were generated using 10-fold dilutions of a T3D S4-encoding plasmid (pT7-T3D S4) (58). The concentration of viral RNA in each sample was extrapolated from standard curves. The final S4 RNA copy number was calculated by multiplying the copy number obtained by extrapolation from the standard curve by four to account for using one-quarter of the extracted RNA as a template.

Histology and immunohistochemical staining for reovirus antigen

Newborn mice 2-3 days old were inoculated intramuscularly or intracranially with reovirus diluted in PBS. Mice were euthanized 8 days post-inoculation, and organs were resected and incubated in 10% formalin at room temperature for 24 to 48 h. Fixed organs were embedded in paraffin, and consecutive 6 mm sections were stained with hematoxylin and eosin for evaluation of histopathologic changes or processed for immunohistochemical detection of reovirus proteins (9).

APPENDIX A

CRYSTAL STRUCTURE OF REOVIRUS ATTACHMENT PROTEIN σ1 COMPLEX WITH SAILYLATED OLIGOSACCHARIDES

Dirk M. Rieter, Johnna M. Frierson, Elizabeth E. Halvorson, Takeshi Kobayashi, Terence S. Dermody, and Thilo S. Stehle

PLoS Pathogen. 7(8):e1002166; 2011

OPEN ACCESS Freely available online

PLoS PATHOGENS

Crystal Structure of Reovirus Attachment Protein σ1 in Complex with Sialylated Oligosaccharides

Dirk M. Reiter[1], Johnna M. Frierson[2,3], Elizabeth E. Halvorson[2,3¤a], Takeshi Kobayashi[3,4¤b], Terence S. Dermody[2,3,4]*, Thilo Stehle[1,4]*

1 Interfaculty Institute of Biochemistry, University of Tuebingen, Tuebingen, Germany, **2** Departments of Pathology, Microbiology, and Immunology, Vanderbilt University School of Medicine, Nashville, Tennessee, United States of America, **3** Elizabeth B. Lamb Center for Pediatric Research, Vanderbilt University School of Medicine, Nashville, Tennessee, United States of America, **4** Department of Pediatrics, Vanderbilt University School of Medicine, Nashville, Tennessee, United States of America

Abstract

Many viruses attach to target cells by binding to cell-surface glycans. To gain a better understanding of strategies used by viruses to engage carbohydrate receptors, we determined the crystal structures of reovirus attachment protein σ1 in complex with α-2,3-sialyllactose, α-2,6-sialyllactose, and α-2,8-di-siallylactose. All three oligosaccharides terminate in sialic acid, which serves as a receptor for the reovirus serotype studied here. The overall structure of σ1 resembles an elongated, filamentous trimer. It contains a globular head featuring a compact β-barrel, and a fibrous extension formed by seven repeating units of a triple β-spiral that is interrupted near its midpoint by a short α -helical coiled coil. The carbohydrate-binding site is located between β-spiral repeats two and three, distal from the head. In all three complexes, the terminal sialic acid forms almost all of the contacts with σ1 in an identical manner, while the remaining components of the oligosaccharides make little or no contacts. We used this structural information to guide mutagenesis studies to identify residues in σ1 that functionally engage sialic acid by assessing hemagglutination capacity and growth in murine erythroleukemia cells, which require sialic acid binding for productive infection. Our studies using σ1 mutant viruses reveal that residues 198, 202, 203, 204, and 205 are required for functional binding to sialic acid by reovirus. These findings provide insight into mechanisms of reovirus attachment to cell-surface glycans and contribute to an understanding of carbohydrate binding by viruses. They also establish a filamentous, trimeric carbohydrate-binding module that could potentially be used to endow other trimeric proteins with carbohydrate-binding properties.

Citation: Reiter DM, Frierson JM, Halvorson EE, Kobayashi T, Dermody TS, et al. (2011) Crystal Structure of Reovirus Attachment Protein σ1 in Complex with Sialylated Oligosaccharides. PLoS Pathog 7(8): e1002166. doi:10.1371/journal.ppat.1002166

Editor: Félix A. Rey, Institut Pasteur, France

Received March 9, 2011; **Accepted** May 31, 2011; **Published** August 4, 2011

Funding: This work was supported by Public Health Service awards T32 AI07611, R37 AI38296, and R01 AI76983 as well as the Elizabeth B. Lamb Center for Pediatric Research. Additional support was provided by Public Health Service awards P30 CA68485 for the Vanderbilt-Ingram Cancer Center and P60 DK20593 for the Vanderbilt Diabetes Research and Training Center. The funders had no role in study design, data collection and analysis, decision to publish, or preparation of the manuscript.

Competing Interests: The authors have declared that no competing interests exist.

* E-mail: thilo.stehle@uni-tuebingen.de (TS); terry.dermody@vanderbilt.edu (TSD)

¤a Current address: Department of Pediatrics, Wake Forest University School of Medicine, Winston-Salem, North Carolina, United States of America.
¤b Current address: Institute for Virus Research, Kyoto University, Kyoto, Japan.

Introduction

Viral infections are initiated by specific attachment of a virus particle to receptors at the surface of the host cell. This process, which serves to firmly adhere the virus to its cellular target, is rarely a bimolecular interaction between one viral attachment protein and one receptor. In most cases, several receptors are employed, and recognition events are frequently accompanied by substantial structural rearrangements that serve to expose new binding sites, strengthen the initial interaction, and prime the virus for cell entry. Structure-function analyses of virus-receptor interactions have provided detailed insights into the attachment strategies of viruses belonging to several different families [1–18]. However, much less is known about structure-function interrelationships between different binding sites for distinct receptors on the same viral attachment molecule.

Reoviruses are useful experimental models for studies of virus-receptor interactions and viral pathogenesis. Moreover, the recent development of plasmid-based reverse genetics for reovirus provides an opportunity to manipulate these viruses for oncolytic and vaccine applications. Reoviruses form icosahedral particles approximately 850 Å in diameter. At the virion five-fold symmetry axes, the trimeric attachment protein, σ1, extends from pentameric turrets formed by the λ2 protein. A similar arrangement of a trimeric attachment protein inserted into a pentameric base is also observed for the adenovirus attachment protein, fiber. The σ1 protein is about 400 Å long and consists of three discrete domains, termed tail, body, and head [19]. Residues 1 to 160 encompass the tail domain, which partially inserts into the virion capsid [20–22]. This region of the molecule is predicted to form an α-helical coiled-coil structure. The body domain encompasses residues 170 to 309 and contains β-spiral repeat motifs [22]. Lastly, the globular head domain incorporates residues 310 to 455 and folds into an 8-stranded β-barrel [22,23].

Reovirus attachment is thought to proceed via a two-step adhesion-strengthening mechanism, in which σ1 first engages widely distributed carbohydrate receptors with lower affinity. The three prototype reovirus strains, type 1 Lang (T1L), type 2 Jones

Author Summary

Human reoviruses bind first with low affinity to a carbohydrate receptor that brings the virus in close proximity to the host cell. This interaction then facilitates high-affinity binding to a second receptor, the tight junction component junctional adhesion molecule-A (JAM-A). While all human reoviruses bind JAM-A, they differ in carbohydrate receptor specificity, and this difference may influence the distinct disease patterns of reovirus serotypes. We present here the structure of the attachment protein of type 3 reovirus in complex with carbohydrates that naturally occur on human cells. Our results show that the protein forms an elongated trimer, with the carbohydrate binding site being located close to the midpoint of the molecule in a fiber-like region. Our findings provide insights into mechanisms of reovirus attachment to cell-surface glycans and contribute to an understanding of carbohydrate binding by viruses. They also establish a filamentous, trimeric carbohydrate-binding module that could potentially be used to introduce carbohydrate-binding properties into other trimeric proteins.

(T2J), and type 3 Dearing (T3D) recognize different carbohydrate structures, which may account for the serotype-specific differences in routes of spread in the host and end-organ tropism. In the case of serotype 3 (T3) reoviruses, the carbohydrate bound is α-linked sialic acid [24–26]. This initial contact, which has lower affinity and may allow for lateral diffusion of the particle at the membrane [27], is followed by high-affinity interactions with junctional adhesion molecule-A (JAM-A) [28], a component of tight junctions [29–31]. All reoviruses, including prototype and field-isolate strains, use JAM-A as a high-affinity receptor [28,32,33]. Firm adherence to the cell triggers uptake of the particle, which is dependent on β1 integrins [34,35].

Discrete regions of σ1 mediate binding to its cell-surface receptors. Structural and functional analyses show that the σ1 head, which projects farthest from the virus capsid, engages JAM-A [33,36,37]. In contrast, sequences in the σ1 body bind to carbohydrates [38]. Sequence analysis of reovirus variants identified three residues, Asn198, Arg202, and Pro204, as likely critical for the interaction of T3 σ1 with sialic acid. These residues lie near the midpoint of the protein, at the lower end of the body domain, about 100 Å away from residues in the head that interact with JAM-A. Earlier structural analyses of T3D σ1 [22,23,36] were based on constructs that did not include this putative carbohydrate-binding site. It is therefore currently unclear how σ1 achieves its specificity for sialic acid, whether the large distance between the two receptor-binding sites on σ1 is relevant for binding, or whether σ1 undergoes rearrangements after engaging its carbohydrate receptor.

To enhance an understanding of mechanisms by which viral attachment proteins engage cell-surface glycans, we determined the crystal structure of T3D σ1 in complex with α-2,3-sialyllactose, α-2,6-sialyllactose, and α-2,8-disialyllactose. All three carbohydrates terminate in sialic acid but feature different linkages that are present in various physiologic glycans. In addition, we used plasmid-based reverse genetics to engineer reoviruses that express mutagenized forms of σ1 to define residues required for functional binding to sialic acid. These studies shed light on the structural basis of σ1-sialic acid interactions and define a new carbohydrate-binding structural motif in a viral attachment protein.

Results

Construct Design and Structure Determination

The σ1 protein belongs to a class of fiber proteins constructed from triple β-spirals, a motif that was first identified in the adenovirus fiber [39]. In a previous study, we crystallized a smaller region of σ1, spanning residues 246 to 455 and containing three β-spiral repeats as well as the globular head domain [22]. While this structure provided no insights into the carbohydrate-binding region of σ1, it served as a basis to predict that β-spiral repeats form the entire body domain of the protein (residues 167–309) [22]. Near residue 170, the body domain transitions into a long α-helical coiled-coil region that forms the N-terminal tail domain (residues 1–156).

To determine the structure of a longer fragment of σ1 including the predicted sialic-acid binding residues 198, 202, and 204, we designed a construct for the expression of residues 170–455. This construct excluded the long α-helical coiled-coil region to simplify protein expression, purification, and crystallization. Prototype strain T3D σ1 is sensitive to trypsin-mediated cleavage after Arg245 [40]. However, a sequence polymorphism occurring in the majority of T3 field-isolate strains, Thr249Ile, renders the protein resistant to trypsin [40]. A construct containing Ile249 was therefore used in our study. Trimerization was promoted by using a hexahistidine-tagged trimerization domain, a modified GCN4 sequence [41], at the N-terminus of the expressed protein. This domain was proteolytically removed before final purification and crystallization.

Overall Structure of σ1

The structure of σ1 residues 170 to 455 reveals a highly elongated, symmetric trimer that measures about 200 Å in length (Table 1 and Figure 1A,B). Tail residues N-terminal to amino acid 170, which were not included in the crystallized protein, are predicted to form an α-helical coiled-coil structure that adds another 200 Å in length to the protein (Figure 1C). As expected,

Table 1. Data collection and refinement statistics.

σ1 in complex with	α-2,3-sl	α-2,6-sl	α-2,8-di-sl
Space group	$P2_12_12$	$P2_12_12$	$P2_12_12$
Unit cell dimensions (Å)	a = 87.15	a = 87.61	a = 87.19
	b = 333.18	b = 333.06	b = 331.84
	c = 58.49	c = 58.29	c = 58.13
Unit cell angles (°)	α = β = γ = 90	α = β = γ = 90	α = β = γ = 90
Resolution range (Å)	38.6–2.25	48.05–2.79	48.06–2.28
Completeness (%)	95.37	98.65	96.03
Total reflections	369038	547842	277926
Unique reflections	78324	43203	75913
R_{merge} (%)#	10.8	6.2	9.6
I/σI	13.5	18.6	18.6
R_{work} (%)*	15.77	15.69	17.31
R_{free} (%)*	19.89	20.48	22.03
r.m.s.d. bond lengths (Å)	0.006	0.007	0.006
r.m.s.d. bond angles (°)	0.960	1.12	1.01

r.m.s.d., root-mean-square deviation. sl, sialyllactose.
*$R_{work} = R_{free} = \Sigma| |F_{obs}(hkl)| - |F_{calc}(hkl)| |/\Sigma |F_{obs}(hkl)|$. R_{free} was calculated with 5% of the data.
#$R_{merge} = \Sigma | I - \langle I \rangle |/\Sigma I$
doi:10.1371/journal.ppat.1002166.t001

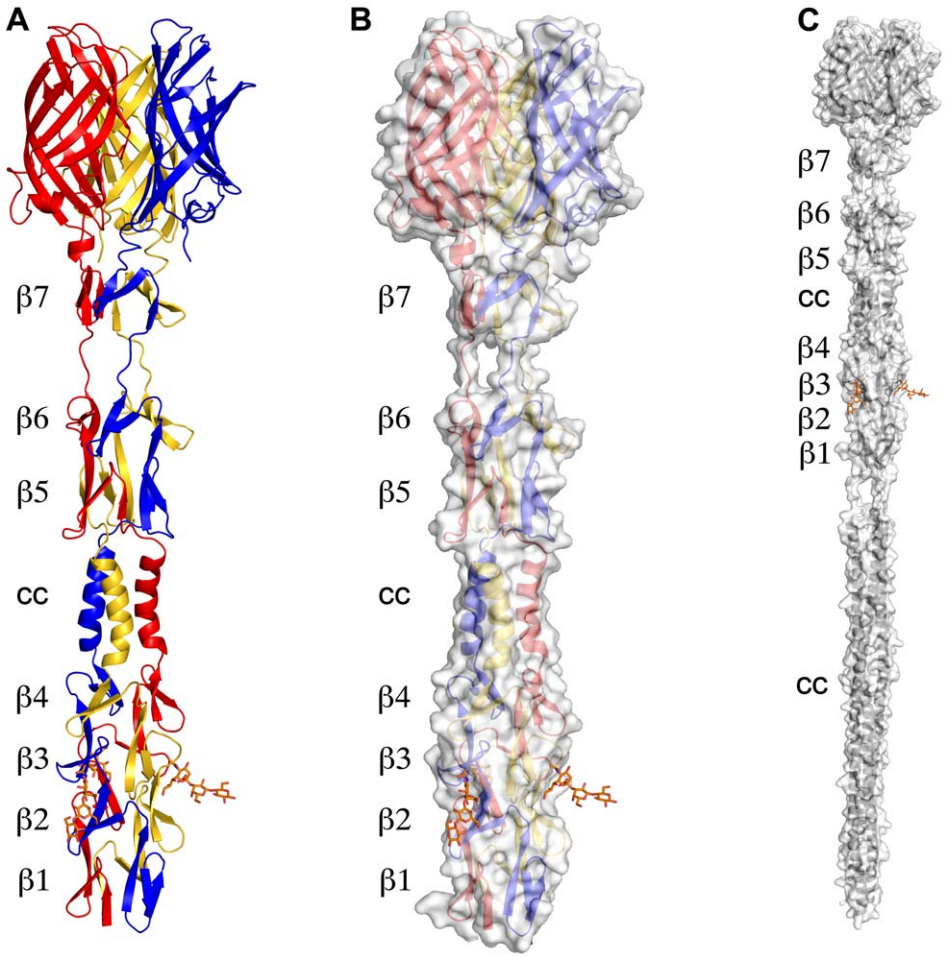

Figure 1. Structure of T3D σ1. (**A**) Ribbon drawing of the T3D σ1 body and head domains in complex with α-2,3-sialyllactose. The σ1 monomers are shown in red, blue, and yellow. The body domain consists of seven triple β-spiral repeats (β1–β7) and an α-helical coiled-coil domain (cc) that is inserted between β-spiral repeats β4 and β5. The bound α-2,3-sialyllactose is shown in stick representation and colored in orange. (**B**) Molecular surface of the σ1 structure, shown in semitransparent white coloring. (**C**) Model of full-length σ1, including a computer-generated trimeric α-helical coiled coil structure spanning σ1 residues 1–160 at the N-terminus.
doi:10.1371/journal.ppat.1002166.g001

the structure of the globular head domain (residues 310 to 455) is essentially identical to that described previously [22]. However, the body domain displays a number of unusual features. Although sequence-based predictions suggested that this region would be composed of eight consecutive triple β-spiral repeats [22], we find that the body domain contains a mixture of α-helical coiled-coil and β-spiral repeats (Figure 1). Four β-spiral repeats at the N-terminus (β1–β4, residues 170 to 235) are followed by a short α-helical coiled-coil (cc, residues 236 to 251) and three additional β-spiral repeats (β5-β7, residues 252 to 309) (Figure 2). Inspection of the sequence indicates a likely reason for the deviation from the β-spiral fold at the center of the body (Figure 2B). Three hydrophilic residues (Thr236, Ser244, and Ser252) are located at positions that are typically occupied by hydrophobic side chains in β-spirals. Moreover, Ser241 replaces a characteristic proline or glycine at the turn in a β-spiral repeat. While some deviations from the β-spiral consensus sequence can be tolerated, even residues replacing the glycine or proline (e.g., residues Gln224 or Thr278), the cumulative effect of the four non-consensus residues results in a β-spiral no longer being the optimal fold. The α-helical coiled-coil structure contains two heptad-repeat sequences, starting with Phe239 and ending with Gln251 (Figure 2A,C).

Structure of σ1 in Complex with α-2,3-Sialyllactose

To elucidate the structural basis of the interaction of the reovirus attachment protein σ1 with its carbohydrate coreceptor, we prepared a complex by soaking crystals of σ1 with 10 mM α-2,3-sialyllactose, a compound that terminates in α-linked sialic acid. The subsequent structure, determined at 2.25 Å resolution (Table 1), unambiguously demonstrated the location of the carbohydrate in an unbiased difference electron-density map (Figure 3A). The oligosaccharide binds in a shallow groove next to the loop connecting the second and third β-spiral repeats. The σ1 protein contains three identical binding sites, one on each chain, and all three are occupied by α-2,3-sialyllactose molecules, with the sialic acid making identical and extensive contacts in each chain (Figure 3B,C). The lactose moieties face different directions, probably as a result of internal flexibility and participation in crystal contacts (Figure 3C).

Sialic acid contains four characteristic functional groups: a carboxylate at C1, a hydroxyl group at C4, an N-acetyl group at C5, and a glycerol chain at C6. All four groups are recognized by σ1 (Figure 3B). Arg202 forms a bidentate salt bridge with the carboxyl group. A single hydrogen bond links the hydroxyl group at C4 to the carbonyl of Gly205. The amide of the N-acetyl group

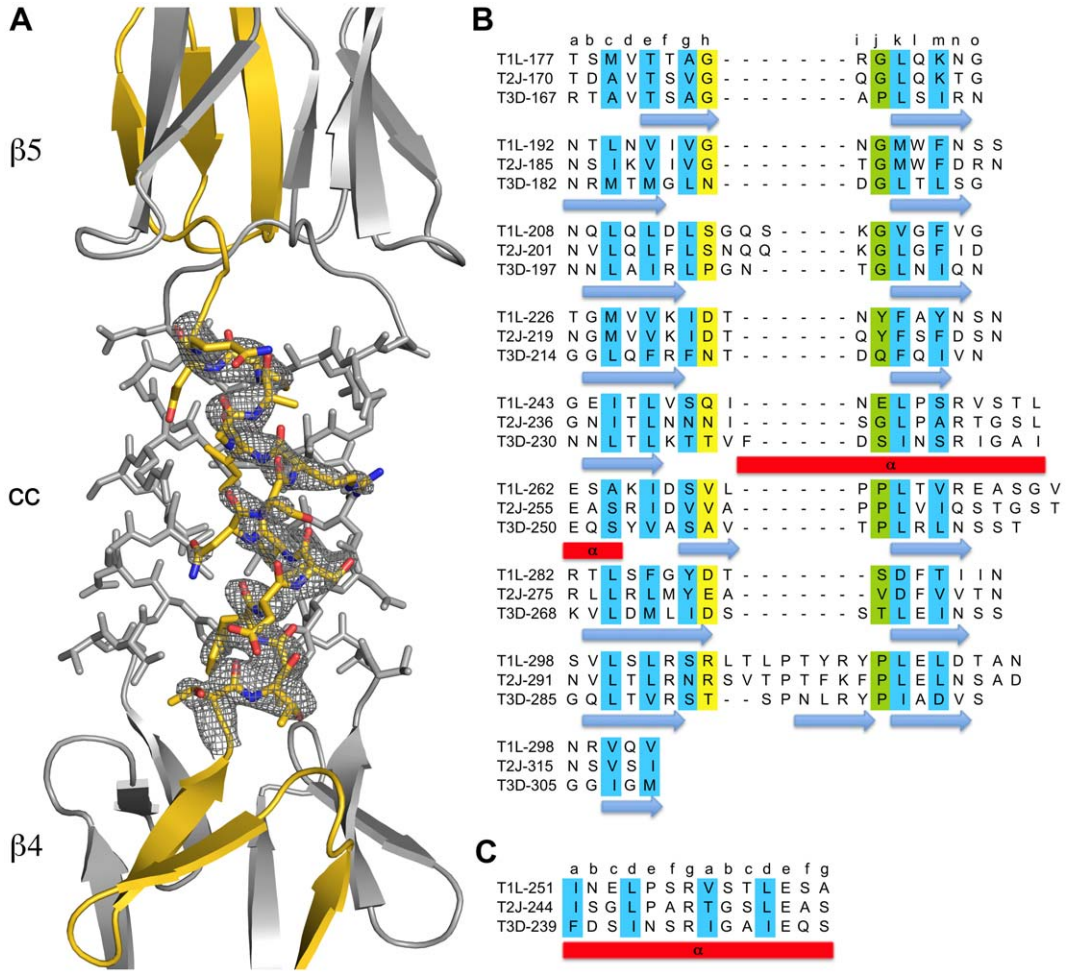

Figure 2. Structural features of the T3D σ1 body domain and sequence alignments with T1L and T2J σ1. (**A**) Close-up view of the α-helical coiled-coil that separates β-spirals 4 and 5 in the T3D σ1 body domain. The coiled-coil region is shown as a stick model, while the adjacent β-spiral repeats are depicted as a ribbon drawing. A simulated annealing omit difference map for one chain is shown with a radius of 2.2 Å and a contour level of 3σ. (**B**) The residues are aligned according to the triple β-spiral consensus sequence (a–o), with typically hydrophobic residues (c, e, g, k, and m) indicated in cyan and the position in the β-turn usually occupied by proline or glycine (j) in green. (**C**) Sequence analysis of the coiled-coil region in the body domain. Residues 239–252 are organized in heptads (a–g), and the coiled-coil consensus is indicated with typically hydrophobic residues (a and d) highlighted in cyan.
doi:10.1371/journal.ppat.1002166.g002

is engaged in a hydrogen bond with the backbone carbonyl of Leu203, and the N-acetyl methyl group is facing into a partially hydrophobic cavity. The glycerol chain lies parallel to the peptide backbone, forming direct hydrogen bonds with the backbone carbonyl of Ile201 and the amide nitrogen of Leu203 and in some of the binding sites water-mediated hydrogen bonds with the Asn210 side chain and the amide nitrogen of Ile211. We note that Arg202, which was previously shown to influence sialic acid binding [42], provides a key contact to the ligand. Moreover, Pro204, which also had been implicated in sialic acid binding [42], is part of a structure that shapes the ligand-binding site.

Structures of σ1 in Complex with α-2,6-Sialyllactose and α-2,8-Disialyllactose

As contacts in the complex of σ1 with α-2,3-sialyllactose exclusively involve the sialic acid moiety, we hypothesized that σ1 should be capable of binding sialic acid in different naturally occurring linkages, including α-2,6- and α-2,8-linked sialic acid. We therefore determined crystal structures of σ1 in complex with α-2,6-sialyllactose (Figure 4A) and α-2,8-disialyllactose (Figure 4B). Refinement statistics for both structures are provided in Table 1. In each case, only two of the binding sites are occupied, as the third is partially blocked by crystal contacts. For the α-2,6-sialyllactose complex, the electron density allowed us to unambiguously identify all three sugar residues (Figure 4A). The electron density for the α-2,8-disialyllactose complex did not allow us to model the terminal glucose. Comparison of these structures with each other and with the α-2,3-sialyllactose complex shows that the terminal sialic acid is bound in the same conformation and with identical contacts in all three cases. However, the remaining moieties of the glycans differ in conformation and contacts with σ1. The α-2,3-sialyllactose and α-2,8-disialyllactose ligands assume an elongated shape in which the lactose groups face away from the protein (Figure 3C, Figure 4B). Inspection of the α-2,8-disialyllactose complex shows that the N-acetyl group of the second sialic acid forms a hydrogen bond to the side chain of Ser195. In contrast, σ1 binds α-2,6-sialyllactose in a folded-back conformation (Figure 4A). This conformation is stabilized by an

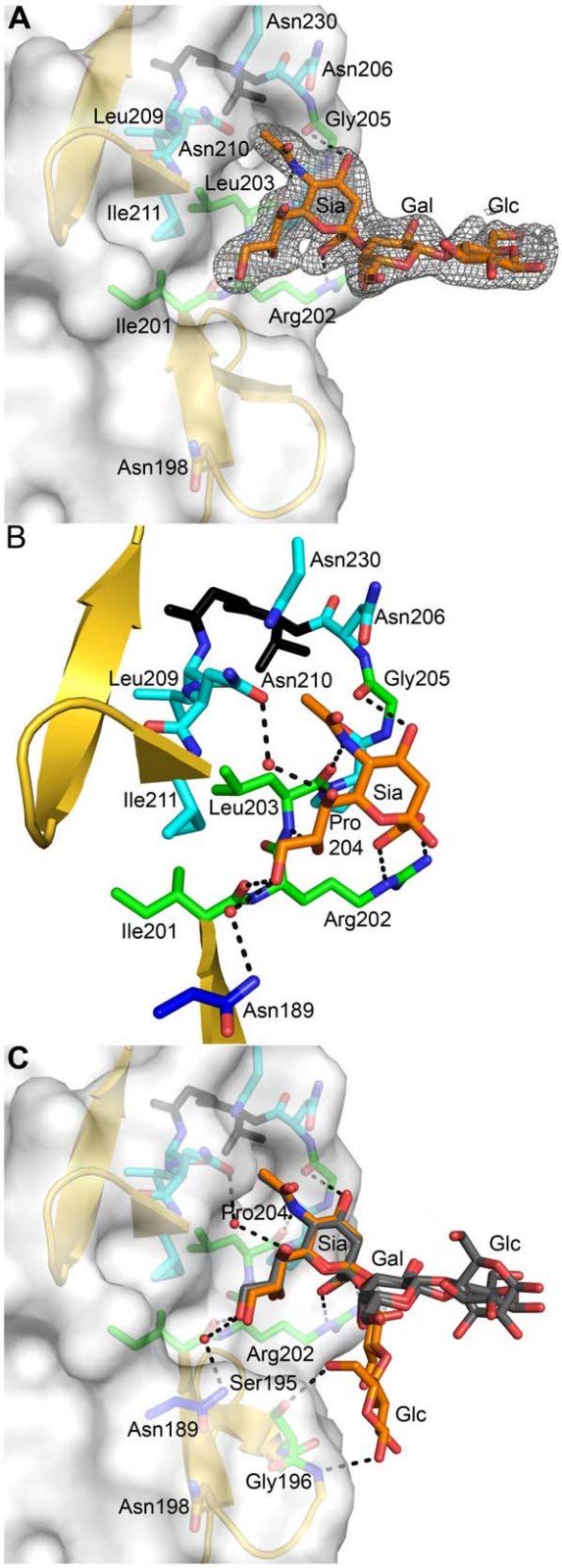

Figure 3. Interactions between σ1 and sialic acid. (**A**) Simulated annealing omit difference density map contoured at 3σ and displayed with a radius of 2.2 Å around the bound α-2,3-sialyllactose. The sugar moieties are labeled Sia (sialic acid), Gal (galactose), and Glc (glucose) here and in subsequent figures. (**B**) Detailed interactions between σ1 and the terminal sialic acid of α-2,3-sialyllactose. Residues in the binding region are drawn in ball and stick representation, while the rest of the protein is shown as a ribbon drawing. The σ1 residues forming hydrogen bonds or salt bridges with the ligand are shown in green, and residues forming van der Waals contacts are shown in cyan. The side chain of Asn189 (colored dark blue) is contributed by a neighboring σ1 monomer (see also Figure 1A). Sialic acid is shown in ball-and-stick representation, with carbons colored orange, oxygens colored red, and nitrogens colored blue. Bridging waters are shown as orange spheres. Hydrogen bonds and salt bridges are represented with broken lines. (**C**) Superposition of all three bound ligands into a single binding site. The superposition was performed using σ1 residues only. While the orientation of the terminal sialic acid is nearly identical, the lactose moieties are facing in different orientations as a result of their participation in different crystal contacts.
doi:10.1371/journal.ppat.1002166.g003

intramolecular hydrogen bond and the galactose O2 and O3 hydroxyl groups, which form hydrogen bonds to the backbone carbonyl atoms of Ser195 and Leu194, respectively.

Residues in Reovirus σ1 Required for Sialic Acid Binding

To identify sequences that influence sialic acid binding, we used plasmid-based reverse genetics [43,44] to introduce point mutations into the σ1 protein of reovirus strain T3D. Mutant viruses were isolated following co-transfection of murine L929 cells with RNA-encoding plasmids corresponding to the T3D *L1-L3*, *M1-M3*, and *S2-S4* genes and a plasmid corresponding to the σ1-encoding *S1* gene incorporating site-specific mutations. Thus, each recombinant virus is isogenic, with the exception of the *S1* gene and its protein product, σ1. Guided by the structure of the σ1-sialic acid complexes, we engineered individual alanine substitutions of amino acids ranging from Asn189 to Asn210. By their location in the structure, we hypothesized that these residues would be required for functional sialic acid binding. In addition, substitutions N198D, R202W, and P204L, which have been implicated in sialic acid binding by sequence comparisons of reovirus strains that differ in sialic acid utilization [26,45] and genetic analysis of reovirus mutants adapted to growth in murine erythroleukemia (MEL) cells [42], were engineered to define the effect of these polymorphisms in an otherwise isogenic background.

After confirming the σ1-encoding S1 gene nucleotide sequences, the mutant viruses were tested for hemagglutination (HA) capacity (Figure 5) and growth in L929 cells and MEL cells (Figure 6). In comparison to rsT3D, rsT3D-σ1N198D, rsT3D-σ1R202A, rsT3D-σ1R202W, rsT3D-σ1L203A, rsT3D-σ1P204A, rsT3D-σ1P204L, and rsT3D-σ1G205A produced little or no agglutination of calf erythrocytes, a sensitive assay for sialic acid binding [26]. However, rsT3D-σ1N189A, rsT3D-σ1S195A, and rsT3D-σ1N210A produced HA titers that were comparable to those of wild-type rsT3D. Each of the point-mutant viruses produced approximately 1000-fold yields of viral progeny after growth in L929 cells (Figure 6), a cell line that does not require sialic acid binding for reovirus to replicate [45]. In contrast, those containing mutations N198D, R202A, R202W, L203A, P204A, P204L, and G205A displayed attenuated growth in MEL cells (Figure 6), a cell line permissive only to sialic acid binding reovirus strains [45]. These findings indicate that viruses with mutations of residues 198, 202, 203, 204, and 205 are altered in sialic acid binding efficiency, suggesting that these residues serve a functional role in T3D σ1-sialic acid interactions.

Discussion

Although all known reovirus strains engage cells by binding to the tight junction protein JAM-A [33], the major reovirus serotypes differ in the routes of dissemination in the host and

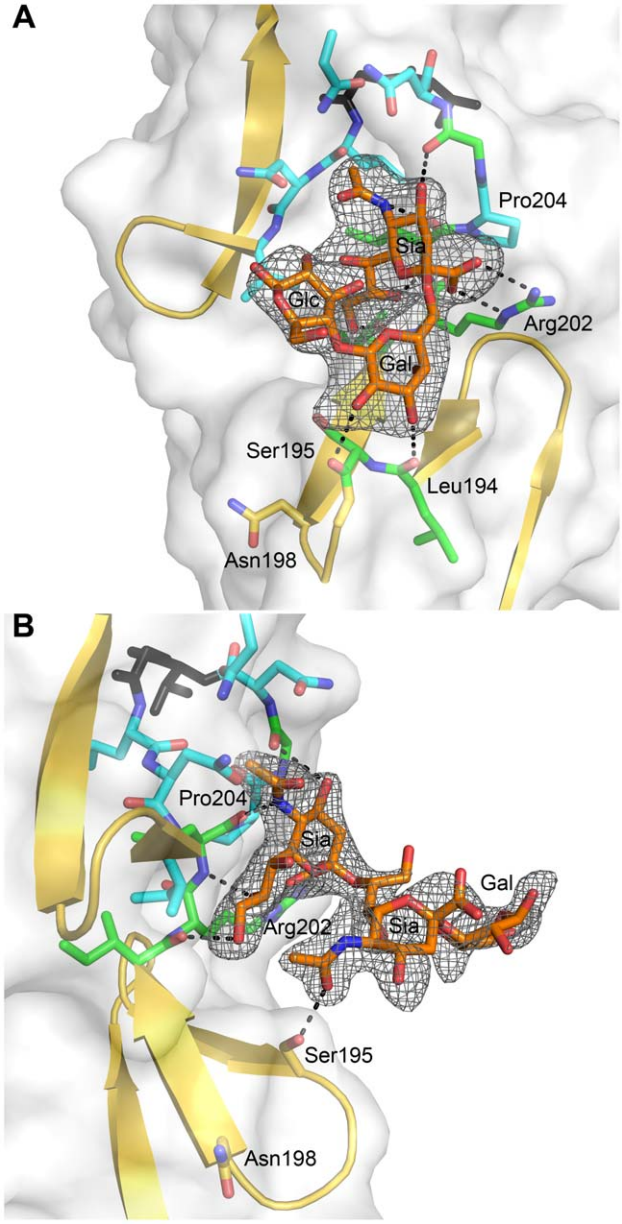

Figure 4. σ1 in complex with sialic acid in different linkages. (A) View into the carbohydrate-binding site of the complex of σ1 with α-2,6-sialyllactose. (B) View into the carbohydrate-binding site of the complex of σ1 with α-2,8-disialyllactose. The orientation in panel (A) differs by 60 degrees along a vertical axis from the orientations shown in panel (B) and Figure 3 to provide a clearer view into of the binding site. In both panels, σ1 residues directly contacting the ligand are shown in green, and surrounding residues making van der Waals contacts are shown in cyan. The ligands are shown in ball-and-stick representation, with carbons colored orange, oxygens colored red, and nitrogens colored blue. Hydrogen bonds are represented with broken black lines. The maps are simulated annealing omit difference density maps contoured at 3σ and displayed with a radius of 2.2 Å around the ligands.
doi:10.1371/journal.ppat.1002166.g004

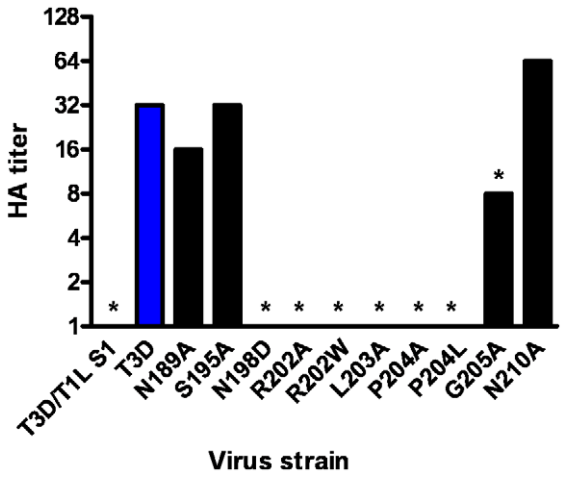

Figure 5. HA assay of T3D σ1 point mutants. Purified reovirus virions (10^{11} particles) were serially diluted in 0.05 ml of PBS in 96-well U-bottom microtiter plates. Bovine erythrocytes were washed twice with PBS and resuspended at a concentration of 1% (vol/vol) in PBS. Erythrocytes (0.05 ml) were added to wells containing virus and incubated at 4°C for at least 2 h. HA titer is expressed as 10^{11} particles divided by the number of particles/HA unit. One HA unit equals the number of particles sufficient to produce HA. *, $P<0.05$ in comparison to T3D (Student's *t* test).
doi:10.1371/journal.ppat.1002166.g005

tropism for host tissues [46–48]. These differences are linked to the σ1-encoding S1 gene segment and most likely attributable to serotype-specific interactions of σ1 with different cell-surface receptors. T3 reoviruses require sialic acid as a coreceptor, but the context in which sialic acid is bound is unknown. To define this interaction, we determined crystal structures of reovirus σ1 in complex with three sialylated glycans that incorporate a terminal sialic acid moiety in different linkages. These structural analyses were complemented with mutagenesis experiments that establish the physiologic relevance of the observed interactions.

The σ1 protein uses a complex network of contacts to engage terminal sialic acid, which is a common feature of all three glycans studied here. The interactions involve σ1 residues at the lower end of the body domain, between β-spirals 2 and 3. At this location, the sialic acid moiety docks into a shallow pocket that is formed mainly by residues in the third β-spiral. All four functional groups of sialic acid make contacts with σ1 through an elaborate network of hydrogen bonds and van der Waals interactions. Mutations that alter these contacts lead to significantly reduced sialic acid binding as assessed by HA profiles and diminished infection of MEL cells. Although all three ligands used for complex formation with σ1 contain additional carbohydrates, these make very few interactions. The complex with α-2,8-disialyllactose identified a hydrogen bond between the N-acetyl group of the second sialic acid and the side chain of Ser195 (Figure 4B). However, the results from mutagenesis experiments demonstrate that a Ser195A mutation has no effect on either HA capacity or viral growth. Therefore, the observed contact is unlikely to have physiologic relevance. The interactions between σ1 and α-2,6-sialyllactose identified two hydrogen bonds that link the galactose to the protein and may help to stabilize the folded-back conformation of the ligand (Figure 4A). As both contacts involve main chain atoms of σ1, their functional significance cannot be easily probed by site-directed mutagenesis. Nevertheless, it is likely that the observed contacts lead to a modest increase in the affinity of σ1 for compounds terminating in α-2,6-linked sialic acid. It is unclear if such an increase is biologically significant.

Naturally occurring sequence variability at three amino acid positions (residues 198, 202, and 204) has been linked to the sialic acid-binding capacity of T3 σ1 [26,42]. Our structures readily identify two of these residues, Arg202 and Pro204, as key

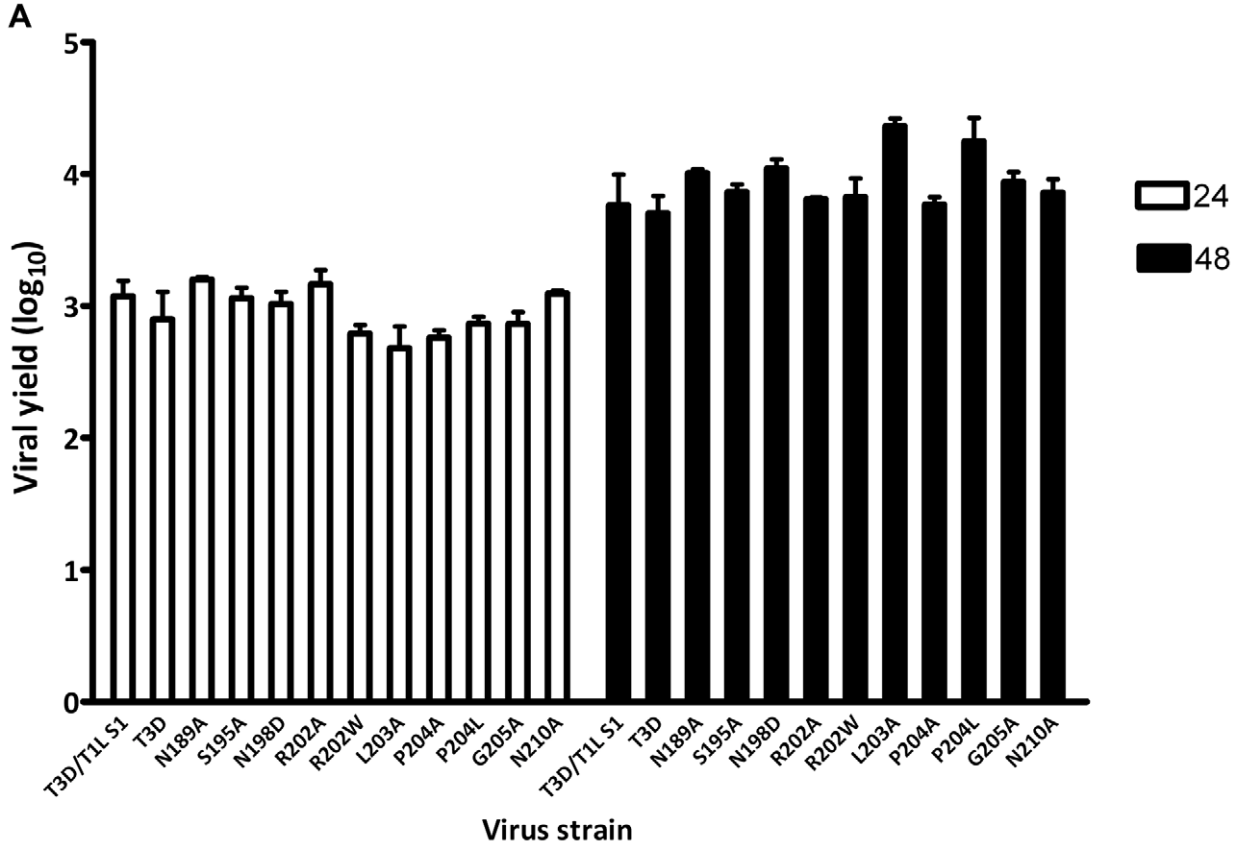
A
Viral yield (log_{10})
0
1
2
3
4
5
24
48
T3D/T1L S1
T3D
N189A
S195A
N198D
R202A
R202W
L203A
P204A
P204L
G205A
N210A
T3D/T1L S1
T3D
N189A
S195A
N198D
R202A
R202W
L203A
P204A
P204L
G205A
N210A
Virus strain

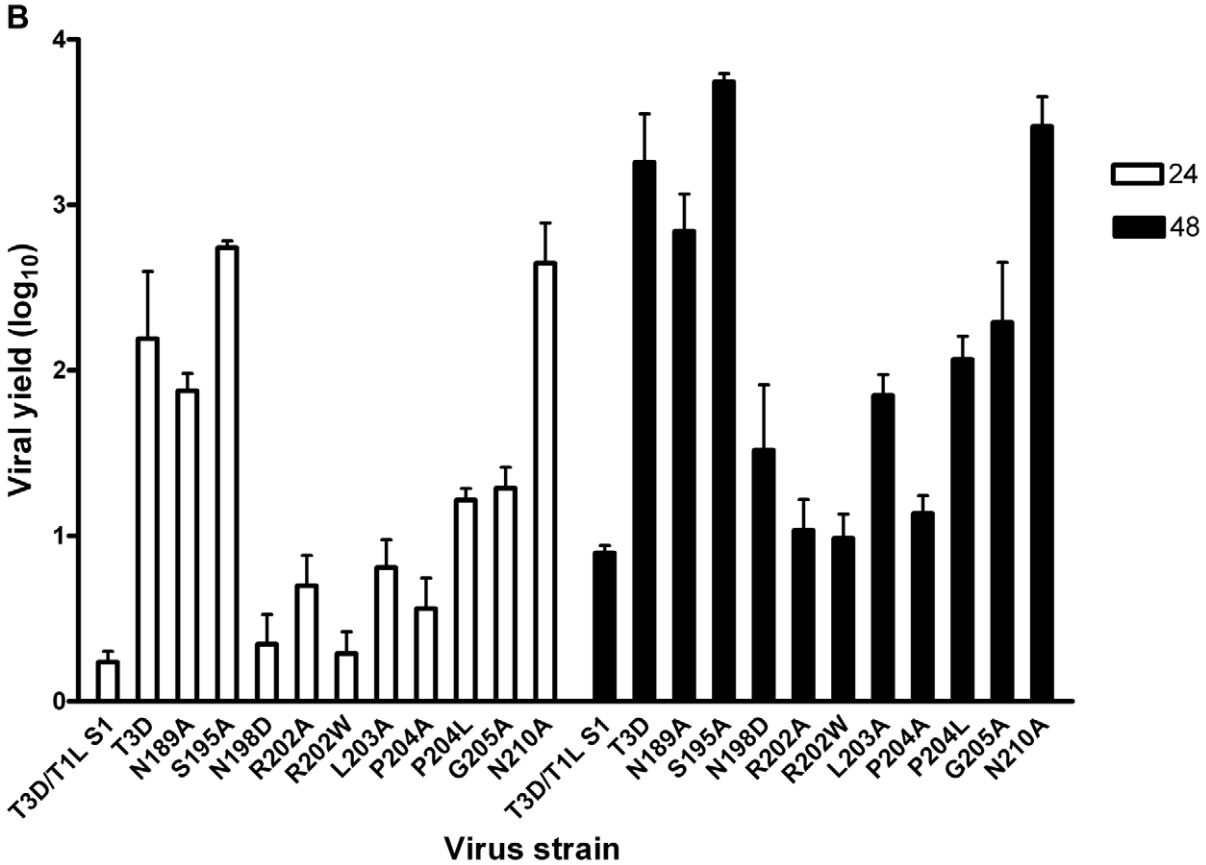
B
Viral yield (log_{10})
0
1
2
3
4
24
48
T3D/T1L S1
T3D
N189A
S195A
N198D
R202A
R202W
L203A
P204A
P204L
G205A
N210A
T3D/T1L S1
T3D
N189A
S195A
N198D
R202A
R202W
L203A
P204A
P204L
G205A
N210A
Virus strain

Figure 6. Identification of σ1 residues required for binding to cell-surface sialic acid. (A) Infection of murine fibroblast (L929) cells or **(B)** murine erythroleukemia (MEL) cells by wild-type or point-mutant viruses. Cells were adsorbed with virus at an MOI of 1 PFU/cell. Following incubation at room temperature for 1 h, the inoculum was removed, and cells were incubated at 37°C for 24 and 48 h. Viral titers were determined by plaque assay. The results are expressed as viral yields ($\log_{10}$ titer at $t = 24$ or 48 h minus $\log_{10}$ titer at $t = 0$ h) for triplicate samples. Error bars indicate S.D. *, $P < 0.05$ in comparison to T3D (Student's t test).
doi:10.1371/journal.ppat.1002166.g006

determinants of sialic acid binding. The side chain of Arg202 forms a salt bridge with the sialic acid carboxylate group, while the Pro204 side chain stacks against the Arg202 guanidinium group. Moreover, the carbonyl oxygen in the peptide bond linking Leu203 and Pro204 forms a hydrogen bond with the sialic acid. Substitutions of either Arg202 or Pro204, as seen in the R202W and P204L variants, would decrease the affinity for sialic acid, and this is confirmed by the mutagenesis data. In contrast, the critical role of residue 198 in ligand recognition is not apparent from the crystal structures. Our mutagenesis data (Figure 5 and Figure 6), in conjunction with previous results [42], clearly demonstrate that Asn198 is required for successful sialic acid-dependent infection, with viruses carrying an N198D mutation having substantially reduced infectivity in MEL cells. However, the crystal structures show that Asn198 is not involved in direct or water-mediated contacts to any of the three oligosaccharides. Furthermore, the Asn198 side chain is solvent-exposed, forming a single hydrogen bond with the Asn189 side chain. Mutation of Asn189 to alanine does not affect sialic acid binding (Figure 5 and Figure 6), suggesting that the observed Asn198-Asn189 hydrogen bond is not relevant for ligand recognition. It is possible that the introduction of a negatively charged side chain at position 198, as is the case with the N198D mutation, leads to long-range electrostatic effects or structural rearrangements that indirectly affect receptor binding. However, given the distance of Asn198 from the binding site and its surface-exposed location, this possibility appears remote. We think it more likely that Asn198 serves as a contact point with a part of the functionally relevant glycan, which has not been included in the structural analysis. Although our results define the interactions of σ1 with terminal sialic acid, the actual receptor may be a more complex sialylated glycan, perhaps carrying several branches. Such complex receptor structures, which can be attached to proteins or lipids, have recently been identified as the true ligands for several adenovirus and polyomavirus capsid proteins [16–18]. Therefore, Asn198 may well define a second receptor contact point for reovirus σ1.

A large collection of structures of viruses or viral attachment proteins in complex with sialylated oligosaccharide receptors is available, and these have produced significant insights into mechanisms of sialic acid binding, receptor specificity, and viral pathogenesis [1–3,5,9,11,14,16–18,49–52]. However, the interactions observed between T3D σ1 and sialic acid differ in important ways from those found in all other virus-receptor complexes, offering new insights into the parameters that guide viral attachment and specificity. In all cases in which structures are available, the receptors are bound by a globular domain in a region that projects farthest from the viral capsid and is easily accessible for interactions with the cell surface. In contrast, the highly elongated T3D σ1 protein engages its carbohydrate ligand at its midpoint, about 150 Å away from the region that projects farthest from the virion. Although the σ1 protein possesses some flexibility at defined regions [19,22], the location of the sialic acid-binding site would not appear optimal for engagement of membrane-bound receptors that feature sialylated ligands close to the membrane. The region of JAM-A that is engaged by the σ1 head domain is fairly close to the membrane [36]. Even when allowing for considerable flexibility between the σ1 head and body, it is difficult to envision a conformation in which the tail of σ1 is still inserted into the virus and the sialic acid binding site can closely approach the membrane. However, σ1 could more easily engage sialic acid that projects far above the membrane, perhaps by being located on a large protein or projecting from prominent loops.

Prior to this study, structural information had been available only for the C-terminal portion of the σ1 protein [22]. Based on analysis of that structure, as well as sequence comparisons with the related adenovirus fiber protein, full-length σ1 was predicted to fold into three distinct regions: an N-terminal α-helical coiled coil (termed the tail), a region containing eight consecutive β-spiral repeats (the body), and a globular β-barrel (the head). Our structural analysis of a fragment comprising the body and head domains show that this model must be revised, as we find an insertion of a short α-helical coiled coil that interrupts the β-spiral sequence in the body, replacing one β-spiral repeat with a helical structure. Thus, it is clear that the structure of σ1 features several transitions between α-helical and β-spiral regions. This topological relationship differs from that of the adenovirus fiber, in which the shaft domain is thought to consist entirely of β-spiral repeats [39]. Examination of the T3D body domain sequence shows that it contains a nearly perfect heptad repeat pattern, which is typical for α-helical coiled coils, in a short stretch of 14 residues (Figure 2). A similar pattern is observed in the T1L and T2J σ1 sequences, but a proline residue within the consensus makes it unlikely that these proteins also feature a continous α-helical coiled coil at the equivalent location.

To our knowledge, the structures presented here are the first examples of any fibrous viral protein engaging a ligand via its repetitive fiber region. Other viral attachment proteins contain fibrous- or stalk-like structures, but they usually engage receptors with globular head domains placed on top of these structural elements, as observed in complexes of adenovirus fiber proteins with their receptors [7,15,18]. Globular head domains offer higher variability in engaging ligands and can more easily create recessed binding pockets suitable for high-affinity binding. Instead, fiber-like structures generally feature short connections between their repeating units and a relatively flat surface, limiting binding options. However, inspection of the β-spirals in σ1 reveals subtle modifications in a single repeat that allow it to create a shallow binding site for sialic acid. One of the hallmarks of β-spirals is a highly conserved β-turn between two strands, involving residues at positions g, h, i, and j (Figure 2). The residue at position j is usually a proline or glycine. This turn is enlarged by two amino acids in the σ1 repeat that engages sialic acid, transforming the turn into a small loop (Figure 7). Interestingly, Pro204 introduces a kink after a β-strand, causing the chain to deviate from the β-spiral motif at this position to provide a pocket for the ligand. Thus, alteration of the typical repeating motif identifies a ligand-binding site in the case of σ1. It is conceivable that similar aberrations in other fibrous protein sequences might also indicate binding sites. The location of a sialic acid binding site in an elongated fiber-like structure also raises the possibility of creating a small sialic acid binding cassette that could be transferred into a variety of trimeric fiber-like proteins constructed from α-helical coiled coils or β-spirals. Our work thus enhances an understanding of reovirus-

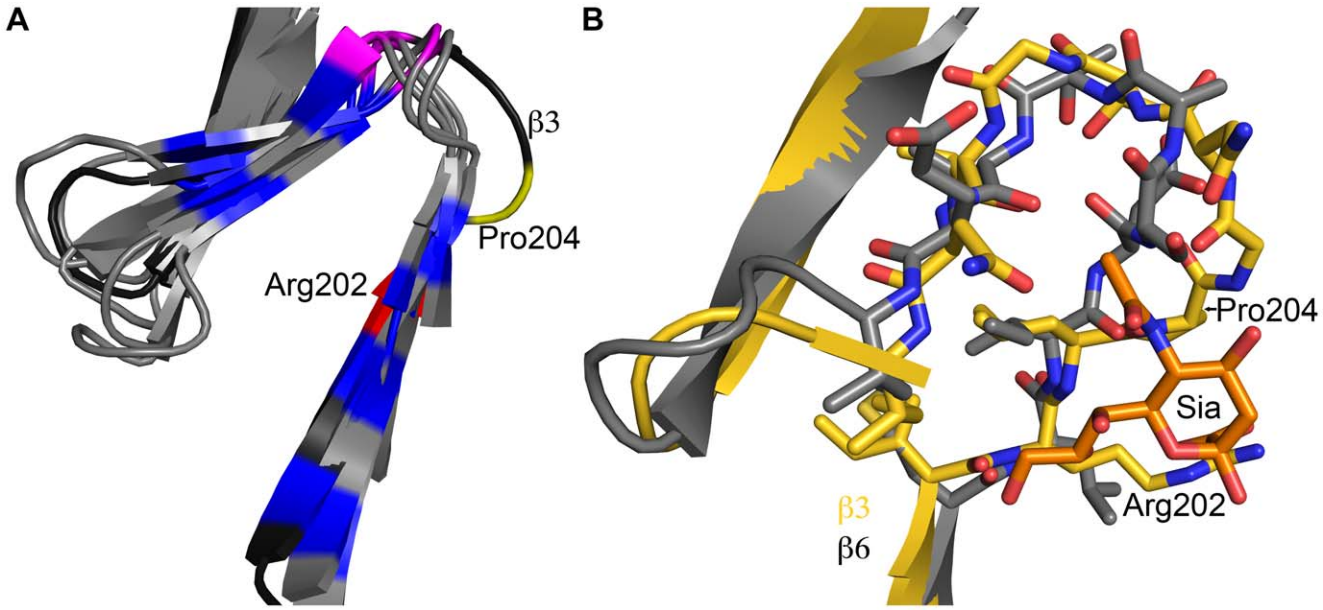

Figure 7. Structural adaption of the binding site. (**A**) Superposition of all seven β-spiral repeats. Repeat β3, which is shown in darker shading, interacts with sialic acid and deviates markedly in its structure from the other repeats. Conserved hydrophobic residues are colored in blue, the position in the β-turn that is usually occupied by proline or glycine is shown in magenta. Arg202 and Pro204, which are part of repeat β3, are highlighted in red and yellow, respectively. (**B**) Superposition of a prototypical β-spiral repeat (β6) onto the sialic acid binding repeat β3. Amino acids are shown in ball and stick representation, and residues Arg202 and Pro204 in β3 are labeled. Panel B is enlarged to provide a clearer view.
doi:10.1371/journal.ppat.1002166.g007

glycan interactions and may also guide the construction of new sialic acid binding platforms to facilitate structure-function analyses and sialic acid-mediated cell targeting.

Materials and Methods

Protein Expression and Purification

The expression of soluble and properly folded T3D σ1 trimers was facilitated by appending a trypsin-cleavable trimerization domain based on the GCN4 leucine zipper [41] N-terminally to a cDNA encoding the entire σ1 body and head domains (amino acids 170–455). The construct was cloned into the pQE-80L expression vector, which encodes a non-cleavable N-terminal hexahistidine-tag. The protein was expressed in *E. coli Rosetta 2 DE3* (Novagen) at 20°C for 16 h post-induction or by autoinduction at 20°C for 48–72 h. Bacteria were lysed by two passages through an EmulsiFlex (Avestin) homogenizer and purified by Ni-IMAC using His-Trap-FF columns (GE-Healthcare). The immobilized protein was eluted by on-column digestion with 0.1 mg/ml trypsin at a flowrate of 0.1 ml/min for 12 h. Size-exclusion chromatography (Superdex-200, GE-Healthcare) was used as the final purification step.

X-ray Structure Determination

Crystals were grown using 15% PEG200, 0.1 M MES (pH 6.5) as a precipitant. The crystals belong to space group $P2_12_12$ and contain one trimer in the asymmetric unit. Complexes with carbohydrate ligands were prepared by soaking crystals with the respective carbohydrate prior to data collection. The crystals were transferred into mother liquor supplemented with 10 mM carbohydrate, incubated for 5 min, and cryoprotected by incubation for 15 s in 35% PEG200, 0.1 M MES, 10 mM carbohydrate (pH 6.5).

Diffraction data were collected at the beamlines PXI (SLS) and ID14-4 (ESRF). Diffraction data were integrated and scaled using XDS [53], and the structure was solved by molecular replacement with AMoRe [54] using the structure of the T3D σ1 head (PDB ID 1KKE) as a search model. Refinement was performed with Refmac5 [55] and Phenix [56], and model building was done in Coot [57]. Ligands were fitted into weighted F_o-F_c difference density maps at a contour level of 3σ and refined using the CCP4 library and user-defined restraints. Coordinates and structure factors for all three complexes have been deposited in the PDB data bank (www.rcsb.org) with accession codes 3S6X (complex with α-2,3-sialyllactose), 3S6Y (complex with α-2,6-sialyllactose) and 3S6Z (complex with α-2,8-di-sialyllactose).

Cells

L929 cells [58] were maintained in Joklik's minimum essential medium (Sigma-Aldrich) supplemented to contain 5% fetal bovine serum, 2 mM L-glutamine, 100 U/ml of penicillin, 100 μg/ml of streptomycin, and 25 ng/ml of amphotericin B. MEL cells, previously designated T3cl.2 cells [59], were maintained in Ham's F-12 medium (CellGro) supplemented to contain 10% fetal bovine serum, 2 mM L-glutamine, 100 U/ml penicillin, 100 μg/ml streptomycin, and 25 ng/ml amphotericin B.

Viruses

Recombinant reoviruses were generated by plasmid-based reverse genetics [43,44]. Reovirus strains rsT3D (wild type), rsT3D-σ1N198D, rsT3D-σ1R202W, and rsT3D-σ1P204L were recovered using monolayers of L929 cells at approximately 90% confluence (3×10^6 cells) in 60-mm dishes (Costar) infected with rDIs-T7pol [60] at an MOI of ~0.5 $TCID_{50}$. At 1 h post-infection, cells were co-transfected with ten plasmid constructs representing the cloned T3D genome using 3 μl of TransIT-LT1 transfection reagent (Mirus) per μg of plasmid DNA [43]. Reovirus strains rsT3D-σ1N189A, rsT3D-σ1S195A, rsT3D-σ1R202A, rsT3D-σ1L203A, rsT3D-σ1P204A, rsT3D-σ1G205A, and

rsT3D-σ1N210A were recovered using BHK-T7 cells at 90% confluence (approximately 3×10^6 cells) seeded in 60-mm dishes. Cells were co-transfected with five plasmids representing the cloned T3D genome using 3 µl of TransIT-LT1 transfection reagent (Mirus) per µg of plasmid DNA [44]. The amount of each plasmid used for transfection was identical to that described for L929 cell transfections. Following 3 to 5 days of incubation, recombinant viruses were isolated from transfected cells by plaque purification using monolayers of L929 cells [61]. For the generation of σ1 mutant viruses, pT7-S1T3D [43] was altered by QuikChange (Stratagene) site-directed mutagenesis. To confirm sequences of the mutant viruses, viral RNA was extracted from purified virions and subjected to Onestep RT-PCR (Qiagen) using *L1*- or *S1*-specific primers. (Primer sequences are available from the corresponding authors upon request.) The purified PCR products were subjected to sequence analysis for the presence of the introduced mutation in the *S1* gene segment and the noncoding signature mutation in the *L1* gene segment [43].

Purified reovirus virions were prepared using second-passage L929-cell lysate stocks of twice plaque-purified reovirus as described [20]. Viral particles were Freon-extracted from infected cell lysates, layered onto CsCl gradients, and centrifuged at 62,000 × *g* for 18 h. Bands corresponding to virions (1.36 g/cm^3) [62] were collected and dialyzed in virion-storage buffer (150 mM NaCl, 15 mM $MgCl_2$, 10 mM Tris-HCl pH 7.4). The concentration of reovirus virions in purified preparations was determined from an equivalence of one OD unit at 260 nm equals 2.1×10^{12} virions [62]. Viral titers were determined by plaque assay using L929 cells [61].

HA Assay

Purified reovirus virions (10^{11} particles) were distributed into 96-well U-bottom microtiter plates (Costar) and serially diluted twofold in 0.05 ml of PBS. Calf erythrocytes (Colorado Serum Co.) were washed twice with PBS and resuspended at a concentration of 1% (vol/vol). Erythrocytes (0.05 ml) were added to wells containing virus particles and incubated at 4°C for at least 2 h. A partial or complete shield of erythrocytes on the well bottom was interpreted as a positive HA result; a smooth, round button of erythrocytes was interpreted as a negative result. HA titer is expressed as 10^{11} particles divided by the number of particles/HA unit. One HA unit equals the number of particles sufficient to produce HA. HA titers from three independent experiments were compared using an unpaired Student's *t* test as applied in Microsoft Excel. *P* values of less than 0.05 were considered statistically significant.

Reovirus Infection of L929 and MEL Cells

L929 cells or MEL cells (2×10^5 cells/well) were plated in 24-well plates (Costar) and incubated at 37°C for at least 2 h. Cells were adsorbed with reovirus strains at an MOI of 1 PFU/cell. Following incubation at room temperature for 1 h, cells were washed three times with PBS and incubated at 37°C for 24 or 48 h. Samples were frozen and thawed twice, and viral titers were determined by plaque assay [61]. For each experiment, samples were infected in triplicate. Mean values from three independent experiments were compared using an unpaired Student's *t* test as applied in Microsoft Excel. *P* values of less than 0.05 were considered statistically significant.

Acknowledgments

We are grateful to Karl Boehme, Laurie Silva and Ursula Neu for helpful discussions and ideas. We thank Jeanne Charles for technical contributions.

Author Contributions

Conceived and designed the experiments: DMR JMF TSD TS. Performed the experiments: DMR JMF EEH TK. Analyzed the data: DMR JMF EEH TK TSD TS. Wrote the paper: DMR JMF TSD TS.

References

1. Weis WI, Brown JH, Cusack S, Paulson JC, Skehel JJ, et al. (1988) Structure of the influenza virus haemagglutinin complexed with its receptor, sialic acid. Nature 333: 426–431.
2. Stehle T, Yan Y, Benjamin TL, Harrison SC (1994) Structure of murine polyomavirus complexed with an oligosaccharide receptor fragment. Nature 369: 160–163.
3. Zhou L, Luo Y, Wu Y, Tsao J, Luo M (2000) Sialylation of the host receptor may modulate entry of demyelinating persistent Theiler's virus. J Virol 74: 1477–1485.
4. Fry EE, Lea SM, Jackson T, Newman JW, Ellard FM, et al. (1999) The structure and function of a foot-and-mouth disease virus- oligosaccharide receptor complex. EMBO J 18: 543–554.
5. Burmeister WP, Guilligay D, Cusack S, Wadell G, Arnberg N (2004) Crystal structure of species D adenovirus fiber knobs and their sialic acid binding sites. J Virol 78: 7727–7736.
6. Kwong PD, Wyatt R, Robinson J, Sweet RW, Sodroski J, et al. (1998) Structure of an HIV gp120 envelope glycoprotein in complex with the CD4 receptor and a neutralizing antibody. Nature 393: 648–659.
7. Bewley MC, Springer K, Zhang YB, Freimuth P, Flanagan JM (1999) Structural analysis of the mechanism of adenovirus binding to its human cellular receptor, CAR. Science 286: 1579–1583.
8. Carfi A, Willis SH, Whitbeck JC, Krummenacher C, Cohen GH, et al. (2001) Herpes simplex virus glycoprotein D bound to the human receptor HveA. Mol Cell 8: 169–179.
9. Dormitzer PR, Sun ZY, Wagner G, Harrison SC (2002) The rhesus rotavirus VP4 sialic acid binding domain has a galectin fold with a novel carbohydrate binding site. EMBO J 21: 885–897.
10. Mullen MM, Haan KM, Longnecker R, Jardetzky TS (2002) Structure of the Epstein-Barr virus gp42 protein bound to the MHC class II receptor HLA-DR1. Mol Cell 9: 375–385.
11. Yuan P, Thompson TB, Wurzburg BA, Paterson RG, Lamb RA, et al. (2005) Structural studies of the parainfluenza virus 5 hemagglutinin-neuraminidase tetramer in complex with its receptor, sialyllactose. Structure 13: 803–815.
12. Seiradake E, Lortat-Jacob H, Billet O, Kremer EJ, Cusack S (2006) Structural and mutational analysis of human Ad37 and canine adenovirus 2 fiber heads in complex with the D1 domain of coxsackie and adenovirus receptor. J Biol Chem 281: 33704–33716.
13. Cao S, Lou Z, Tan M, Chen Y, Liu Y, et al. (2007) Structural basis for the recognition of blood group trisaccharides by norovirus. J Virol 81: 5949–5957.
14. Blanchard H, Yu X, Coulson BS, von Itzstein M (2007) Insight into host cell carbohydrate-recognition by human and porcine rotavirus from crystal structures of the virion spike associated carbohydrate-binding domain (VP8*). J Mol Biol 367: 1215–1226.
15. Persson BD, Reiter DM, Marttila M, Mei YF, Casasnovas JM, et al. (2007) Adenovirus type 11 binding alters the conformation of its receptor CD46. Nat Struct Mol Biol 14: 164–166.
16. Neu U, Woellner K, Gauglitz G, Stehle T (2008) Structural basis of GM1 ganglioside recognition by simian virus 40. Proc Natl Acad Sci U S A 105: 5219–5224.
17. Neu U, Maginnis MS, Palma AS, Ströh L, Feizi T, et al. (2010) Structure-function analysis of the human JC polyomavirus establishes the LSTc pentasaccharide as a functional receptor motif. Cell Host Microbe 8: 309–319.
18. Nilsson EC, Storm RJ, Bauer J, Johansson SM, Lookene A, et al. (2011) The GD1a glycan is a cellular receptor for adenoviruses causing epidemic keratoconjunctivitis. Nat Med 17: 105–109.
19. Fraser RD, Furlong DB, Trus BL, Nibert ML, Fields BN, et al. (1990) Molecular structure of the cell-attachment protein of reovirus: correlation of computer-processed electron micrographs with sequence- based predictions. J Virol 64: 2990–3000.
20. Furlong DB, Nibert ML, Fields BN (1988) Sigma 1 protein of mammalian reoviruses extends from the surfaces of viral particles. J Virol 62: 246–256.
21. Dryden KA, Wang G, Yeager M, Nibert ML, Coombs KM, et al. (1993) Early steps in reovirus infection are associated with dramatic changes in supramolecular structure and protein conformation: analysis of virions and subviral particles by cryoelectron microscopy and image reconstruction. J Cell Biol 122: 1023–1041.

22. Chappell JD, Prota AE, Dermody TS, Stehle T (2002) Crystal structure of reovirus attachment protein sigma 1 reveals evolutionary relationship to adenovirus fiber. EMBO J 21: 1–11.
23. Schelling P, Guglielmi KM, Kirchner E, Paetzold B, Dermody TS, et al. (2007) The reovirus sigma1 aspartic acid sandwich: a trimerization motif poised for conformational change. J Biol Chem 282: 11582–11589.
24. Gentsch JR, Pacitti AF (1985) Effect of neuraminidase treatment of cells and effect of soluble glycoproteins on type 3 reovirus attachment to murine L cells. J Virol 56: 356–364.
25. Paul RW, Choi AH, Lee PW (1989) The alpha-anomeric form of sialic acid is the minimal receptor determinant recognized by reovirus. Virology 172: 382–385.
26. Dermody TS, Nibert ML, Bassel-Duby R, Fields BN (1990) A sigma 1 region important for hemagglutination by serotype 3 reovirus strains. J Virol 64: 5173–5176.
27. Barton ES, Connolly JL, Forrest JC, Chappell JD, Dermody TS (2001) Utilization of sialic acid as a coreceptor enhances reovirus attachment by multistep adhesion strengthening. J Biol Chem 276: 2200–2211.
28. Barton ES, Forrest JC, Connolly JL, Chappell JD, Liu Y, et al. (2001) Junction adhesion molecule is a receptor for reovirus. Cell 104: 441–451.
29. Martin-Padura I, Lostaglio S, Schneemann M, Williams L, Romano M, et al. (1998) Junctional adhesion molecule, a novel member of the immunoglobulin superfamily that distributes at intercellular junctions and modulates monocyte transmigration. J Cell Biol 142: 117–127.
30. Del Maschio A, De Luigi A, Martin-Padura I, Brockhaus M, Bartfai T, et al. (1999) Leukocyte recruitment in the cerebrospinal fluid of mice with experimental meningitis is inhibited by an antibody to junctional adhesion molecule (JAM). J Exp Med 190: 1351–1356.
31. Liu JH, Nusrat A, Schnell FJ, Reaves TA, Walsh S, et al. (2000) Human junction adhesion molecule regulates tight junction resealing in epithelia. J Cell Sci 113: 2363–2374.
32. Prota AE, Campbell JA, Schelling P, Forrest JC, Watson MJ, et al. (2003) Crystal structure of human junctional adhesion molecule 1: Implications for reovirus binding. Proc Natl Acad Sci U S A 100: 5366–5371.
33. Campbell JA, Schelling P, Wetzel JD, Johnson EM, Forrest JC, et al. (2005) Junctional adhesion molecule a serves as a receptor for prototype and field-isolate strains of mammalian reovirus. J Virol 79: 7967–7978.
34. Maginnis MS, Forrest JC, Kopecky-Bromberg SA, Dickeson SK, Santoro SA, et al. (2006) Beta1 integrin mediates internalization of mammalian reovirus. J Virol 80: 2760–2770.
35. Maginnis MS, Mainou BA, Derdowski A, Johnson EM, Zent R, et al. (2008) NPXY motifs in the beta1 integrin cytoplasmic tail are required for functional reovirus entry. J Virol 82: 3181–3191.
36. Kirchner E, Guglielmi KM, Strauss HM, Dermody TS, Stehle T (2008) Structure of Reovirus Sigma1 in Complex with Its Receptor Junctional Adhesion Molecule-A. PLoS Pathog 4: e1000235.
37. Guglielmi KM, Kirchner E, Holm GH, Stehle T, Dermody TS (2007) Reovirus binding determinants in junctional adhesion molecule-A. J Biol Chem 282: 17930–17940.
38. Chappell JD, Duong JL, Wright BW, Dermody TS (2000) Identification of carbohydrate-binding domains in the attachment proteins of type 1 and type 3 reoviruses. J Virol 74: 8472–8479.
39. van Raaij MJ, Mitraki A, Lavigne G, Cusack S (1999) A triple beta-spiral in the adenovirus fibre shaft reveals a new structural motif for a fibrous protein. Nature 401: 935–938.
40. Chappell JD, Barton ES, Smith TH, Baer GS, Duong DT, et al. (1998) Cleavage susceptibility of reovirus attachment protein sigma 1 during proteolytic disassembly of virions is determined by a sequence polymorphism in the sigma 1 neck. J Virol 72: 8205–8213.
41. Harbury PB, Kim PS, Alber T (1994) Crystal structure of an isoleucine-zipper trimer. Nature 371: 80–83.
42. Chappell JD, Gunn VL, Wetzel JD, Baer GS, Dermody TS (1997) Mutations in type 3 reovirus that determine binding to sialic acid are contained in the fibrous tail domain of viral attachment protein sigma 1. J Virol 71: 1834–1841.
43. Kobayashi T, Antar AA, Boehme KW, Danthi P, Eby EA, et al. (2007) A plasmid-based reverse genetics system for animal double-stranded RNA viruses. Cell Host Microbe 1: 147–157.
44. Kobayashi T, Ooms LS, Ikizler M, Chappell JD, Dermody TS (2010) An improved reverse genetics system for mammalian orthoreoviruses. Virology 398: 194–200.
45. Rubin DH, Wetzel JD, Williams WV, Cohen JA, Dworkin C, et al. (1992) Binding of type 3 reovirus by a domain of the sigma 1 protein important for hemagglutination leads to infection of murine erythroleukemia cells. J Clin Invest 90: 2536–2542.
46. Weiner HL, Drayna D, Averill DR, Jr., Fields BN (1977) Molecular basis of reovirus virulence: role of the S1 gene. Proc Natl Acad Sci U S A 74: 5744–5748.
47. Weiner HL, Powers ML, Fields BN (1980) Absolute linkage of virulence and central nervous system cell tropism of reoviruses to viral hemagglutinin. J Infect Dis 141: 609–616.
48. Tyler KL, McPhee DA, Fields BN (1986) Distinct pathways of viral spread in the host determined by reovirus S1 gene segment. Science 233: 770–774.
49. Eisen MB, Sabesan S, Skehel JJ, Wiley DC (1997) Binding of the influenza A virus to cell-surface receptors: structures of five hemagglutinin-sialyloligosaccharide complexes determined by X- ray crystallography. Virology 232: 19–31.
50. Stehle T, Harrison SC (1996) Crystal structures of murine polyomavirus in complex with straight-chain and branched-chain sialyloligosaccharide receptor fragments. Structure, Fold Des 4: 183–194.
51. Stehle T, Harrison SC (1997) High-resolution structure of a polyomavirus VP1-oligosaccharide complex: implications for assembly and receptor binding. EMBO J 16: 5139–5148.
52. Fry EE, Tuthill TJ, Harlos K, Walter TS, Rowlands DJ, et al. (2010) Crystal structure of equine rhinitis A virus in complex with its sialic acid receptor. J Gen Virol 91: 1971–1977.
53. Kabsch W (1993) Automatic processing of rotation diffraction data from crystals of initially unknown symmetry and cell constants. J Appl Cryst 26: 795–800.
54. Navaza J (1994) AMoRe: an automated package for molecular replacement. Acta Crystallogr A50: 157–163.
55. Murshudov GN, Vagin AA, Dodson EJ (1997) Refinement of Macromolecular Structures by the Maximum-Likelihood Method. Acta Crystallogr D53: 240–255.
56. Adams PD, Grosse-Kunstleve RW, Hung LW, Ioerger TR, McCoy AJ, et al. (2002) PHENIX: building new software for automated crystallographic structure determination. Acta Crystallogr D58: 1948–1954.
57. Emsley P, Cowtan K (2004) Coot: model building tools for molecular graphics. Acta Crystallogr D60: 2126–2132.
58. Sanford KK, Earle WR, Likely GD (1948) The growth in vitro of single isolated tissue cells. J Natl Cancer Inst 9: 229–246.
59. Ross J, Gielen J, Packman S, Ikawa Y, Leder P (1974) Globin gene expression in cultured erythroleukemic cells. J Mol Biol 87: 697–714.
60. Ishii K, Ueda Y, Matsuo K, Matsuura Y, Kitamura T, et al. (2002) Structural analysis of vaccinia virus DIs strain: application as a new replication-deficient viral vector. Virology 302: 433–444.
61. Virgin HW, III, Bassel-Duby R, Fields BN, Tyler KL (1988) Antibody protects against lethal infection with the neurally spreading reovirus type 3 (Dearing). J Virol 62: 4594–4604.
62. Smith RE, Zweerink HJ, Joklik WK (1969) Polypeptide components of virions, top component and cores of reovirus type 3. Virology 39: 791–810.

APPENDIX B

THE REOVIRUS SIGMA1S PROTEIN IS A DETERMINANT OF HEMATOGENOUS BUT NOT NEURAL VIRUS DISSEMINATION IN MICE

Karl W. Boehme, Johnna M. Frierson, Jennifer L. Konopka, Takeshi Kobayashi, and Terence S. Dermody

Journal of Virology. 85(22):11781-90;2011

Journal of Virology

The Reovirus σ1s Protein Is a Determinant of Hematogenous but Not Neural Virus Dissemination in Mice

Karl W. Boehme, Johnna M. Frierson, Jennifer L. Konopka, Takeshi Kobayashi and Terence S. Dermody

J. Virol. **2011, 85(22):11781. DOI: 10.1128/JVI.02289-10. Published Ahead of Print 14 September 2011.**

JOURNAL OF VIROLOGY, Nov. 2011, p. 11781–11790 Vol. 85, No. 22
0022-538X/11/$12.00 doi:10.1128/JVI.02289-10

The Reovirus σ1s Protein Is a Determinant of Hematogenous but Not Neural Virus Dissemination in Mice▽

Karl W. Boehme,[1,3] Johnna M. Frierson,[2,3] Jennifer L. Konopka,[1,3] Takeshi Kobayashi,[1,3]† and Terence S. Dermody[1,2,3]*

Departments of Pediatrics[1] and Pathology, Microbiology, and Immunology[2] and Elizabeth B. Lamb Center for Pediatric Research,[3] Vanderbilt University School of Medicine, Nashville, Tennessee 37232

Received 2 November 2010/Accepted 31 August 2011

Nonstructural protein σ1s is a critical determinant of hematogenous dissemination by type 1 reoviruses, which reach the central nervous system (CNS) by a strictly blood-borne route. However, it is not known whether σ1s contributes to neuropathogenesis of type 3 reoviruses, which disseminate by both vascular and neural pathways. Using isogenic type 3 viruses that vary only in σ1s expression, we observed that mice survived at a higher frequency following hind-limb inoculation with σ1s-null virus than when inoculated with wild-type virus. This finding suggests that σ1s is essential for reovirus virulence when inoculated at a site that requires systemic spread to cause disease. Wild-type and σ1s-null viruses produced comparable titers in the spinal cord, suggesting that σ1s is dispensable for invasion of the CNS. Although the two viruses ultimately achieved similar peak titers in the brain, loads of wild-type virus were substantially greater than those of the σ1s-null mutant at early times after inoculation. In contrast, wild-type virus produced substantially higher titers than the σ1s-null virus in peripheral organs to which reovirus spreads via the blood, including the heart, intestine, liver, and spleen. Concordantly, viral titers in the blood were higher following infection with wild-type virus than following infection with the σ1s-null mutant. These results suggest that differences in viral brain titers at early time points postinfection are due to limited virus delivery to the brain by hematogenous pathways. Transection of the sciatic nerve prior to hind-limb inoculation diminished viral spread to the spinal cord. However, wild-type virus retained the capacity to disseminate to the brain following sciatic nerve transection, indicating that wild-type reovirus can spread to the brain by the blood. Together, these results indicate that σ1s is not required for reovirus spread by neural mechanisms. Instead, σ1s mediates hematogenous dissemination within the infected host, which is required for full reovirus neurovirulence.

Many viral diseases occur as a consequence of systemic dissemination within the infected host. Some viruses, such as herpes simplex virus (20, 28) and rabies virus (3, 39), spread within their hosts by neural routes. Others, including human immunodeficiency virus (42) and measles virus (47), use hematogenous pathways to spread systemically. Although the general principles of virus dissemination are understood, little is known about the viral and cellular determinants that govern virus spread. Defining the mechanisms used by viruses to disseminate within their hosts is essential to an understanding of how viruses cause systemic disease and may foster development of therapeutics that arrest viral replication prior to the seeding of target tissues.

Mammalian orthoreoviruses (reoviruses) are highly tractable models for studies of viral pathogenesis. Reoviruses are nonenveloped, icosahedral viruses that contain 10 segments of double-stranded RNA (dsRNA) (24). In newborn mice, type 1 and type 3 reoviruses invade the central nervous system (CNS) following oral or intramuscular inoculation but use different routes and produce distinct pathological consequences. Type 1 reoviruses access the CNS by hematogenous routes and infect ependymal cells, causing ependymitis and hydrocephalus (41, 45, 46). Type 3 reoviruses spread to the CNS by neural routes (41) and infect neurons, causing lethal encephalitis (22, 41). However, type 3 reoviruses also use hematogenous routes to disseminate to other organs, including the heart, liver, and spleen (1, 12). Serotype-specific differences in neurotropism and disease segregate with the viral S1 dsRNA gene segment (10, 38), which encodes attachment protein σ1 and nonstructural protein σ1s (33, 44). Receptor engagement is critical for target cell selection by many viruses, suggesting that the σ1 attachment protein is the primary determinant of viral tropism. However, σ1s is required for hematogenous dissemination of type 1 reovirus to sites of secondary replication in mice (6). Because of the serotype-specific differences in reovirus tropism, routes of spread, and outcome of infection, it is possible that the σ1s protein from different serotypes mediates serotype-specific functions.

Protein σ1s is a 14-kDa nonstructural protein encoded by the viral S1 gene segment (7, 11, 33). The σ1s open reading frame (ORF) completely overlaps the σ1 coding sequence; however, σ1s lies in a different reading frame (7–9, 11, 33). Little amino acid sequence identity exists among the σ1s proteins from the different reovirus serotypes (7, 9). The only feature of the σ1s protein that is conserved across the serotypes is a cluster of positively charged amino acids near the amino terminus (7, 9). For type 3 reovirus, this cluster functions as a nuclear localization signal (15). The σ1s protein has

* Corresponding author. Mailing address: Lamb Center for Pediatric Research, D7235 MCN, Vanderbilt University School of Medicine, Nashville, TN 37232. Phone: (615) 343-9943. Fax: (615) 343-9723. E-mail: terry.dermody@vanderbilt.edu.

† Present address: Institute for Virus Research, Kyoto University, Kyoto 606-8507, Japan.

▽ Published ahead of print on 14 September 2011.

been implicated in reovirus-induced cell cycle arrest at the G_2/M boundary (29, 30) and may function in reovirus neurovirulence by influencing reovirus-induced apoptosis in the murine CNS (16). However, interpreting these studies of σ1s function is complicated because the σ1s-null mutant virus used in previous experiments is not isogenic to the parental strain from which it was derived (32). Thus, a role for σ1s in the pathogenesis of type 3 reovirus is undefined.

In this study, we used plasmid-based reverse genetics to generate a σ1s-null reovirus to determine how σ1s influences systemic dissemination of type 3 reovirus. Following intramuscular inoculation, mice infected with the σ1s-null mutant survive at a higher frequency than those infected with wild-type virus. This result suggests that σ1s is a determinant of reovirus virulence when reovirus is inoculated at a site that requires systemic dissemination. Wild-type and mutant viruses produced equivalent titers in the spinal cord, indicating that σ1s is not required for reovirus invasion of the CNS. Although the two viruses produced similar peak titers in the brain, titers of the σ1s-null mutant in the brain were markedly lower than those of wild-type virus at early times postinfection. Viral blood titers were substantially higher following infection with wild-type virus than those produced by the σ1s-null mutant. In addition, titers of σ1s-null virus in organs that reovirus accesses via the bloodstream, including the heart, intestine, liver, and spleen, were substantially lower than those produced by wild-type virus. These data suggest that σ1s is essential for reovirus hematogenous spread within an infected host but dispensable for dissemination by neural routes. Sectioning the sciatic nerve prior to hind-limb inoculation diminished but did not eliminate spread of wild-type virus to the brain. However, dissemination of σ1s-null virus to the brain was almost completely abolished following sciatic nerve transection. These data indicate that reovirus accesses the brain by a combination of hematogenous and neural routes. Collectively, the results described in this study suggest that reovirus trafficking to the brain via hematogenous dissemination precedes spread by neural routes and that blood-borne viral transport is essential for reovirus neurovirulence.

MATERIALS AND METHODS

Cell lines. HeLa cells were maintained in Dulbecco modified Eagle medium supplemented to contain 10% fetal bovine serum (FBS), 2 mM L-glutamine, 100 U/ml of penicillin, 100 μg/ml streptomycin, and 25 ng/ml of amphotericin B (Invitrogen). L929 cells were maintained in Joklik's minimum essential medium supplemented to contain 10% FBS, 2 mM L-glutamine, 100 U/ml of penicillin, 100 μg/ml streptomycin, and 25 ng/ml of amphotericin B.

Viruses. Recombinant reoviruses were generated using plasmid-based reverse genetics (19). Monolayers of L929 cells at approximately 90% confluence (3×10^6 cells) in 60-mm-diameter dishes (Corning) were infected with rDIs-T7 pol at a multiplicity of infection (MOI) of ~0.5 50% tissue culture infective doses ($TCID_{50}$) per cell. At 1 h postinfection, cells were cotransfected with nine plasmid constructs representing cloned gene segments from the strain type 3 Dearing (T3D) genome—pT7-L1T3D (2 μg), pT7-L2T3D (2 μg), pT7-L3T3D (2 μg), pT7-M1T3D (1.75 μg), pT7-M2T3D (1.75 μg), pT7-M3T3D (1.75 μg), pT7-S2T3D (1.5 μg), pT7-S3T3D (1.5 μg), and pT7-S4T3D (1.5 μg)—in combination with 2 μg of pBacT7-S1T3D or pBacT7-S1T3D σ1s-null. For each, 3 μl of TransIT-LT1 transfection reagent (Mirus) was used per μg of plasmid DNA. Following 5 days of incubation, recombinant virus was isolated from transfected cells by plaque purification using monolayers of L929 cells (43). For generation of σ1s-deficient virus, pBacT7-S1T3D (T3D S1; GenBank accession number HM159619) was altered by QuikChange (Stratagene) site-directed mutagenesis. To confirm sequences of the mutant virus, viral RNA was extracted from purified virions and subjected to OneStep reverse transcription-PCR (RT-PCR) (Qiagen) using S1-specific primers. Primer sequences are available from the corresponding author upon request. PCR products were analyzed following electrophoresis in Tris-borate-EDTA agarose gels or purified and subjected directly to sequence analysis. The presence of a noncoding signature mutation in the L1 gene of viruses generated by plasmid-based rescue was confirmed using RT-PCR and L1-specific primers (19).

Purified reovirus virions were generated using second- or third-passage L929 cell lysate stocks of twice-plaque-purified reovirus as described previously (13). Viral particles were Freon extracted from infected cell lysates, layered onto 1.2- to 1.4-g/cm^3 CsCl gradients, and centrifuged at 62,000 × *g* for 18 h. Bands corresponding to virions (1.36 g/cm^3) (36) were collected and dialyzed in virion storage buffer (150 mM NaCl, 15 mM $MgCl_2$, 10 mM Tris-HCl [pH 7.4]). The concentration of reovirus virions in purified preparations was determined from the following equivalence: 1 optical density at 260 nm (OD_{260}) unit = 2.1×10^{12} virions (36). Viral titer was determined by plaque assay using L929 cells (43).

Virus replication assays. Monolayers of cells in 24-well plates (Corning) were adsorbed in triplicate with each reovirus strain at an MOI of 0.01, 0.1, or 1 PFU/cell at room temperature for 1 h in serum-free medium, washed once with phosphate-buffered saline (PBS), and incubated in serum-containing medium for various intervals. Cells were frozen and thawed twice prior to determination of viral titer by plaque assay using L929 cells (43). Viral yields were calculated according to the following formula: $\log_{10}\text{yield}_{t_x} = \log_{10}(\text{PFU/ml})_{t_x} - \log_{10}(\text{PFU/ml})_{t_0}$, where t_x is the time postinfection.

Assessment of σ1s expression by indirect immunofluorescence. Monolayers of HeLa cells (2×10^5 cells/well) grown on coverslips in 24-well plates were adsorbed with reovirus at an MOI of 50 PFU/cell at room temperature for 1 h. Following removal of the inoculum, cells were washed with PBS and incubated in complete medium at 37°C for 18 h to permit completion of a single cycle of viral replication. Monolayers were fixed with 1 ml of methanol at −20°C for at least 30 min, washed twice with PBS, and blocked with 0.1% gelatin, 0.1% Tween 20 (Sigma), and 20% normal goat serum (Vector Laboratories) in PBS. For detection of σ1s, cells were washed with PBS and incubated with mouse monoclonal anti-σ1s antibody 2F4 (32) at a dilution of 1:500 in PBS with 0.1% gelatin, 2% normal goat serum, and 0.1% Tween 20. For detection of reovirus proteins, cells were washed once with PBS and stained with polyclonal rabbit anti-reovirus serum at a 1:1,000 dilution in PBS–0.5% Triton X-100 at room temperature for 1 h. Monolayers were washed twice with PBS–0.5% Triton X-100 and incubated with a 1:1,000 dilution of Alexa 488- or Alexa 546-labeled anti-rabbit or anti-mouse IgG (Invitrogen), respectively. Monolayers were washed with PBS, and infected cells were visualized by indirect immunofluorescence using an Axiovert 200 fluorescence microscope (Carl Zeiss).

Infection of mice. C57BL/6J mice were obtained from Jackson Laboratory. Swiss Webster mice were obtained from Harlan Biosciences. Animal husbandry and experimental procedures were performed in accordance with Public Health Service policy and approved by the Vanderbilt University School of Medicine Institutional Animal Care and Use Committee.

Two-day-old mice were inoculated intramuscularly or intracranially with purified reovirus diluted in PBS. Intramuscular inoculations (10 μl) were delivered into the left hind limb (hamstring muscle) using a Hamilton syringe and 30-gauge needle. Intracranial inoculations (5 μl) were delivered into the left cerebral hemisphere using a Hamilton syringe and 30-gauge needle (40). For analysis of viral virulence, mice were monitored for weight loss and symptoms of disease for 25 days postinoculation. For survival experiments, mice were euthanized when found to be moribund (defined by rapid or shallow breathing, lethargy, or paralysis). Death was not used as an endpoint. Data from these experiments are reported as "percent survival." For analysis of virus replication, mice were euthanized at various intervals following inoculation, and organs were collected into 1 ml of PBS and homogenized by freezing, thawing, and sonication. For analysis of viremia, mice were euthanized and decapitated at various intervals following inoculation, and whole blood was collected from the neck into a 1-ml syringe containing 100 μl Alsever's solution (Sigma). Viral titers in organ homogenates were determined by plaque assay using L929 cells.

Sciatic nerve sectioning. Two-day-old C57/BL6 mice were anesthetized by hypothermia. The proper depth of anesthesia was assessed visually by absence of a withdrawal reflex and lack of response to external stimuli. The area around the incision site was cleaned with Betadine using a cotton swab. A 0.5-cm incision was made along the back of the thigh using surgical scissors (Fine Science Tools). The sciatic nerve was isolated using forceps (Fine Science Tools), and a segment of the nerve was excised using surgical scissors. The incision was closed by bringing the skin flaps into apposition and applying liquid skin (Webster Veterinary). The pups were warmed gradually by placement in a room temperature cage. Following recovery of activity, pups were moved to a cage that had been

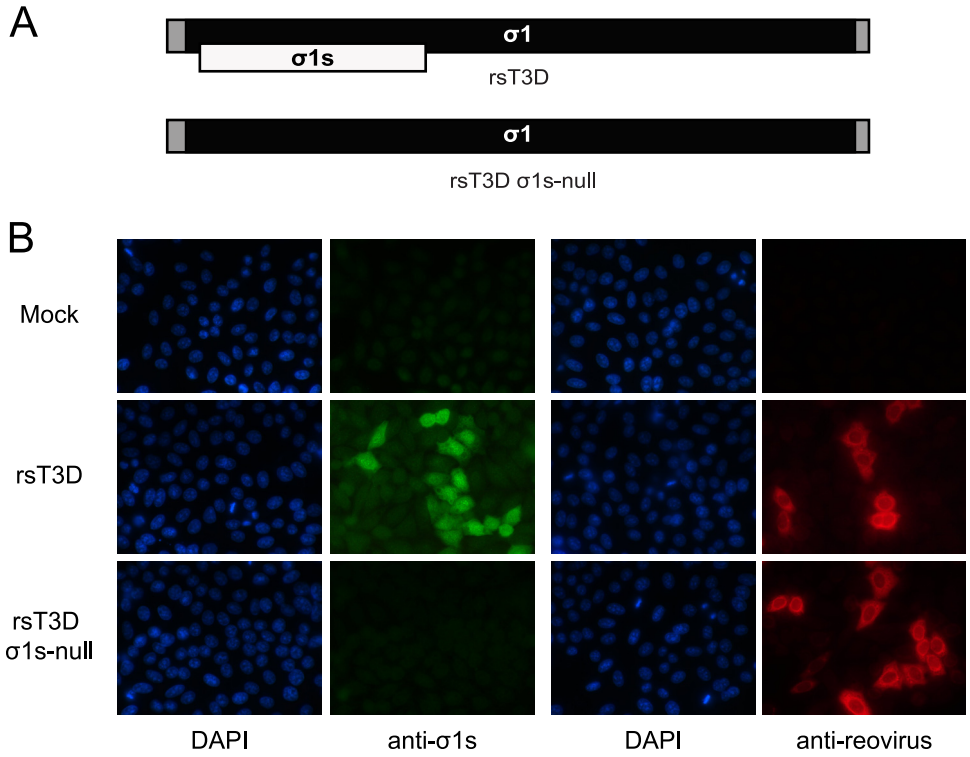

FIG. 1. Construction and characterization of a σ1s-deficient type 3 reovirus. (A) Schematic of the reovirus S1 gene segment. The σ1 ORF is shown in black, the σ1s ORF in white, and the 5′ and 3′ untranslated regions (UTRs) in gray. The wild-type (upper panel) and σ1s-null (lower panel) S1 gene alleles are shown. (B) rsT3D σ1s-null does not express the σ1s protein. HeLa cells were either mock infected or adsorbed with rsT3D or rsT3D σ1s-null at an MOI of 10 PFU/cell. At 24 h postinfection, cells were fixed and stained with a T3D σ1s-specific monoclonal antibody or reovirus-specific polyclonal antiserum. Nuclei were stained with 4′,6-diamidino-2-phenylindole (DAPI).

placed atop a warming pad (Braintree Scientific). Pups were then inoculated intramuscularly with 1×10^6 PFU of rsT3D or rsT3D σ1s-null reovirus prior to returning them to the dam. Mice were euthanized at 2 or 4 days following inoculation, and organs were collected into 1 ml of PBS and homogenized by freezing, thawing, and sonication.

Quantification of viral RNA using RT-qPCR. Total RNA was extracted from 200 μl of whole blood/Alsever's mixture using the High Pure viral RNA kit (Roche). RNA was eluted into a final volume of 40 μl. Reverse transcription-quantitative PCR (RT-qPCR) was performed using the ABI 7000 sequence detection system (Applied Biosystems) and EZ RT-PCR System (Roche) according to the manufacturer's instructions with minor modifications. Reovirus RNA was quantified using 10 μl of RNA extract. Forward (S4 83F, 5′-CGCTT TTGAAGGTCGTGTATCA-3′) and reverse (S4 153R, 5′-CTGGCTGTGCTG AGATTGTTTT-3′) primers corresponding to the viral S4 gene were used for reverse transcription and quantitative PCR amplification. The S4-specific fluorogenic probe used was 5′-dFAM-AGCGCGCAAGAGGGATGGGA-BHQ-1-3′ (Biosearch Technologies). Reverse transcription was performed at 50°C for 2 min, followed by incubation at 60°C for 30 min. The reaction was terminated by incubation at 95°C for 5 min. Subsequently, 40 cycles of quantitative PCR were performed at 95°C for 15 s followed by incubation at 60°C for 30 s. Standard curves relating threshold cycle values to copies of plasmid DNA template were generated using 10-fold dilutions of a T3D S4-encoding plasmid (pT7-T3D S4) (19). The concentration of viral RNA in each sample was extrapolated from standard curves. The final S4 RNA copy number was calculated by multiplying by 4 the copy number obtained by extrapolation from the standard curve to account for using one-quarter of the extracted RNA as a template.

Preparation of murine cortical neuron cultures. Primary cultures of mouse cortical neurons were established using cerebral cortices of C57/BL6 embryos at developmental day E15 (1). Fetuses were decapitated, brains were removed, and cortical lobes were dissected and submerged in Hanks' balanced salt solution (Gibco) on ice. Cortices were incubated in 0.6 mg/ml trypsin solution at room temperature for 30 min, washed twice, and manually dissociated twice with a Pasteur pipette. Viable cells were plated at a density of 2.75×10^5 cells/ml in 24-well plates or on glass coverslips (BD Biosciences) placed in 24-well plates. Wells were treated prior to plating with a 10-μg/ml poly-D-lysine solution (BD Biosciences) and a 1.64-μg/ml laminin solution (BD Biosciences). Cultures were incubated for the first 24 h in neurobasal medium (Gibco) supplemented to contain 10% FBS (Gibco), 0.6 mM L-glutamine, 50 U/ml penicillin, and 50 μg/ml streptomycin. Cultures were thereafter maintained in neurobasal medium supplemented to contain 1× B27 (Gibco), 50 U/ml penicillin, and 50 μg/ml streptomycin. One-half of the medium was replaced with fresh medium every 3 to 4 days. Neurons were allowed to mature for 7 days prior to use.

Statistical analysis. A log-rank test was used for comparison of survival curves. For experiments in which viral titers were determined in an organ or blood, the Mann-Whitney test was used to calculate two-tailed *P* values. This test is appropriate for experimental data that display a non-Gaussian distribution (31). When all values are less than the limit of detection, a Mann-Whitney test *P* value cannot be calculated. Statistical analyses were performed using Prism software (GraphPad Software, Inc.).

RESULTS

Construction and characterization of a σ1s-deficient type 3 reovirus. To determine the function of σ1s in the pathogenesis of type 3 reovirus, we used plasmid-based reverse genetics to engineer a recombinant reovirus deficient in σ1s expression (19). The start codon for the σ1s open reading frame was disrupted by introducing a single nucleotide change (^{71}AUG to ^{71}ACG) into the plasmid encoding the cDNA for the S1 gene segment derived from prototype type 3 reovirus strain T3D (Fig. 1A). This mutation alters the σ1s translational start site; however, the coding sequence of the overlapping σ1 open reading frame is not affected. Viable viruses were recovered that contain nine gene segments from T3D in combination

with either the wild-type or σ1s-null T3D S1 gene segment. Analysis of genomic dsRNA from each virus verified that the rescued viruses contain the expected combination of gene segments (data not shown). The sequence of the S1 gene segment and the integrity of the σ1s translational start site from each virus were confirmed by direct sequencing of viral RNA using serotype-specific S1 primers (data not shown). The S1 genes of both strains contained no additional mutations.

To confirm that altering the σ1s translational start site prevents σ1s synthesis, we assessed σ1s expression following infection of HeLa cells with rsT3D or rsT3D σ1s-null by indirect immunofluorescence using T3D σ1s-specific monoclonal antibody 2F4 (Fig. 1B). At 24 h postinfection, σ1s protein was detected in cells infected with wild-type virus but not in those infected with the σ1s-null mutant. In parallel, staining with reovirus-specific polyclonal antiserum showed equivalent levels of infection for both viruses. Thus, rsT3D and rsT3D σ1s-null are isogenic viruses that differ only in σ1s expression.

The σ1s protein is not required for reovirus replication in cell culture. To determine whether σ1s influences reovirus growth in cell culture, we quantified viral yields following infection of mouse L929 cells (Fig. 2A). Cells were infected with rsT3D or rsT3D σ1s-null at MOIs of 0.01 or 1 PFU per cell, and viral titers were determined by plaque assay over a 48-h time course. At each MOI tested, the replication kinetics and yields of viral progeny for the σ1s-null virus were indistinguishable from those of wild-type virus. Furthermore, no differences in replication kinetics or viral yields were observed between wild-type and σ1s-deficient viruses following infection of HeLa cells at an MOI of 0.1 or 1 PFU per cell (Fig. 2B). To determine whether σ1s expression contributes to reovirus protein production, we assessed steady-state viral protein levels by immunoblotting using reovirus-specific antiserum after infection of murine L929 cells with rsT3D or rsT3D σ1s-null (Fig. 2C). At both 24 and 48 h postinfection, no differences in protein levels were observed between the wild-type and mutant viruses. Together, these data are consistent with previous studies showing that σ1s is dispensable for reovirus replication in cultured cells (6, 32).

The σ1s protein is a determinant of reovirus virulence following intramuscular inoculation. To determine whether σ1s contributes to reovirus virulence, we inoculated newborn C57/BL6 mice intramuscularly with 10^6 PFU of rsT3D or rsT3D σ1s-null (Fig. 3A). Reovirus normally infects by the oral route, and spread to the CNS is required for reovirus-induced disease. However, reovirus strain T3D replicates poorly in the gastrointestinal tract due to cleavage of its attachment protein by intestinal proteases (4, 5, 23). Inoculation of type 3 reoviruses intramuscularly leads to invasion of the brain by neural routes (41). Infected mice were monitored for signs of disease and euthanized when moribund. Approximately 75% of mice infected with rsT3D succumbed to infection, whereas only 25% of mice died following infection with rsT3D σ1s-null. These data indicate that σ1s influences reovirus virulence following inoculation of the virus at a peripheral site.

The σ1s protein is dispensable for reovirus spread to the CNS by neural routes. To determine whether σ1s is required for reovirus transmission by neural routes, we quantified viral titers in hind limb muscle, spinal cord, and brain at days 4, 8, and 12 following intramuscular inoculation of 10^6 PFU of rsT3D or rsT3D σ1s-null virus (Fig. 3B). In the hind-limb muscle, the σ1s-null virus produced higher titers than wild-type virus at day 4. Titers at day 8 were equivalent for the two viruses. At day 12, higher titers of the wild-type virus than of the σ1s-null mutant were detected. These data indicate that the levels of infection were comparable between the wild-type virus and σ1s-null mutant at the site of inoculation.

In the spinal cord, titers of wild-type and σ1s-null viruses at days 4 and 8 were comparable. At day 12, wild-type virus produced higher titers than mutant virus, but this difference was not statistically significant. In the brain, titers of wild-type virus were greater than those of the σ1s-null mutant at days 1, 2, and 4. However, titers of the two viruses were equivalent at days 8 and 12. Both viruses reached a peak titer approaching 10^7 PFU/brain. Sequence analysis of the S1 gene from 5 viruses recovered from the spinal cord and brain of mice inoculated with rsT3D σ1s-null indicate that the mutant virus retained the σ1s-null mutation. This finding indicates that the σ1s-null virus is stable in the murine CNS. Together, these data suggest that the σ1s protein is not required for reovirus spread by neural routes. Rather, σ1s appears to either facilitate reovirus transport to the brain or enhance viral replication at that site.

The σ1s protein modestly enhances reovirus neurovirulence following intracranial inoculation. To determine whether σ1s influences reovirus virulence in the murine CNS, we inoculated newborn C57/BL6 mice intracranially with 100 PFU of rsT3D or rsT3D σ1s-null (Fig. 4A). Mice were monitored for signs of disease and euthanized when moribund. Animals infected with either virus developed clinical signs of encephalitis and succumbed to infection. However, mice infected with rsT3D σ1s-null survived approximately 1 day longer than those inoculated with wild-type virus. The average survival times for mice infected with rsT3D or rsT3D σ1s-null were 12 or 13 days, respectively. Similar results were obtained in experiments performed using Swiss Webster mice (Fig. 4B). The average survival time for mice infected with rsT3D σ1s-null was slightly longer than that for rsT3D-infected mice. However, the difference was not statistically significant. Together, these data suggest that σ1s contributes only modestly to reovirus virulence following intracranial inoculation.

The σ1s protein is not required for reovirus replication in the murine CNS. To determine whether σ1s expression is required for reovirus replication within the murine CNS, we inoculated newborn C57/BL6 mice intracranially with 100 PFU of rsT3D or rsT3D σ1s-null and quantified viral titers in the brain at days 4, 8, and 12 postinoculation (Fig. 4C). Wild-type and σ1s-null viruses produced equivalent titers at days 4 and 8. At day 12, the σ1s-null mutant produced higher titers than wild-type virus, although the difference was not statistically significant. Similar results were obtained following intracranial inoculation of Swiss Webster mice (Fig. 4D). Titers of wild-type and σ1s-null viruses were equivalent in the brain at each time point assessed. These data indicate that σ1s is dispensable for reovirus replication in the murine CNS.

To test directly whether σ1s influences reovirus replication in neurons, we compared replication of wild-type and σ1s-null virus in primary cultures of murine cortical neurons (Fig. 5). Viral yields following infection of primary neuronal cultures were quantified at 24, 48, and 72 h following infection with rsT3D or rsT3D σ1s-null at an MOI of 1 PFU per cell. Wild-

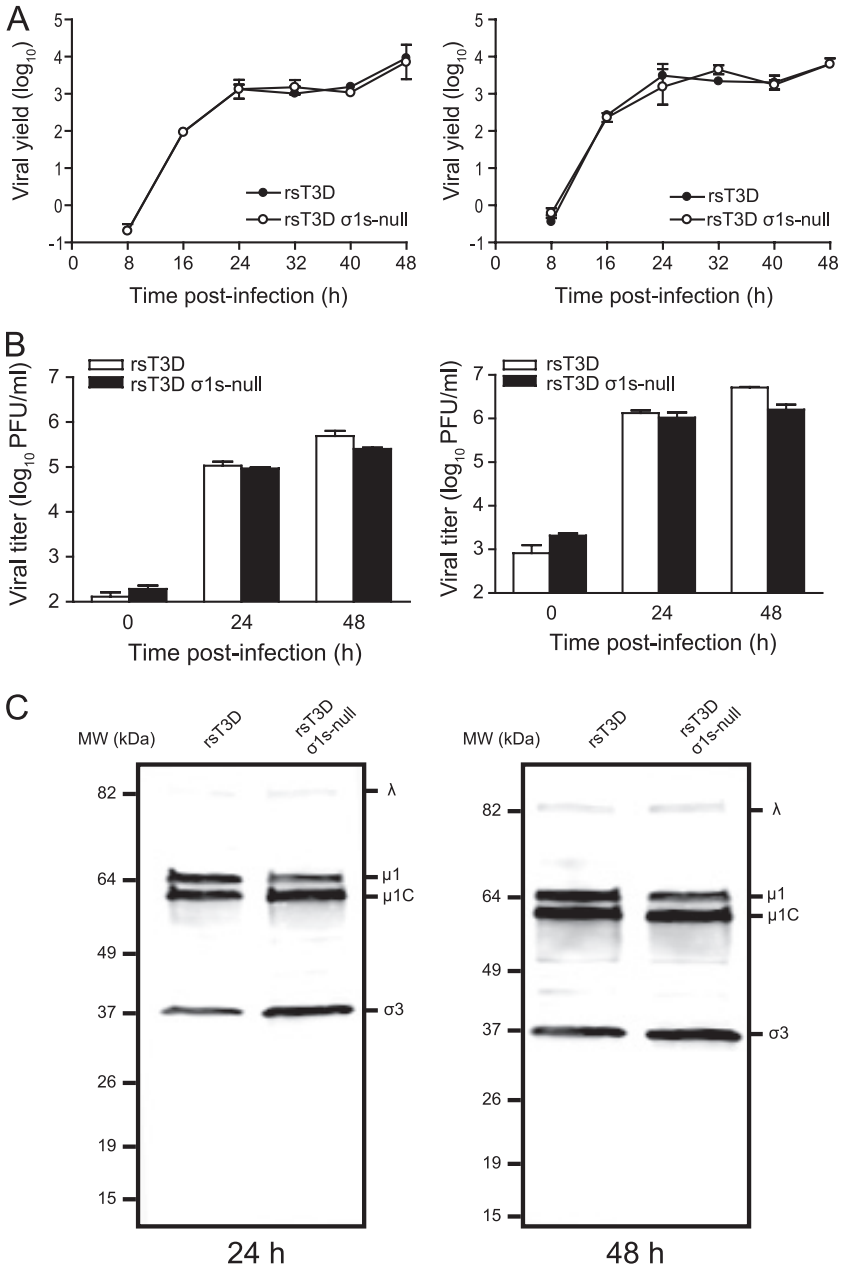

FIG. 2. The σ1s protein is dispensable for reovirus growth in cell culture. (A) L cells were adsorbed with rsT3D or rsT3D σ1s-null at MOIs of 0.01 (left) or 1 (right) PFU/cell. (B) HeLa cells were adsorbed with rsT3D or rsT3D σ1s-null at MOIs of 0.1 (left) or 1 (right) PFU/cell. Titers of virus in cell lysates were determined by plaque assay at the indicated times postinfection. Results are expressed as mean viral yield or titers for triplicate samples. Error bars indicate standard deviations. (C) Expression of reovirus proteins by wild-type and σ1s-null viruses. Whole-cell lysates from infected cells were immunoblotted using reovirus-specific antiserum.

type virus produced slightly higher (although not statistically significant) yields than the σ1s-null virus at 24 h postinfection. However, at 48 and 72 h, yields of the σ1s-null virus were indistinguishable from those of wild-type virus. Thus, σ1s is dispensable for reovirus replication in neurons.

The σ1s protein enhances reovirus dissemination by hematogenous routes. To determine whether σ1s is required for reovirus spread by the bloodstream, newborn C57/BL6 mice were inoculated intramuscularly with 10^6 PFU of rsT3D or rsT3D σ1s-null, and viral loads in the blood were quantified by RT-qPCR at days 1, 2, and 4 postinoculation (Fig. 6). Low levels of both viruses were detected at day 1. However, although levels of wild-type virus increased substantially by days 2 and 4, loads of the σ1s-null virus in the blood remained low at these time points. By day 4, loads of wild-type virus were approximately 10-fold higher than those of the σ1s-null mutant. These data indicate that σ1s functions to promote the establishment of reovirus viremia.

To determine whether σ1s is required for hematogenous spread of type 3 reovirus to tissues that support secondary

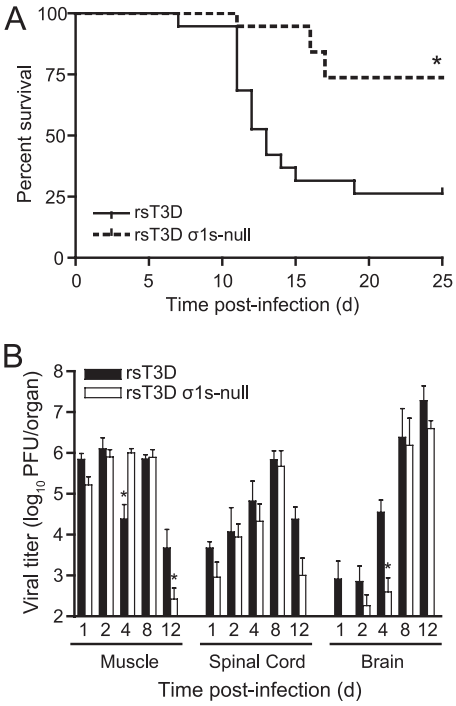

FIG. 3. (A) The σ1s protein enhances reovirus virulence following intramuscular inoculation. Newborn C57/BL6 mice were inoculated in the left hind limb with 10^6 PFU of rsT3D or rsT3D σ1s-null. Mice (n = 19 for each virus strain) were monitored for survival for 25 days. *, $P < 0.001$ as determined by log-rank test in comparison to rsT3D. (B) The σ1s protein is not required for reovirus spread by neural routes. Newborn C57/BL6 mice were inoculated in the left hind limb with 10^6 PFU of rsT3D or rsT3D σ1s-null. At days 1, 2, 4, 8, and 12 postinoculation, mice were euthanized, hind-limb muscle, spinal cord, and brain were resected, and viral titers were determined by plaque assay. Results are expressed as mean viral titers for 6 to 9 animals for each time point. Error bars indicate standard errors of the means. *, $P < 0.05$ as determined by Mann-Whitney test in comparison to rsT3D.

rounds of viral replication, we inoculated newborn C57/BL6 mice intramuscularly with 10^6 PFU of rsT3D or rsT3D σ1s-null virus (Fig. 7A). Viral titers were quantified in peripheral organs that reovirus infects via the bloodstream, including heart, liver, intestine, and spleen. At each time point assessed, titers of wild-type virus in the organs assayed were greater than those of the σ1s-null virus. To determine whether σ1s is required for hematogenous reovirus spread following intracranial inoculation, we inoculated newborn C57/BL6 mice intracranially with 100 PFU of rsT3D or rsT3D σ1s-null and determined titers in the heart, intestine, liver, and spleen at days 4, 8, and 12 postinoculation (Fig. 7B). Again, titers of wild-type virus were higher than those of σ1s-deficient virus in each of the target organs tested at days 4 and 8. Only at day 12 did titers of the σ1s-null mutant approximate, or in some cases exceed, those of wild-type virus. These data suggest that σ1s is required for efficient reovirus spread by hematogenous routes, regardless of the site of inoculation.

Analysis of S1 gene sequences of virus isolates from organs containing disseminated σ1s-null virus following intracranial inoculation revealed a reversion to wild-type sequence in 20 of 47 viruses tested (43%). These data provide further support for the contention that σ1s acts to facilitate hematogenous reovirus dissemination.

Reovirus disseminates to the brain by hematogenous and neural routes. To determine whether type 3 reovirus can disseminate to the brain using hematogenous pathways, we transected the sciatic nerve prior to hind limb inoculation. The sciatic nerve is the principal neural conduit by which reovirus spreads from the hind limb to the spinal cord (41). Sectioning the sciatic nerve should inhibit virus transmission to the CNS by neural routes but not affect spread by hematogenous pathways (41). The left sciatic nerve of two-day-old C57/BL6 mice was transected prior to inoculation in the left hind limb muscle with 10^6 PFU of rsT3D or rsT3D σ1s-null virus. In parallel, mice that were not subjected to sciatic nerve section were inoculated intramuscularly with 10^6 PFU of rsT3D or rsT3D σ1s-null virus. At 2 and 4 days postinoculation, viral titers were quantified in the hind limb muscle, spinal cord, brain, heart, intestine, liver, and spleen (Fig. 8). Titers of wild-type and σ1s-null virus at the site of inoculation were unaffected by the neurectomy (Fig. 8A). However, sciatic nerve sectioning resulted in a modest decrease in spinal cord titers of both viruses at day 2 and a 100-fold decrease at day 4 in comparison to those in mice with intact sciatic nerves. This finding suggests that viral spread to the spinal cord by neural pathways was successfully interrupted by sciatic nerve transection. The residual virus in the spinal cord likely results from spread via the femoral nerve, which enervates the quadriceps muscle that opposes the hamstring muscle into which virus was inoculated.

Following disruption of neural transmission by sciatic nerve section, rsT3D was still detected in the brain (Fig. 8A). Although titers of wild-type virus in the spinal cord were reduced 100-fold compared to those in controls following sciatic nerve transection, neurectomy reduced viral titers in the brain less than 10-fold. In addition, viral titers in organs that reovirus infects via the blood, including the heart, intestine, liver, and spleen, were largely unaffected by sciatic nerve transection. These findings confirm that spread to these organs is achieved by hematogenous routes and indicate that hematogenous pathways disseminate type 3 reovirus to every organ system in the animal, including the brain. Most strikingly, titers of the σ1s-null virus in the brain were markedly reduced following sciatic nerve section. Thus, type 3 reovirus uses both neural and hematogenous routes to spread to the brain, and σ1s is required for dissemination only by the hematogenous pathway.

DISCUSSION

In this study, we found that nonstructural protein σ1s is a critical determinant of type 3 reovirus dissemination within its host by hematogenous routes but is dispensable for spread by neural pathways. Following intramuscular inoculation of newborn mice, viral loads were markedly higher in the blood of animals infected with wild-type virus than in those inoculated with σ1s-null virus. Concordantly, wild-type virus produced higher titers in organs that reovirus targets via the bloodstream, including the heart, intestine, liver, and spleen. In contrast, wild-type and σ1s-null viruses traffic to the spinal cord with equivalent efficiency. Together, these data support a role for σ1s in promoting reovirus spread through the bloodstream

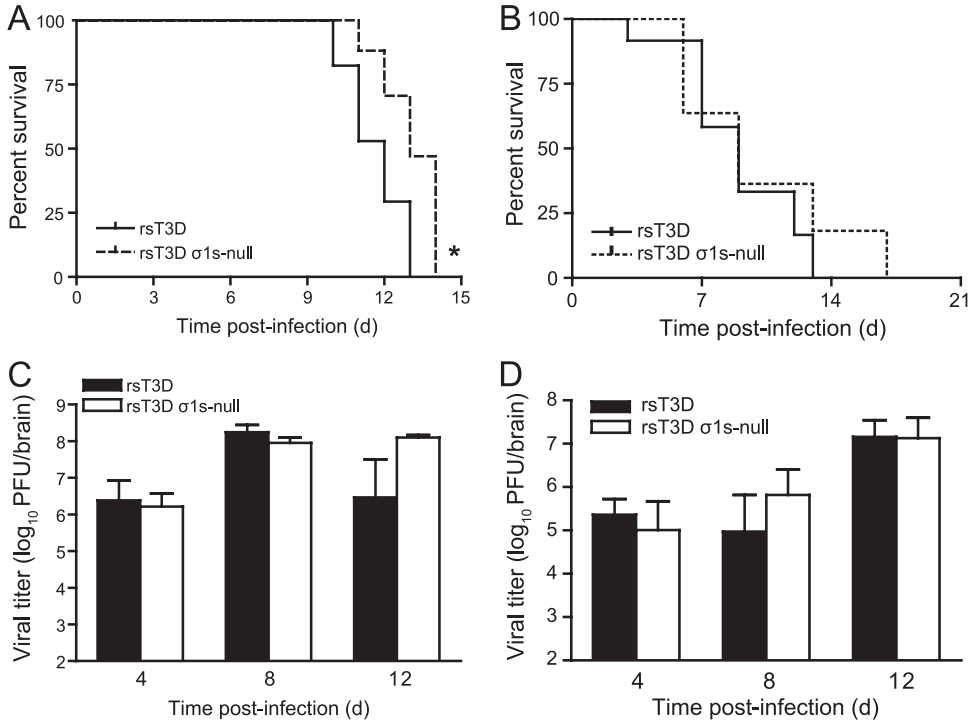

FIG. 4. (A and B) The σ1s protein modestly enhances reovirus neurovirulence after intracranial inoculation. (A) Newborn C57/BL6 mice were inoculated intracranially with 100 PFU of rsT3D or rsT3D σ1s-null. Mice (n = 17 for each virus strain) were monitored for survival for 14 days. *, $P < 0.005$ as determined by log-rank test in comparison to rsT3D. (B) Newborn Swiss Webster ND4 mice were inoculated intracranially with 100 PFU of rsT3D or rsT3D σ1s-null. Mice (n = 8 to 12) were monitored for survival for 17 days. (C and D) The σ1s protein is dispensable for reovirus replication in the CNS. (C) Newborn C57/BL6 mice were inoculated intracranially with 100 PFU of rsT3D or rsT3D σ1s-null. At days 4, 8, and 12 postinoculation, viral titers in the brain were determined by plaque assay. Results are expressed as mean viral titers for 5 to 8 animals for each time point. Error bars indicate standard errors of the means. (D) Newborn Swiss Webster ND4 mice were inoculated intracranially with 100 PFU of rsT3D or rsT3D σ1s-null. At days 4, 8, and 12 postinoculation, viral titers in the brain were determined by plaque assay. Results are expressed as mean viral titers for 5 to 8 animals for each time point. Error bars indicate standard errors of the means.

and indicate that σ1s is dispensable for reovirus neurotransmission.

Type 3 reoviruses disseminate within their hosts by hematogenous (1) and neural (41) pathways. Severing the sciatic nerve prior to hind-limb inoculation blocks virus spread to the spinal cord (41). This finding indicates that neural, but not hematogenous, pathways are important for delivering reovirus to the CNS. Consistent with the hypothesis that type 3 reoviruses invade the CNS by neural routes, we found that titers of wild-type and σ1s-null viruses were equivalent in the spinal

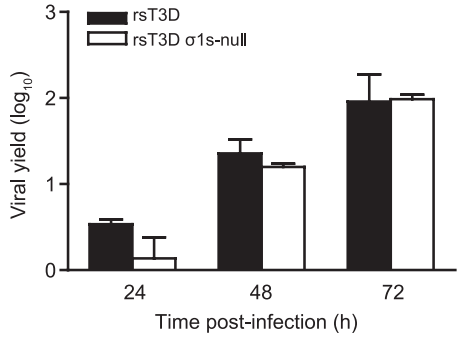

FIG. 5. The σ1s protein is not required for reovirus replication in primary mouse neurons. Cortical neurons were harvested from C57/BL6 mouse embryos at developmental day E15 and cultured for 7 days prior to infection. Neurons were adsorbed with rsT3D or rsT3D σ1s-null at an MOI of 1 PFU/cell. Titers of virus in cell lysates were determined by plaque assay at the indicated times postinfection. Results are expressed as mean viral yield for triplicate samples. Error bars indicate standard deviations.

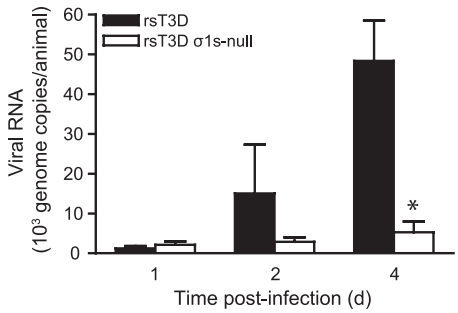

FIG. 6. The σ1s protein is required for the establishment of reovirus viremia. Newborn C57/BL6 mice were inoculated intramuscularly with 10^6 PFU of rsT3D or rsT3D σ1s-null. At days 1, 2, or 4 postinoculation, mice were euthanized, blood was collected, and viral genome copies in blood were determined by RT-qPCR. Results are expressed as mean viral genome copies per animal for 3 to 5 animals at each time point. Error bars indicate standard errors of the means. *, $P < 0.05$ as determined by Mann-Whitney test in comparison to rsT3D.

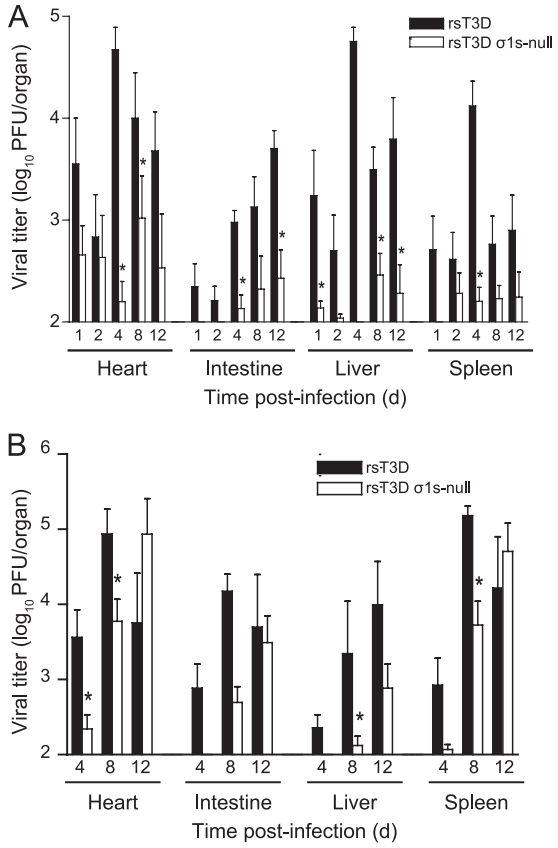

FIG. 7. (A) The σ1s protein is required for hematogenous reovirus dissemination following intramuscular inoculation. Newborn C57/BL6 mice were inoculated in the left hind limb with 10^6 PFU of rsT3D or rsT3D σ1s-null. At days 1, 2, 4, 8, and 12 postinoculation, mice were euthanized, the organs shown were resected, and viral titers were determined by plaque assay. Results are expressed as mean viral titers for 6 to 9 animals for each time point. Error bars indicate standard errors of the means. *, $P < 0.05$ as determined by Mann-Whitney test in comparison to rsT3D. (B) The σ1s protein enhances reovirus dissemination following intracranial inoculation. Newborn C57/BL6 mice were inoculated intracranially with 100 PFU of rsT3D or rsT3D σ1s-null. At days 4, 8, and 12 postinoculation, mice were euthanized, the organs shown were resected, and viral titers were determined by plaque assay. Results are expressed as mean viral titers for 5 to 8 animals for each time point. Error bars indicate SEM. *, $P < 0.05$ as determined by Mann-Whitney test in comparison to rsT3D.

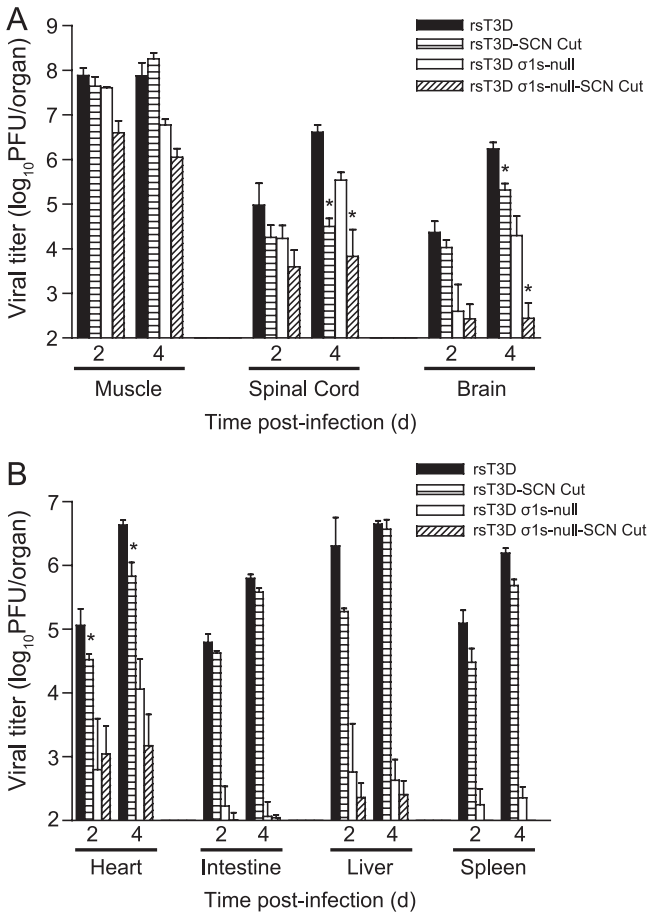

FIG. 8. Reovirus disseminates to the CNS by hematogenous and neural routes. The left sciatic nerve of newborn C57/BL6 mice was sectioned prior to inoculation in the left hind limb with 10^6 PFU of rsT3D or rsT3D σ1s-null. In parallel, mice in which the left sciatic nerve was not sectioned were inoculated in the left hind limb with 10^6 PFU of rsT3D or rsT3D σ1s-null. At days 2 and 4 postinoculation, mice were euthanized, hind limb muscle, spinal cord, and brain (A) and heart, intestine, liver, and spleen (B) were resected, and viral titers were determined by plaque assay. Results are expressed as mean viral titers for 6 animals for each time point. Error bars indicate standard errors of the means. *, $P < 0.05$ as determined by Mann-Whitney test in comparison to animals in which the sciatic nerve was not sectioned.

cord at each time point examined (Fig. 3B). In contrast, viral titers in the brain were substantially higher at day 4 for mice inoculated with wild-type virus in comparison to those infected with the σ1s-null mutant (Fig. 3B). These data suggest that invasion of the brain by type 3 reovirus by neural pathways is preceded by virus delivered hematogenously. At days 8 and 12 postinoculation, titers in the brain were equivalent for wild-type and σ1s-null virus (Fig. 3B), suggesting that the majority of reovirus transport to the brain by neural pathways occurs subsequent to delivery of virus to the brain via the bloodstream.

To determine whether hematogenous mechanisms can disseminate type 3 reovirus to the brain, we interrupted virus transmission via neural routes by sectioning the sciatic nerve prior to hind limb inoculation. Consistent with previous work (41), we found that sciatic nerve transection markedly reduced viral titers in the spinal cord (Fig. 8A), presumably as a consequence of limited neural transmission. However, although brain titers were diminished by sciatic nerve section, significant levels of wild-type virus were detected at this site. In addition, section of the sciatic nerve prior to inoculation with the σ1s-null virus almost completely eliminated its spread to the brain. These results indicate that both hematogenous and neural pathways function to disseminate type 3 reovirus to the brain.

How reovirus accesses the bloodstream after intramuscular inoculation is not known. It also has not been determined whether reovirus disseminates hematogenously using cell-free or cell-associated mechanisms. Following viral replication in the hind limb muscle (12), virus may reach the blood by infecting endothelial cells that form the lymphatic and blood

vessels that supply muscle tissue. Alternatively, virus may infect phagocytic cells that subsequently migrate to lymphatic channels and eventually the bloodstream. Based on these possibilities, we think that there are three mechanisms by which σ1s may promote reovirus dissemination following intramuscular inoculation. First, σ1s may be essential for replication in a cell type that is required for hematogenous spread, such as lymphocytes or mononuclear cells. Second, σ1s may trigger apoptosis in cells at the site of viral inoculation (16), which is required for viral release and subsequent bloodstream invasion. Third, σ1s may inhibit some component of the host antiviral response to reovirus infection. It is possible that σ1s disrupts innate or adaptive immune mechanisms that allow reovirus to evade immune detection. In this scenario, the absence of σ1s would lead to more efficient reovirus clearance.

Although titers of wild-type and σ1s-null virus in the brain are equivalent at day 4 following intracranial inoculation, only a small fraction of infected animals contain σ1s-null virus in other organs in comparison to those infected with wild-type virus (Fig. 7B). The percentage of organs with disseminated σ1s-null virus increases at day 8, and by day 12, titers of the σ1s-null virus approximate those of wild-type virus. We envision three possibilities to explain the kinetics of reovirus dissemination from the brain following intracranial inoculation. First, the block to hematogenous dissemination for the σ1s-null virus may not be absolute, and a small percentage of the virus may reach the bloodstream even in the absence of σ1s expression. Thus, the low titers of σ1s-null virus in peripheral organs results from this limited level of disseminated virus that is capable of seeding organs such as the heart, liver, and spleen. Second, virus might spread from the brain by neural pathways and thus not require functional σ1s for this mode of transit. Much like the vasculature, neuronal pathways traverse every organ in the animal and provide a direct conduit for virus to access peripheral sites. The delayed kinetics with which the σ1s-null virus spreads to peripheral organs would be consistent with the idea that bloodstream dissemination is more rapid than neural dissemination. Third, hematogenous spread of the σ1s-null virus may result from reversion of the σ1s-null mutation to the wild type. In our experiments, a substantial portion of the disseminated σ1s-null virus had reverted to the wild type, supporting this possibility and further underscoring the importance of σ1s in promoting viremic spread. These mechanisms are not mutually exclusive, and it is possible that reovirus disseminates systemically from the brain following intracranial inoculation by a combination of neural and hematogenous pathways.

The means by which reovirus traffics within neurons is not known. The administration of colchicine to inhibit fast axonal transport (18, 35) prior to intramuscular inoculation inhibits spread of virus to the spinal cord (41). In contrast, transport to the spinal cord is not affected by treatment with β-β′-iminodipropronitrile (41), which selectively inhibits slow axonal transport (14). These data indicate that fast axonal transport pathways facilitate virus spread from the hind-limb muscle through the sciatic nerve to the spinal cord and presumably to the brain. However, the delay in invasion of the brain by the σ1s-null virus suggests that neural transmission of virus from the spinal cord to the brain is not rapid. Other viruses that traffic by neural routes from peripheral sites to the brain using fast axonal transport reach the brain with rapid kinetics (25, 48). For example, poliovirus is detected in the spinal cord within 2 h and reaches the brain by 24 h following intramuscular inoculation (21). Thus, it is possible that a mechanism other than fast axonal transport mediates transit of reovirus from the spinal cord to the brain.

Reovirus serotypes differ in tropism within the murine CNS (22, 45, 46). These differences segregate with the S1 gene (10, 38), which encodes attachment protein σ1 and nonstructural protein σ1s (33, 44). We previously demonstrated that type 1 reovirus σ1s protein is not required for viral infection and replication in the mouse brain (6). In this study, we found that a type 3 σ1s-null virus replicates in the murine CNS as efficiently as wild-type virus (Fig. 4B and C). Moreover, identical cell types and brain regions are infected by wild-type and σ1s-null viruses (data not shown). The σ1s protein also is dispensable for replication in primary cultures of neurons (Fig. 5). Collectively, these findings demonstrate that σ1s is not a determinant of viral tropism or replication in the brain. Instead, σ1s mediates hematogenous spread within the infected host. Differences in viral tropism in the murine CNS appear to be governed by attachment protein σ1. It remains unclear why infection with type 1 and type 3 reoviruses differs in the mouse brain. However, our work clearly indicates that σ1s does not influence this difference; rather, the basis for this distinction is likely differential binding to host cell receptors by the σ1 protein.

Following intramuscular inoculation, the survival of mice infected with the σ1s-null mutant was markedly increased compared to that of mice infected with wild-type virus (Fig. 3A). It is possible that systemic infection, leading to disease in multiple organ systems, is a major contributor to reovirus-induced mortality. In experimental mouse models, reovirus can cause a variety of diseases, including myocarditis (34), hepatitis (17, 26, 27), and biliary obstruction (2). Following intramuscular inoculation, higher titers of wild-type virus than of the σ1s-null mutant at sites of secondary replication may cause increased injury to other organ systems that leads to the dramatic differences in survival. The kinetics of reovirus delivery to the CNS also may be critical for the onset of encephalitis. Susceptibility to reovirus encephalitis is age dependent, and mice are refractory to reovirus disease when inoculated later than 8 days of age (37). It is possible that titers of the σ1s-null mutant in the brain do not reach the threshold required to cause disease within the necessary time frame.

We previously showed that the σ1s protein is required for hematogenous spread of type 1 reoviruses (6), which disseminate within the host by strictly blood-borne mechanisms. A type 1 σ1s-null virus replicates equivalently to wild-type virus in the intestine following peroral inoculation. Although both viruses are taken up by Peyer's patches, only the wild-type virus spreads to the mesenteric lymph node and bloodstream. These findings suggest that σ1s is essential for reovirus spread from intestinal lymphatics to the circulation, thereby allowing the establishment of viremia and dissemination to sites of secondary replication. Here, we demonstrate that type 3 reovirus σ1s promotes viral bloodstream dissemination but is dispensable for transmission by neural routes. Collectively, these studies suggest that following replication at a site of inoculation, reoviruses use a serotype-independent pathway that requires σ1s

to disseminate through the lymphatic-hematogenous system to organs that support secondary viral replication. This work reveals how different mechanisms of dissemination contribute to reovirus pathogenesis and provides insight into the events at the pathogen-host interface that lead to systemic infection and disease.

ACKNOWLEDGMENTS

We thank members of our laboratory for many useful discussions and Pranav Danthi, Geoff Holm, and Bernardo Mainou for reviews of the manuscript. We thank Laura Ooms for assistance with quantitative RT-PCR. We are grateful to Patty Chen and Ken Tyler for assistance in developing the sciatic nerve section protocol.

This research was supported by Public Health Service awards T32 CA09385 (K.W.B.), F32 AI075776 (K.W.B.), T32 AI07611 (J.M.F.), T32 CA09385 (J.L.K.), F32 AI081486 (J.L.K.), and R37 AI38296 (T.S.D.) and the Elizabeth B. Lamb Center for Pediatric Research. Additional support was provided by Public Health Service awards CA68485 for the Vanderbilt-Ingram Cancer Center and DK20593 for the Vanderbilt Diabetes Research and Training Center.

REFERENCES

1. **Antar, A. A. R., et al.** 2009. Junctional adhesion molecule-A is required for hematogenous dissemination of reovirus. Cell Host Microbe **5:**59–71.
2. **Barton, E. S., et al.** 2003. Utilization of sialic acid as a coreceptor is required for reovirus-induced biliary disease. J. Clin. Invest. **111:**1823–1833.
3. **Bijlenga, G.** 1978. A potency test which simulates natural exposure for measuring post-exposure activity of rabies vaccines. A proposal for preparing a relevant international reference preparation. Dev. Biol. Stand. **40:**203–208.
4. **Bodkin, D. K., and B. N. Fields.** 1989. Growth and survival of reovirus in intestinal tissue: role of the L2 and S1 genes. J. Virol. **63:**1188–1193.
5. **Bodkin, D. K., M. L. Nibert, and B. N. Fields.** 1989. Proteolytic digestion of reovirus in the intestinal lumens of neonatal mice. J. Virol. **63:**4676–4681.
6. **Boehme, K. W., K. M. Guglielmi, and T. S. Dermody.** 2009. Reovirus nonstructural protein σ1s is required for establishment of viremia and systemic dissemination. Proc. Natl. Acad. Sci. U. S. A. **106:**19986–19991.
7. **Cashdollar, L. W., R. A. Chmelo, J. R. Wiener, and W. K. Joklik.** 1985. Sequences of the S1 genes of the three serotypes of reovirus. Proc. Natl. Acad. Sci. U. S. A. **82:**24–28.
8. **Cenatiempo, Y., et al.** 1984. Two initiation sites detected in the small s1 species of reovirus mRNA by dipeptide synthesis in vitro. Proc. Natl. Acad. Sci. U. S. A. **81:**1084–1088.
9. **Dermody, T. S., M. L. Nibert, R. Bassel-Duby, and B. N. Fields.** 1990. Sequence diversity in S1 genes and S1 translation products of 11 serotype 3 reovirus strains. J. Virol. **64:**4842–4850.
10. **Dichter, M. A., and H. L. Weiner.** 1984. Infection of neuronal cell cultures with reovirus mimics in vitro patterns of neurotropism. Ann. Neurol. **16:**603–610.
11. **Ernst, H., and A. J. Shatkin.** 1985. Reovirus hemagglutinin mRNA codes for two polypeptides in overlapping reading frames. Proc. Natl. Acad. Sci. U. S. A. **82:**48–52.
12. **Flamand, A., J. P. Gagner, L. A. Morrison, and B. N. Fields.** 1991. Penetration of the nervous systems of suckling mice by mammalian reoviruses. J. Virol. **65:**123–131.
13. **Furlong, D. B., M. L. Nibert, and B. N. Fields.** 1988. Sigma 1 protein of mammalian reoviruses extends from the surfaces of viral particles. J. Virol. **62:**246–256.
14. **Hansson, G., K. Kristensson, Y. Olsson, and J. Sjostrand.** 1971. Embryonal and postnatal development of mast cells in rat peripheral nerve. Acta Neuropathol. **17:**139–149.
15. **Hoyt, C. C., R. J. Bouchard, and K. L. Tyler.** 2004. Novel nuclear herniations induced by nuclear localization of a viral protein. J. Virol. **78:**6360–6369.
16. **Hoyt, C. C., et al.** 2005. Nonstructural protein σ1s is a determinant of reovirus virulence and influences the kinetics and severity of apoptosis induction in the heart and central nervous system. J. Virol. **79:**2743–2753.
17. **Johnson, E. M., et al.** 2009. Genetic and pharmacologic alteration of cathepsin expression influences reovirus pathogenesis. J. Virol. **83:**9630–9640.
18. **Karlsson, J. O., and J. Sjostrand.** 1969. The effect of colchicine on the axonal transport of protein in the optic nerve and tract of the rabbit. Brain Res. **13:**617–619.
19. **Kobayashi, T., et al.** 2007. A plasmid-based reverse genetics system for animal double-stranded RNA viruses. Cell Host Microbe **1:**147–157.
20. **Kristensson, K., E. Lycke, and J. Sjostrand.** 1971. Spread of herpes simplex virus in peripheral nerves. Acta Neuropathol. **17:**44–53.
21. **Lancaster, K. Z., and J. K. Pfeiffer.** 2010. Limited trafficking of a neurotropic virus through inefficient retrograde axonal transport and the type I interferon response. PLoS Pathog. **6:**e1000791.
22. **Morrison, L. A., R. L. Sidman, and B. N. Fields.** 1991. Direct spread of reovirus from the intestinal lumen to the central nervous system through vagal autonomic nerve fibers. Proc. Natl. Acad. Sci. U. S. A. **88:**3852–3856.
23. **Nibert, M. L., J. D. Chappell, and T. S. Dermody.** 1995. Infectious subvirion particles of reovirus type 3 Dearing exhibit a loss in infectivity and contain a cleaved σ1 protein. J. Virol. **69:**5057–5067.
24. **Nibert, M. L., and L. A. Schiff.** 2001. Reoviruses and their replication, p. 1679–1728. *In* D. M. Knipe and P. M. Howley (ed.), Fields virology, fourth ed. Lippincott Williams & Wilkins, Philadelphia, PA.
25. **Ohka, S., W. X. Yang, E. Terada, K. Iwasaki, and A. Nomoto.** 1998. Retrograde transport of intact poliovirus through the axon via the fast transport system. Virology **250:**67–75.
26. **Papadimitriou, J. M.** 1965. Electron micrographic features of acute murine reovirus hepatitis. Am. J. Pathol. **47:**565–585.
27. **Papadimitriou, J. M.** 1966. Ultrastructural features of chronic murine hepatitis after reovirus type 3 infection. Br. J. Exp. Pathol. **47:**624–631.
28. **Penfold, M. E., P. Armati, and A. L. Cunningham.** 1994. Axonal transport of herpes simplex virions to epidermal cells: evidence for a specialized mode of virus transport and assembly. Proc. Natl. Acad. Sci. U. S. A. **91:**6529–6533.
29. **Poggioli, G. J., T. S. Dermody, and K. L. Tyler.** 2001. Reovirus-induced 1s-dependent G_2/M cell cycle arrest results from inhibition of p34cdc2. J. Virol. **75:**7429–7434.
30. **Poggioli, G. J., C. J. Keefer, J. L. Connolly, T. S. Dermody, and K. L. Tyler.** 2000. Reovirus-induced G_2/M cell cycle arrest requires σ1s and occurs in the absence of apoptosis. J. Virol. **74:**9562–9570.
31. **Richardson, B. A., and J. Overbaugh.** 2005. Basic statistical considerations in virological experiments. J. Virol. **79:**669–676.
32. **Rodgers, S. E., J. L. Connolly, J. D. Chappell, and T. S. Dermody.** 1998. Reovirus growth in cell culture does not require the full complement of viral proteins: identification of a σ1s-null mutant. J. Virol. **72:**8597–8604.
33. **Sarkar, G., et al.** 1985. Identification of a new polypeptide coded by reovirus gene S1. J. Virol. **54:**720–725.
34. **Sherry, B.** 1998. Pathogenesis of reovirus myocarditis. Curr. Top. Microbiol. Immunol. **233**(Pt 2)**:**51–66.
35. **Sjostrand, J., and J. O. Karlsson.** 1969. Axoplasmic transport in the optic nerve and tract of the rabbit: a biochemical and radioautographic study. J. Neurochem. **16:**833–844.
36. **Smith, R. E., H. J. Zweerink, and W. K. Joklik.** 1969. Polypeptide components of virions, top component and cores of reovirus type 3. Virology **39:**791–810.
37. **Tardieu, M., M. L. Powers, and H. L. Weiner.** 1983. Age-dependent susceptibility to reovirus type 3 encephalitis: role of viral and host factors. Ann. Neurol. **13:**602–607.
38. **Tardieu, M., and H. L. Weiner.** 1982. Viral receptors on isolated murine and human ependymal cells. Science **215:**419–421.
39. **Tsiang, H.** 1979. Evidence for intraaxonal transport of fixed and street rabies virus. J. Neuropathol. Exp. Neurol. **38:**286–297.
40. **Tyler, K. L., R. T. Bronson, K. B. Byers, and B. N. Fields.** 1985. Molecular basis of viral neurotropism: experimental reovirus infection. Neurology **35:**88–92.
41. **Tyler, K. L., D. A. McPhee, and B. N. Fields.** 1986. Distinct pathways of viral spread in the host determined by reovirus S1 gene segment. Science **233:**770–774.
42. **van't Wout, A. B., et al.** 1994. Macrophage-tropic variants initiate human immunodeficiency virus type 1 infection after sexual, parenteral, and vertical transmission. J. Clin. Invest. **94:**2060–2067.
43. **Virgin, H. W., IV. R. Bassel-Duby, B. N. Fields, and K. L. Tyler.** 1988. Antibody protects against lethal infection with the neurally spreading reovirus type 3 (Dearing). J. Virol. **62:**4594–4604.
44. **Weiner, H. L., K. A. Ault, and B. N. Fields.** 1980. Interaction of reovirus with cell surface receptors. I. Murine and human lymphocytes have a receptor for the hemagglutinin of reovirus type 3. J. Immunol. **124:**2143–2148.
45. **Weiner, H. L., D. Drayna, D. R. Averill, Jr., and B. N. Fields.** 1977. Molecular basis of reovirus virulence: role of the S1 gene. Proc. Natl. Acad. Sci. U. S. A. **74:**5744–5748.
46. **Weiner, H. L., M. L. Powers, and B. N. Fields.** 1980. Absolute linkage of virulence and central nervous system tropism of reoviruses to viral hemagglutinin. J. Infect. Dis. **141:**609–616.
47. **Yanagi, Y., M. Takeda, and S. Ohno.** 2006. Measles virus: cellular receptors, tropism and pathogenesis. J. Gen. Virol. **87:**2767–2779.
48. **Yang, W. X., et al.** 1997. Efficient delivery of circulating poliovirus to the central nervous system independently of poliovirus receptor. Virology **229:**421–428.

APPENDIX C

INTESTINAL MICROBIOTA PROMOTE ENTERIC VIRUS REPLICATION AND SYSTEMIC PATHOGENESIS

Sharon K. Kuss, Gavin T. Best, Chris A. Etheredge, Andrea J. Pruijssers, Johnna M. Frierson, Lora V. Hooper, Terence S. Dermody, and Julie K. Pfeiffer

Science. 334(6053): 249-252; 2011

Intestinal Microbiota Promote Enteric Virus Replication and Systemic Pathogenesis

Sharon K. Kuss *et al.*

Science **334**, 249 (2011);
DOI: 10.1126/science.1211057

Science (print ISSN 0036-8075; online ISSN 1095-9203) is published weekly, except the last week in December, by the American Association for the Advancement of Science, 1200 New York Avenue NW, Washington, DC 20005.

$CD14^{KO}$, but not $TLR2^{KO}$, mice (Fig. 4B and table S1). Thus, our results support a model (fig. S7) whereby LPS-induced signaling drives a viral "subversion" pathway via IL-10 production that promotes viral transmission to successive generations.

Detailed analysis of the actual viral load in subsequent generations of infected $IL\text{-}10^{KO}$ and $IL\text{-}6^{KO}$ mice revealed that it was reduced gradually and that it took different numbers of passages for various families to completely eliminate the virus (table S1 and fig. S8). Thus, it appears that, in early generations, a high viral load can compensate for the loss of the TLR4-dependent subversion pathway and overpower the adaptive immune response. However, the virus is eventually lost in each infected mouse pedigree, as the virus load is reduced with each subsequent passage (fig. S8).

Commensal microbiota are required for many homeostatic functions of the intestinal mucosa and other barrier tissues. Microbiota control tissue repair (*16*), induction of tolerance to self [including tolerance to itself (*17*) and to autoantigens of the host (*18*)], and oral tolerance of adults to ingested antigens (*19*, *20*). At present, it is unknown whether neonatal oral tolerance is also dependent on microbiota or whether MMTV induces neonatal oral tolerance to itself by a unique mechanism available to retroviruses. Commensals interact with various pathogens and protect the host against infection with pathogenic and opportunistic bacteria (*21*), protozoa (*22*), and fungi (*23*) or facilitate infection with helminthes (*24*). However, the role of commensal bacteria in viral transmission and/or pathogenesis is only beginning to unravel. It is highly likely that bacterial microbiota can play both protective (*25*) and abetting roles (present report) in their interactions with viruses. The lack of knowledge in this area makes it important to expand such investigations to other systems. It is not yet clear whether other viruses take advantage of bacterial products, such as LPS, to achieve successful transmission. Retroviruses transmitted through mucosal surfaces may also use similar strategies. In humans, the highest risk of human immunodeficiency virus (HIV) transmission occurs across mucosal surfaces among individuals who practice receptive anal intercourse (*26*), and risk is also high in infants breastfed by HIV-infected mothers (*27*, *28*). This study sheds light on the previously unknown role of commensal microbiota in retroviral pathogenesis and suggests new approaches to the prevention of mucosal transmission, viral-specific vaccination, and therapies.

References and Notes

1. E. P. Browne, D. R. Littman, *PLoS Pathog.* **5**, e1000298 (2009).
2. A. W. Hardy, D. R. Graham, G. M. Shearer, J. P. Herbeuval, *Proc. Natl. Acad. Sci. U.S.A.* **104**, 17453 (2007).
3. M. Kane *et al*., *Immunity* **35**, 135 (2011).
4. M. H. Malim, M. Emerman, *Cell Host Microbe* **3**, 388 (2008).
5. U. Dittmer *et al*., *Immunity* **20**, 293 (2004).
6. B. A. Jude *et al*., *Nat. Immunol.* **4**, 573 (2003).
7. R. Medzhitov, P. Preston-Hurlburt, C. A. Janeway Jr., *Nature* **388**, 394 (1997).
8. A. Poltorak *et al*., *Science* **282**, 2085 (1998).
9. T. Kawai, S. Akira, *Nat. Immunol.* **11**, 373 (2010).
10. J. C. Rassa, J. L. Meyers, Y. Zhang, R. Kudaravalli, S. R. Ross, *Proc. Natl. Acad. Sci. U.S.A.* **99**, 2281 (2002).
11. T. V. Golovkina, J. P. Dudley, S. R. Ross, *J. Immunol.* **161**, 2375 (1998).
12. P. Marrack, E. Kushnir, J. Kappler, *Nature* **349**, 524 (1991).
13. D. A. Hill, D. Artis, *Annu. Rev. Immunol.* **28**, 623 (2010).
14. T. V. Golovkina, M. Shlomchik, L. Hannum, A. Chervonsky, *Science* **286**, 1965 (1999).
15. F. E. Dewhirst *et al*., *Appl. Environ. Microbiol.* **65**, 3287 (1999).
16. S. Rakoff-Nahoum, J. Paglino, F. Eslami-Varzaneh, S. Edberg, R. Medzhitov, *Cell* **118**, 229 (2004).
17. S. Rakoff-Nahoum, R. Medzhitov, *Mucosal Immunol.* **1**, (Suppl 1), S10 (2008).
18. L. Wen *et al*., *Nature* **455**, 1109 (2008).
19. M. C. Moreau, G. Corthier, *Infect. Immun.* **56**, 2766 (1988).
20. N. Sudo *et al*., *J. Immunol.* **159**, 1739 (1997).
21. B. Stecher, W. D. Hardt, *Trends Microbiol.* **16**, 107 (2008).
22. A. Benson, R. Pifer, C. L. Behrendt, L. V. Hooper, F. Yarovinsky, *Cell Host Microbe* **6**, 187 (2009).
23. M. J. Wargo, D. A. Hogan, *Curr. Opin. Microbiol.* **9**, 359 (2006).
24. K. S. Hayes *et al*., *Science* **328**, 1391 (2010).
25. T. Ichinohe *et al*., *Proc. Natl. Acad. Sci. U.S.A.* **108**, 5354 (2011).
26. R. A. Royce, A. Seña, W. Cates Jr., M. S. Cohen, *N. Engl. J. Med.* **336**, 1072 (1997).
27. R. Nduati *et al*., *JAMA* **283**, 1167 (2000).
28. J. H. Humphrey *et al*.; ZVITAMBO study group, *BMJ* **341**, c6580 (2010).

Acknowledgments: We thank B. Theriault and A. Vest for their help in monitoring gnotobiotic animals. This work was supported by T32GM007183 to M.K., K.K., and C.M.; by T32 AI065382-01 to L.C.; by Juvenile Diabetes Research Foundation grants 2005-204 and 2007-353; by the National Institute of Allergy and Infectious Diseases (NIAID) NIH AI082418 and the National Institute of Diabetes and Digestive and Kidney Diseases, NIH, Digestive Disease Research Core Center grant DK42086 to A.V.C.; by National Cancer Institute, NIH, grant CA100383 and NIAID grant AI090084 to T.V.G.; and by a grant (P30 CA014599) to The University of Chicago. A material transfer agreement is required for use of the SPF and GF C3H-based mutant strains of mice. The data reported in this paper are tabulated in the main paper and the supporting online material.

Supporting Online Material

www.sciencemag.org/cgi/content/full/334/6053/245/DC1
Materials and Methods
Figs. S1 to S8
Table S1
References (*29*–*48*)

5 July 2011; accepted 24 August 2011
10.1126/science.1210718

Intestinal Microbiota Promote Enteric Virus Replication and Systemic Pathogenesis

Sharon K. Kuss,[1] Gavin T. Best,[1] Chris A. Etheredge,[1]* Andrea J. Pruijssers,[2,3] Johnna M. Frierson,[3,4] Lora V. Hooper,[1,5,6] Terence S. Dermody,[2,3,4] Julie K. Pfeiffer[1]†

Intestinal bacteria aid host health and limit bacterial pathogen colonization. However, the influence of bacteria on enteric viruses is largely unknown. We depleted the intestinal microbiota of mice with antibiotics before inoculation with poliovirus, an enteric virus. Antibiotic-treated mice were less susceptible to poliovirus disease and supported minimal viral replication in the intestine. Exposure to bacteria or their *N*-acetylglucosamine–containing surface polysaccharides, including lipopolysaccharide and peptidoglycan, enhanced poliovirus infectivity. We found that poliovirus binds lipopolysaccharide, and exposure of poliovirus to bacteria enhanced host cell association and infection. The pathogenesis of reovirus, an unrelated enteric virus, also was more severe in the presence of intestinal microbes. These results suggest that antibiotic-mediated microbiota depletion diminishes enteric virus infection and that enteric viruses exploit intestinal microbes for replication and transmission.

Enteric viruses encounter up to 10^{14} bacteria in the mammalian intestine (*1*). It is unclear whether commensal microorganisms affect enteric viruses. Poliovirus is an enteric human pathogen transmitted by the fecal-oral route and serves as a model for enteric virus infections (*2*). Orally acquired poliovirus undergoes a primary replication cycle in the gastrointestinal tract before dissemination. Poliovirus occasionally disseminates from the intestine to the central nervous system, which results in paralytic poliomyelitis days to weeks after initial infection in the gastrointestinal tract. A key question is whether microbiota influence viral replication in the gastrointestinal tract to augment systemic dissemination.

To investigate the effect of intestinal microbiota on poliovirus infection, mice susceptible to

[1]Department of Microbiology, University of Texas Southwestern Medical Center, Dallas, TX 75390, USA. [2]Department of Pediatrics, Vanderbilt University School of Medicine, Nashville, TN 37240, USA. [3]Elizabeth B. Lamb Center for Pediatric Research, Vanderbilt University School of Medicine, Nashville, TN 37240, USA. [4]Department of Pathology, Microbiology, and Immunology, Vanderbilt University School of Medicine, Nashville, TN 37240, USA. [5]Department of Immunology, University of Texas Southwestern Medical Center, Dallas, TX 75390, USA, [6]Howard Hughes Medical Institute.

*Present address: Neurosciences Department, Medical University of South Carolina, Charleston, SC 29425, USA.
†To whom correspondence should be addressed. E-mail: julie.pfeiffer@utsouthwestern.edu

poliovirus were treated with antibiotics to deplete microbes, and viral disease was monitored (fig. S1) (*3*). Murine poliovirus infection requires expression of the human poliovirus receptor, PVR (*4*–*6*). PVR-transgenic mice (PVRtg), however, are not susceptible to oral poliovirus infection unless rendered immunodeficient by interferon-α/β receptor gene inactivation (PVRtg-*Ifnar1*$^{-/-}$) (*7*, *8*). PVRtg-*Ifnar1*$^{-/-}$ mice were untreated or treated orally with four antibiotics before oral inoculation with poliovirus. Antibiotic treatment reduced culturable intestinal bacteria by a millionfold (Fig. 1A). The mortality of untreated mice was twice that of antibiotic-treated mice (Fig. 1B). Reintroduction of fecal bacteria into antibiotic-treated mice enhanced poliovirus disease, which suggested that microbiota promote poliovirus pathogenesis. However, when the intestinal lumen was bypassed by intraperitoneal inoculation of poliovirus, pathogenesis was microbiota-independent (Fig. 1C and fig. S2). Given that orally inoculated poliovirus enters the intestine and encounters the large number of bacteria that reside there, the microbiota-mediated enhancement of poliovirus pathogenesis in orally inoculated mice is likely initiated in the intestine.

To determine whether mice harboring microbiota support more efficient poliovirus replication than mice with depleted microbiota, we quantified viral titers from fecal samples (Fig. 1D and fig. S3A), because poliovirus was undetectable in intestinal tissue (fig. S4), and minimal intestinal pathology was evident (fig. S5). Peak poliovirus titers in feces from antibiotic-treated animals were lower than those from untreated mice, but titers from antibiotic-treated mice were higher at later times. Prolonged shedding from antibiotic-treated mice was due to slower peristalsis, because dye transit also was delayed (fig. S6) (*9*). We postulated that increased poliovirus titers from antibiotic-treated mice at late times might be due to extended shedding of unreplicated inoculum virus. To differentiate between replicated and inoculum virus, we first quantified fecal shedding of poliovirus from nonpermissive mice lacking PVR and observed elevated late titers in antibiotic-treated mice, which suggested that total viral titers in feces and replication are not linked (fig. S3B). We then quantified viral replication in PVR mice using light-sensitive poliovirus. Poliovirus propagated in the presence of neutral red dye is sensitive to light-induced inactivation by RNA cross-linking but loses light sensitivity upon replication in the dark inside mice, facilitating assessment of replication (*10*). We orally inoculated untreated or antibiotic-treated mice with light-sensitive poliovirus and collected feces in the dark. Fecal viruses were light-exposed or unexposed and quantified to determine replication status (fig. S7). PVRtg-*Ifnar1*$^{-/-}$ and PVRtg mice harboring microbiota supported efficient intestinal poliovirus replication, whereas antibiotic-treated mice did not (Fig. 1, E and F). Therefore, total fecal titers do not reflect viral replication, a fact only revealed by using light-sensitive viruses. Moreover, poliovirus intestinal replication was equivalent in *Ifnar1M*$^{+/+}$ and *Ifnar1*$^{-/-}$ mice, which suggested that intestinal replication was IFNAR-independent. Because poliovirus infection was lethal for a fraction of antibiotic-treated mice (Fig. 1B), it is possible that either minimal viral replication was sufficient for lethality or inoculum virus breached the epithelium and replicated in extraintestinal sites, occasionally initiating disease. Collectively, these results indicate that the microbiota enhance gastrointestinal poliovirus replication.

We gathered several lines of evidence suggesting that diminished poliovirus replication and disease in antibiotic-treated mice is due to microbiota depletion rather than direct effects of antibiotic treatment. We first tested whether antibiotics directly affect poliovirus and found that

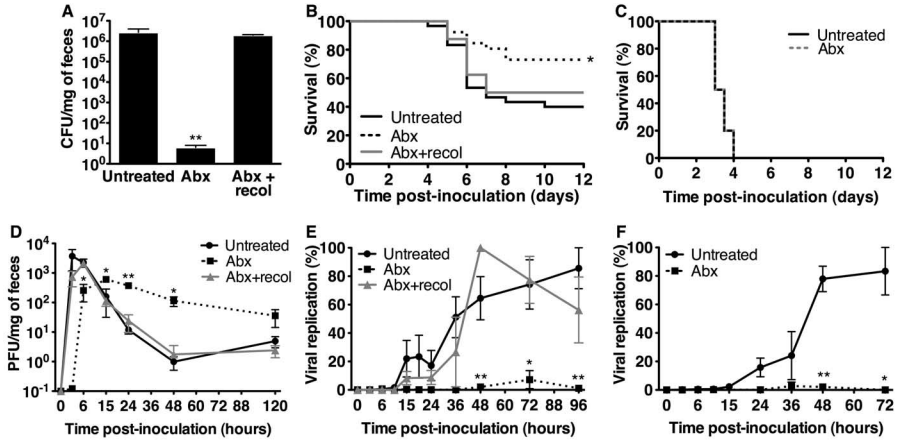

Fig. 1. Poliovirus pathogenesis, shedding, and replication in microbiota-depleted mice. (**A**) Bacterial loads in feces. PVRtg-*Ifnar1*$^{-/-}$ mice (n = 4 to 7) were untreated, antibiotic-treated (Abx) for 10 days, or antibiotic-treated for 8 days and recolonized for 2 days with fecal bacteria (Abx + recol). Feces were plated and grown anaerobically, yielding colony-forming units (CFU) per milligram of feces. (**B**) Survival of PVRtg-*Ifnar1*$^{-/-}$ mice orally inoculated with poliovirus (untreated, n = 30; Abx, n = 26; Abx + recol, n = 8). *P = 0.012, log-rank test. (**C**) Survival of PVRtg-*Ifnar1*$^{-/-}$ mice intraperitoneally inoculated with poliovirus (n = 10 mice each). (**D**) Poliovirus shedding from PVRtg-*Ifnar1*$^{-/-}$ mice. Mice were orally inoculated with poliovirus, feces were collected (n = 2 to 26 per interval), and poliovirus was isolated and quantified by plaque assay, yielding plaque-forming units (PFU) per milligram of feces. (**E** and **F**) Poliovirus replication in intestinal tracts of PVRtg-*Ifnar1*$^{-/-}$ (E) or PVRtg (F) mice orally inoculated with light-sensitive poliovirus (n = 3 to 9 mice per interval). Feces were harvested, and virus was quantified with or without light exposure to determine percent replication. Symbols represent means + SEM, *P < 0.05, **P < 0.01, Student's t test. n = 2 to 6 experiments for all.

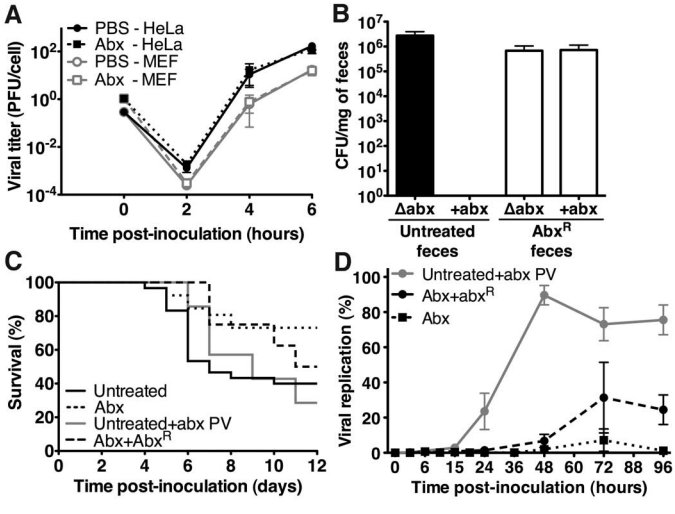

Fig. 2. The effects of antibiotic treatment on poliovirus replication and pathogenesis. (**A**) Poliovirus replication kinetics in MEFs and HeLa cells with or without antibiotics. (**B**) Fecal bacterial loads from untreated or antibiotic-treated mice harboring antibiotic-resistant (abxR) bacteria. Feces were plated on rich medium with or without four antibiotics. (**C**) Survival of PVRtg-*Ifnar1*$^{-/-}$ mice orally inoculated with poliovirus premixed with four antibiotics (Untreated+abx PV, n = 9 mice) or poliovirus alone in antibiotic-treated mice harboring AbxR bacteria (Abx + abxR, n = 8 mice). (Results from untreated and antibiotic-treated mice are from Fig. 1B.) (**D**) Replication of light-sensitive poliovirus in untreated mice receiving poliovirus + antibiotics inoculum and antibiotic-treated mice harboring abxR bacteria in comparison with antibiotic-treated mice. (Results from antibiotic-treated mice are from Fig. 1E.) Each symbol represents mean ± SEM. (A) and (B), n = 2 to 5 experiments, (C) and (D) are from a representative experiment.

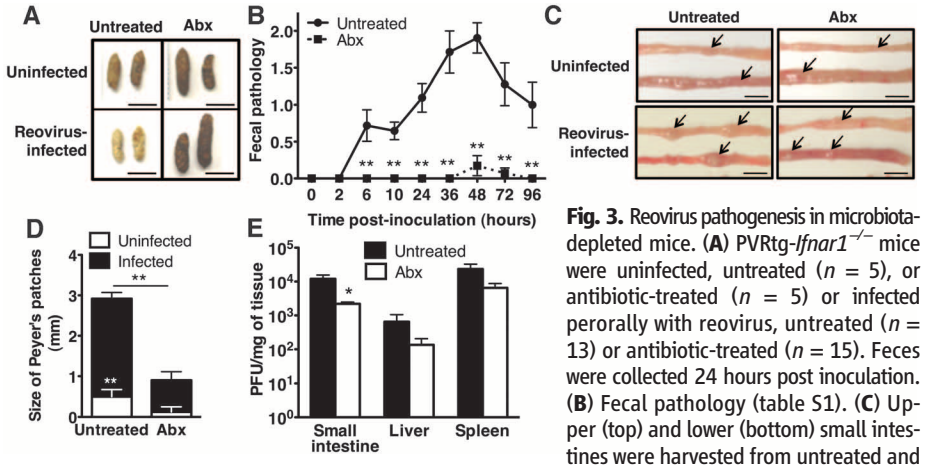

Fig. 3. Reovirus pathogenesis in microbiota-depleted mice. (**A**) PVRtg-*Ifnar1*$^{-/-}$ mice were uninfected, untreated (n = 5), or antibiotic-treated (n = 5) or infected perorally with reovirus, untreated (n = 13) or antibiotic-treated (n = 15). Feces were collected 24 hours post inoculation. (**B**) Fecal pathology (table S1). (**C**) Upper (top) and lower (bottom) small intestines were harvested from untreated and antibiotic-treated PVRtg-*Ifnar1*$^{-/-}$ mice on day 4 post infection or from uninfected mice. Arrows indicate Peyer's patches. (**D**) Quantification of Peyer's patch sizes [from (C)] from uninfected and infected mice. (**E**) Reovirus titers from day 4 post infection PVRtg-*Ifnar1*$^{-/-}$mouse tissues. Plaque assays were performed using murine L929 cells, yielding PFU per milligram of tissue. For (B) to (E), n = 4 to 9 untreated mice, n = 2 to 9 antibiotic-treated mice. Each symbol or bar denotes the mean + SEM. *P < 0.05, **P < 0.01, Student's t test. Scale bars in (A) and (C), 5 mm. (A) and (C), representative of 3 to 5 experiments; n = 2 to 4 experiments for (B), (D), and (E).

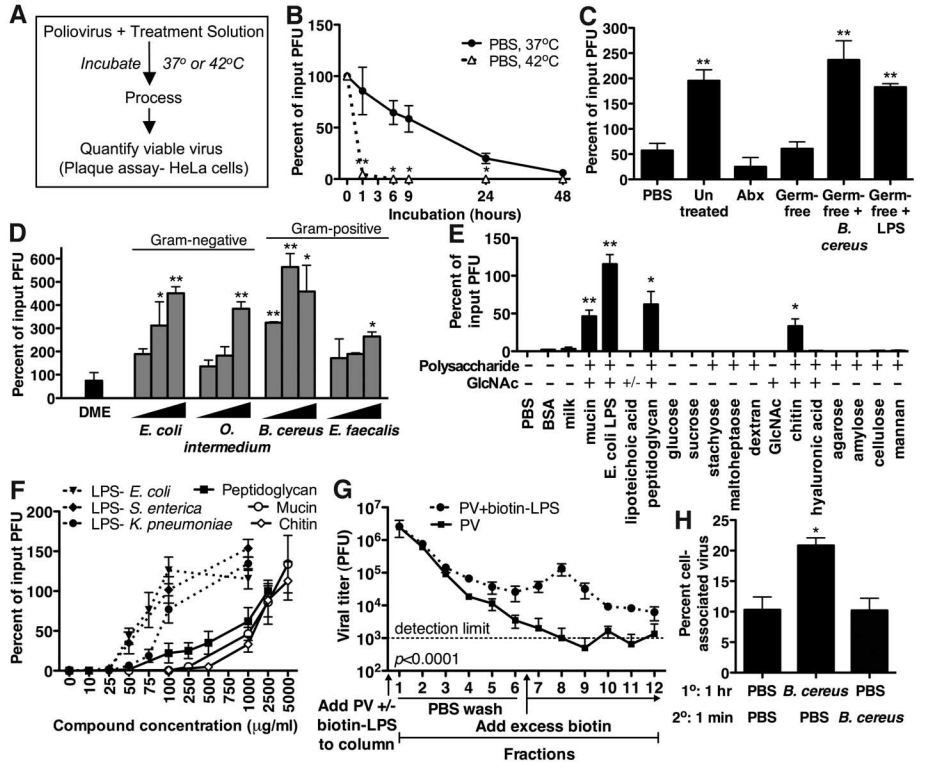

Fig. 4. Effects of bacteria and polysaccharides on poliovirus. (**A**) Strategy for in vitro poliovirus infectivity experiments. (**B**) Poliovirus recovered after incubation in PBS. (**C**) Poliovirus infectivity after exposure to PBS, feces, or feces supplemented with *B. cereus* or LPS (6 hours at 37°C). (**D**) Poliovirus infectivity after exposure to medium (DME) or bacterial strains (10^7, 10^8, or 10^9 CFU) (6 hours at 37°C). (**E**) Poliovirus infectivity after incubation with compounds (1 mg/ml) (6 hours at 42°C). (**F**) Poliovirus infectivity after incubation with various concentrations of compounds (6 hours at 42°C). (**G**) Poliovirus binding to LPS. Poliovirus was incubated with or without biotinylated LPS for 1 hour at 37°C. A monomeric avidin column was loaded with samples and washed with PBS to collect fractions 1 to 6. Excess biotin was added to elute (fractions 7 to 12). Poliovirus was quantified yielding PFU per fraction, P < 0.0001, two-way analysis of variance (ANOVA). (**H**) Binding of radiolabeled poliovirus to HeLa cells. ^{35}S-labeled poliovirus was incubated with PBS or 10^8 CFU *B. cereus* for 1 hour at 37°C. An equal volume of PBS or *B. cereus* was added, followed by immediate incubation with HeLa cells. After washing, cell-associated radioactivity was quantified. For all, n = 2 to 8 experiments, and bars and symbols denote mean ± SEM, *P < 0.05, **P < 0.01, Student's t test.

poliovirus replication kinetics were identical in the presence and absence of antibiotics in HeLa cells and PVRtg mouse embryo fibroblasts (MEFs) (Fig. 2A). We next assayed poliovirus replication and pathogenesis in antibiotic-treated mice harboring antibiotic-resistant bacteria. For these experiments, we treated PVRtg-*Ifnar1*$^{-/-}$ mice with antibiotics to select antibiotic-resistant microbiota (fig. S8). After several weeks, fecal bacteria were insensitive to antibiotics in vitro (Fig. 2B). The strain resistant to multiple antibiotics was identified as *Ochrobactrum intermedium,* a Gram-negative aerobe, by 16*S* ribosomal DNA sequencing of fecal-derived subclones (fig. S9). Poliovirus replicated and was pathogenic in antibiotic-treated mice harboring *O. intermedium* (Fig. 2, C and D). Finally, poliovirus mixed with antibiotics before oral inoculation of mice replicated and was pathogenic (Fig. 2, C and D). Therefore, diminished poliovirus replication and pathogenesis in antibiotic-treated mice is not due to direct antiviral effects of antibiotics.

Because all enteric viruses encounter intestinal bacteria within the host, we examined the specificity of the microbiota effects using reovirus, an enteric virus that infects most mammals (*11*). Although immunocompetent adult mice do not display overt reovirus disease symptoms, immunocompromised adult mice develop nonfatal disease after oral inoculation with reovirus strain T3SA+. We orally inoculated untreated or antibiotic-treated immunocompromised PVRtg-*Ifnar1*$^{-/-}$ mice with reovirus. Feces from untreated mice were yellow, oily, and hardened, typical of biliary obstruction from T3SA+ reovirus replication and damage (*12*), whereas feces from antibiotic-treated mice appeared normal (Fig. 3, A and B). Furthermore, analysis of intestines revealed severe reovirus-induced pathology, with enlarged Peyer's patches in untreated, but not antibiotic-treated, mice (Fig. 3, C and D). Reovirus titers in intestines from untreated mice were significantly higher than those from antibiotic-treated mice (Fig. 3E). These results suggest that intestinal microbes promote reovirus disease and, therefore, may promote infection with other enteric viruses.

The microbiota-dependent enhancement of poliovirus replication and pathogenesis could be mediated by microbiota-induced host effects, viral effects, or both. To discriminate between these possibilities, we investigated whether intestinal microbes alter poliovirus infectivity. First, we tested whether poliovirus infectivity was altered by exposure to intestinal microbiota in vivo. We orally inoculated untreated, antibiotic-treated, and germ-free mice with poliovirus; harvested lumenal contents from the lower small intestine 2 hours postinfection; and quantified infectivity of isolated poliovirus in primary MEFs and HeLa cells. The infectivity in MEFs of poliovirus isolated from untreated mice was twice that of tissue culture–derived virus and antibiotic-treated and germ-free intestinal virus (fig. S10). Second, we developed an ex vivo–in vitro assay to examine

poliovirus infectivity (Fig. 4A). Poliovirus was incubated at 37° or 42°C, and viable virus was quantified by plaque assay. Poliovirus incubated in phosphate-buffered saline (PBS), feces from antibiotic-treated mice, and germ-free feces lost viability (Fig. 4, B and C). However, poliovirus incubated in untreated feces or germ-free feces supplemented with bacteria had significantly increased viability (Fig. 4C). Similarly, poliovirus incubated with Gram-negative (*Escherichia coli* or *O. intermedium*) or Gram-positive (*Bacillus cereus* or *Enterococcus faecalis*) bacteria had significantly increased viability (Fig. 4D). Exposure to *B. cereus* increased poliovirus infectivity more than 500%. Enhancement of poliovirus infectivity did not require live bacteria (fig. S11). Moreover, poliovirus incubated with certain bacterial surface polysaccharides, including lipopolysaccharide (LPS) and peptidoglycan (PG), had significantly enhanced yield over PBS-treated controls (Fig. 4, C and E, and fig. S12). The enhancement was not due to cellular effects of LPS or PG treatment (fig. S13). We tested a variety of glycans and other compounds, and only *N*-acetylglucosamine (GlcNAc)–containing polysaccharides (e.g., chitin) demonstrated activity (Fig. 4E). Mucin, a host protein modified with GlcNAc-containing polysaccharides, also had activity (*13*). Of the purified components tested, LPS was the most potent enhancer of poliovirus infectivity, with activity at concentrations 1/20th those of chitin or mucin (Fig. 4F). Using biotinylated LPS and monomeric avidin columns, we found that poliovirus binds LPS (Fig. 4G). Because *B. cereus* exposure produced the largest increase in poliovirus yield, we tested whether exposure to *B. cereus* enhanced radiolabeled poliovirus binding to HeLa cells, which would aid infection. Poliovirus incubated with *B. cereus* displayed adherence to HeLa cells 2 times that of controls (Fig. 4H). Overall, poliovirus infectivity was enhanced in the presence of intestinal microbiota in vitro and in vivo, which likely contributed to the enhanced replication and pathogenesis in microbiota-harboring mice.

Despite the well-known beneficial effects of intestinal microbes, we discovered that they augment enteric virus pathogenesis by enhancing viral replication. Intestinal microbes also induce egg hatching of an intestinal nematode in mice (*14*), which suggests that diverse pathogens exploit intestinal microbes for propagation. Our work implies that antibiotic-mediated microbiota depletion can have antiviral effects, although we do not advocate the use of antibiotics to prevent viral disease. However, understanding how microbiota promote enteric virus infections may reveal new antiviral strategies. Our results suggest that poliovirus binds specific microbe–associated surface polysaccharides, which enhances viral thermostability and attachment to host cells. Contrary to the known benefits of intestinal microbiota to the host (*1*), enteric viruses may have evolved to use intestinal microbes as a trigger for replication at a site optimal for transmission.

References and Notes

1. W. S. Garrett, J. I. Gordon, L. H. Glimcher, *Cell* **140**, 859 (2010).
2. M. A. Pallansch, R. P. Roos, in *Fields Virology*, D. M. Knipe, P. M. Howley, Eds. (Lippincott Williams & Wilkins, Philadelphia, ed. 4, 2001), pp. 723–775.
3. Materials and methods are available as supporting material on *Science* online.
4. R. B. Ren, F. Costantini, E. J. Gorgacz, J. J. Lee, V. R. Racaniello, *Cell* **63**, 353 (1990).
5. S. Koike *et al.*, *Proc. Natl. Acad. Sci. U.S.A.* **88**, 951 (1991).
6. M. Ida-Hosonuma *et al.*, *Arch. Virol.* **148**, 29 (2003).
7. M. Ida-Hosonuma *et al.*, *J. Virol.* **79**, 4460 (2005).
8. S. Ohka *et al.*, *J. Virol.* **81**, 7902 (2007).
9. G. D. Abrams, J. E. Bishop, *Proc. Soc. Exp. Biol. Med.* **126**, 301 (1967).
10. S. K. Kuss, C. A. Etheredge, J. K. Pfeiffer, *PLoS Pathog.* **4**, e1000082 (2008).
11. K. L. Tyler, in *Fields Virology*, D. M. Knipe, P. M. Howley, Eds. (Lippincott Williams & Wilkins, Philadelphia, ed. 4, 2001), vol. 1, pp. 1729–1945.
12. E. S. Barton *et al.*, *J. Clin. Invest.* **111**, 1823 (2003).
13. D. K. Podolsky, *J. Biol. Chem.* **260**, 8262 (1985).
14. K. S. Hayes *et al.*, *Science* **328**, 1391 (2010).

Acknowledgments: We thank B. Duerkop, C. Behrendt-Boyd, J. Charles, J. Richardson, and S. Gore for assistance; B. Levine and V. Sperandio for manuscript comments; and S. Koike for PVRtg mice. This research was supported by Public Health Service awards T32 AI007520 (S.K.K.); F32 NS071986 (A.J.P.); T32 AI07611 (J.M.F.); R37 AI38296, P30 CA68485, and P60 DK20593 (T.S.D.); R01 AI74668 (J.K.P.); the Elizabeth B. Lamb Center for Pediatric Research (T.S.D.); and a Pew Scholar award (J.K.P.). The data reported in the paper are tabulated in the main manuscript and in the supporting online material. The sequence data are available in GenBank (accession no. BankIt1475845 SEq. 10 JN613288).

Supporting Online Material

www.sciencemag.org/cgi/content/full/334/6053/249/DC1
Materials and Methods
Figs. S1 to S13
Table S1
References (*15*–*19*)

12 July 2011; accepted 7 September 2011
10.1126/science.1211057

MED12, the *Mediator Complex Subunit 12* Gene, Is Mutated at High Frequency in Uterine Leiomyomas

Netta Mäkinen,[1]* Miika Mehine,[1]* Jaana Tolvanen,[1] Eevi Kaasinen,[1] Yilong Li,[1] Heli J. Lehtonen,[1] Massimiliano Gentile,[2] Jian Yan,[3] Martin Enge,[3] Minna Taipale,[1,3] Mervi Aavikko,[1] Riku Katainen,[1] Elina Virolainen,[4] Tom Böhling,[4,5] Taru A. Koski,[1] Virpi Launonen,[1] Jari Sjöberg,[6] Jussi Taipale,[1,3] Pia Vahteristo,[1] Lauri A. Aaltonen[1]†

Uterine leiomyomas, or fibroids, are benign tumors that affect millions of women worldwide and that can cause considerable morbidity. To study the genetic basis of this tumor type, we examined 18 uterine leiomyomas derived from 17 different patients by exome sequencing and identified tumor-specific mutations in the *mediator complex subunit 12* (*MED12*) gene in 10. Through analysis of 207 additional tumors, we determined that *MED12* is altered in 70% (159 of 225) of tumors from a total of 80 patients. The Mediator complex is a 26-subunit transcriptional regulator that bridges DNA regulatory sequences to the RNA polymerase II initiation complex. All mutations resided in exon 2, suggesting that aberrant function of this region of *MED12* contributes to tumorigenesis.

Uterine leiomyomas, also called fibroids, are benign tumors that occur in 60% of women by the age of 45 years and that cause symptoms in about half of the cases (*1*). These symptoms include abdominal pain and discomfort and abnormal bleeding. Uterine leiomyomas are also an important cause of infertility [reviewed in (*2*, *3*)], and they are the most common medical reason for hysterectomy (*4*). Several recurrent genetic aberrations such as deletions in 7q, trisomy of chromosome 12, and various rearrangements affecting the *high mobility group AT-hook 2* (*HMGA2*) gene mapping to chromosome 12q14 (*5*–*7*) have been observed in uterine leiomyomas, but these occur at low frequency. To investigate whether these tumors have high-frequency genetic alterations, we investigated all protein-coding genes by exome sequencing in 18 uterine leiomyomas and the respective normal tissue DNAs. These tumors came from 17 different patients.

The most frequent tumor-specific alterations in the set of 18 tumors affected the *MED12* gene on chromosome Xq13.1. *MED12* is a subunit of the Mediator complex, which is thought to regulate global, as well as gene-specific, transcription (*8*). Ten tumors displayed a mutation, and eight

[1]Department of Medical Genetics, Genome-Scale Biology Research Program, 00014 University of Helsinki, Helsinki, Finland. [2]Center for Science Ltd., 02101 Espoo, Finland. [3]Science for Life Laboratory, Department of Biosciences and Nutrition, Karolinska Institutet, 14183 Stockholm, Sweden. [4]Department of Pathology, Haartman Institute, 00014 University of Helsinki, Helsinki, Finland. [5]Laboratory of Hospital District of Helsinki and Uusimaa, 00029 Helsinki University Central Hospital, Helsinki, Finland. [6]Department of Obstetrics and Gynecology, 00029 Helsinki University Central Hospital, Helsinki, Finland.

*These authors contributed equally to this work.
†To whom correspondence should be addressed. E-mail: lauri.aaltonen@helsinki.fi

APPENDIX D

UTILIZATION OF SIALYLATED GLYCANS AS CORECEPTORS ENHANCES THE NEUROVIRULENCE OF SEROTYPE 3 REOVIRUS

Johnna M. Frierson, Andrea J. Pruijssers, Jennifer Konopka, Dirk M. Rieter, Ty W. Abel, Thilo S. Stehle and Terence S. Dermody

Journal of Virology.Manuscript accepted with revisions*;*2012

Utilization of Sialylated Glycans as Coreceptors Enhances the Neurovirulence of Serotype 3 Reovirus

Johnna M. Frierson,[1,2] Andrea J. Pruijssers,[2,3] Jennifer L. Konopka,[2,3] Dirk M. Reiter,[4] Ty W. Abel,[1] Thilo Stehle,[3,4] and Terence S. Dermody[1,2,3,*]

Departments of Pathology, Microbiology, and Immunology[1] and Pediatrics[3] and Elizabeth B. Lamb Center for Pediatric Research,[2] Vanderbilt University School of Medicine, Nashville, TN 37232 and Interfaculty Institute of Biochemistry,[4] University of Tübingen, Hoppe-Seyler-Str. 4, D-72076 Tübingen

[*]Corresponding author. Mailing address: Lamb Center for Pediatric Research, D7235 MCN, Vanderbilt University School of Medicine, Nashville, TN 37232. Tel.: 615-343-9943. Fax: 615-343-9723. E-mail: terry.dermody@vanderbilt.edu.

Running title: Sialic acid binding enhances reovirus neurovirulence

ABSTRACT

Mammalian reoviruses display serotype-specific patterns of tropism and disease in the murine central nervous system (CNS) attributable to polymorphisms in viral attachment protein σ1. While all reovirus serotypes use junctional adhesion molecule-A as a cellular receptor, they differ in utilization of carbohydrate coreceptors. This observation raises the possibility that carbohydrate binding by σ1 influences reovirus pathology in the CNS. In this study, we sought to define the function of carbohydrate binding in reovirus neuropathogenesis. Newborn mice were inoculated intramuscularly with wild-type strain type 3 Dearing (T3D) and T3D-σ1R202W, a point-mutant T3D derivative that does not bind sialic acid (SA). Infected mice were monitored for survival, and viral loads at sites of primary and secondary replication were quantified. Fewer mice inoculated with wild-type virus survived in comparison to those inoculated with the mutant virus. Wild-type virus also produced higher titers in the spinal cord and brain at late times post-inoculation but lower titers in the liver in comparison to those produced by the mutant virus. In addition, wild-type virus was more virulent and produced higher titers in the brain than the mutant following intracranial inoculation. These animal infectivity studies suggest that T3D-σ1R202W harbors a defect in neural growth. Concordantly, compared with wild-type virus, mutant virus displayed a decreased capacity to infect and replicate in primary cultures of cortical neurons, a property dependent on cell-surface SA. These results suggest that SA binding enhances the kinetics of reovirus replication in neural tissues and highlight a functional role for sialylated glycans as reovirus coreceptors in the CNS.

INTRODUCTION

Attachment to specific cell-surface molecules is the initial step in viral infection. As such, receptor engagement can influence many aspects of viral pathogenesis, perhaps most prominently systemic dissemination and tropism for distinct host cells and tissues. Tropism of human immunodeficiency virus (HIV) (27), poliovirus (32), and SARS-coronavirus (15), among others, is strongly influenced by the capacity of the virus to bind specific receptors. Infection of discrete regions within the central nervous system (CNS) by strains of adeno-associated virus (AAV) is dependent on carbohydrate-binding specificity. AAV4 infects ependymal cells and utilizes α(2,3)-linked sialic acid (SA) as a receptor. In contrast, AAV5 uses both α(2,3)- and α(2,6)-linked SA to infect neurons (22). While much is known about the importance of these receptor-mediated functions in viral spread and tropism, precise mechanisms by which receptor utilization regulates viral infection in the CNS are not fully understood.

Mammalian orthoreoviruses (reoviruses), members of the *Reoviridae*, are nonenveloped viruses comprised of two concentric protein shells that enclose the 10 segments of the viral double-stranded RNA genome (37). These viruses are genetically tractable tools for studies of virus-receptor interactions and viral pathogenesis. In neonatal mice, reovirus serotypes 1 and 3 disseminate from sites of primary replication to the CNS. However, tropism for neural cells and resulting disease outcomes vary in a serotype-specific manner. Type 1 reovirus strains spread to the CNS via hematogenous routes and infect ependymal cells in the brain, which leads to a non-lethal hydrocephalus (40, 43, 44). In contrast, type 3 reovirus strains spread to the CNS using both neural and hematogenous routes and target neurons in the brain, which results in lethal encephalitis

(1, 6, 28, 40). These serotype-specific differences in tropism and disease segregate genetically with the viral S1 gene (43, 44), which encodes attachment protein σ1 (26, 45) and nonstructural protein σ1s (9, 17, 35). Both S1 gene products influence reovirus pathogenesis (1, 5-7, 23), with the σ1 protein thought to target the virus to discrete cell types in the CNS (14, 39).

Reovirus attachment protein σ1 is a filamentous trimer with three discrete domains: the tail, body, and head (11, 19, 31). Residues 1 to 160 encompass the tail domain, which inserts into the virion capsid (11, 20). This region of the molecule is predicted to form an α-helical coiled coil (16, 29). The body domain encompasses residues 170 to 309 and is comprised of a β-spiral repeat motif interrupted by a short α-helical coiled coil (31). The globular head domain incorporates residues 310 to 455 and folds into an 8-stranded β-barrel (11, 24, 36).

Receptors for reovirus are engaged by a multistep adhesion-strengthening process in which σ1 first binds to an abundant cell-surface carbohydrate with low affinity (3), which is followed by high-affinity interactions with junctional adhesion molecule-A (JAM-A) (2, 4). Sequences in the σ1 body domain mediate SA binding by type 3 strains (10, 31), whereas sequences in the σ1 head domain engage JAM-A (24). Interactions between σ1 and SA involve residues at the N-terminal portion of the body domain, between β-spiral repeats 2 and 3, where the SA moiety docks into a shallow pocket that is formed mainly by residues in the third β-spiral repeat (31).

While all reovirus serotypes engage JAM-A (8, 30), they differ in carbohydrate coreceptor utilization, suggesting that carbohydrate binding by σ1 influences reovirus pathology in the CNS. Studies comparing pathogenesis in newborn mice of reovirus

strains that differ in glycan utilization revealed that SA-binding enhances spread from the intestine to peripheral sites of replication such as the liver, spleen, and brain (5). In addition, the capacity to bind SA confers reovirus tropism for bile duct epithelium (5). However, it is not known whether SA-binding influences reovirus dissemination, tropism, and replication within the CNS.

In this study, we sought to define the function of carbohydrate binding in reovirus neuropathogenesis. We monitored survival of newborn mice inoculated with wild-type type 3 Dearing (T3D) and T3D-σ1R202W, a T3D point-mutant virus that does not bind SA (31), and quantified viral loads in various organs of infected animals. We found that the wild-type virus was more virulent and produced higher titers in neural tissues than the mutant virus following intramuscular or intracranial inoculation. Furthermore, we found that wild-type virus displayed an increased capacity to infect and replicate in primary cultures of cortical neurons in an SA-dependant manner. Collectively, these results suggest that binding to SA enhances the kinetics of reovirus replication in neural tissues and point to a functional role for sialylated glycan engagement in reovirus neurovirulence.

MATERIALS AND METHODS

Cells and viruses. L929 cells (34) were maintained in Joklik's minimum essential medium supplemented to contain 5% fetal bovine serum, 2 mM L-glutamine, 100 U/ml of penicillin, 100 μg/ml of streptomycin, and 25 ng/ml of amphotericin B (Invitrogen).

Strains T3D (25) and T3D-σ1R202W (31) used for this study were generated by plasmid-based reverse genetics. Purified reovirus virions were obtained using second- or third-passage L929 cell-lysate stocks of twice-plaque-purified reovirus as described (20). Viral particles were Freon-extracted from infected cell lysates, layered onto 1.2- to 1.4-g/cm^3 CsCl gradients, and centrifuged at 62,000 × g for 18 h. Bands corresponding to virions (1.36 g/cm^3) (38) were collected and dialyzed in virion-storage buffer (150 mM NaCl, 15 mM $MgCl_2$, 10 mM Tris-HCl [pH 7.4]). The concentration of reovirus virions in purified preparations was determined from an equivalence of one OD unit at 260 nm equals 2.1×10^{12} virions (38). Viral titer was determined by plaque assay using L929 cells (42). The average particle-to-PFU ratios for T3D and T3D-σ1R202W were 893 (n=4) and 1050 (n=5), respectively. These values do not differ statistically.

Infection of mice. C57BL/6J mice were obtained from Jackson Laboratory to establish breeding colonies. Newborn mice 2-3 days old were inoculated intramuscularly or intracranially with purified reovirus diluted in PBS. Intramuscular (IM) inoculations (5 μl) were delivered into the right hindlimb, and intracranial (IC) inoculations (5 μl) were delivered into the left cerebral hemisphere, in both cases using a Hamilton syringe and 30-gauge needle. For analysis of viral virulence, mice were monitored for symptoms of disease for 21 days post-inoculation. For survival experiments, mice were euthanized when found to be moribund (defined by rapid or shallow breathing, lethargy, or paralysis).

123 Death was not used as an endpoint. For analysis of virus replication, mice were
124 euthanized at various intervals following inoculation, and organs were collected into 1 ml
125 of phosphate-buffered saline (PBS) and homogenized by freezing, thawing, and
126 sonication. For analysis of viremia, mice were euthanized and decapitated at various
127 intervals following inoculation, and whole blood was collected from the neck into a 1 ml
128 syringe containing 100 μl Alsever's solution (Sigma). Viral titers in organ homogenates
129 were determined by plaque assay using L929 cells (42).

130 For experiments in which viral titers were determined in an organ or blood, the
131 Mann-Whitney test was used to calculate two-tailed *P* values. This test is appropriate for
132 experimental data that display a non-Gaussian distribution (33). *P* values of less than 0.05
133 were considered to be statistically significant. When all values are less than the limit of
134 detection, a Mann-Whitney test *P* value cannot be calculated. Statistical analyses were
135 performed using Prism software (GraphPad Software, Inc.).

136 All animal husbandry and experimental procedures were performed in accordance
137 with Public Health Service policy and approved by the Vanderbilt University School of
138 Medicine Institutional Animal Care and Use Committee.

139 **Histology and immunohistochemical staining for reovirus antigen.** Newborn
140 mice 2-3 days old were inoculated intramuscularly or intracranially with reovirus diluted
141 in PBS. Mice were euthanized 8 days post-inoculation, and organs were resected and
142 incubated in 10% formalin at room temperature for 24 to 48 h. Fixed organs were
143 embedded in paraffin, and consecutive 6 mm sections were stained with hematoxylin and
144 eosin (H&E) for evaluation of histopathologic changes or processed for

145 immunohistochemical detection of reovirus proteins (5) or the activated form of caspase-
146 3 (Cell Signaling, Inc.) (12).

147 **Quantification of viral RNA using RT-qPCR**. Total RNA was extracted from
148 200 µl of whole blood/Alsever's mixture using the High Pure Viral RNA kit (Roche).
149 RNA was eluted into a final volume of 40 µl. Reverse transcription-quantitative PCR
150 (RT-qPCR) was performed using an ABI 7000 sequence detection system (Applied
151 Biosystems) and EZ RT-PCR (Roche) according to the manufacturer's instructions with
152 minor modifications. Reovirus RNA was quantified using 10 µl of RNA extract. Forward
153 (S4 83F, 5′-CGCTTTTGAAGGTCGTGTATCA-3′) and reverse (S4 153R, 5′-
154 CTGGCTGTGCTGAGATTGTTTT-3′) primers corresponding to the viral S4 gene were
155 used for RT and qPCR amplification. The S4-specific fluorogenic probe used was 5′-
156 dFAM-AGCGCGCAAGAGGGATGGGA-BHQ-1-3′ (Biosearch Technologies). RT was
157 performed at 50°C for 2 min, followed by incubation at 60°C for 30 min. The reaction
158 was terminated by incubation at 95°C for 5 min. Subsequently, 40 cycles of qPCR were
159 performed at 95°C for 15 s followed by incubation at 60°C for 30 s. Standard curves
160 relating threshold cycle values to copies of plasmid DNA template were generated using
161 10-fold dilutions of a T3D S4-encoding plasmid (pT7-T3D S4) (25). The concentration
162 of viral RNA in each sample was extrapolated from standard curves. The final S4 RNA
163 copy number was calculated by multiplying the copy number obtained by extrapolation
164 from the standard curve by four to account for using one-quarter of the extracted RNA as
165 a template.
166

Preparation of cortical neuron cultures from embryonic mice. Primary cultures of mouse cortical neurons were established using cerebral cortices of C57/BL6 embryos at developmental day E15 (1). Fetuses were decapitated, brains were removed, and cortical lobes were dissected and submerged in Hanks' balanced salt solution (Gibco) on ice. Cortices were incubated in 0.6 mg/ml trypsin solution at room temperature for 30 min, washed twice, and manually dissociated twice using a Pasteur pipette. Viable cells were plated at a density of 2.5×10^5 cells/ml in 24-well plates. Wells were treated prior to plating with a 10 μg/ml poly-D-lysine solution (BD Biosciences) and a 1.64 μg/ml laminin solution (BD Biosciences). Cultures were incubated for the first 24 h in neurobasal medium (Gibco) supplemented to contain 10% FBS (Gibco), 0.6 mM L-glutamine, 50 units/ml penicillin, and 50 μg/ml streptomycin. Cultures were thereafter maintained in neurobasal medium supplemented to contain B27 (Gibco), 50 units/ml penicillin, and 50 μg/ml streptomycin. One-half of the medium was replaced with fresh medium every 3 to 4 days. Neurons were cultivated for 7 days prior to use.

Assessment of reovirus infectivity by indirect immunofluorescence. Monolayers of murine cortical neurons (2.5×10^5 cells/well) seeded in 24-well plates were adsorbed with reovirus at a multiplicity of infection (MOI) of 1000 plaque-forming units (PFU)/cell at room temperature for 1 h. Cells were incubated with either PBS or 40 mU *Arthrobacter ureafaciens* neuraminidase at 37°C for 1 h and washed three times with PBS prior to virus adsorption. Following removal of the virus inoculum, cells were washed with PBS and incubated in complete medium at 37°C for 21 h to permit completion of a single cycle of viral replication. Monolayers were fixed with 1 ml of methanol at -20°C for at least 30 min, washed twice with PBS, and blocked with 0.1%

Tween-20 (Sigma) and 20% normal goat serum (Vector Laboratories) in PBS. Cells were washed once with PBS and stained with polyclonal rabbit anti-reovirus serum at a 1:1000 dilution in PBS-0.5% Triton X-100 at room temperature for 1 h. Neurons were visualized after washing three times with PBS and staining with a monoclonal mouse anti-β-tubulin antibody (TUJ1; Covance) at a 1:1000 dilution in PBS-0.5% Triton X-100 at room temperature for 1 h. Monolayers were washed twice with PBS-0.5% Triton X-100 and incubated with a 1:1000 dilution of Alexa488-labeled anti-rabbit and Alexa546-labeled anti-mouse IgG (Invitrogen). Nuclei were stained with 4′,6-diamidino-2-phenylindole (DAPI; Invitrogen) at a 1:10,000 dilution. Monolayers were washed with PBS, and infected cells were visualized by indirect immunofluorescence using an Axiovert 200 fluorescence microscope (Carl Zeiss).

Assessment of reovirus replication by plaque assay. Murine primary cortical neurons (10^5 cells/well) were adsorbed with reovirus strains at an MOI of 1 PFU/cell. Cells were incubated with either PBS or 40 mU *A. ureafaciens* neuraminidase at 37°C for 1 h and washed three times with PBS prior to virus adsorption. Following incubation with virus at room temperature for 1 h, cells were washed three times with PBS and incubated at 37°C for various intervals. Samples were frozen and thawed twice, and viral titers were determined by plaque assay using L929 cells (42). For each experiment, samples were infected in triplicate. Viral yields were calculated according to the following formula: $\log_{10}\text{yield}_{tx} = \log_{10}(\text{PFU/ml})_{tx} - \log_{10}(\text{PFU/ml})_{t0}$, where t_x is the time postinfection. Mean values from two independent experiments were compared using an unpaired Student's *t* test as applied in Microsoft Excel. *P* values of less than 0.05 were considered to be statistically significant.

RESULTS

SA binding enhances reovirus neurovirulence and spinal cord injury. To determine whether SA binding influences reovirus neuropathogenesis, we monitored survival and clinical signs of disease in two-day-old mice following IM inoculation with 5×10^6 PFU of either wild-type T3D or mutant T3D-σ1R202W (Fig. 1A). Reovirus strain T3D-σ1R202W contains a point mutation in σ1 that ablates SA-binding capacity (31). Mice were observed for 21 days after inoculation and euthanized when moribund. Significantly fewer mice infected with T3D survived in comparison to those infected with T3D-σ1R202W. The survival frequency of mice infected with T3D was 25.9% compared with 63.6% for mice infected with T3D-σ1R202W ($P < 0.005$). These results suggest that SA binding enhances reovirus virulence.

Following IM inoculation of newborn mice, serotype 3 reovirus causes acute flaccid paralysis (AFP) between 8 and 10 days post-inoculation (21). Infected mice exhibit ipsilateral, followed by contralateral, hindlimb paralysis as a consequence of injury within the anterior horn of the spinal cord associated with motor neuron loss and spread of viral antigen (21). We observed differences in development of AFP in mice infected with wild-type and mutant virus. On day 8 post-inoculation, mice infected with wild-type virus displayed hindlimb paralysis at a five-fold greater frequency than those infected with the mutant virus (33% vs. 6%, respectively) (Fig. 1B). Furthermore, the percentage of mice infected with wild-type virus exhibiting bilateral hindlimb paralysis was almost four times greater than that in mice infected with the mutant virus (11% vs. 3%, respectively) (Fig. 1B). These data are concordant with results gathered from the

survival experiments and provide further evidence that SA binding enhances reovirus virulence.

To investigate whether enhanced virulence and AFP development in mice infected with wild-type virus compared with mutant virus corresponds with more extensive reovirus infection and tissue damage in the spinal cord, we compared histologic sections of spinal cords resected from mice inoculated intramuscularly with 5×10^6 PFU of either T3D or T3D-σ1R202W (Fig. 2). Transverse sections of the inferior spinal cord were sectioned and processed for H&E staining, staining for reovirus antigen, or staining for the activated form of caspase-3, a marker of apoptosis. Following H&E staining, spinal cords of mice infected with wild-type virus displayed more widespread injury, as indicated by increased apoptotic bodies, reactive endothelium, inflammatory infiltrates, and neurons with eosinophilic cytoplasmic inclusions. Immunohistochemistry for reovirus antigen showed correspondingly more abundant and intense staining in mice infected with wild-type virus compared with spinal cords from mice infected with the mutant virus. Staining for the activated form of caspase-3 demonstrated more apoptotic neurons in spinal cord tissues of mice infected with wild-type virus in comparison to those from mutant-infected mice. Quantification of caspase-3-positive cells revealed that mice infected with wild-type virus contained a significantly higher number of apoptotic cells in spinal cord sections ($P < 0.005$) (Fig. 3). These findings suggest that binding to SA leads to increased reovirus infection and apoptotic injury to motor neurons in the spinal cord.

SA binding influences reovirus replication at sites of secondary replication. To better understand how SA-binding capacity influences reovirus virulence, we

inoculated two-day-old mice intramuscularly with 5×10^6 PFU of either T3D or T3D-σ1R202W and quantified viral titers in the hindlimb, spinal cord, brain, and liver on days 2, 4, 8, and 10 post-inoculation (Fig. 4). In the hindlimb muscle, titers of both viruses were comparable, except on day 4 when the mutant virus produced higher titers than the wild-type virus ($P < 0.005$). In the spinal cord and brain, the mutant virus produced significantly higher titers than the wild-type virus at day 4 ($P < 0.05$). However, on days 8 and 10, titers of the wild-type virus were significantly higher than those of the mutant ($P < 0.05$). Interestingly, titers in the liver of mice infected with the wild-type virus were significantly less than those in mice infected with the mutant virus throughout the experimental time course of infection ($P < 0.05$ on day 2 and $P < 0.005$ on days 4 and 8).

To determine whether SA-binding capacity influences the kinetics of hematogenous spread, we again inoculated two-day-old mice intramuscularly with 5×10^6 PFU of either T3D or T3D-σ1R202W. In this experiment, we quantified viral titers in the heart and spleen (Fig. 5A) and monitored viral genome copies in the serum (Fig. 5B). There were statistically significant differences in titers produced by wild-type and mutant virus in the heart on day 4 post-inoculation and in the spleen on days 4 and 10 post-inoculation. On day 4 post-inoculation, the wild-type virus produced higher titer in the heart but lower titer in the spleen in comparison to the mutant virus. On day 10 post-inoculation, the wild-type virus produced higher titer than the mutant virus in the spleen. Although these differences are statistically significant, because of the modest magnitude of the differences, we do not think that they are biologically relevant. Furthermore, the number of viral genome copies detected in the serum of mice infected with either virus also was comparable. Thus, SA-binding capacity enhances overall peak titers in the

281 murine CNS. However, utilization of SA is not required for infection of the liver and
282 does not appear to influence hematogenous dissemination in mice.

283 **SA binding enhances reovirus neurovirulence and replication in the brain.**
284 Differences in titers produced by T3D and T3D-σ1R202W in the spinal cord and brain
285 could result from more efficient spread of wild-type virus from the muscle to the CNS,
286 enhanced replication of wild-type virus in the CNS, or both effects. To distinguish
287 between these possibilities, we inoculated three-day-old mice intracranially with 2 PFU
288 of either wild-type or mutant virus. We monitored infected mice for survival and clinical
289 signs of disease for 21 days and quantified viral loads in the brain at days 4, 8, and 12
290 following inoculation (Fig. 6). We again observed that mice infected with the wild-type
291 virus displayed a lower frequency of survival (33%) compared with those infected with
292 the mutant virus (85%) ($P < 0.001$) (Fig. 6A). In addition, wild-type virus produced
293 higher titers in the brain than did the mutant following IC inoculation (Fig. 6B), reaching
294 statistical significance on day 8 post-inoculation ($P < 0.05$). Taken together, these
295 findings suggest that SA binding enhances reovirus virulence by augmenting viral
296 replication in the CNS.

297 **SA binding does not alter reovirus tropism in the brain.** To test whether σ1-
298 SA interactions are required for neural tropism of type 3 reovirus, we compared
299 histologic sections of brains resected from mice inoculated intracranially with 100 PFU
300 of either T3D or T3D-σ1R202W (Fig. 7). Brains chosen for histologic analysis were
301 matched anatomically based on the size and shape of landmarks such as the hippocampus
302 as well as displaying comparable viral titers. The intensity of reovirus antigen staining as
303 well as the cellular distribution of reovirus antigen was similar in brain sections from

304 mice infected with either T3D or T3D-σ1R202W. Characteristic reovirus tropism
305 involving several areas the brain including the cortex, the C2-C4 region of the
306 hippocampus, and the thalamus was apparent in mice infected with either virus (Fig. 7A).
307 In addition, involvement of the cerebellum, specifically infection of the Purkinje cells,
308 was observed in brain sections of mice infected with either virus (Fig. 7B). Staining for
309 the activated form of caspase-3 demonstrated apoptotic foci in sections of brain tissue
310 from animals infected with either T3D or T3D-σ1R202W. However, the number of
311 apoptotic cells did not appear to differ in these sections (data not shown), perhaps due to
312 the inoculum dose used in this experiment. Therefore, SA-binding capacity of type 3
313 reovirus does not influence targeting of reovirus to specific regions within the brain, but
314 rather appears to influence replication efficiency in brain tissue.
315 **SA binding enhances infection of murine primary cortical neurons.** Results
316 gathered thus far reveal that SA-binding enhances the capacity of reovirus to replicate in
317 the brain following IM or IC inoculation. We hypothesized that this difference is
318 attributable to enhanced infection and replication in neurons by SA-binding reovirus
319 strains. To test this hypothesis, we quantified infection of primary cortical neuron
320 cultures using an immunoflorescence assay (Figs. 8A and 8B) and compared titers of
321 T3D and T3D-σ1R202W following replication in primary cortical neuron cultures at 24,
322 48, and 72 h post-infection (Fig. 8C). Primary cultures of mouse cortical neurons were
323 established using cerebral cortices of C57/BL6 embryos at developmental day E15 and
324 cultured for 7 days prior to infection (1). Wild-type virus infected a significantly higher
325 percentage of cortical neurons (5%) in comparison to the mutant (1%) ($P < 0.0001$) (Fig.
326 8B). Concordantly, at 24 h post-infection, yields of wild-type and mutant virus were

327 comparable (Fig. 8C). However, by 48 and 72 h post-infection, wild-type virus produced
328 significantly higher yields than those produced by the mutant ($P < 0.05$) (Fig. 8C). These
329 findings suggest that engagement of SA by reovirus enhances infection and replication
330 efficiency in neurons.

331 To confirm the importance of SA binding for infectivity and replication of
332 primary cultures of neurons, cells were treated with *A. ureafaciens* neuraminidase to
333 remove cell-surface SA. *A. ureafaciens* neuraminidase is a broad-spectrum enzyme that
334 cleaves α-2,3-, α-2,6-, and α-2,8- terminally-linked SA present on glycan chains (41).
335 Neuraminidase treatment diminished the infectivity and replication of wild-type virus to
336 the levels observed for the mutant virus (Fig. 8A-C). These findings demonstrate that
337 both infectivity and replication in primary neuronal cultures by type 3 reovirus is
338 enhanced by SA binding. Collectively, these results suggest that the capacity of reovirus
339 to bind cell-surface SA enhances the efficiency of infection of cells in the murine CNS.

DISCUSSION

In this study, we found that the capacity to bind cell-surface SA enhances the neurovirulence of type 3 reovirus. Following either IM or IC inoculation of newborn mice, wild-type strain T3D was more virulent and produced higher titers in neural tissues compared with non-SA-binding mutant virus T3D-σ1R202W. Furthermore, mice infected with wild-type virus displayed a higher frequency of AFP and enhanced tissue injury compared with mutant-infected mice. Injury in the spinal cord and the brain is associated with apoptosis, with the number of apoptotic neurons in the spinal cord correlating with the extent of neurological symptoms. The key finding of this study is that SA-binding capacity dictates increased reovirus infectivity and replicative capacity in murine neurons. These data suggest that SA binding enhances the neurovirulence of type 3 reovirus by mediating efficient infection of target cells in the CNS, resulting in increased replication and pathology.

We found that wild-type T3D displays increased infectivity and replicative capacity in primary cultures of murine cortical neurons, a phenotype that is dependent on cell-surface SA. Binding of type 3 reovirus strains to SA facilitates viral attachment through low-affinity adhesion that places the virus on the cell surface where access to the higher-affinity, but lower-abundance, proteinaceous receptor is thermodynamically favored (3). This adhesion-strengthening mechanism may be the basis for the enhanced replication and neurovirulence of T3D. Although the proteinaceous receptor on neurons for type 3 reovirus is not known, our findings suggest that its optimal engagement likely requires initial low-affinity glycan binding to anchor the virus to the cell surface. We favor this scenario because neuraminidase treatment of primary murine cortical neurons

363 decreases but does not abolish infection or replication (Fig. 8), consistent with the
364 existence of other host mediators of infection.
365 We previously identified residues in type 3 σ1 that are required for functional
366 binding of reovirus to SA, i.e., binding that results in productive infection (31). Using
367 reverse genetics, we introduced structure-guided mutations in the type 3 σ1 molecule and
368 characterized the resultant mutant viruses using assays to quantify SA-binding capacity.
369 This analysis highlighted the importance of Arg202 in the interaction of type 3 σ1 with
370 SA. The Arg202 sidechain forms a bidentate salt bridge with the carboxylate moiety of
371 SA, which is an important electrostatic contact between the protein and its carbohydrate
372 ligand. Replacement of Arg202 with a tryptophan in T3D-σ1R202W would remove the
373 electrostatic interaction between the arginine and SA and introduce a structural clash with
374 the glycan (Fig. 9). It is therefore unlikely that the mutant can bind to SA, even in the
375 improbable case that the overall structure of the binding site is not altered by the mutation.
376 This model provides a structural framework for understanding the decreased virulence
377 displayed by T3D-σ1R202W.
378 Following IM inoculation, wild-type T3D produced lower titers in the livers of
379 infected mice than did non-SA binding stain T3D-σ1R202W (Fig. 4). This is an
380 interesting result because previous studies from our laboratory revealed that SA binding
381 confers tropism of reovirus for bile duct epithelium and reovirus-induced injury to the
382 liver (5). The SA-binding strain used in that study, T3SA+, produces higher titers in liver
383 tissue than its non-SA-binding counterpart, T3SA-, at early times after infection.
384 However, SA-binding-capacity is not strictly required for infection and replication in the
385 liver, as T3SA- produces titers in the liver that approximate those of T3SA+ at late times

386 of infection (1, 5). It is possible that the genetic backgrounds of the strains used by
387 Barton et al (5) (T1L) and here (T3D) account for the observed differences. It also is
388 possible that the routes of inoculation, peroral (5) vs. IM (current study) influence hepatic
389 tropism. We also noted that T3D-σ1R202W produced higher titers than wild-type virus in
390 the spinal cord and brain of infected mice on day 4 post-inoculation. Since reovirus is
391 delivered initially to the CNS by hematogenous routes (1, 6), it is possible that
392 bloodstream dissemination of the mutant virus is subtly enhanced in comparison to wild-
393 type virus, although if so, this difference was not sufficient to permit detection in our
394 assays.

395 Data presented in this study and others (5) indicate that the capacity of type 3
396 reovirus to bind cell-surface SA can target the virus to specific sites of replication and
397 lead to enhanced replication and disease. These observations suggest that SA-binding
398 capacity confers a fitness advantage for reovirus. For example, it is possible that an SA-
399 mediated replication enhancement leads to increased viral shedding and transmission of
400 virus from host to host. However, there are naturally circulating strains of reovirus that do
401 not bind to SA (13), suggesting that SA-binding capacity is a balanced polymorphism in
402 nature that also imposes a fitness cost. For example, SA-binding capacity diminishes
403 reovirus infection of polarized human airway epithelial cells (18). Strain T3SA+ does not
404 efficiently infect these cells, whereas T3SA- does. Moreover, neuraminidase pre-
405 treatment to remove cell-surface SA enhances T3SA+ infection of these cells (18).
406 Determination of the precise contribution of SA binding to viral fitness will require
407 competition studies using strains that vary solely in SA-binding capacity and populations
408 of susceptible mice.

For many viruses, including several important human pathogens, glycan engagement plays an important role in infection and pathogenesis. Here, we demonstrate that utilization of sialylated glycans as coreceptors enhances the neurovirulence of type 3 reovirus. This study broadens an understanding of mechanisms of reovirus attachment to neuronal cells and supports the hypothesis that type 3 reovirus-glycan interactions are key determinants of reovirus neurovirulence in the CNS.

ACKNOWLEDGMENTS

We thank Jim Chappell and members of our laboratory for many helpful suggestions and useful discussions. We thank Karl Boehme and Bernardo Mainou for careful review of the manuscript. We are grateful to Laura Ooms for assistance with the PCR assays.

This work was supported by Public Health Service awards T32 AI07611 (J.M.F.), R01 AI76983 (T.S.D. and T.S.), and R37 AI38296 (T.S.D.) and the Elizabeth B. Lamb Center for Pediatric Research. Additional support was provided by Public Health Service awards P30 CA68485 for the Vanderbilt-Ingram Cancer Center and P60 DK20593 for the Vanderbilt Diabetes Research and Training Center. We have no financial conflicts of interest.

REFERENCES

1. **Antar, A. A. R., J. L. Konopka, J. A. Campbell, R. A. Henry, A. L. Perdigoto, B. D. Carter, A. Pozzi, T. W. Abel, and T. S. Dermody.** 2009. Junctional adhesion molecule-A is required for hematogenous dissemination of reovirus. Cell Host Microbe **5:**59-71.
2. **Barton, E. S., J. D. Chappell, J. L. Connolly, J. C. Forrest, and T. S. Dermody.** 2001. Reovirus receptors and apoptosis. Virology **290:**173-180.
3. **Barton, E. S., J. L. Connolly, J. C. Forrest, J. D. Chappell, and T. S. Dermody.** 2001. Utilization of sialic acid as a coreceptor enhances reovirus attachment by multistep adhesion strengthening. J. Biol. Chem. **276:**2200-2211.
4. **Barton, E. S., J. C. Forrest, J. L. Connolly, J. D. Chappell, Y. Liu, F. Schnell, A. Nusrat, C. A. Parkos, and T. S. Dermody.** 2001. Junction adhesion molecule is a receptor for reovirus. Cell **104:**441-451.
5. **Barton, E. S., B. E. Youree, D. H. Ebert, J. C. Forrest, J. L. Connolly, T. Valyi-Nagy, K. Washington, J. D. Wetzel, and T. S. Dermody.** 2003. Utilization of sialic acid as a coreceptor is required for reovirus-induced biliary disease. J. Clin. Invest. **111:**1823-1833.
6. **Boehme, K. W., J. M. Frierson, J. L. Konopka, T. Kobayashi, and T. S. Dermody.** 2011. The reovirus sigma1s protein is a determinant of hematogenous but not neural virus dissemination in mice. J. Virol. **85:**11781-90.
7. **Boehme, K. W., K. M. Guglielmi, and T. S. Dermody.** 2009. Reovirus nonstructural protein σ1s is required for establishment of viremia and systemic dissemination. Proc. Natl. Acad. Sci. U. S. A. **106:**19986-19991.

8. **Campbell, J. A., P. Shelling, J. D. Wetzel, E. M. Johnson, G. A. R. Wilson, J. C. Forrest, M. Aurrand-Lions, B. Imhof, T. Stehle, and T. S. Dermody.** 2005. Junctional adhesion molecule-A serves as a receptor for prototype and field-isolate strains of mammalian reovirus. J. Virol. **79:**7967-7978.

9. **Cashdollar, L. W., R. A. Chmelo, J. R. Wiener, and W. K. Joklik.** 1985. Sequences of the S1 genes of the three serotypes of reovirus. Proc. Natl. Acad. Sci. U. S. A. **82:**24-28.

10. **Chappell, J. D., J. L. Duong, B. W. Wright, and T. S. Dermody.** 2000. Identification of carbohydrate-binding domains in the attachment proteins of type 1 and type 3 reoviruses. J. Virol. **74:**8472-8479.

11. **Chappell, J. D., A. Prota, T. S. Dermody, and T. Stehle.** 2002. Crystal structure of reovirus attachment protein σ1 reveals evolutionary relationship to adenovirus fiber. EMBO J. **21:**1-11.

12. **Danthi, P., T. Kobayashi, G. H. Holm, M. W. Hansberger, T. W. Abel, and T. S. Dermody.** 2008. Reovirus apoptosis and virulence are regulated by host cell membrane-penetration efficiency. J. Virol. **82:**161-172.

13. **Dermody, T. S., M. L. Nibert, R. Bassel-Duby, and B. N. Fields.** 1990. Sequence diversity in S1 genes and S1 translation products of 11 serotype 3 reovirus strains. J. Virol. **64:**4842-4850.

14. **Dichter, M. A., and H. L. Weiner.** 1984. Infection of neuronal cell cultures with reovirus mimics in vitro patterns of neurotropism. Ann. Neurol. **16:**603-610.

15. **Ding, Y., L. He, Q. Zhang, Z. Huang, X. Che, J. Hou, H. Wang, H. Shen, L. Qiu, Z. Li, J. Geng, J. Cai, H. Han, X. Li, W. Kang, D. Weng, P. Liang, and S.**

Jiang. 2004. Organ distribution of severe acute respiratory syndrome (SARS) associated coronavirus (SARS-CoV) in SARS patients: implications for pathogenesis and virus transmission pathways. J. Pathol. **203:**622-630.

16. **Duncan, R., D. Horne, L. W. Cashdollar, W. K. Joklik, and P. W. K. Lee.** 1990. Identification of conserved domains in the cell attachment proteins of the three serotypes of reovirus. Virology **174:**399-409.

17. **Ernst, H., and A. J. Shatkin.** 1985. Reovirus hemagglutinin mRNA codes for two polypeptides in overlapping reading frames. Proc. Natl. Acad. Sci. U. S. A. **82:**48-52.

18. **Excoffon, K. J. D. A., K. M. Guglielmi, J. D. Wetzel, N. D. Gansemer, J. A. Campbell, T. S. Dermody, and J. Zabner.** 2008. Reovirus preferentially infects the basolateral surface and is released from the apical surface of polarized human respiratory epithelial cells. J. Infect. Dis. **197:**1189-1197.

19. **Fraser, R. D. B., D. B. Furlong, B. L. Trus, M. L. Nibert, B. N. Fields, and A. C. Steven.** 1990. Molecular structure of the cell-attachment protein of reovirus: correlation of computer-processed electron micrographs with sequence-based predictions. J. Virol. **64:**2990-3000.

20. **Furlong, D. B., M. L. Nibert, and B. N. Fields.** 1988. Sigma 1 protein of mammalian reoviruses extends from the surfaces of viral particles. J. Virol. **62:**246-256.

21. **Goody, R. J., S. A. Schittone, and K. L. Tyler.** 2008. Experimental reovirus-induced acute flaccid paralysis and spinal motor neuron cell death. J. Neuropathol. Exp. Neurol. **67:**231-239.

22. **Kaludov, N., K. E. Brown, R. W. Walters, J. Zabner, and J. A. Chiorini.** 2001. Adeno-associated virus serotype 4 (AAV4) and AAV5 both require sialic acid binding for hemagglutination and efficient transduction but differ in sialic acid linkage specificity. J. Virol. **75:**6884-6893.

23. **Kaye, K. M., D. R. Spriggs, R. Bassel-Duby, B. N. Fields, and K. L. Tyler.** 1986. Genetic basis for altered pathogenesis of an immune-selected antigenic variant of reovirus type 3 Dearing. J. Virol. **59:**90-97.

24. **Kirchner, E., K. M. Guglielmi, H. M. Strauss, T. S. Dermody, and T. Stehle.** 2008. Structure of reovirus σ1 in complex with its receptor junctional adhesion molecule-A. PLoS Pathog. **4:**e1000235.

25. **Kobayashi, T., A. A. R. Antar, K. W. Boehme, P. Danthi, E. A. Eby, K. M. Guglielmi, G. H. Holm, E. M. Johnson, M. S. Maginnis, S. Naik, W. B. Skelton, J. D. Wetzel, G. J. Wilson, J. D. Chappell, and T. S. Dermody.** 2007. A plasmid-based reverse genetics system for animal double-stranded RNA viruses. Cell Host Microbe **1:**147-157.

26. **Lee, P. W. K., E. C. Hayes, and W. K. Joklik.** 1981. Protein σ1 is the reovirus cell attachment protein. Virology **108:**156-163.

27. **Maddon, P. J., A. G. Dalgleish, J. S. Mcdougal, P. R. Clapham, R. A. Weiss, and R. Axel.** 1986. The T4 gene encodes the AIDS virus receptor and is expressed in the immune system and the brain. Cell **47:**333-348.

28. **Morrison, L. A., R. L. Sidman, and B. N. Fields.** 1991. Direct spread of reovirus from the intestinal lumen to the central nervous system through vagal autonomic nerve fibers. Proc. Natl. Acad. Sci. U. S. A. **88:**3852-3856.

29. **Nibert, M. L., T. S. Dermody, and B. N. Fields.** 1990. Structure of the reovirus cell-attachment protein: a model for the domain organization of σ1. J. Virol. **64:**2976-2989.

30. **Prota, A. E., J. A. Campbell, P. Schelling, J. C. Forrest, T. R. Peters, M. J. Watson, M. Aurrand-Lions, B. Imhof, T. S. Dermody, and T. Stehle.** 2003. Crystal structure of human junctional adhesion molecule 1: implications for reovirus binding. Proc. Natl. Acad. Sci. U. S. A. **100:**5366-5371.

31. **Reiter, D. M., J. M. Frierson, E. E. Halvorson, T. Kobayashi, T. S. Dermody, and T. Stehle.** 2011. Crystal structure of reovirus attachment protein σ1 in complex with sialylated oligosaccharides. PLoS Pathog. **7:**e1002166.

32. **Ren, R., F. C. Costantini, E. J. Gorgacz, J. J. Lee, and V. R. Racaniello.** 1990. Transgenic mice expressing a human poliovirus receptor: a new model for poliomyelitis. Cell **63:**353-362.

33. **Richardson, B. A., and J. Overbaugh.** 2005. Basic statistical considerations in virological experiments. J. Virol. **79:**669-676.

34. **Sanford, K. K., W. R. Earle, and G. D. Likely.** 1948. The growth in vitro of single isolated tissue cells. J. Natl. Cancer Inst. **9:**229-46.

35. **Sarkar, G., J. Pelletier, R. Bassel-Duby, A. Jayasuriya, B. N. Fields, and N. Sonenberg.** 1985. Identification of a new polypeptide coded by reovirus gene S1. J. Virol. **54:**720-725.

36. **Schelling, P., K. M. Guglielmi, E. Kirchner, B. Paetzold, T. S. Dermody, and T. Stehle.** 2007. The reovirus σ1 aspartic acid sandwich: a trimerization motif poised for conformational change. J. Biol. Chem. **282:**11582-11589.

37. **Schiff, L. A., M. L. Nibert, and K. L. Tyler.** 2007. Orthoreoviruses and their replication, p. 1853-1915. *In* D. M. Knipe and P. M. Howley (ed.), Fields Virology, Fifth ed, vol. 2. Lippincott Williams & Wilkins, Philadelphia.

38. **Smith, R. E., H. J. Zweerink, and W. K. Joklik.** 1969. Polypeptide components of virions, top component and cores of reovirus type 3. Virology **39:**791-810.

39. **Tardieu, M., and H. L. Weiner.** 1982. Viral receptors on isolated murine and human ependymal cells. Science **215:**419-421.

40. **Tyler, K. L., D. A. McPhee, and B. N. Fields.** 1986. Distinct pathways of viral spread in the host determined by reovirus S1 gene segment. Science **233:**770-774.

41. **Uchida, Y., Y. Tsukada, and T. Sugimori.** 1979. Enzymatic properties of neuraminidases from Arthrobacter ureafaciens. J. Biochem. **86:**1573-1585.

42. **Virgin, H. W., IV, R. Bassel-Duby, B. N. Fields, and K. L. Tyler.** 1988. Antibody protects against lethal infection with the neurally spreading reovirus type 3 (Dearing). J. Virol. **62:**4594-4604.

43. **Weiner, H. L., D. Drayna, D. R. Averill, Jr, and B. N. Fields.** 1977. Molecular basis of reovirus virulence: role of the S1 gene. Proc. Natl. Acad. Sci. U. S. A. **74:**5744-5748.

44. **Weiner, H. L., M. L. Powers, and B. N. Fields.** 1980. Absolute linkage of virulence and central nervous system tropism of reoviruses to viral hemagglutinin. J. Infect. Dis. **141:**609-616.

45. **Weiner, H. L., R. F. Ramig, T. A. Mustoe, and B. N. Fields.** 1978. Identification of the gene coding for the hemagglutinin of reovirus. Virology **86:**581-584.

FIGURE LEGENDS

FIG 1 SA-binding capacity enhances reovirus virulence and paralysis following IM inoculation. Newborn C57/BL6 mice were inoculated in the right hindlimb with 5×10^6 PFU of either T3D or T3D-σ1R202W (R202W). (A) Mice (n = 22-27 for each virus strain) were monitored for survival for 21 days. *, $P < 0.005$, as determined by log-rank test in comparison to T3D. (B) Mice were monitored for development of reovirus-induced AFP on day 8 post-inoculation (n = 32-44 for each virus strain). Complete paralysis was first observed at this time point; survival frequencies of wild-type and mutant-infected mice at this time point were comparable.

FIG 2 SA-binding capacity enhances reovirus-induced injury in the spinal cord following IM inoculation. Newborn C57/BL6 mice were inoculated in the right hindlimb with 5×10^6 PFU of either T3D or T3D-σ1R202W (R202W). The inferior spinal cord was resected on day 8 post-inoculation, and consecutive lumbosacral sections were stained with hematoxylin and eosin (H&E), polyclonal reovirus antiserum (Reovirus), or antibodies specific for the cleaved (active) form of caspase-3 (Caspase-3). Representative sections of spinal cord matched for lumbar depth are shown. Boxes indicate areas of enlargement.

FIG 3 Quantification of apoptotic cells in the spinal cord of reovirus-infected mice. Lumbosacral sections of the inferior spinal cord resected from newborn mice inoculated intramuscularly in the right hindlimb with 5×10^6 PFU of either T3D or T3Dσ1-R202W (R202W) were stained for the cleaved form of caspase-3. Cells staining positive for

586 caspase-3 were enumerated in individual sections obtained from four animals infected
587 with each virus strain. Results are expressed as mean caspase-3-positive cells per tissue
588 section. Error bars represent SD. *, $P < 0.005$, as determined by Student's *t* test in
589 comparison to T3D.
590
591 **FIG 4 SA binding is associated with higher peak titers of reovirus in neural tissues.**
592 Newborn C57/BL6 mice were inoculated in the right hindlimb with 5×10^6 PFU of either
593 T3D or T3D-σ1R202W. At days 2, 4, 8, and 10 post-inoculation, mice were euthanized,
594 hindlimb muscle, spinal cord, brain, and liver were resected, and viral titers in organ
595 homogenates were determined by plaque assay. Results are expressed as mean viral titers
596 for 6-9 animals for each time point. Error bars indicate SEM. *, $P < 0.05$ and **, $P <$
597 0.005, as determined by Mann-Whitney test in comparison to T3D.
598
599 **FIG 5 Binding to SA is not required for dissemination by hematogenous routes.**
600 Newborn C57/BL6 mice were inoculated in the right hindlimb with 5×10^6 PFU of either
601 T3D or T3D-σ1R202W. (A) At days 2, 4, 8, and 10 post-inoculation, mice were
602 euthanized, and heart and spleen were resected. Viral titers in organ homogenates were
603 determined by plaque assay. Results are expressed as mean viral titers for 7 to 10 animals
604 for each time point. Error bars indicate SEM. *, $P < 0.05$, as determined by Mann-
605 Whitney test in comparison to T3D. (B) At days 2, 4, 8, and 10 post-inoculation, mice
606 were euthanized, blood was collected, and viral genome copies in serum were determined
607 by RT-qPCR. Results are expressed as mean viral genome copies per animal for 3 to 5
608 animals at each time point. Error bars indicate SEM.

FIG 6 SA-binding capacity enhances reovirus neurovirulence and replicative capacity following IC inoculation. Newborn C57/BL6 mice were inoculated intracranially with 2 PFU of either T3D or T3D-σ1R202W. (A) Mice (n = 18-21 for each virus strain) were monitored for survival for 21 days. **, $P < 0.001$, as determined by log-rank test in comparison to T3D. (B) At days 4, 8, and 12 post-inoculation, viral titers in brain homogenates were determined by plaque assay. Results are expressed as mean viral titers for 4 to 7 animals for each time point. Error bars indicate SEM. *, $P < 0.05$, as determined by Mann-Whitney test in comparison to T3D.

FIG 7 Binding to SA does not alter reovirus tropism in the brain. Newborn C57/BL6 mice were inoculated intracranially with 100 PFU of either T3D or T3D-σ1R202W (R202W). On day 8 post-inoculation, brains of infected mice were resected. The brains were bisected, and the left hemispheres were processed for histopathology and the right hemispheres were prepared for viral titer determination by plaque assay. Consecutive coronal sections of the brain were stained with hematoxylin and eosin (H&E) or polyclonal reovirus antiserum (Reovirus). Representative sections of brain hemisphere matched for hippocampal depth (A) and cerebellum (B) are shown. T3D-infected brain sections are from the right hemisphere of a brain with a titer of 8×10^8 PFU, and T3D-σ1R202W-infected brain sections are from the right hemisphere of a brain with a titer of 3.5×10^8 PFU.

FIG 8 SA-binding capacity increases the efficiency of reovirus infection of primary cortical neurons. Cortical neurons were harvested from C57/BL6 mouse embryos at developmental day E15.5 and cultured for 5-7 days prior to infection. (A) Neurons were adsorbed with either T3D or T3D-σ1R202W at an MOI of 1000 PFU/cell following pre-treatment with either PBS or 40 mM *A. ureafaciens* neuraminidase and incubated for 21 h. Cells were stained with TUJ1 neural-specific marker to detect neurons (red), DAPI to detect nuclei (blue), and polyclonal reovirus antiserum to detect reovirus antigen (green) and visualized using indirect immunofluorescence microscopy. Representative wells from duplicate experiments are shown. (B) The percentage of infected cells was quantified by dividing the number of neurons exhibiting reovirus staining by the total number of cell nuclei exhibiting DAPI staining in three fields of 400X view in triplicate wells (n=2). Fields of view contained between 200 and 600 nuclei. Error bars indicate SEM. *, $P < 0.0001$, as determined by Student's *t* test in comparison to T3D. (C) Neurons were adsorbed with either T3D or T3D-σ1R202W at an MOI of 1 PFU/cell. Titers of virus in cell lysates were determined by plaque assay at the indicated times post-adsorption. Results are expressed as mean viral yield for duplicate samples. Error bars indicate SD. *, $P < 0.05$, as determined by Student's *t* test in comparison to T3D.

FIG 9 Comparison of T3D and T3D-σ1R202W σ1 interactions with the terminal SA of α(2,3) sialyllactose. (A) Ribbon drawing of the T3D σ1 body and head domains in complex with α(2,3) sialyllactose. The σ1 monomers are shown in red, blue, and yellow. The body domain consists of seven triple β-spiral repeats (β1–β7) and an α-helical coiled-coil domain (cc) that is inserted between β-spiral repeats β4 and β5. The bound α(2,3)

sialyllactose is shown in stick representation and colored in orange (enclosed by the red box). (B) An enlarged view of the T3D σ1 SA-binding domain. The σ1 residue 202 of a single σ1 monomer is drawn in stick representation, while the remainder of the monomer is shown as a ribbon tracing. The other monomers are shown in a surface-shaded representation. The SA moiety of α(2,3) sialyllactose is shown in stick representation, with carbons colored orange, oxygens colored red, and nitrogens colored blue. Residue Arg202 (cyan) of wild-type T3D forms a salt bridge with the carboxylate group of SA (31). This bond is represented by a dashed red line, illustrating that it is likely lost when Arg202 is replaced with a tryptophan (yellow) in T3D-σ1R202W.

REFERENCES

1. **Adams, P. D., et al.** 2002. PHENIX: building new software for automated crystallographic structure determination. Acta Crystallogr D Biol Crystallogr 58:1948-54.

2. **Alexander, D. A., et al.** 2002. Sialic acid functions in enterovirus 70 binding and infection. J. Virol 76:11265-72.

3. **Antar, A. A. R., J. L. Konopka, J. A. Campbell, R. A. Henry, A. L. Perdigoto, B. D. Carter, A. Pozzi, T. W. Abel, and T. S. Dermody.** 2009. Junctional adhesion molecule-A is required for hematogenous dissemination of reovirus. Cell Host Microbe 5:59-71.

4. **Arrate, M. P., J. M. Rodriguez, T. M. Tran, T. A. Brock, and S. A. Cunningham.** 2001. Cloning of human junctional adhesion molecule 3 (JAM3) and its identification as the JAM2 counter-receptor. Journal of Biological Chemistry 276:45826-45832.

5. **Aurrand-Lions, M., L. Duncan, C. Ballestrem, and B. A. Imhof.** 2001. JAM-2, a novel immunoglobulin superfamily molecule, expressed by endothelial and lymphatic cells. J Biol Chem 276:2733-41.

6. **Barton, E. S., J. D. Chappell, J. L. Connolly, J. C. Forrest, and T. S. Dermody.** 2001. Reovirus receptors and apoptosis. Virology 290:173-180.

7. **Barton, E. S., J. L. Connolly, J. C. Forrest, J. D. Chappell, and T. S. Dermody.** 2001. Utilization of sialic acid as a coreceptor enhances reovirus attachment by multistep adhesion strengthening. Journal of Biological Chemistry 276:2200-2211.

8. **Barton, E. S., J. C. Forrest, J. L. Connolly, J. D. Chappell, Y. Liu, F. Schnell, A. Nusrat, C. A. Parkos, and T. S. Dermody.** 2001. Junction adhesion molecule is a receptor for reovirus. Cell 104:441-451.

9. **Barton, E. S., B. E. Youree, D. H. Ebert, J. C. Forrest, J. L. Connolly, T. Valyi-Nagy, K. Washington, J. D. Wetzel, and T. S. Dermody.** 2003. Utilization of sialic acid as a coreceptor is required for reovirus-induced biliary disease. Journal of Clinical Investigation 111:1823-1833.

10. **Bassel-Duby, R., A. Jayasuriya, D. Chatterjee, N. Sonenberg, J. V. Maizel, Jr, and B. N. Fields.** 1985. Sequence of reovirus haemagglutinin predicts a coiled-coil structure. Nature 315:421-423.

11. **Bassel-Duby, R., D. R. Spriggs, K. L. Tyler, and B. N. Fields.** 1986. Identification of attenuating mutations on the reovirus type 3 S1 double-stranded RNA segment with a rapid sequencing technique. Journal of Virology 60:64-67.

12. **Bergelson, J. M., J. A. Cunningham, G. Droguett, E. A. Kurt-Jones, A. Krithivas, J. S. Hong, M. S. Horwitz, R. L. Crowell, and R. W. Finberg.** 1997. Isolation of a common receptor for Coxsackie B viruses and adenoviruses 2 and 5. Science 275:1320-1323.

13. **Bertolotti-Ciarlet, A., L. J. White, R. Chen, B. V. Prasad, and M. K. Estes.** 2002. Structural requirements for the assembly of Norwalk virus-like particles. J Virol 76:4044-55.

14. **Blanchard, H., X. Yu, B. S. Coulson, and M. von Itzstein.** 2007. Insight into host cell carbohydrate-recognition by human and porcine rotavirus from crystal structures of the virion spike associated carbohydrate-binding domain (VP8*). Journal of Molecular Biology 367:1215-1226.

15. **Boehme, K. W., J. M. Frierson, J. L. Konopka, T. Kobayashi, and T. S. Dermody.** 2011. The reovirus sigma1s protein is a determinant of hematogenous but not neural virus dissemination in mice. J Virol 85:11781-90.

16. **Buchholz, U. J., S. Finke, and K. K. Conzelmann.** 1999. Generation of bovine respiratory syncytial virus (BRSV) from cDNA: BRSV NS2 is not essential for virus replication in tissue culture, and the human RSV leader region acts as a functional BRSV genome promoter. J Virol 73:251-9.

17. **Burmeister, W. P., D. Guilligay, S. Cusack, G. Wadell, and N. Arnberg.** 2004. Crystal structure of species D adenovirus fiber knobs and their sialic acid binding sites. Journal of Virology 78:7727-7736.

18. **Campbell, J. A., P. Shelling, J. D. Wetzel, E. M. Johnson, G. A. R. Wilson, J. C. Forrest, M. Aurrand-Lions, B. Imhof, T. Stehle, and T. S. Dermody.** 2005. Junctional adhesion molecule-A serves as a receptor for prototype and field-isolate strains of mammalian reovirus. Journal of Virology 79:7967-7978.

19. **Cavalli, A., A. E. Prota, T. Stehle, T. S. Dermody, M. Recanatini, G. Folkers, and L. Scapozza.** 2004. A molecular dynamics study of reovirus attachment protein σ1 reveals conformational changes in σ1 structure. Biophysical Journal 86:3423-3431.

20. **Chappell, J. D., E. S. Barton, T. H. Smith, G. S. Baer, D. T. Duong, M. L. Nibert, and T. S. Dermody.** 1998. Cleavage susceptibility of reovirus attachment protein σ1 during proteolytic disassembly of virions is determined by a sequence polymorphism in the σ1 neck. Journal of Virology 72:8205-8213.

21. **Chappell, J. D., J. L. Duong, B. W. Wright, and T. S. Dermody.** 2000. Identification of carbohydrate-binding domains in the attachment proteins of type 1 and type 3 reoviruses. Journal of Virology 74:8472-8479.

22. **Chappell, J. D., V. L. Gunn, J. D. Wetzel, G. S. Baer, and T. S. Dermody.** 1997. Mutations in type 3 reovirus that determine binding to sialic acid are contained in the fibrous tail domain of viral attachment protein σ1. Journal of Virology 71:1834-1841.

23. **Chappell, J. D., A. Prota, T. S. Dermody, and T. Stehle.** 2002. Crystal structure of reovirus attachment protein σ1 reveals evolutionary relationship to adenovirus fiber. EMBO Journal 21:1-11.

24. **Chen, B., E. M. Vogan, H. Gong, J. J. Skehel, D. C. Wiley, and S. C. Harrison.** 2005. Structure of an unliganded simian immunodeficiency virus gp120 core. Nature 433:834-841.

25. **Cunningham, S. A., M. P. Arrate, J. M. Rodriguez, R. J. Bjercke, P. Vanderslice, A. P. Morris, and T. A. Brock.** 2000. A novel protein with homology to the junctional adhesion molecule. Characterization of leukocyte interactions. Journal of Biological Chemistry 275:34750-34756.

26. **Dermody, T. S., J. Parker, and B. Sherry.** In Press. Orthoreovirus. *In* D. M. K. a. P. M. Howley (ed.), Fields Virology, 6 ed, vol. 2. Lippincott Williams & Wilkins, Philadelphia.

27. **Dermody, T. S., M. L. Nibert, R. Bassel-Duby, and B. N. Fields.** 1990. A σ1 region important for hemagglutination by serotype 3 reovirus strains. Journal of Virology 64:5173-5176.

28. **Dermody, T. S., M. L. Nibert, R. Bassel-Duby, and B. N. Fields.** 1990. Sequence diversity in S1 genes and S1 translation products of 11 serotype 3 reovirus strains. Journal of Virology 64:4842-4850.

29. **Dichter, M. A., and H. L. Weiner.** 1984. Infection of neuronal cell cultures with reovirus mimics in vitro patterns of neurotropism. Annals of Neurology 16:603-610.

30. **Ding, Y., L. He, Q. Zhang, Z. Huang, X. Che, J. Hou, H. Wang, H. Shen, L. Qiu, Z. Li, J. Geng, J. Cai, H. Han, X. Li, W. Kang, D. Weng, P. Liang, and S. Jiang.** 2004. Organ distribution of severe acute respiratory syndrome (SARS) associated coronavirus (SARS-CoV) in SARS patients: implications for pathogenesis and virus transmission pathways. The Journal of Pathology 203:622-630.

31. **Doms, R. W., and S. C. Peipert.** 1997. Unwelcomed guests with master keys: How HIV uses chemokine receptors for cellular entry. Virology 235:179-190.

32. **Dormitzer, P. R., Z. Y. Sun, G. Wagner, and S. C. Harrison.** 2002. The rhesus rotavirus VP4 sialic acid binding domain has a galectin fold with a novel carbohydrate binding site. EMBO Journal 21:885-897.

33. **Dryden, K. A., D. L. Farsetta, G. Wang, J. M. Keegan, B. N. Fields, T. S. Baker, and M. L. Nibert.** 1998. Internal structures containing transcriptase-related proteins in top component particles of mammalian orthoreovirus. Virology 245:33-46.

34. **Dryden, K. A., G. Wang, M. Yeager, M. L. Nibert, K. M. Coombs, D. B. Furlong, B. N. Fields, and T. S. Baker.** 1993. Early steps in reovirus infection are associated with dramatic changes in supramolecular structure and protein conformation: analysis of virions and subviral particles by cryoelectron microscopy and image reconstruction. Journal of Cell Biology 122:1023-1041.

35. **Duncan, R., D. Horne, L. W. Cashdollar, W. K. Joklik, and P. W. K. Lee.** 1990. Identification of conserved domains in the cell attachment proteins of the three serotypes of reovirus. Virology 174:399-409.

36. **Eisen, M. B., S. Sabesan, J. J. Skehel, and D. C. Wiley.** 1997. Binding of the influenza A virus to cell-surface receptors: structures of five hemagglutinin-sialyloligosaccharide complexes determined by X-ray crystallography. Virology 232:19-31.

37. **Emsley, P., and K. Cowtan.** 2004. Coot: model building tools for molecular graphics. Acta Crystallogr. D 60:2126-2132.

38. **Excoffon, K. J. D. A., K. M. Guglielmi, J. D. Wetzel, N. D. Gansemer, J. A. Campbell, T. S. Dermody, and J. Zabner.** 2008. Reovirus preferentially infects the basolateral surface and is released from the apical surface of polarized human respiratory epithelial cells. Journal of Infectious Diseases 197:1189-1197.

39. **Fraser, R. D. B., D. B. Furlong, B. L. Trus, M. L. Nibert, B. N. Fields, and A. C. Steven.** 1990. Molecular structure of the cell-attachment protein of reovirus: correlation of computer-processed electron micrographs with sequence-based predictions. Journal of Virology 64:2990-3000.

40. **Frierson, J. M., A. J. Pruijssers, J. L. Konopka, D. M. Reiter, T. W. Abel, T. Stehle, and T. S. Dermody.** 2012. Utilization of sialylated glycans as coreceptors enhances the neurovirulence of serotype 3 reovirus
Journal of Virology *Manuscript accepted with revisions*.

41. **Fry, E. E., et al.** 2010. Crystal structure of equine rhinitis A virus in complex with its sialic acid receptor. J Gen Virol 91:1971-77.

42. **Furlong, D. B., M. L. Nibert, and B. N. Fields.** 1988. Sigma 1 protein of mammalian reoviruses extends from the surfaces of viral particles. Journal of Virology 62:246-256.

43. **Gagneux, P., et al.** 2003. Human-specific regulation of alpha 2-6-linked sialic acids. J Biol Chem 278:48245-50.

44. **Gentsch, J. R., and A. F. Pacitti.** 1987. Differential interaction of reovirus type 3 with sialylated receptor components on animal cells. Virology 161:245-248.

45. **Goody, R. J., S. A. Schittone, and K. L. Tyler.** 2008. Experimental reovirus-induced acute flaccid paralysis and spinal motor neuron cell death. Journal of Neuropathology and Experimental Neurology 67:231-239.

46. **Guglielmi, K. M., E. M. Johnson, T. Stehle, and T. S. Dermody.** 2006. Attachment and cell entry of mammalian orthoreovirus. Curr. Top. Microbiol. Immunol. 309:1-38.

47. **Harbury, B., P. S. Kim, and T. Alber.** 1994. Crystal structure of an isoleucine-zipper trimer. Nature 371:80-83.

48. **Haselhorst, T., et al.** 2009. Sialic acid dependence in rotavirus host cell invasion. Nat Chem Biol 5:91-93.

49. **Helander, A., K. J. Silvey, N. J. Mantis, A. B. Hutchings, K. Chandran, W. T. Lucas, M. L. Nibert, and M. R. Neutra.** 2003. The viral σ1 protein and glycoconjugates containing α2-3-linked sialic acid are involved in type 1 reovirus adherence to M cell apical surfaces. Journal of Virology 77:7964-7977.

50. **Hettmer, S., R. McCarter, S. Ladisch, and K. Kaucic.** 2004. Alterations in neuroblastoma ganglioside synthesis by induction of GD1b synthase by retinoic acid. Br J Cancer 91:389-97.

51. **Isa, P., et al.** 2006. Role of sialic acids in rotavirus infection. Glycoconj J. 23:27-37.

52. **Ishii, K., Y. Ueda, K. Matsuo, Y. Matsuura, T. Kitamura, K. Kato, Y. Izumi, K. Someya, T. Ohsu, M. Honda, and T. Miyamura.** 2002. Structural analysis of vaccinia virus DIs strain: application as a new replication-deficient viral vector. Virology 302:433-444.

53. **Johnson, D. C., R. L. Burke, and T. Gregory.** 1990. Soluble forms of herpes simplex virus glycoprotein D bind to a limited number of cell surface receptors and inhibit virus entry into cells. Journal of Virology 64:2569-2576.

54. **Kabsch, W.** 1993. Automatic processing of rotation diffraction data from crystals of initially unknown symmetry and cell constants. J Appl Cryst 26:795–800.

55. **Kaludov, N., K. E. Brown, R. W. Walters, J. Zabner, and J. A. Chiorini.** 2001. Adeno-associated virus serotype 4 (AAV4) and AAV5 both require sialic acid binding for hemagglutination and efficient transduction but differ in sialic acid linkage specificity. J Virol 75:6884-6893.

56. **Kaye, K. M., D. R. Spriggs, R. Bassel-Duby, B. N. Fields, and K. L. Tyler.** 1986. Genetic basis for altered pathogenesis of an immune-selected antigenic variant of reovirus type 3 Dearing. Journal of Virology 59:90-97.

57. Kirchner, E., K. M. Guglielmi, H. M. Strauss, T. S. Dermody, and T. Stehle. 2008. Structure of reovirus s1 in complex with its receptor junctional adhesion molecule-A. PLoS Pathog 4:e1000235.

58. Kobayashi, T., A. A. R. Antar, K. W. Boehme, P. Danthi, E. A. Eby, K. M. Guglielmi, G. H. Holm, E. M. Johnson, M. S. Maginnis, S. Naik, W. B. Skelton, J. D. Wetzel, G. J. Wilson, J. D. Chappell, and T. S. Dermody. 2007. A plasmid-based reverse genetics system for animal double-stranded RNA viruses. Cell Host Microbe 1:147-157.

59. Kobayashi, T., L. S. Ooms, M. Ikizler, J. D. Chappell, and T. S. Dermody. 2010. An improved reverse genetics system for mammalian orthoreoviruses. Virology 2:194-200.

60. Kostrewa, D., M. Brockhaus, A. D'Arcy, G. E. Dale, P. Nelboeck, G. Schmid, F. Mueller, G. Bazzoni, E. Dejana, T. Bartfai, F. K. Winkler, and M. Hennig. 2001. X-ray structure of junctional adhesion molecule: structural basis for homophilic adhesion via a novel dimerization motif. EMBO Journal 20:4391-4398.

61. Kotani, M., I. Kawashima, H. Ozawa, T. Terashima, and T. Tai. 1993. Differential distribution of major gangliosides in rat central nervous system detected by specific monoclonal antibodies. Glycobiology 3:137-46.

62. Ledeen, R. W., and R. K. Yu. 1982. Gangliosides: structure, isolation, and analysis. Methods Enzymol 83:139-91.

63. Lerner, A. M., J. D. Cherry, and M. Finland. 1963. Haemagglutination with reoviruses. Virology 19:58-65.

64. Liang, T. W., H. H. Chiu, A. Gurney, A. Sidle, D. B. Tumas, P. Schow, J. Foster, T. Klassen, K. Dennis, R. A. DeMarco, T. Pham, G. Frantz, and S. Fong. 2002. Vascular endothelial-junctional adhesion molecule (VE-JAM)/JAM 2 interacts with T, NK, and dendritic cells through JAM 3. J Immunol 168:1618-26.

65. Liemann, S., K. Chandran, T. S. Baker, M. L. Nibert, and S. C. Harrison. 2002. Structure of the reovirus membrane-penetration protein, m1, in a complex with its protector protein, s3. Cell 108:283-295.

66. **Liu, Y., A. Nusrat, F. J. Schnell, T. A. Reaves, S. Walsh, M. Ponchet, and C. A. Parkos.** 2000. Human junction adhesion molecule regulates tight junction resealing in epithelia. Journal of Cell Science 113:2363-2374.

67. **Low, J. A., et al.** 2006. Identification of gangliosides GD1b and GT1b as receptors for BK virus. J. Virol 80:1361-6.

68. **Maddon, P. J., A. G. Dalgleish, J. S. Mcdougal, P. R. Clapham, R. A. Weiss, and R. Axel.** 1986. The T4 gene encodes the AIDS virus receptor and is expressed in the immune system and the brain. Cell 47:333-348.

69. **Mann, M. A., D. M. Knipe, G. D. Fischbach, and B. N. Fields.** 2002. Type 3 reovirus neuroinvasion after intramuscular inoculation: direct invasion of nerve terminals and age-dependent pathogenesis. Virology 303:222-231.

70. **Martin-Padura, I., S. Lostaglio, M. Schneemann, L. Williams, M. Romano, P. Fruscella, C. Panzeri, A. Stoppacciaro, L. Ruco, A. Villa, D. Simmons, and E. Dejana.** 1998. Junctional adhesion molecule, a novel member of the immunoglobulin superfamily that distributes at intercellular junctions and modulates monocyte transmigration. Journal of Cell Biology 142:117-127.

71. **Mathias, P., T. Wickham, M. Moore, and G. Nemerow.** 1994. Multiple adenovirus serotypes use av integrins for infection. Journal of Virology 68:6811-6814.

72. **Miller-Podraza, H., et al.** 2009. Biosynthesis and localization of gangliosides in cultured cells. Biochemistry 21:3260-5.

73. **Morrison, L. A., R. L. Sidman, and B. N. Fields.** 1991. Direct spread of reovirus from the intestinal lumen to the central nervous system through vagal autonomic nerve fibers. Proceedings of the National Academy of Sciences USA 88:3852-3856.

74. **Murshudov, G. N., A. A. Vagin, and E. J. Dodson.** 1997. Refinement of macromolecular structures by the maximum-likelihood method. Acta Crystallogr. D Biol. Crystallogr. 53:240-255.

75. **Naik, U. P., M. U. Naik, K. Eckfeld, P. Martin-DeLeon, and J. Spychala.** 2001. Characterization and chromosomal localization of JAM-1, a platelet receptor for a stimulatory monoclonal antibody. J Cell Sci 114:539-47.

76. **Nason, E. L., J. D. Wetzel, S. K. Mukherjee, E. S. Barton, B. V. V. Prasad, and T. S. Dermody.** 2001. A monoclonal antibody specific for reovirus outer-capsid protein s3 inhibits s1-mediated hemagglutination by steric hindrance. Journal of Virology 75:6625-6634.

77. **Navaza, J.** 1994. AMoRe: an automated package for molecular replacement. Acta Crystallogr. A 50:157-163.

78. **Neu, U., et al.** 2010. Structure-function analysis of the human JC polyomavirus establishes the LSTc pentasaccharide as a functional receptor motif. Cell Host Microbe 8:309-19.

79. **Neu, U., K. Woellner, G. Gauglitz, and T. Stehle.** 2008. Structural basis of GM1 ganglioside recognition by simian virus 40. Proceedings of the National Academy of Sciences USA:5219–5224.

80. **Nibert, M. L., J. D. Chappell, and T. S. Dermody.** 1995. Infectious subvirion particles of reovirus type 3 Dearing exhibit a loss in infectivity and contain a cleaved s1 protein. Journal of Virology 69:5057-5067.

81. **Nibert, M. L., T. S. Dermody, and B. N. Fields.** 1990. Structure of the reovirus cell-attachment protein: a model for the domain organization of s1. Journal of Virology 64:2976-2989.

82. **Nilsson, E. C., et al.** 2011. The GD1a glycan is a cellular receptor for adenoviruses causing epidemic keratoconjunctivitis. Nat Med 17:105-109.

83. **Nilsson, E. C., F. Jamshidi, S. A. C. Johansson, M. S. Oberste, and N. Arnberg.** 2008. Sialic acid is a cellular receptor for coxsackievirus A24 variant, an emerging virus with pandemic potential. Journal of Virology 82:5115-5115.

84. **Paul, R. W., and P. W. K. Lee.** 1987. Glycophorin is the reovirus receptor on human erythrocytes. Virology 159:94-101.

85. **Persson, B. D., D. M. Reiter, M. Marttila, Y. F. Mei, J. M. Casasnovas, N. Arnberg, and T. Stehle.** 2007. Adenovirus type 11 binding alters the conformation of its receptor CD46. Nat. Struct. Mol. Biol. 14:164-166.

86. **Prota, A. E., J. A. Campbell, P. Schelling, J. C. Forrest, T. R. Peters, M. J. Watson, M. Aurrand-Lions, B. Imhof, T. S. Dermody, and T. Stehle.** 2003. Crystal structure of human junctional adhesion molecule 1: implications for reovirus binding. Proceedings of the National Academy of Sciences USA 100:5366-5371.

87. **Raaij, M. J. v., N. Louis, J. Chroboczek, and S. Cusack.** 1999. Structure of the human adenovirus serotype 2 fiber head domain at 1.5 A resolution. Virology 262:333-343.

88. **Raaij, M. J. v., A. Mitraki, G. Lavigne, and S. Cusack.** 1999. A triple b-spiral in the adenovirus fibre shaft reveals a new structural motif for a fibrous protein. Nature 401:935-938.

89. **Ramos-Alvarez, M., and A. B. Sabin.** 1958. Enteropathogenic viruses and bacteria. Role in summer diarrheal diseases of infancy and early childhood. Journal of the American Medical Association 167:147-158.

90. **Reiss, K., J. E. Stencel, B. S. Blaum, D. Reiter, Y. Liu, T. Feizi, T. S. Dermody, and T. Stehle.** 2012. The GM2 glycan serves as a functional co-receptor for serotype 1 reovirus. PLoS Pathogens *Manuscript accepted with revisions*.

91. **Reiter, D. M., J. M. Frierson, E. E. Halvorson, T. Kobayashi, T. S. Dermody, and T. Stehle.** 2011. Crystal structure of reovirus attachment protein σ1 in complex with sialylated oligosaccharides. PLoS Pathog 7:e1002166.

92. **Ren, R., F. C. Costantini, E. J. Gorgacz, J. J. Lee, and V. R. Racaniello.** 1990. Transgenic mice expressing a human poliovirus receptor: a new model for poliomyelitis. Cell 63:353-362.

93. **Richardson, B. A., and J. Overbaugh.** 2005. Basic statistical considerations in virological experiments. Journal of Virology 79:669-676.

94. **Ross, J., J. Glelen, S. Packman, Y. Ikawa, and P. Leder.** 1974. Globin gene expression in cultured erythroleukemic cells. Journal of Molecular Biology 87:697-714.

95. **Rubin, D. H.** 1987. Reovirus serotype 1 binds to the basolateral membrane of intestinal epithelial cells. Microbial Pathogenesis 3:215-220.

96. **Rubin, D. H., M. J. Kornstein, and A. O. Anderson.** 1985. Reovirus serotype 1 intestinal infection: a novel replicative cycle with ileal disease. Journal of Virology 53:391-398.

97. **Rubin, D. H., D. B. Weiner, C. Dworkin, M. I. Greene, G. G. Maul, and W. V. Williams.** 1992. Receptor utilization by reovirus type 3: distinct binding sites on thymoma and fibroblast cell lines result in differential compartmentalization of virions. Microbial Pathogenesis 12:351-365.

98. **Rubin, D. H., J. D. Wetzel, W. V. Williams, J. A. Cohen, C. Dworkin, and T. S. Dermody.** 1992. Binding of type 3 reovirus by a domain of the σ1 protein important for hemagglutination leads to infection of murine erythroleukemia cells. Journal of Clinical Investigation 90:2536-2542.

99. **Sabin, A. B.** 1959. Reoviruses: a new group of respiratory and enteric viruses formerly classified as ECHO type 10 is described. Science 130:1387-1389.

100. **Sanford, K. K., W. R. Earle, and G. D. Likely.** 1948. The growth in vitro of single isolated tissue cells. Journal of the National Cancer Institute 9:229-46.

101. **Schelling, P., K. M. Guglielmi, E. Kirchner, B. Paetzold, T. S. Dermody, and T. Stehle.** 2007. The reovirus σ1 aspartic acid sandwich: a trimerization motif poised for conformational change. Journal of Biological Chemistry 282:11582-11589.

102. **Smith, R. E., H. J. Zweerink, and W. K. Joklik.** 1969. Polypeptide components of virions, top component and cores of reovirus type 3. Virology 39:791-810.

103. **Spear, P. G.** 1993. Entry of alphaherpesviruses into cells. Seminars in Virology 4:167-180.

104. **Stehle, T., and S. C. Harrison.** 1996. Crystal structures of murine polyomavirus in complex with straight-chain and branched-chain sialyloligosaccharide receptor fragments. Structure 4:183-194.

105. **Stehle, T., and S. C. Harrison.** 1997. High-resolution structure of a polyomavirus VP1-oligosaccharide complex: implications for assembly and receptor binding. Embo J 16:5139-48.

106. Stehle, T., Y. Yan, T. L. Benjamin, and S. C. Harrison. 1994. Structure of murine polyomavirus complexed with an oligosaccharide receptor fragment. Nature 369:160-163.

107. Stevens, J., O. Blixt, T. M. Tumpey, J. K. Taubenberger, J. C. Paulson, and I. A. Wilson. 2006. Structure and receptor specificity of the hemagglutinin from an H5N1 influenza virus. Science 312:404-410.

108. Suzuki, Y. 2005. Sialobiology of influenza: molecular mechanism of host range variation of influenza viruses. Biol. Pharm. Bull. 28:399-408.

109. Svennerholm, L. 1963. Chromatographic separation of human brain gangliosides. J. Neurochem. 10:1613-23.

110. Tai, J. H., J. V. Williams, K. M. Edwards, P. F. Wright, J. E. Crowe, and T. S. Dermody. 2005. Prevalence of reovirus-specific antibodies in young children in Nashville, Tennessee. Journal of Infectious Diseases 191:1221-1224.

111. Tardieu, M., M. L. Powers, and H. L. Weiner. 1983. Age-dependent susceptibility to reovirus type 3 encephalitis: role of viral and host factors. Annals of Neurology 13:602-607.

112. Tardieu, M., and H. L. Weiner. 1982. Viral receptors on isolated murine and human ependymal cells. Science 215:419-421.

113. Tomko, R. P., R. Xu, and L. Philipson. 1997. HCAR and MCAR: the human and mouse cellular receptors for subgroup C adenoviruses and group B coxsackieviruses. Proceedings of the National Academy of Sciences USA 94:3352-6.

114. Trkola, A., T. Dragic, J. Arthos, J. M. Binley, W. C. Olson, G. P. Allaway, C. Cheng-Mayer, J. Robinson, P. J. Maddon, and J. P. Moore. 1996. CD4-dependent, antibody-sensitive interaction between HIV-1 and its co-receptor CCR-5. Nature 384:184-187.

115. Tyler, K. L., D. A. McPhee, and B. N. Fields. 1986. Distinct pathways of viral spread in the host determined by reovirus S1 gene segment. Science 233:770-774.

116. Uchida, Y., Y. Tsukada, and T. Sugimori. 1979. Enzymatic properties of neuraminidases from Arthrobacter ureafaciens. J. Biochem. 86:1573-1585.

117. van Raaij, M. J., A. Mitraki, G. Lavigne, and S. Cusack. 1999. A triple β-spiral in the adenovirus fibre shaft reveals a new structural motif for a fibrous protein. Nature 401:935-938.

118. Virgin, H. W., IV, R. Bassel-Duby, B. N. Fields, and K. L. Tyler. 1988. Antibody protects against lethal infection with the neurally spreading reovirus type 3 (Dearing). Journal of Virology 62:4594-4604.

119. Virgin, H. W., K. L. Tyler, and T. S. Dermody. 1997. Reovirus, p. 669-699. *In* N. Nathanson (ed.), Viral Pathogenesis. Lippincott-Raven, New York.

120. Weiner, D. B., K. Girard, W. V. Williams, T. McPhillips, and D. H. Rubin. 1988. Reovirus type 1 and type 3 differ in their binding to isolated intestinal epithelial cells. Microbial Pathogenesis 5:29-40.

121. Weiner, H. L., D. Drayna, D. R. Averill, Jr, and B. N. Fields. 1977. Molecular basis of reovirus virulence: role of the S1 gene. Proceedings of the National Academy of Sciences USA 74:5744-5748.

122. Weiner, H. L., M. L. Powers, and B. N. Fields. 1980. Absolute linkage of virulence and central nervous system tropism of reoviruses to viral hemagglutinin. Journal of Infectious Diseases 141:609-616.

123. Weis, W., J. H. Brown, S. Cusack, J. C. Paulson, J. J. Skehel, and D. C. Wiley. 1988. Structure of the influenza virus haemagglutinin complexed with its receptor, sialic acid. Nature 333:426-431.

124. Whitbeck, J. C., C. Peng, H. Lou, R. Xu, S. H. Willis, M. PonceDeLeon, T. Peng, A. V. Nicola, R. I. Montgomery, M. S. Warner, A. M. Soulika, L. A. Spruce, W. T. Moore, J. D. Lambris, P. G. Spear, G. H. Cohen, and R. J. Eisenberg. 1997. Glycoprotein D of herpes simplex virus (HSV) binds directly to HVEM, a member of the tumor necrosis factor receptor superfamily and a mediator of HSV entry. Journal of Virology 71:6083-6093.

125. Wickham, T. J., P. Mathias, D. A. Cheresh, and G. R. Nemerow. 1993. Integrins $\alpha_v\beta_3$ and $\alpha_v\beta_5$ promote adenovirus internalization but not virus attachment. Cell 73:309-319.

126. Williams, L. A., I. Martin-Padura, E. Dejana, N. Hogg, and D. L. Simmons. 1999. Identification and characterisation of human junctional adhesion molecule (JAM). Molecular Immunology 36:1175-1188.

127. Williams, R. K., and S. E. Straus. 1997. Specificity and affinity of binding of herpes simplex virus type 2 glycoprotein B to glycosaminoglycans. Journal of Virology 71:1375-1380.

128. Wolf, J. L., R. Dambrauskas, A. H. Sharpe, and J. S. Trier. 1987. Adherence to and penetration of the intestinal epithelium by reovirus type 1 in neonatal mice. Gastroenterology 92:82-91.

129. Wolf, J. L., R. S. Kauffman, R. Finberg, R. Dambrauskas, B. N. Fields, and J. S. Trier. 1983. Determinants of reovirus interaction with the intestinal M cells and absorptive cells of murine intestine. Gastroenterology 85:291-300.

130. Wolf, J. L., D. H. Rubin, R. Finberg, R. S. Kaufman, A. H. Sharpe, J. S. Trier, and B. N. Fields. 1981. Intestinal M cells: a pathway of entry of reovirus into the host. Science 212:471-472.

131. Wu, L., N. P. Gerard, R. Wyatt, H. Choe, C. Parolin, N. Ruffing, A. Borsetti, A. A. Cardoso, E. Desjardin, W. Newman, C. Gerard, and J. Sodroski. 1996. CD4-induced interaction of primary HIV-1 gp120 glycoproteins with the chemokine receptor CCR-5. Nature 384:179-83.

132. Yuan, P., T. B. Thompson, B. A. Wurzburg, R. G. Paterson, R. A. Lamb, and T. S. Jardetzky. 2005. Structural studies of the parainfluenza virus 5 hemagglutinin-neuraminidase tetramer in complex with its receptor, sialyllactose. Structure 13:803-815.

133. Zhou, L., Y. Luo, Y. Wu, J. Tsao, and M. Luo. 2000. Sialylation of the host receptor may modulate entry of demyelinating persistent Theiler's virus. J Virol 74:1477-85.